

#625

SME

Earth Sc

U.V. OZONE DATA
 U.V. OZONE RADIANCE DATA
 I.R. OZONE DATA
 NEAR I.R. RADIANCE DATA
 NO2 OZONE DATA
 DAILY AVERAGED SOLAR IRRADIANCES

81-100A-01A, 01B, 03A, 03B, 04A, 05A
-01C, 01D, 01E, 01F, 01G, 04B, C.

625	81-100A-01A	<i>NO #</i>
625	81-100A-01B	SPIO-00256
625	81-100A-01C	ESAC-00034
625	81-100A-01D	
625	81-100A-01E	ESAC-00006
625	81-100A-01F	SPIO-00278
625	81-100A-01G	SPIO-00287
625	81-100A-03A	
625	81-100A-03B	ESAC-00022
625	81-100A-04A	
625	81-100A-05A	SOUV-00019

Table of Contents

1. Introduction
2. Errata/Change Log
3. LINKS TO RELEVANT INFORMATION IN THE ONLINE NSSDC INFORMATION SYSTEM
4. Catalog Materials
 - a. Associated Documents
 - b. Core Catalog Materials

1. INTRODUCTION:

The documentation for this data set was originally on paper, kept in NSSDC's Data Set Catalogs (DSCs). The paper documentation in the Data Set Catalogs have been made into digital images, and then collected into a single PDF file for each Data Set Catalog. The inventory information in these DSCs is current as of July 1, 2004. This inventory information is now no longer maintained in the DSCs, but is now managed in the inventory part of the NSSDC information system. The information existing in the DSCs is now not needed for locating the data files, but we did not remove that inventory information.

The offline tape datasets have now been migrated from the original magnetic tape to Archival Information Packages (AIP's).

A prior restoration may have been done on data sets, if a requestor of this data set has questions; they should send an inquiry to the request office to see if additional information exists.

2. ERRATA/CHANGE LOG:

NOTE: Changes are made in a text box, and will show up that way when displayed on screen with a PDF reader.

When printing, special settings may be required to make the text box appear on the printed output.

Version	Date	Person	Page	Description of Change
01				
02				

3 LINKS TO RELEVANT INFORMATION IN THE ONLINE NSSDC INFORMATION SYSTEM:

<http://nssdc.gsfc.nasa.gov/nmc/>

[NOTE: This link will take you to the main page of the NSSDC Master Catalog. There you will be able to perform searches to find additional information]

4. CATALOG MATERIALS:

- a. Associated Documents To find associated documents you will need to know the document ID number and then click here.
<http://nssdcftp.gsfc.nasa.gov/miscellaneous/documents/>

- b. Core Catalog Materials

SME

OZONE RADIANCE DATA

DAILY ORBITAL OZONE PROFILE

1 DAY + 30 DAY AVERAGE OZONE VMR PFL, TAPE

ORBITAL NO DENISTY PFL MAGNETIC LATITUDE

ORBITAL NO DENSITY PFL GEOGRAPHIC LATITUDE

IRR, LIMB RAD PROFILE, 6.8 + 9.6 MIC

RADIANCE DATA, TAPE

DAILY ORBITAL OZONE PROFILE, TAPE

IR 1 DAY + 30 DAY OZONE VMR PFL, TAPE

ORBITAL NITROGEN DIOXIDE PFL, TAPE

30 DAY AVG, NITROGEN DIOXIDE PFL, TAPE

VISIBLE LIMB RADIANCE

SOLAR IRRADIANCE DATA TAPE

81-100-01B,01C,01E,01F,01G,02A,03B,03C,03E,04B,04C,04D,05A

THIS DATA SET CATALOG CONSISTS OF 117 MAGNETIC TAPES. THE TAPES ARE 9 TRACK, 1600 BPI, ASCII AND WERE CREATED ON A VAX 11/780 COMPUTER. THE TAPES CONTAIN A HEADER FILE, TRAILER FILE AND A DATA FILE FOR EACH DATA SET CONTAINED ON THE TAPE. THE TAPES HAVE MULTIPLE DATA FILES. THE D AND C NUMBERS ARE AS FOLLOWS:

81-100A-01B SPIO-00256

<u>D#</u>	<u>C#</u>	<u>FILES</u>	<u>TIME SPAN</u>
D-64437	C-24482	1125	12/16/81 - 04/22/82
D-64438	C-24483	1266	04/23/82 - 08/12/82
D-64439	C-24484	1221	08/13/82 - 12/04/82
D-64440	C-24485	1059	12/04/82 - 03/19/83
D-64441	C-24486	1362	03/19/83 - 08/24/83
D-64442	C-24487	405	08/24/83 - 10/07/83
D-68864	C-25087	1404	10/08/83 - 03/15/84

81-100A-01B **SPIO-00256**

<u>D#</u>	<u>C#</u>	<u>FILES</u>	<u>TIME SPAN</u>
D-68865	C-25088	1449	03/16/84 - 08/27/84
D-68866	C-25089	291	08/28/84 - 09/30/84
D-76260	C-26671	1686	10/01/84 - 03/26/85
D-76261	C-26672	1380	03/27/85 - 07/23/85
D-76262	C-26673	822	07/23/85 - 09/30/85
D-78041	C-27230	1629	10/01/85 - 01/24/86
D-78042	C-27231	1563	01/24/86 - 05/02/86
D-78043	C-27232	1527	05/03/86 - 08/26/86
D-78044	C-27233	1938	08/26/86 - 10/14/86
D-78045	C-27234	804	10/14/86 - 12/18/86

81-100A-01C,03C **ESAC-00034**

D-78573	C-26829	6	12/15/81 - 09/30/82
D-78574	C-26830	6	10/01/82 - 09/30/83
D-78575	C-26831	6	10/01/83 - 09/30/84
D-78576	C-26832	6	10/01/84 - 09/30/85
D-79164	C-27243	3	01/01/86 - 12/18/86
D-79165	C-27244	3	01/01/86 - 12/18/86

81-100A-01E,03E **ESAC-00006**

D-79161	C-27171	12	01/01/82 - 12/18/86
---------	---------	----	---------------------

81-100A-01F **SPIO-00278**

D-79158	C-27237	9	01/06/82 - 06/30/83
D-79159	C-27238	12	07/01/83 - 06/30/85
D-79160	C-27239	9	07/01/85 - 12/11/86

81-100A-01G **SPIO-00287**

D-79155	C-27240	9	01/06/82 - 06/30/83
D-79156	C-27241	12	07/01/83 - 06/30/85
D-79157	C-27242	9	07/01/85 - 12/11/86

81-100A-02A **ESAC-00014**

D-75500	C-27252	1	01/01/82 - 12/31/82
D-75501	C-27253	1	01/01/82 - 12/31/82
D-75502	C-27254	1	01/01/83 - 12/31/83
D-75503	C-27255	1	01/01/83 - 12/31/83
D-75504	C-27256	1	01/01/84 - 12/31/84
D-75505	C-27257	1	01/01/84 - 12/31/84
D-75506	C-27258	1	01/01/85 - 09/30/85
D-75507	C-27259	1	01/01/85 - 09/30/85

<u>D#</u>	<u>C#</u>	<u>FILES</u>	<u>TIME SPAN</u>
D-64443	C-24488	900	12/16/81 - 02/12/82
D-64444	C-24489	918	02/12/82 - 04/03/82
D-64445	C-24490	903	04/03/82 - 05/19/82
D-64446	C-24491	918	05/19/82 - 07/02/82
D-64447	C-24492	924	07/02/82 - 08/11/82
D-64448	C-24493	900	08/11/82 - 09/14/82
D-64449	C-24494	900	09/14/82 - 10/21/82
D-64450	C-24495	909	10/21/82 - 11/26/82
D-64451	C-24496	942	11/26/82 - 01/01/83
D-64452	C-24497	924	01/01/83 - 02/06/83
D-64453	C-24498	942	02/06/83 - 03/13/83
D-64454	C-24499	921	03/14/83 - 04/18/83
D-64455	C-24500	942	04/19/83 - 05/24/83
D-64456	C-24501	885	05/24/83 - 06/29/83
D-64457	C-24502	843	06/29/83 - 08/04/83
D-64458	C-24503	834	08/04/83 - 09/09/83
D-64459	C-24504	639	09/09/83 - 10/07/83
D-68867	C-25090	987	09/26/83 - 11/18/83
D-68868	C-25091	1017	11/18/83 - 01/05/84
D-68869	C-25092	762	01/07/84 - 02/12/84
D-68870	C-25093	432	02/12/84 - 03/03/84
D-68871	C-25094	411	03/03/84 - 03/23/84
D-68872	C-25095	552	03/23/84 - 04/18/84
D-68873	C-25096	567	04/19/84 - 05/15/84
D-68874	C-25097	549	05/19/84 - 06/11/84
D-68875	C-25098	408	06/11/84 - 06/30/84
D-68876	C-25099	555	07/01/84 - 07/27/84
D-68877	C-25100	552	07/27/84 - 08/22/84
D-68878	C-25101	765	08/23/84 - 09/30/84
D-76263	C-26674	939	10/02/84 - 11/29/84
D-76264	C-26675	888	11/29/84 - 01/19/85
D-76265	C-26676	894	01/20/85 - 02/28/85
D-76266	C-26677	1008	02/28/85 - 04/02/85
D-76267	C-26678	1137	04/02/85 - 05/12/85
D-76268	C-26679	954	05/12/85 - 06/07/85
D-76269	C-26680	975	06/07/85 - 07/10/85
D-76270	C-26681	948	07/01/85 - 08/05/85
D-76271	C-26682	933	08/06/85 - 09/01/85
D-76272	C-26683	1038	09/01/85 - 09/30/85
D-78040	C-27272	933	10/01/85 - 10/29/85
D-78028	C-27260	1224	10/30/85 - 12/08/85
D-78029	C-27261	1233	12/09/85 - 01/16/86
D-78030	C-27262	888	01/17/86 - 02/11/86
D-78031	C-27263	891	02/12/86 - 03/10/86
D-78032	C-27264	1185	03/11/86 - 04/12/86
D-78033	C-27265	1110	04/13/86 - 05/15/86
D-78034	C-27266	930	05/16/86 - 06/17/86
D-78035	C-27267	930	06/18/86 - 07/20/86
D-78036	C-27268	1023	07/21/86 - 08/22/86
D-78037	C-27269	1323	08/23/86 - 09/23/86

81-100A-03B **ESAC-00022**

<u>D#</u>	<u>C#</u>	<u>FILES</u>	<u>TIME SPAN</u>
D-78038	C-27270	1146	09/24/86 - 10/26/86
D-78039	C-27271	436	10/27/86 - 11/26/86

81-100A-04B **ESAC-00051**

D-79162	C-27235	9	02/17/82 - 12/31/84
D-79163	C-27236	6	01/10/85 - 12/31/86

81-100A-04C **ESAC-00049**

D-79154	C-27185	3	01/01/82 - 12/31/86
---------	---------	---	---------------------

81-100A-04D **ESAC-00002**

D-78459	C-27276	759	01/01/82 - 02/15/82
D-78460	C-27277	1074	02/16/82 - 04/22/82
D-78461	C-27278	1278	04/23/82 - 06/27/82
D-78462	C-27279	1224	06/28/82 - 08/26/82
D-78463	C-27280	1143	08/26/82 - 11/07/82
D-78464	C-27281	843	11/07/82 - 01/12/83
D-78465	C-27282	993	01/12/83 - 03/19/83
D-78466	C-27283	969	03/19/83 - 05/23/83
D-78467	C-27284	969	05/24/83 - 07/29/83
D-78468	C-27285	972	07/29/83 - 10/02/83
D-78469	C-27286	978	10/03/83 - 12/07/83
D-78470	C-27287	957	12/08/83 - 02/11/84
D-78471	C-27288	972	02/11/84 - 04/17/84
D-78472	C-27289	1272	04/19/84 - 07/12/84
D-78473	C-27290	1260	07/13/84 - 10/25/84
D-78474	C-27291	1440	10/26/84 - 03/13/85
D-78475	C-27292	1197	03/13/85 - 07/07/85
D-78476	C-27293	1383	07/10/85 - 11/05/85
D-78477	C-27294	1362	11/06/85 - 02/06/86
D-78478	C-27295	1341	02/06/86 - 05/15/86
D-78479	C-27296	1401	05/16/86 - 08/16/86
D-78480	C-27297	1776	08/16/86 - 10/08/86
D-78481	C-27298	933	10/08/86 - 12/18/86

81-100A-05A **SOUV-00019**

D-78572	C-26835	3	01/01/82 - 06/30/88
---------	---------	---	---------------------

SME

SOLAR IRRADIANCE DATA, TAPE

81-100A-05A SOUV-00019

THIS DATA SET HAS BEEN RESTORED. THERE WAS ORIGINALLY ONE 9-TRACK, 1600 BPI, STANDARD LABELED TAPE, WRITTEN IN ASCII. THERE IS ONE RESTORED TAPE. THE DR TAPE IS A 3480 CARTRIDGE AND THE DS TAPE IS 9-TRACK, 6250 BPI. THE ORIGINAL TAPE WAS CREATED ON AN VAX 11/780 COMPUTER AND WAS RESTORED ON AN IBM 9021 COMPUTER. THE DR AND DS NUMBER ALONG WITH THE CORRESPONDING D NUMBER AND TIME SPAN IS AS FOLLOWS:

DR#	DS#	D#	FILES	TIME SPAN
DR006132	DS006132	D078572	3	01/01/82 - 06/30/88

9/22/87

To : POST, HOROWITZ
Cc : SME file

From : NG

Re : SME status ; Phone conversation with
Ronald Thomas, NCAR

- ① UV & IR ozone data are not good for long-term trend studies. Warning was included in the user's guide distributed previously.
- ② NSSDC may continue to distribute data with the appropriate user's guide until we are told otherwise.
- ③ There is no more UV, IR data after December 1986*. But the solar UV irradiance data are still being collected and are useful to many.
- ④ Anyone can log onto the SME database :
SET HOST ORION
Username : SME DATA
Password : GUEST
Comments can be sent to KNAPP [ORION::KNAPP]
Communication w/ Ron Thomas : ORION::RTHOMAS

* Day 352, 1986

ORION NO LONGER EXIST 1/94

Node: ORION
UN: SMEDATA
PW: GUEST

SME

9/87

(i)

81-100A-04

Visible Spectrometer

Products: NO_2 density on alt. grid

Potential: {
1) Temp on alt-grid
2) Ch 1 grad
3) Ch 2 " " "

86/334

(ii)

81-100-01

UV Spectrometer

Products

ORB004

1) Ozone density, orbital 86/289
2) Ozone mixing ratio on press grid, orbital 86/289
3) Daily averaged ozone 86/289
4) " variance
5) Monthly averaged ozone 86/June
6) monthly variance
7) grad.

1A
1B

MON002

OZ 010-0202

(iii)

81-100-02

IR Radiometer

Potential products:

- 1) 6.8- μm grad alt. grid
- 2) 9.6- μm " " "
- 3) H_2O mixing ratio press grid
- 4) O_3 " " " "
- 5) Night 6.8- μm grad alt. grid
- 6) Night 9.6- μm " " "
- 7) Trailing 6.8- μm - - -
- 8) Trailing 9.6- μm - - -
- 9) Night trailing 6.8 - - -
- 10) Night trailing 9.6 - - -

iv) S1-100-03 Near IR Spectrometer

Products ^{ORB004}
a) O₃ density on alt. grid; orbital 86/352
b) Daily averaged 86/347
c) Daily Variance 86/347

MON002 2 a) O₃ mixing ratio press grid; orbital 86/352
b) Daily averaged 86/347
c) Daily Variance 86/347

3. Airglow vol. emission on alt. grid; orbital

AG0030 } 4. 1.27- μ m cloud data on alt. grid (radiance)
AG0039 } 5. 1.87- μ m cloud data " " " (radiance?)

Monthly averaged \rightarrow 86/August
Monthly Variance \rightarrow "

v) S1-100-05 Solar UV Spectrometer

Products ^{SME005}
1) Daily Avg Solar irradiance
2) Daily Avg Solar Lyman- α irradiance
SME004 87/155

Laboratory for Atmospheric and Space Physics (LASP)

Campus Box 392
Boulder, Colorado 80309-0392
(303) 492-7677 TWX 910-940-3441

October 22, 1986

National Space Science Data Center
Goddard Space Flight Center
Code 633
Greenbelt, Md 20771

Attn: Ralph Post

Dear Mr. Post:

I am sending 16 tapes with one year of SME science and radiance data. Documentation for each tape is included.

Monthly average ozone are on the tape labeled MON002. Monthly average ozone mixing ratios on a pressure-latitude grid, from October 1984 to September 1985, from both the Near-Infrared Spectrometer and the Ultraviolet Spectrometer are included.

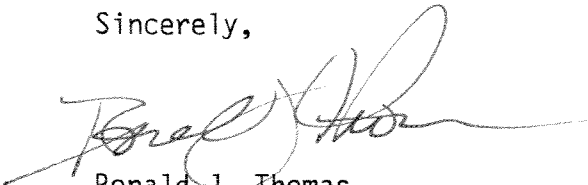
Daily average ozone and solar flux are on the tape labeled SME005. Daily average ozone mixing ratios on a pressure-latitude grid, from 1 October 1984 to 30 September 1985.

Ozone data along the orbit track are on tape ORB004. The ozone mixing ratios on a pressure-latitude grid, from 1 October 1984 to 30 September 1985, from both the Near-Infrared Spectrometer and the Ultraviolet Spectrometer are included.

Radiance data from the Near-Infrared Spectrometer are on ten tapes: AG0030 to AG0039. Radiance data for the Ultraviolet Spectrometer are on 3 tapes: OZ010 to OZ012.

Please call me at (303) 492-7672 if there are any questions.

Sincerely,



Ronald J. Thomas
Research Associate

cc: G. Esenwein
C.A. Barth

-01D
-03D
-01A
-03A
-05A
-01C
-03C
-03B
-01B
OK

Not for users

UNIVERSITY OF COLORADO, BOULDER

Laboratory for Atmospheric and
Space Physics (LASP)



October 15, 1985

National Space Science Data Center
Goddard Space Flight Center
Code 633
Greenbelt, Md 20771

Attn: Ralph Post

Dear Mr. Post:

I am sending 15 SME radiance data tapes and documentation. The tapes include ozone and radiance data for the period 1 October 1983 to 30 September 1984. *01B* → Three of the tapes are radiance data from the Ultraviolet Spectrometer and are labeled OZ007 to OZ009. Twelve tapes are radiance data from the Near Infrared Spectrometer and are labeled AG0018 to AG0029. Please call me at *03B* → (303) 492-7672 if you have any questions. *OK*

Sincerely,

A handwritten signature in cursive script, appearing to read "Ronald J. Thomas".

Ronald J. Thomas

RJT/mh

Enclosure

cc: G. Eesenwein
C.A. Barth

B R I E F D E S C R I P T I O N
SME,Limb View UV Ozone Spect
81-100A-01

The objective of the Ultraviolet Ozone Experiment was to measure ozone absorption of Rayleigh-scattered sunlight in the middle ultraviolet region. A dual-channel Ebert-Fastie spectrometer operated in the regions 1880-3100 A and 2230-3404 A and viewed normal to the spin axis. There were 208 or 11 grating steps per scan, respectively. At half maximum the full width of the signal was 15 A.

SOLAR MESOSPHERE EXPLORER
UV OZONE RADIANCE DATA

1981-1986

The ultraviolet spectrometer on the Solar Mesosphere Explorer (SME) records limb radiance profiles at two wavelengths simultaneously. For these data, these wavelengths are 2650.7 Angstroms (Channel 1), and 2964.3 Angstrom (Channel 2). The raw counts for both channels recorded and transmitted by the SME are converted into calibrated radiances with units of photons/(sq.cm-sec). For each channel, sets of six consecutive spin profiles are merged together to improve the signal to noise ratio for future data processing. If more than one spin profile in a given set of six is determined to be of poor quality, the merged profile is rejected. The saved merged radiance profiles are the ones contained in this dataset. The radiance data for both channels begin at an altitude of 41.0 km, and increase to a maximum altitude of 83.0 km, with a constant spacing of 3.5 km. See Rusch, et al. 1984 for more information.

These radiance data are contained in 17 tapes, and cover the time period from December 16, 1981 through December 18, 1986. Each tape is written in standard ASCII labeled format. The volume labels are OZ001 through OZ0017. Each file has a name of the form OZxxxxx.NSS, where xxxxx is the SME transorbit number (transorbits start at 3 a.m. local time). The following is a listing of tapes and orbit intervals contained on the tapes.

Tape Label	Orbit Interval	No. Data Files on Tape
OZ0001	1074 - 2996	375
OZ0002	3010 - 4691	422
OZ0003	4704 - 6414	407
OZ0004	6415 - 7991	353
OZ0005	8001 - 10395	454
OZ0006	10395 - 11067	135
OZ0007	11075 - 13493	468
OZ0008	13501 - 15996	483
OZ0009	16004 - 16510	97
OZ0010	16516 - 19194	562
OZ0011	19203 - 20994	460
OZ0012	21000 - 22047	274
OZ0013	22056 - 23797	543
OZ0014	23801 - 25296	521
OZ0015	25304 - 27049	509
OZ0016	27050 - 27799	646
OZ0017	27801 - 28786	268

Handwritten notes:
-01B
File # & time span
File # & orb interval
BD: Vax labelled tape

Each file contains 304-byte fixed-length records described as follows:

Record 1:

Transorbit number

No. of good radiance profile sets in this orbit (= N)

Year at start of orbit

Julian day at start of orbit

Time in seconds at start of orbit (GMT)

FORTRAN format: (I5,1X,I2,1X,I4,1X,I3,1X,F7.1)

Records 2 through N+1:

Absolute profile number for this orbit

Average latitude (degrees)

Average longitude (degrees)

Year

Julian day

Time in seconds (GMT)

Solar zenith angle (degrees)

No. of merged single-spin profiles (5 or 6)

Limb flag (1=leading limb, 2=trailing limb)

Channel 1 radiance profile of 13 points

Channel 2 radiance profile of 13 points

FORTRAN format: (I2,1X,F5.1,1X,F6.1,1X,I4,1X,I3,1X,F7.1,
1X,F5.1,1X,I1,1X,I1,1X,26(E9.2,1X))

Dr. C.A. Barth is the principal investigator for the SME experiment. Co-investigators Drs. R.J. Thomas, D.W. Rusch, G.E. Thomas, and G.J. Rottman are resident at The Laboratory for Atmospheric and Space Physics at the University of Colorado, Boulder, Colorado 80309.

SME REFERENCES

Barth, C.A., R.W. Sanders, G.E. Thomas, G.J. Rottman, D.W. Rusch, R.J. Thomas, G.H. Mount, G.M. Lawrence, J.M. Zawodny, R.A. West and J. London, Solar Mesosphere Explorer Measurements of the El Chicon Volcanic Cloud, Bull. Amer. Meteor. Soc. 63, 1314, 1982.

Barth, C.A., D.W. Rusch, R.J. Thomas, G.H. Mount, G.J. Rottman, G.E. Thomas, R.W. Sanders, G.M. Lawrence, Solar Mesosphere Explorer: Scientific Objectives and Results, Geophys. Res. Lett. 10, 237-240, 1983.

Mount, G.H., D.W. Rusch, J.M. Zawodny, J.F. Noxon, C.A. Barth, G.J. Rottman, R.J. Thomas, G.E. Thomas, R.W. Sanders, G.M. Lawrence, Measurements of NO₂ in the Earth's Stratosphere Using a Limb Scanning Visible Light Spectrometer, Geophys. Res. Lett. 10, 265-268, 1983.

Mount, G.H., D.W. Rusch, J.F. Noxon, J.M. Zawodny, and C.A. Barth, Measurements of Stratospheric NO₂ from the Solar Mesosphere Explorer Satellite. 1. An Overview of the Results, J. Geophys. Res. 89, 1327-1340, 1984.

Rottman, G.J., "Solar Ultraviolet Irradiance 1982 and 1983" in Atmospheric Ozone (ed. C.S. Zerefos) D. Reidel Pub. Co., 1985.

Rottman, G.J., C.A. Barth, R.J. Thomas, G.H. Mount, G.M. Lawrence, D.W. Rusch, R.W. Sanders, G.E. Thomas, and J. London: Solar Spectral Irradiance, 120 to 190 nm, October 13, 1981 - January 3, 1982, Geophys. Res. Lett. 9, 587-590, 1982.

Rusch, D.W., R.S. Eckman, and S. Solomon, Implications of the Comparison of Ozone Abundances Measured by the Solar Mesosphere Explorer to Model Calculations, J. Geophys. Res., in press, 1985.

Rusch, D.W., G.H. Mount, C.A. Barth, G.J. Rottman, R.J. Thomas, G.E. Thomas, R.W. Sanders, G.M. Lawrence, R.S. Eckman, Ozone Densities in the Lower Mesosphere Measured by a Limb Scanning Ultraviolet Spectrometer, Geophys. Res. Lett. 10, 241-244, 1983.

Rusch, D.W., G.H. Mount, C.A. Barth, R.J. Thomas, and M.T. Callan, Solar Mesosphere Explorer Ultraviolet Spectrometer: Measurements of Ozone in the 1.0 to 0.1 mb Region, J. Geophys. Res. 89, 11677-11687, 1984.

- Rusch, D.W., G.H. Mount, J.M. Zawodny, C.A. Barth, G.J. Rottman, R.J. Thomas, G.E. Thomas, R.W. Sanders, G.M. Lawrence, Temperature Measurements in the Earth's Stratosphere Using a Limb Scanning Visible Light Spectrometer, Geophys. Res. Lett. 10, 261-264, 1983.
- Solomon, S., G.H. Mount, and J.M. Zawodny, Measurements of Stratospheric NO₂ from the Solar Mesosphere Explorer Satellite. 2. General Morphology of observed NO₂ and derived N₂O₅, J. Geophys. Res. 89, 7317-7321, 1984.
- Thomas, G.E., C.A. Barth, E.R. Hansen, C.W. Hord, G.M. Lawrence, G.H. Mount, G.J. Rottman, D.W. Rusch, A.I. Stewart, R.J. Thomas, J. London, P.L. Bailey, P.J. Crutzen, R.E. Dickenson, J.C. Gille, S.C. Liu, J.F. Noxon, and C.B. Farmer: Scientific Objectives of the Solar Mesosphere Explorer Mission, Pageoph 118, 591-615, 1980.
- Thomas, R.J., C.A. Barth, G.J. Rottman, D.W. Rusch, G.H. Mount, G.M. Lawrence, R.W. Sanders, G.E. Thomas, L.E. Clemens, Ozone Density Distribution in the Mesosphere (50-90 km) Measured by the SME Limb Scanning Near Infrared Spectrometer, Geophys. Res. Lett. 10, 245-248, 1983.
- Thomas, R.J., C.A. Barth, G.J. Rottman, D.W. Rusch, G.H. Mount, G.M. Lawrence, R.W. Sanders, G.E. Thomas, L.E. Clemens, Mesospheric Ozone Depletion During the Solar Proton Event of July 13, 1982, Part I Measurement, Geophys. Res. Lett. 10, 253-255, 1983.
- Thomas, R.J., C.A. Barth, D.W. Rusch, and R.W. Sanders, Solar Mesosphere Explorer Near Infrared Spectrometer: Measurements of 1.2 μ m Radiances and the Inference of Mesospheric Ozone, J. Geophys. Res. 89, 9569-9580, 1984.
- Thomas, R.J., C.A. Barth, and S. Solomon, Seasonal Variations of Ozone in the Upper Mesosphere and Gravity Waves, Geophys. Res. Lett. 11, 673-676, 1984.

-01B
p. 6

LABORATORY FOR ATMOSPHERIC AND SPACE PHYSICS

SOLAR MESOSPHERE EXPLORER

UV SPECTROMETER RADIANCE DATA FOR THE

NATIONAL SPACE SCIENCE DATA CENTER

APPENDIX

Each of the enclosed tapes has the following characteristics:

1. 9-track, 1600 bpi. Written on a Digital TU77 drive.
2. ANSI STANDARD tape headers and End-of-File (EOF) structure (7-bit ASCII characters) as per VAX 11/780 system software. After the Volume Header record (80 bytes), there are four File Header records (80 bytes each), one EOF, the data records (304 bytes each), one EOF, four File Trailer records (80 bytes each), and one EOF for each of the data files on this tape.
3. Physical data blocks are 304 bytes long; each block contains one logical record. If the logical record is less than 304 bytes long, a hexadecimal value of 20 is used as fill from the end of the logical record to the end of the physical record.
4. The VAX writes bytes onto a 9-track tape in the following order:

Vax word	0	1	2	3	4	5	6	7	8	9	10	11	12	13	14	15
Vax tape	<----->							<----->								
Word written	2nd							1st								

The resulting tape (up is the tape beginning direction)

	8	9	10	11	12	13	14	15	Word part 2
	0	1	2	3	4	5	6	7	Word part 1

5. An annotated dump is attached which shows the contents of the first eight physical blocks. The left side of the dump shows the hexadecimal word (read from right to left) and the right side of the dump shows the ASCII equivalent word contents (read from left to right). The last column on the right is the hexadecimal 4-byte word number for the rightmost four bytes in the hexadecimal dump section.

Dump of device MTA3: on 21-NOV-1987 00:04:14.75

Block number 1 (00000001), 80 (0050) bytes

20202020	20202020	20202020	20202020	20202020	20203331	30305A4F	314C4F56	VOL10Z0013		000000
20202020	20202020	20202020	20202020	20202020	20202020	20202020	20202020			000020
				33202020	20202020	20202020	20202020		3.....	000040

Dump of device MTA3: on 21-NOV-1987 00:04:14.75

Block number 2 (00000002), 80 (0050) bytes

30313030	30333130	305A4F20	20202020	2053534E	2E363530	32325A4F	31F24448	HDR10Z22056.NSS	EZ001300010	000000
46434544	30303030	30302030	30303030	20343233	37382030	30313030	30313030	001000100 87324	00000 000000	DECF 000020
				20202020	20202020	20204131	31454C49	ILE11A	000040

Dump of device MTA3: on 21-NOV-1987 00:04:14.75

Block number 3 (00000003), 80 (0050) bytes

20202020	20202020	20202020	20202020	20343033	30303430	33303046	32524448	HDR2F0030400304		000000
20202020	20202020	20202020	30302020	20202020	20202020	20202041	20202020	A	00	000020
				20202020	20202020	20202020	20202020		000040

Dump of device MTA3: on 21-NOV-1987 00:04:14.75

Block number 4 (00000004), 80 (0050) bytes

30303030	30303030	31303030	30303030	30303030	31303130	30333130	33524448	HDR30130010100000000000001000000000		000000
30303030	30303030	30303030	30303030	30303030	30333130	30303030	30303030	0000000001300000000000000000000000		000020
				20202020	20202020	20202020	30303030	0000	000040

Dump of device MTA3: on 21-NOV-1987 00:04:14.75

Block number 5 (00000005), 80 (0050) bytes

20202020	20202020	20202020	20202020	20202020	20202020	20202020	34524448	HDR4		000000
20202020	20202020	20202020	20202020	20202020	20202020	20202020	20202020			000020
				20202020	20202020	20202030	30202020	00	000040

*** End of file ***

-018
p.7

Dump of device MTA3: on 21-NOV-1987 00:04:14.75

Block number 6 (00000006), 304 (0130) bytes

20202020	2020332E	31393233	32203437	32203538	39312039	31203635	30323220	22056	18	1985	274	23291.3	000000
20202020	20202020	20202020	20202020	20202020	20202020	20202020	20202020						000020
20202020	20202020	20202020	20202020	20202020	20202020	20202020	20202020						000040
20202020	20202020	20202020	20202020	20202020	20202020	20202020	20202020						000060
20202020	20202020	20202020	20202020	20202020	20202020	20202020	20202020						000080
20202020	20202020	20202020	20202020	20202020	20202020	20202020	20202020						0000A0
20202020	20202020	20202020	20202020	20202020	20202020	20202020	20202020						0000C0
20202020	20202020	20202020	20202020	20202020	20202020	20202020	20202020						0000E0
20202020	20202020	20202020	20202020	20202020	20202020	20202020	20202020						000100
20202020	20202020	20202020	20202020	20202020	20202020	20202020	20202020						000120

Dump of device MTA3: on 21-NOV-1987 00:04:14.75

Block number 7 (00000007), 304 (0130) bytes

2E333036	34322034	37322035	38393120	392E3532	31202032	2E333720	20323220	22	-78.2	125.9	1985	274	24603.	000000
2030312B	4535372E	31202030	312B4537	362E3120	20312036	20342E39	37202035	5	79.4	6	1	1.67E+10	1.75E+10	000020
32202030	312E4531	342E3220	2030312B	4537302E	32202030	312B4536	382E3120		1.86E+10	2.07E+10	2.41E+10	2	000040	
362E3120	2030312B	4536322E	32202030	312B4531	372E3220	2030312B	4532372E		.72E+10	2.71E+10	2.26E+10	1.6	000060	
4538392E	33202039	302B4530	362E3620	2030312B	4534302E	31202030	312B4530		0E+10	1.04E+10	6.60E+09	3.98E	000080	
312B4539	352E3220	2031312B	4532332E	32202039	302E4537	302E3220	2039302B	+09	2.07E+09	2.32E+11	2.59E+1	0000A0		
2031312B	4530382E	31202031	312B4533	332E3220	2031312B	4534362E	32202031	1	2.64E+11	2.33E+11	1.80E+11	0000C0		
33202030	312B4533	342E3520	2030312B	4533342E	38202031	312B4537	322E3120		1.27E+11	8.43E+10	5.48E+10	3	0000E0	
372E3620	2030312B	4535322E	31202030	312B4536	312E3220	2030312B	4536342E		.46E+10	2.16E+10	1.25E+10	6.7	000100	
				2039302B	4536312E	34202039	302B4537	7E+09	4.16E+09	000120	

Dump of device MTA3: on 21-NOV-1987 00:04:14.75

Block number 8 (00000008), 304 (0130) bytes

2E383437	34322034	37322035	38393120	352E3033	31202032	2E393620	20343220	24	-69.2	130.5	1985	274	24748.	000000
2030312B	4536382E	31202030	312B4538	372E3120	20312035	20352E35	37202035	5	75.5	5	1	1.78E+10	1.86E+10	000020
32202030	312B4539	332E3220	2030312B	4535312E	32202030	312B4538	392E3120		1.98E+10	2.15E+10	2.39E+10	2	000040	
362E3120	2030312B	4536322E	32202030	312B4533	362E3220	2030312B	4533362E		.63E+10	2.63E+10	2.26E+10	1.6	000060	
4533372E	33202039	302B4532	342E3620	2030312B	4537302E	31202030	312B4535		5E+10	1.07E+10	6.42E+09	3.73E	000080	
312B4534	342E3220	2031312B	4539312E	32202039	302B4535	332E3220	2039302B	+09	2.35E+09	2.19E+11	2.44E+1	0000A0		
2031312B	4538382E	31202031	312B4531	332E3220	2031312B	4531352E	32202031	1	2.51E+11	2.31E+11	1.88E+11	0000C0		
33202030	312B4531	392E3520	2030312B	4532302E	39202031	312B4535	332E3120		1.35E+11	9.02E+10	5.91E+10	3	0000E0	
322E3820	2030312B	4530332E	31202030	312B4531	312E3220	2030312B	4533362E		.63E+10	2.11E+10	1.30E+10	8.2	000100	
				2039302B	4532362E	34202039	302B4539	9E+09	4.62E+09	000120	

-018
P.8

81-100A-010103C
Dec 88

LABORATORY FOR ATMOSPHERIC AND SPACE PHYSICS
SOLAR MESOSPHERE EXPLORER
PROCESSED ORBIT DATA FOR THE
NATIONAL SPACE SCIENCE DATA CENTER
1981-1986 DATA

The SOLAR MESOSPHERE EXPLORER (SME) orbit data consists of ozone mixing ratios measured by two instruments. A description of the mission, the instruments, the scientific objectives, and the initial results is contained in a series of articles in the April 1983 issue of Geophysical Research Letters. In JGR in 1984 there are more comprehensive papers on the instruments and data analysis.

The ozone mixing ratios in parts per million by volume from the near infrared spectrometer are given on pressure surfaces from about 50 to 90 km between 85 degrees North and 85 degrees South at each 5 degrees. The analysis is described in "Thomas et. al., 1983, 1984".

The ozone mixing ratios in parts per million by volume from the ultraviolet spectrometer are given in pressure levels from 1.0 to 0.1 mb from 85 degrees South to 85 degrees North in 5 degree latitude intervals (see "Rusch et. al., 1983, 1984").

The previous SME ozone data (both UV and IR) contain slow steady drifts. We believe these drifts were due to a slow small sensitivity drift in the UV spectrometer. This has now been corrected, and we expect that the long term behavior is now meaningful.

Dr. C.A. Barth is the principal investigator for the SME experiment. Co-investigators Drs. R.J. Thomas, D.W. Rusch, G.E. Thomas, and G.J. Rottman are resident at the Laboratory for Atmospheric and Space Physics at the University of Colorado, Boulder, Colorado, 80309.

Orbit ozone mixing ratio data for the entire SME mission is contained on six tapes. The contents of these tapes, labeled ORB001 through ORB006, is shown in the following table.

SME OZONE MIXING RATIO DATA, 1981 - 1986

TAPE	FILE	NO.BLOCKS	CONTENTS
ORB001	AOZORB1.DAT	6365	Airglow ozone, 12/15/81 - 12/31/82
	UVOZORB1.DAT	2914	UV ozone, 12/15/81 - 12/31/82
ORB002	AOZORB2.DAT	5300	Airglow ozone, 1/ 1/83 - 12/31/83
	UVOZORB2.DAT	2404	UV ozone, 1/ 1/83 - 12/31/83
ORB003	AOZORB3.DAT	5000	Airglow ozone, 1/ 1/84 - 12/31/84
	UVOZORB3.DAT	2255	UV ozone, 1/ 1/84 - 12/31/84
ORB004	AOZORB4.DAT	7075	Airglow ozone, 1/ 1/85 - 12/31/85
	UVOZORB4.DAT	3254	UV ozone 1/ 1/85 - 12/31/85
ORB005	AOZORB5.DAT	10235	Airglow ozone, 1/ 1/86 - 12/18/86
ORB006	UVOZORB5.DAT	4654	UV ozone, 1/ 1/86 - 12/18/86

Detailed data record formats for the two files on the first tape, ORB001, are described in the following two tables.

Description of AOZORB1.DAT, airglow ozone mixing ratios in parts per million by volume. The pressure in mb for each record is found by $\log(\text{pressure}) = I * (-0.125)$ where I goes from 1 to 22. No data is indicated by -1.

DATE: 1981 DAY 349

Record	Format	Description
1	3I5,F10.2	Orbit, Year, Day, Equatorial Long.
2	35E10.3	For pressure = 0.74989 mb Field 1: Latitude = -85. Field 2: Latitude = -80. ... Field N: Latitude = (N-18)*5. ... Field 35: Latitude = 85.
3	35E10.3	For pressure = 0.56234 mb Field 1: Latitude = -85. Field 2: Latitude = -80. ... Field N: Latitude = (N-18)*5. ... Field 35: Latitude = 85.
4	35E10.3	For pressure = 0.42170 mb ... Field 35: Latitude = 85.
23	35E10.3	For pressure = 0.00178 mb
24	35F7.2	Longitudes
25	35F7.2	Solar zenith angles
26	35F9.2	Seconds of day
27	35F6.2	Roll angles

DATE: 1981 DAY 350

28	3I5,F10.2	Orbit, Year, Day, Equatorial Long.
29	35E10.3	For pressure = 0.74989 mb Field 1: Latitude = -85. Field 2: Latitude = -80. ... Field N: Latitude = (N-18)*5. ... Field 35: Latitude = 85.
30	35E10.3	For pressure = 0.56234 mb Field 1: Latitude = -85. Field 2: Latitude = -80. ... Field N: Latitude = (N-18)*5. ... Field 35: Latitude = 85.
31	35E10.3	For pressure = 0.42170 mb ... Field 35: Latitude = 85.
50	35E10.3	For pressure = 0.00178 mb
51	35F7.2	Longitudes
52	35F7.2	Solar zenith angles
53	35F9.2	Seconds of day
54	35F6.2	Roll angles

etc., for dates 1981 DAY 349 through 1982 DAY 365 for which we have data.

Description of UVOZORB1.DAT, UV ozone mixing ratios in parts per million by volume. The pressure in mb for each record is found by $\log(\text{pressure}) = I * (-0.125)$ where I goes from 0 to 8. No data is indicated by -1.

DATE: 1981 DAY 349

Record	Format	Description
1	3I5,F10.2	Orbit, Year, Day, Equatorial Long.
2	35E10.3	For pressure = 1.0 mb Field 1: Latitude = -85. Field 2: Latitude = -80. ... Field N: Latitude = (N-18)*5. ... Field 35:Latitude = 85.
3	35E10.3	For pressure = 0.74989 mb Field 1: Latitude = -85. Field 2: Latitude = -80. ... Field N: Latitude = (N-18)*5. ... Field 35:Latitude = 85.
4	35E10.3	For pressure = 0.56234 mb ... Field 35:Latitude = 85.
10	35E10.3	For pressure = 0.1 mb
11	35F7.2	Longitudes
12	35F7.2	Solar zenith angles
13	35F9.2	Seconds of day
14	35F6.2	Roll angles

DATE: 1981 DAY 350

15	3I5,F10.2	Orbit, Year, Day, Equatorial Long.
16	35E10.3	For pressure = 1.0 mb Field 1: Latitude = -85. Field 2: Latitude = -80. ... Field N: Latitude = (N-18)*5. ... Field 35:Latitude = 85.
17	35E10.3	For pressure = 0.74989 mb Field 1: Latitude = -85. Field 2: Latitude = -80. ... Field N: Latitude = (N-18)*5. ... Field 35:Latitude = 85.
18	35E10.3	For pressure = 0.56234 mb ... Field 35:Latitude = 85.
24	35E10.3	For pressure = 0.1 mb
25	35F7.2	Longitudes
26	35F7.2	Solar zenith angles
27	35F9.2	Seconds of day
28	35F6.2	Roll angles

etc., for dates 1981 DAY 349 through 1982 DAY 365 for which we have data.

-010
-020

P 5

LABORATORY FOR ATMOSPHERIC AND SPACE PHYSICS
SOLAR MESOSPHERE EXPLORER
PROCESSED DATA FOR THE
NATIONAL SPACE SCIENCE DATA CENTER

APPENDIX

Each of the enclosed tapes has the following characteristics:

1. 9-track, 1600 bpi. Written on a Digital TU77 drive.
2. ANSI STANDARD tape headers and End-of-File (EOF) structure (7-bit ASCII characters) as per VAX 11/780 system software. After the Volume Header record (80 bytes), there are four File Header records (80 bytes each), one EOF, the data records (2048 bytes each), one EOF, four File Trailer records (80 bytes each), and one EOF for each of the data files on this tape.
3. Physical data blocks are 2048 bytes long; data files are 7-bit ASCII records containing a four byte "control" word followed by the ASCII bytes. The control word contains the logical record length as a right-justified ASCII number. The length refers to the total number of bytes and includes the 4-byte control word. Logical records are blocked into physical records and a hexadecimal value of 5E is used as fill from the end of the last logical record to the end of the physical record.
4. The VAX writes bytes onto a 9-track tape in the following order:

Vax word	0	1	2	3	4	5	6	7	8	9	10	11	12	13	14	15
Vax tape	<----->							<----->								
Word written								2nd		1st						

The resulting tape (up is the tape beginning direction)

	8	9	10	11	12	13	14	15	Word part 2
	0	1	2	3	4	5	6	7	Word part 1

5. An annotated dump is attached which shows the contents of the first six physical blocks. The left side of the dump shows the hexadecimal word (read from right to left) and the right side of the dump shows the ASCII equivalent word contents (read from left to right). The last column on the right is the hexadecimal 4-byte word number for the rightmost four bytes in the hexadecimal dump section.

-003
-002

SME REFERENCES

- Barth, C.A., R.W. Sanders, G.E. Thomas, G.J. Rottman, D.W. Rusch, R.J. Thomas, G.H. Mount, G.M. Lawrence, J.M. Zawodny, R.A. West and J. London, Solar Mesosphere Explorer Measurements of the El Chicon Volcanic Cloud, Bull. Amer. Meteor. Soc. 63, 1314, 1982.
- Barth, C.A., D.W. Rusch, R.J. Thomas, G.H. Mount, G.J. Rottman, G.E. Thomas, R.W. Sanders, G.M. Lawrence, Solar Mesosphere Explorer: Scientific Objectives and Results, Geophys. Res. Lett. 10, 237-240, 1983.
- Mount, G.H., D.W. Rusch, J.M. Zawodny, J.F. Noxon, C.A. Barth, G.J. Rottman, R.J. Thomas, G.E. Thomas, R.W. Sanders, G.M. Lawrence, Measurements of NO₂ in the Earth's Stratosphere Using a Limb Scanning Visible Light Spectrometer, Geophys. Res. Lett. 10, 265-268, 1983.
- Mount, G.H., D.W. Rusch, J.F. Noxon, J.M. Zawodny, and C.A. Barth, Measurements of Stratospheric NO₂ from the Solar Mesosphere Explorer Satellite. 1. An Overview of the Results, J. Geophys. Res. 89, 1327-1340, 1984.
- Rottman, G.J., "Solar Ultraviolet Irradiance 1982 and 1983" in Atmospheric Ozone (ed. C.S. Zerefos) D. Reidel Pub. Co., 1985.
- Rottman, G.J., C.A. Barth, R.J. Thomas, G.H. Mount, G.M. Lawrence, D.W. Rusch, R.W. Sanders, G.E. Thomas, and J. London: Solar Spectral Irradiance, 120 to 190 nm, October 13, 1981 - January 3, 1982, Geophys. Res. Lett. 9, 587-590, 1982.
- Rusch, D.W., R.S. Eckman, and S. Solomon, Implications of the Comparison of Ozone Abundances Measured by the Solar Mesosphere Explorer to Model Calculations, J. Geophys. Res. in press, 1985.
- Rusch, D.W., G.H. Mount, C.A. Barth, G.J. Rottman, R.J. Thomas, G.E. Thomas, R.W. Sanders, G.M. Lawrence, R.S. Eckman, Ozone Densities in the Lower Mesosphere Measured by a Limb Scanning Ultraviolet Spectrometer, Geophys. Res. Lett. 10, 241-244, 1983.
- Rusch, D.W., G.H. Mount, C.A. Barth, R.J. Thomas, and M.T. Callan, Solar Mesosphere Explorer Ultraviolet Spectrometer: Measurements of Ozone in the 1.0 to 0.1 mb Region, J. Geophys. Res. 89, 11677-11687, 1984.

-010
-322

Rusch, D.W., G.H. Mount, J.M. Zawodny, C.A. Barth, G.J. Rottman, R.J. Thomas, G.E. Thomas, R.W. Sanders, G.M. Lawrence, Temperature Measurements in the Earth's Stratosphere Using a Limb Scanning Visible Light Spectrometer, Geophys. Res. Lett. 10, 261-264, 1983.

Solomon, S., G.H. Mount, and J.M. Zawodny, Measurements of Stratospheric NO₂ from the Solar Mesosphere Explorer Satellite. 2. General Morphology of observed NO₂ and derived N₂O₅, J. Geophys. Res. 89, 7317-7321, 1984.

Thomas, G.E., C.A. Barth, E.R. Hansen, C.W. Hord, G.M. Lawrence, G.H. Mount, G.J. Rottman, D.W. Rusch, A.I. Stewart, R.J. Thomas, J. London, P.L. Bailey, P.J. Crutzen, R.E. Dickenson, J.C. Gille, S.C. Liu, J.F. Noxon, and C.B. Farmer: Scientific Objectives of the Solar Mesosphere Explorer Mission, Pageoph 118, 591-615, 1980.

Thomas, R.J., C.A. Barth, G.J. Rottman, D.W. Rusch, G.H. Mount, G.M. Lawrence, R.W. Sanders, G.E. Thomas, L.E. Clemens, Ozone Density Distribution in the Mesosphere (50-90 km) Measured by the SME Limb Scanning Near Infrared Spectrometer, Geophys. Res. Lett. 10, 245-248, 1983.

Thomas, R.J., C.A. Barth, G.J. Rottman, D.W. Rusch, G.H. Mount, G.M. Lawrence, R.W. Sanders, G.E. Thomas, L.E. Clemens, Mesospheric Ozone Depletion During the Solar Proton Event of July 13, 1982, Part I Measurement, Geophys. Res. Lett. 10, 253-255, 1983.

Thomas, R.J., C.A. Barth, D.W. Rusch, and R.W. Sanders, Solar Mesosphere Explorer Near Infrared Spectrometer: Measurements of 1.2 um Radiances and the Inference of Mesospheric Ozone, J. Geophys. Res. 89, 9569-9580, 1984.

Thomas, R.J., C.A. Barth, and S. Solomon, Seasonal Variations of Ozone in the Upper Mesosphere and Gravity Waves, Geophys. Res. Lett. 11, 673-676, 1984.

- 010
- 010

LABORATORY FOR ATMOSPHERIC AND SPACE PHYSICS
SOLAR MESOSPHERE EXPLORER
PROCESSED DATA FOR THE
NATIONAL SPACE SCIENCE DATA CENTER

APPENDIX

Each of the enclosed tapes has the following characteristics:

1. 9-track, 1600 bpi. Written on a Digital TU77 drive.
2. ANSI STANDARD tape headers and End-of-File (EOF) structure (7-bit ASCII characters) as per VAX 11/780 system software. After the Volume Header record (80 bytes), there are four File Header records (80 bytes each), one EOF, the data records (2048 bytes each), one EOF, four File Trailer records (80 bytes each), and one EOF for each of the data files on this tape.
3. Physical data blocks are 2048 bytes long; data files are 7-bit ASCII records containing a four byte "control" word followed by the ASCII bytes. The control word contains the logical record length as a right-justified ASCII number. The length refers to the total number of bytes and includes the 4-byte control word. Logical records are blocked into physical records and a hexadecimal value of 5E is used as fill from the end of the last logical record to the end of the physical record.
4. The VAX writes bytes onto a 9-track tape in the following order:

Vax word	0	1	2	3	4	5	6	7	8	9	10	11	12	13	14	15
Vax tape	<----->							<----->								
Word written	2nd							1st								

The resulting tape (up is the tape beginning direction)

	8	9	10	11	12	13	14	15		Word part 2
	0	1	2	3	4	5	6	7		Word part 1

5. An annotated dump is attached which shows the contents of the first six physical blocks. The left side of the dump shows the hexadecimal word (read from right to left) and the right side of the dump shows the ASCII equivalent word contents (read from left to right). The last column on the right is the hexadecimal 4-byte word number for the rightmost four bytes in the hexadecimal dump section.

B R I E F D E S C R I P T I O N
1-D & 30-D Avg Ozone VMR Pfl, Tape
81-100A-01E

This data set was transferred to the Goddard DAAC in May 1995,
but the data was unreadable.

D A T A S E T R E M A R K S
81-100A-01E
1-D & 30-D Avg Ozone VMR Pfl, Tape

This data set replaces -01A, -01D, -03A and -03D.

A C K N O W L E D G E M E N T S

When using the data in any reports, publications, or presentations, please
acknowledge the National Space Science Data Center and the following
individuals or groups:

81-100A-01E
The Principal Investigator, Dr. C. A. Barth

6-1000 2-1/85
R010 12/1/88

LABORATORY FOR ATMOSPHERIC AND SPACE PHYSICS
SOLAR MESOSPHERE EXPLORER
DAILY AND MONTHLY AVERAGE DATA FOR THE
NATIONAL SPACE SCIENCE DATA CENTER
1981-1986 DATA

The SOLAR MESOSPHERE EXPLORER (SME) daily and monthly average data consists of ozone mixing ratios measured by two instruments. A description of the mission, the instruments, the scientific objectives, and the initial results is contained in a series of articles in the April 1983 issue of Geophysical Research Letters. In JGR in 1984 there are more comprehensive papers on the instruments and data analysis.

The ozone mixing ratios in parts per million by volume from the near infrared spectrometer are given on pressure surfaces from about 50 to 90 km between 85 degrees North and 85 degrees South at each 5 degrees. The analysis is described in "Thomas et. al., 1983, 1984".

The ozone mixing ratios in parts per million by volume from the ultraviolet spectrometer are given in pressure levels from 1.0 to 0.1 mb from 85 degrees South to 85 degrees North in 5 degree latitude intervals (see "Rusch et. al., 1983, 1984").

The previous SME ozone data (both UV and IR) contain slow steady drifts. We believe these drifts were due to a slow small sensitivity drift in the UV spectrometer. This has now been corrected, and we expect that the long term behavior is now meaningful.

Dr. C.A. Barth is the principal investigator for the SME experiment. Co-investigators Drs. R.J. Thomas, D.W. Rusch, G.E. Thomas, and G.J. Rottman are resident at the Laboratory for Atmospheric and Space Physics at the University of Colorado, Boulder, Colorado, 80309.

The data on this tape is contained in four files. The first file, labeled AOZAVEM.DAT, has 260 physical data records and contains ozone monthly average mixing ratios obtained from the near infrared spectrometer. The second file, labeled UVOZAVEM.DAT, has 105 physical data records and consists of monthly average ozone mixing ratios derived from the ultraviolet spectrometer. The third file, labeled AVEAOZ.DAT, has 7815 physical data records and consists of daily average ozone mixing ratios derived from the near infrared spectrometer. The fourth and last file, labeled AVEUVOZ.DAT, has 3210 physical data records and consists of daily average ozone mixing ratios derived from the ultraviolet spectrometer. The data record formats for these four files are described in the following four tables.

Description of AOZAVEM.DAT, monthly averages of airglow ozone mixing ratios in parts per million by volume. The pressure in mb for each record is found by $\log(\text{pressure}) = I * (-0.125)$ where I goes from 1 to 22. No data is indicated by -1.

DATE: 1982 MONTH 1

Record	Format	Description
1	2I5	Year, Month
2	35E10.3	For pressure = 0.74989 mb Field 1: Latitude = -85. Field 2: Latitude = -80. ... Field N: Latitude = (N-18)*5. ... Field 35:Latitude = 85.
3	35E10.3	For pressure = 0.56234 mb Field 1: Latitude = -85. Field 2: Latitude = -80. ... Field N: Latitude = (N-18)*5. ... Field 35:Latitude = 85.
4	35E10.3	For pressure = 0.42170 mb
23	35E10.3	For pressure = 0.00178 mb

DATE: 1982 MONTH 2

24	2I5	Year, Month
25	35E10.3	For pressure = 0.74989 mb Field 1: Latitude = -85. Field 2: Latitude = -80. ... Field N: Latitude = (N-18)*5. ... Field 35:Latitude = 85.
26	35E10.3	For pressure = 0.56234 mb Field 1: Latitude = -85. Field 2: Latitude = -80. ... Field N: Latitude = (N-18)*5. ... Field 35:Latitude = 85.
27	35E10.3	For pressure = 0.42170 mb
46	35E10.3	For pressure = 0.00178 mb

etc., for dates 1982 MONTH 1 through 1986 MONTH 11 for which we have data.

Description of UVOZAVEM.DAT, monthly averages of UV ozone mixing ratios in parts per million by volume. The pressure in mb for each record is found by $\log(\text{pressure}) = I * (-0.125)$ where I goes from 0 to 8. No data is indicated by -1.

DATE: 1982 MONTH 1

Record	Format	Description
1	2I5	Year, Day
2	35E10.3	For pressure = 1.0 mb Field 1: Latitude = -85. Field 2: Latitude = -80. ... Field N: Latitude = (N-18)*5. ...
3	35E10.3	Field 35:Latitude = 85. For pressure = 0.74989 mb Field 1: Latitude = -85. Field 2: Latitude = -80. ... Field N: Latitude = (N-18)*5. ...
4	35E10.3	Field 35:Latitude = 85. For pressure = 0.56234 mb
10	35E10.3	... For pressure = 0.1 mb

DATE: 1982 MONTH 2

11	2I5	Year, Day
12	35E10.3	For pressure = 1.0 mb Field 1: Latitude = -85. Field 2: Latitude = -80. ... Field N: Latitude = (N-18)*5. ...
13	35E10.3	Field 35:Latitude = 85. For pressure = 0.74989 mb Field 1: Latitude = -85. Field 2: Latitude = -80. ... Field N: Latitude = (N-18)*5. ...
14	35E10.3	Field 35:Latitude = 85. For pressure = 0.56234 mb
20	35E10.3	... For pressure = 0.1 mb

etc., for dates 1982 MONTH 1 through 1986 MONTH 10 for which we have data.

Description of AVEAOZ.DAT, daily averages of airglow ozone mixing ratios in parts per million by volume. The pressure in mb for each record is found by $\log(\text{pressure}) = I * (-0.125)$ where I goes from 1 to 22. No data is indicated by -1.

DATE: 1981 DAY 349

Record	Format	Description
1	2I5	Year, Day
2	35E10.3	For pressure = 0.74989 mb Field 1: Latitude = -85. Field 2: Latitude = -80. ... Field N: Latitude = (N-18)*5. ... Field 35:Latitude = 85.
3	35E10.3	For pressure = 0.56234 mb Field 1: Latitude = -85. Field 2: Latitude = -80. ... Field N: Latitude = (N-18)*5. ... Field 35:Latitude = 85.
4	35E10.3	For pressure = 0.42170 mb
23	35E10.3	For pressure = 0.00178 mb

DATE: 1981 DAY 350

24	2I5	Year, Day
25	35E10.3	For pressure = 0.74989 mb Field 1: Latitude = -85. Field 2: Latitude = -80. ... Field N: Latitude = (N-18)*5. ... Field 35:Latitude = 85.
26	35E10.3	For pressure = 0.56234 mb Field 1: Latitude = -85. Field 2: Latitude = -80. ... Field N: Latitude = (N-18)*5. ... Field 35:Latitude = 85.
27	35E10.3	For pressure = 0.42170 mb
46	35E10.3	For pressure = 0.00178 mb

etc., for dates 1981 DAY 349 through 1986 DAY 352 for which we have data.

Description of AVEUVOZ.DAT, daily averages of UV ozone mixing ratios in parts per million by volume. The pressure in mb for each record is found by $\log(\text{pressure}) = I * (-0.125)$ where I goes from 0 to 8. No data is indicated by -1.

DATE: 1981 DAY 349

Record	Format	Description
1	2I5	Year, Day
2	35E10.3	For pressure = 1.0 mb Field 1: Latitude = -85. Field 2: Latitude = -80. ... Field N: Latitude = (N-18)*5. ... Field 35:Latitude = 85.
3	35E10.3	For pressure = 0.74989 mb Field 1: Latitude = -85. Field 2: Latitude = -80. ... Field N: Latitude = (N-18)*5. ... Field 35:Latitude = 85.
4	35E10.3	For pressure = 0.56234 mb
10	35E10.3	For pressure = 0.1 mb

DATE: 1981 DAY 350

11	2I5	Year, Day
12	35E10.3	For pressure = 1.0 mb Field 1: Latitude = -85. Field 2: Latitude = -80. ... Field N: Latitude = (N-18)*5. ... Field 35:Latitude = 85.
13	35E10.3	For pressure = 0.74989 mb Field 1: Latitude = -85. Field 2: Latitude = -80. ... Field N: Latitude = (N-18)*5. ... Field 35:Latitude = 85.
14	35E10.3	For pressure = 0.56234 mb
20	35E10.3	For pressure = 0.1 mb

etc., for dates 1981 DAY 349 through 1986 DAY 352 for which we have data.

SME REFERENCES

- Barth, C.A., R.W. Sanders, G.E. Thomas, G.J. Rottman, D.W. Rusch, R.J. Thomas, G.H. Mount, G.M. Lawrence, J.M. Zawodny, R.A. West and J. London, Solar Mesosphere Explorer Measurements of the El Chicon Volcanic Cloud, Bull. Amer. Meteor. Soc. 63, 1314, 1982.
- Barth, C.A., D.W. Rusch, R.J. Thomas, G.H. Mount, G.J. Rottman, G.E. Thomas, R.W. Sanders, G.M. Lawrence, Solar Mesosphere Explorer: Scientific Objectives and Results, Geophys. Res. Lett. 10, 237-240, 1983.
- Mount, G.H., D.W. Rusch, J.M. Zawodny, J.F. Noxon, C.A. Barth, G.J. Rottman, R.J. Thomas, G.E. Thomas, R.W. Sanders, G.M. Lawrence, Measurements of NO₂ in the Earth's Stratosphere Using a Limb Scanning Visible Light Spectrometer, Geophys. Res. Lett. 10, 265-268, 1983.
- Mount, G.H., D.W. Rusch, J.F. Noxon, J.M. Zawodny, and C.A. Barth, Measurements of Stratospheric NO₂ from the Solar Mesosphere Explorer Satellite. 1. An Overview of the Results, J. Geophys. Res. 89, 1327-1340, 1984.
- Rottman, G.J., "Solar Ultraviolet Irradiance 1982 and 1983" in Atmospheric Ozone (ed. C.S. Zerefos) D. Reidel Pub. Co., 1985.
- Rottman, G.J., C.A. Barth, R.J. Thomas, G.H. Mount, G.M. Lawrence, D.W. Rusch, R.W. Sanders, G.E. Thomas, and J. London: Solar Spectral Irradiance, 120 to 190 nm, October 13, 1981 - January 3, 1982, Geophys. Res. Lett. 9, 587-590, 1982.
- Rusch, D.W., R.S. Eckman, and S. Solomon, Implications of the Comparison of Ozone Abundances Measured by the Solar Mesosphere Explorer to Model Calculations, J. Geophys. Res., in press, 1985.
- Rusch, D.W., G.H. Mount, C.A. Barth, G.J. Rottman, R.J. Thomas, G.E. Thomas, R.W. Sanders, G.M. Lawrence, R.S. Eckman, Ozone Densities in the Lower Mesosphere Measured by a Limb Scanning Ultraviolet Spectrometer, Geophys. Res. Lett. 10, 241-244, 1983.
- Rusch, D.W., G.H. Mount, C.A. Barth, R.J. Thomas, and M.T. Callan, Solar Mesosphere Explorer Ultraviolet Spectrometer: Measurements of Ozone in the 1.0 to 0.1 mb Region, J. Geophys. Res. 89, 11677-11687, 1984.

Rusch, D.W., G.H. Mount, J.M. Zawodny, C.A. Barth, G.J. Rottman, R.J. Thomas, G.E. Thomas, R.W. Sanders, G.M. Lawrence, Temperature Measurements in the Earth's Stratosphere Using a Limb Scanning Visible Light Spectrometer, Geophys. Res. Lett. 10, 261-264, 1983.

Solomon, S., G.H. Mount, and J.M. Zawodny, Measurements of Stratospheric NO₂ from the Solar Mesosphere Explorer Satellite. 2. General Morphology of observed NO₂ and derived N₂O₅, J. Geophys. Res. 89, 7317-7321, 1984.

Thomas, G.E., C.A. Barth, E.R. Hansen, C.W. Hord, G.M. Lawrence, G.H. Mount, G.J. Rottman, D.W. Rusch, A.I. Stewart, R.J. Thomas, J. London, P.L. Bailey, P.J. Crutzen, R.E. Dickenson, J.C. Gille, S.C. Liu, J.F. Noxon, and C.B. Farmer: Scientific Objectives of the Solar Mesosphere Explorer Mission, Pageoph 118, 591-615, 1980.

Thomas, R.J., C.A. Barth, G.J. Rottman, D.W. Rusch, G.H. Mount, G.M. Lawrence, R.W. Sanders, G.E. Thomas, L.E. Clemens, Ozone Density Distribution in the Mesosphere (50-90 km) Measured by the SME Limb Scanning Near Infrared Spectrometer, Geophys. Res. Lett. 10, 245-248, 1983.

Thomas, R.J., C.A. Barth, G.J. Rottman, D.W. Rusch, G.H. Mount, G.M. Lawrence, R.W. Sanders, G.E. Thomas, L.E. Clemens, Mesospheric Ozone Depletion During the Solar Proton Event of July 13, 1982, Part I Measurement, Geophys. Res. Lett. 10, 253-255, 1983.

Thomas, R.J., C.A. Barth, D.W. Rusch, and R.W. Sanders, Solar Mesosphere Explorer Near Infrared Spectrometer: Measurements of 1.2 μ m Radiances and the Inference of Mesospheric Ozone, J. Geophys. Res. 89, 9569-9580, 1984.

Thomas, R.J., C.A. Barth, and S. Solomon, Seasonal Variations of Ozone in the Upper Mesosphere and Gravity Waves, Geophys. Res. Lett. 11, 673-676, 1984.

LABORATORY FOR ATMOSPHERIC AND SPACE PHYSICS
 SOLAR MESOSPHERE EXPLORER
 PROCESSED DATA FOR THE
 NATIONAL SPACE SCIENCE DATA CENTER

APPENDIX

Each of the enclosed tapes has the following characteristics:

1. 9-track, 1600 bpi. Written on a Digital TU77 drive.
2. ANSI STANDARD tape headers and End-of-File (EOF) structure (7-bit ASCII characters) as per VAX 11/780 system software. After the Volume Header record (80 bytes), there are four File Header records (80 bytes each), one EOF, the data records (2048 bytes each), one EOF, four File Trailer records (80 bytes each), and one EOF for each of the data files on this tape.
3. Physical data blocks are 2048 bytes long; data files are 7-bit ASCII records containing a four byte "control" word followed by the ASCII bytes. The control word contains the logical record length as a right-justified ASCII number. The length refers to the total number of bytes and includes the 4-byte control word. Logical records are blocked into physical records and a hexadecimal value of 5E is used as fill from the end of the last logical record to the end of the physical record.
4. The VAX writes bytes onto a 9-track tape in the following order:

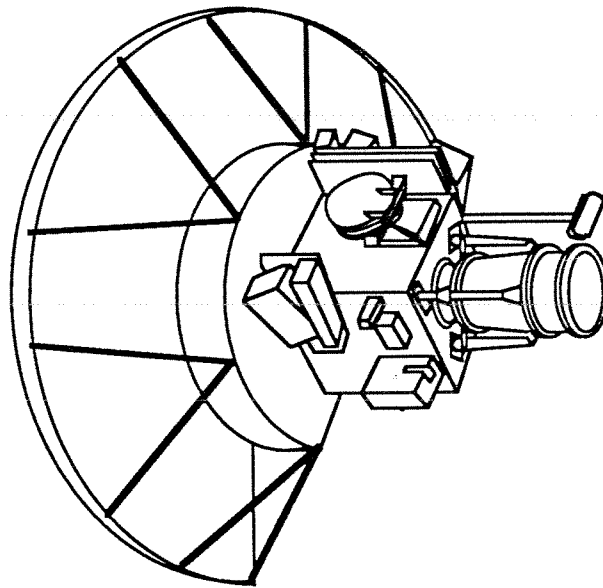
Vax word	0	1	2	3	4	5	6	7	8	9	10	11	12	13	14	15
Vax tape	<----->							<----->								
Word written								2nd		1st						

The resulting tape (up is the tape beginning direction)

8	9	10	11	12	13	14	15	Word part 2
0	1	2	3	4	5	6	7	Word part 1

5. An annotated dump is attached which shows the contents of the first six physical blocks. The left side of the dump shows the hexadecimal word (read from right to left) and the right side of the dump shows the ASCII equivalent word contents (read from left to right). The last column on the right is the hexadecimal 4-byte word number for the rightmost four bytes in the hexadecimal dump section.

SME



Solar Mesosphere Explorer
Scientific Data & Publications
Final Report

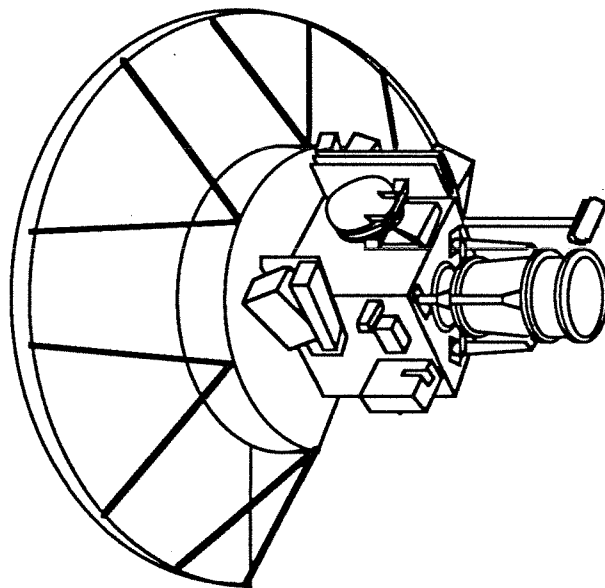
Laboratory for Atmospheric and Space Physics
University of Colorado at Boulder
Box 392
Boulder, Colorado 80309-0392

December 1989

LABORATORY FOR ATMOSPHERIC AND SPACE PHYSICS
UNIVERSITY OF COLORADO
BOULDER, COLORADO

**SOLAR MESOSPHERE EXPLORER (SME)
FINAL REPORT**

Scientific Data & Publications



December 1989

Scientific Data Archives and Scientific Publications from the Solar Mesosphere Explorer

December 1989

The Solar Mesosphere Explorer satellite was launched on October 6, 1981, into a 3:00 am — 3:00 pm Sun-synchronous polar orbit at an altitude of 530 km. The satellite is expected to re-enter Earth's atmosphere late in 1990 due to orbit decay from atmospheric drag. The satellite was operational from October 6, 1981, until April 13, 1989. The ultraviolet, visible, and near-infrared spectrometers were used to measure the properties of the mesosphere from December 15, 1981, until December 22, 1986, a period of five years from solstice to solstice. The ultraviolet and near-infrared spectrometers measured the density of ozone in the mesosphere as a function of altitude, latitude, and time. The ultraviolet spectrometer measured the density of nitric oxide in the lower thermosphere as a function of altitude, density, and time. The visible spectrometer measured the density of nitrogen dioxide in the upper stratosphere as a function of altitude, latitude, and time. The solar ultraviolet spectrometer measured the solar ultraviolet irradiance from October 8, 1981, until April 13, 1989, a period of seven years during the declining phase of the solar cycle, through solar minimum, and during the beginning of the rising phase. The SME data have been archived in the National Space Science Data Center and in the SME database at the University of Colorado. This report describes the content of those archives and lists the scientific papers published from the SME data together with their abstracts

OZONE: ORBIT-TRACK

The SME orbit-track data consist of ozone mixing ratios measured by two instruments. The archived data cover the period from 1981 through 1986. The ozone mixing ratios in parts per million by volume from the Near-Infrared Spectrometer are given on pressure surfaces from about 50 to 90 km between 85° North and 85° South at each 5 degrees. The analysis is described by Thomas *et. al.*, 1983, 1984.¹ The ozone mixing ratios in parts per million by volume from the Ultraviolet Spectrometer are given in pressure levels from 1.0 to 0.1 mb from 85° South to 85° North in 5-degree latitude intervals (see Rusch *et. al.*, 1983, 1984²).

SME OZONE MIXING RATIO DATA, 1981 - 1986

FILE	NO. BLOCKS	CONTENTS
AOZORB1.DAT	6365	Airglow ozone, 12/15/81 - 12/31/82
UVOZORB1.DAT	2914	UV ozone, 12/15/81 - 12/31/82
AOZORB2.DAT	5300	Airglow ozone, 1/ 1/83 - 12/31/83
UVOZORB2.DAT	2404	UV ozone, 1/ 1/83 - 12/31/83
AOZORB3.DAT	5000	Airglow ozone, 1/ 1/84 - 12/31/84
UVOZORB3.DAT	2255	UV ozone, 1/ 1/84 - 12/31/84
AOZORB4.DAT	7075	Airglow ozone, 1/ 1/85 - 12/31/85
UVOZORB4.DAT	3254	UV ozone 1/ 1/85 - 12/31/85
AOZORB5.DAT	10235	Airglow ozone, 1/ 1/86 - 12/18/86
UVOZORB5.DAT	4654	UV ozone, 1/ 1/86 - 12/18/86

¹Thomas R. J., C. A. Barth, G. J. Rottman, D. W. Rusch, G. H. Mount, G. M. Lawrence, R. W. Sanders, G. E. Thomas, and L. E. Clemens, Ozone Density Distribution in the Mesosphere (50-90 km) Measured by the SME Limb-Scanning Near-Infrared Spectrometer, *Geophys. Res. Letters* 10, 245-248, 1983.

Thomas, R. J., C. A. Barth, D. W. Rusch, and R. W. Sanders, Solar Mesosphere Explorer Near-Infrared Spectrometer: Measurements of 1.2 μ m Radiances and the Inference of Mesospheric Ozone, *J. Geophys. Res.* 89, 9569-9580, 1984.

²Rusch, D. W., G. H. Mount, C. A. Barth, G. J. Rottman, R. J. Thomas, G. E. Thomas, R. W. Sanders, G. M. Lawrence, and R. S. Eckman, Ozone Densities in the Lower Mesosphere Measured by a Limb-Scanning Ultraviolet Spectrometer, *Geophys. Res. Letters* 10, 241-244, 1983.

Rusch, D. W., G. H. Mount, C. A. Barth, R. J. Thomas, and M. T. Callan, Solar Mesosphere Explorer Ultraviolet Spectrometer: Measurements of Ozone in the 1.0 to 0.1 mb Region, *J. Geophys. Res.* 89, 11677-11687, 1984.

OZONE: DAILY AND MONTHLY AVERAGE

The SME daily and monthly average data consist of ozone mixing ratios measured by two instruments. The archived data cover the period from 1981 through 1986. The ozone mixing ratios in parts per million by volume from the Near Infrared Spectrometer are given on pressure surfaces from about 50 to 90 km between 85° North and 85° South at each 5 degrees. The ozone mixing ratios in parts per million by volume from the ultraviolet spectrometer are given in pressure levels from 1.0 to 0.1 mb from 85° South to 85° North in 5-degree latitude intervals.

SME OZONE MIXING RATIO DATA, 1981-1986

FILE	NO.BLOCKS	CONTENTS
AOZAVEM.DAT	260	Near-Infrared Spectrometer: Monthly average ozone mixing ratios
UVOZAVEM.DAT	105	Ultraviolet Spectrometer: Monthly average ozone mixing ratios
AVEAOZDAT	7815	Near-Infrared Spectrometer: Daily average ozone mixing ratios
AVEUVOZ.DAT	3210	Ultraviolet Spectrometer: Daily average ozone mixing ratios

NITRIC OXIDE: ORBIT-TRACK

The SME orbit-track NO data were derived from Ultra-violet Spectrometer radiance measurements. The archived data cover the years 1982 through 1986. The nitric oxide densities are given on altitude surfaces from 100 to 160 km. There are two sets of NO densities, one on a grid of magnetic latitudes, and the other on geographic latitudes. Each set also includes longitudes and solar zenith angles.

SME NO DENSITY DATA, 1981 - 1986

MAGNETIC LATITUDE GRIDDED NO DENSITY

FILE	NO. BLOCKS	CONTENTS	FIRST ORBIT
NOM82A.DAT	10718	1/ 6/82 - 6/30/82	1387
NOM82B.DAT	9269	7/ 1/82 - 12/31/82	4046
NOM83A.DAT	7774	1/ 1/83 - 6/30/83	6834
NOM83B.DAT	7843	7/ 1/83 - 12/31/83	9576
NOM84A.DAT	7889	1/ 1/84 - 6/29/84	12365
NOM84B.DAT	5267	6/30/84 - 12/31/84	15110
NOM85A.DAT	3703	1/ 1/85 - 6/30/85	17915
NOM85B.DAT	3979	7/ 1/85 - 12/31/85	20659
NOM86A.DAT	4048	1/ 1/86 - 6/30/86	23451
NOM86B.DAT	2323	7/ 1/86 - 12/11/86	26211

GEOGRAPHIC LATITUDE GRIDDED NO DENSITY

NOG82A.DAT	10718	1/ 6/82 - 6/30/82	1387
NOG82B.DAT	9269	7/ 1/82 - 12/31/82	4046
NOG83A.DAT	7774	1/ 1/83 - 6/30/83	6834
NOG83B.DAT	7843	7/ 1/83 - 12/31/83	9576
NOG84A.DAT	7889	1/ 1/84 - 6/29/84	12365
NOG84B.DAT	5267	6/30/84 - 12/31/84	15110
NOG85A.DAT	3703	1/ 1/85 - 6/30/85	17915
NOG85B.DAT	3979	7/ 1/85 - 12/31/85	20659
NOG86A.DAT	4048	1/ 1/86 - 6/30/86	23451
NOG86B.DAT	2323	7/ 1/86 - 12/11/86	26211

NITROGEN DIOXIDE: ORBIT-TRACK

The SME orbit-track NO₂ data were derived from Visible Spectrometer radiance measurements. The archived data cover the years 1982 through 1986. Nitrogen dioxide mixing ratios in parts per billion by volume are given on pressure surfaces from about 24 to 40 km between 120° South and 120° North at each 5 degrees.

SME NO₂ MIXING RATIO DATA, 1981 - 1986

FILE	NO.BLOCKS	CONTENTS
NO282.DAT	4137	2/17/82 - 12/31/82
NO283.DAT	3237	1/ 1/83 - 12/31/83
NO284.DAT	2829	1/ 1/84 - 12/31/84
NO285.DAT	3335	1/ 1/85 - 12/31/85
NO286.DAT	4683	1/ 1/86 - 12/18/86

NITROGEN DIOXIDE: MONTHLY AVERAGE

The SME monthly average NO₂ data were also derived from Visible Spectrometer radiance measurements. The archived data cover the years 1982 through 1986. The nitrogen dioxide mixing ratios in parts per billion by volume are given on pressure surfaces from about 24 to 40 km between 120° South and 120° North at each 5 degrees.

SME NO₂ MIXING RATIO DATA, 1982-1986

FILE	NO. BLOCKS	CONTENTS
SMENO2M.DAT	396	Visible Spectrometer: Monthly averages of NO ₂ mixing ratios in ppbv

SOLAR ULTRAVIOLET IRRADIANCE

The Solar Ultraviolet Spectrometer made daily measurements of the solar flux from 115 nm to 302 nm with 1 nm resolution. The archived data cover the period 1 January 1982 through 30 June 1988. The SME Solar UVS daily solar irradiance data are reduced from multiple scans, in 0.25-nm steps, of the full disk solar irradiance at the SME by a spectrometer with a full-width half-maximum resolution of 0.75 nm (Rottman *et al.*, 1982³). That is, multiple measurements spaced at 0.25 nm are convolved with an instrument response function and integrated to a resolution of 1 nm. The absolute flux is normalized to a rocket experiment of 17 May 1982 (Mount and Rottman, 1983⁴) and is accurate to $\pm 15\%$.

SME SOLAR FLUX DATA, 1981-1988

FILE	NO. BLOCKS	CONTENTS
SMESOL.TXT	2373	Solar flux and quality index 1/1/82 - 6/30/88

Data for the last year of the SME mission (*i.e.*, 1 July 1988 to 13 April 1989) will be available in both the NSSDC and University of Colorado archives after 30 June 1990. This will constitute the final database of the SME solar measurements, and, in addition, it will include the 1981 data (13 October 1981 - 31 December 1981). Estimates of the precision and long-term relative accuracy of the entire solar data set are presently being determined. These parameters are essential to establishing solar-cycle variability and will be made available to the data users.

³Rottman, G. J., C. A. Barth, R. J. Thomas, G. H. Mount, G. M. Lawrence, D. W. Rusch, R. W. Sanders, G. E. Thomas, and J. London: Solar Spectral Irradiance, 120 to 190 nm, October 13, 1981 -- January 3, 1982, *Geophys. Res. Letters* **9**, 587--590, 1982.

⁴Mount, G. H., and G. J. Rottman, The Solar Absolute Spectral Irradiance 1150--3173 Å : May 17, 1982, *J. Geophys. Res.* **88**, 5403--5410, 1983.

Scientific Publications from the Solar Mesosphere Explorer

December 1989

Barth, C. A., Reference Models for Thermospheric NO, *Adv. Space Res.* **10**, 103-115, 1989.

Nitric oxide has been measured with an ultraviolet spectrometer on the polar-orbiting satellite Solar Mesosphere Explorer (SME) for the period January 1982 to August 1986. The nitric oxide database contains densities at all latitudes sorted into 5°-bins and at altitudes between 100 and 140 km sorted into 3.3-km-bins. The largest densities occur at latitudes in the auroral zones where the density varies as a function of geomagnetic activity. Variations of a factor of 10 occur between times of intense activity and quiet times. At low latitudes, the nitric oxide density at 110 km varies from a mean value of 3×10^7 molecules/cm³ in January 1982 to a mean value of 4×10^6 molecules/cm³ during solar minimum conditions in 1986. In addition, the low-latitude nitric oxide density varies $\pm 50\%$ with a period of 27 days during times of high solar activity.

Barth, C. A., R. W. Sanders, G. E. Thomas, G. J. Rottman, D. W. Rusch, R. J. Thomas, G. H. Mount, G. M. Lawrence, J. M. Zawodny, R. A. West, and J. London, Solar Mesosphere Explorer Measurements of the El Chichon Volcanic Cloud, *Bull. Amer. Meteor. Soc.* **63**, 1314, 1982.

Instruments onboard the NASA Solar Mesosphere Explorer (SME) satellite have been measuring the formation and dispersal of the stratospheric cloud produced from the major eruption of the El Chichon volcano on 4 April 1982. SME is a polar-orbiting satellite in a sun-synchronous orbit. Its instruments view the stratosphere and mesosphere by limb-scanning along the track of the orbit. This observational technique has provided altitude-latitude maps of the atmosphere every day since the eruption.

Barth, C. A., D. W. Rusch, R. J. Thomas, G. H. Mount, G. J. Rottman, G. E. Thomas, R. W. Sanders, and G. M. Lawrence, Solar Mesosphere Explorer: Scientific Objectives and Results, *Geophys. Res. Letters* **10**, 237-240, 1983.

Instruments on the Solar Mesosphere Explorer simultaneously measure ozone density, temperature, and solar ultraviolet flux. Results from six months of observations show that ozone density in the mesosphere changes from day-to-day and with the seasons and that the principal cause of these changes is the variation in atmospheric temperature. The dependence between ozone density and temperature is inverse, with a decrease in temperature producing an increase in ozone density. This dependence is observable in the seasonal patterns and also in orbit-to-orbit observations during dramatic atmosphere changes such as stratospheric warmings.

Barth, C. A., R. W. Sanders, R. J. Thomas, G. E. Thomas, B. M. Jakosky, and R. A. West, Formation of the El Chichon Aerosol Cloud, *Geophys. Res. Letters* **10**, 993-996, 1983.

Thermal emission at 6.8 μm and particle-scattered radiation at 1.9 μm from the El Chichon aerosol cloud were measured by instruments on board the Solar Mesosphere Explorer satellite. The cloud moved westward circling the globe in twenty-one days. During its initial formation the cloud was centered at an altitude of 27 km and was confined to the altitude band between the equator and 30°N. At the 27 km level, the maximum density was reached eight to nine weeks after the eruption. Following that time, the maximum in the density gradually moved lower in altitude.

Barth, C. A., W. K. Tobiska, D. E. Siskind, and D. D. Cleary, Solar Terrestrial Coupling: Low-Latitude Thermospheric Nitric Oxide, *Geophys. Res. Letters* **15**, 92-94, 1988.

As measured by the Solar Mesosphere Explorer satellite, the density of nitric oxide at low latitudes (30°S to 30°N) and at 110 km (E-region) decreased from a mean value of 3×10^7 molecules/cm³ in January 1982 to a mean value of 4×10^6 molecules/cm³ in April 1985. In addition, the nitric oxide density varied $\pm 50\%$ with a 27-day period during times of high solar activity. The variation of nitric oxide correlates with variations in the solar Lyman-alpha irradiance which is also measured by the Solar Mesosphere Explorer satellite. The Lyman-alpha irradiance is interpreted as an index of the variations in the solar EUV and soft X-ray flux. The hypothesis is proposed that the solar X-ray flux between 20 and 100 Å has a larger variation than the solar EUV flux between 100 and 1050 Å and that the solar X-rays produce photoelectrons which are the source of the nitric oxide.

Barth, C. A., W. K. Tobiska, G. J. Rottman, and O. R. White, Comparison of 10.7 cm Radio Flux with SME Solar Lyman Alpha Flux Analysis, *Geophys. Res. Letters*, *in press*, 1990.

Measurements of the solar Lyman alpha flux that were made over a seven-and-one-half-year period between October 8, 1981 and April 13 1986 have been compared with ground-based measurements of the solar 10.7 cm radio flux made over the same time period. There is a long-term correlation between these two measures of solar flux between October 8, 1981 and July 26, 1984 during the declining part of the solar cycle. During the period July 26, 1984 — April 11, 1987, during the solar minimum period, there is not a correlation between the two solar fluxes because the 10.7 cm radio flux reaches a minimum of 65×10^{-22} W m⁻² Hz⁻¹ and does not vary below this value while the Lyman alpha flux continues to decline and show long-term and short-term variations. During the period April 11, 1987 — November 25, 1988, during the rising part of the solar cycle, there is again a correlation between the two fluxes, although the proportionality between the two is different from the proportionality during the declining phase of the solar cycle. During the period November 25, 1988 — April 13, 1989, the last period when observations of Lyman alpha were made, a medium-term correlation exists

and the proportionality of the two indices is similar to what it was during the declining phase of the solar cycle. A study of the correlation of the 10.7 cm flux with the Lyman alpha for a 999-day period during the declining phase showed that for the short-term (27-day) variation there is a correlation between the two fluxes but the proportionality between them varies from one solar rotation to the next. The conclusion is that the solar 10.7 cm radio flux is not a useful index for the solar Lyman alpha flux for the short-term, 27-day variations.

Clancy, R. T., El Chichon and "Mystery Cloud" Aerosols between 30 and 55 km: Global Observations from the SME Visible Spectrometer, *Geophys. Res. Letters* **13**, 937-940, 1986.

Visible limb radiances measured by the Solar Mesosphere Explorer (SME) are used to obtain volume scattering ratios for aerosol loading in the 30-55 km altitude range of the stratosphere. Global maps of these ratios are presented for the period January 1982 to August 1984. Significant aerosol scattering from the "mystery cloud" and El Chichon aerosol layers are found above 30 km. A timescale of approximately 2 months between the appearance of the aerosol at 30.5 km and at 37.5 km is consistent with vertical transport of aerosol or vapor by eddy diffusion above 30 km. An anticorrelation exists between aerosol scattering and stratospheric temperatures. Periods of lower stratospheric temperatures may account for the formation of aerosol between 40 and 55 km altitude.

Clancy, R. T., and D. W. Rusch, Climatology and Trends of Mesospheric (58-90 km) Temperatures Based upon 1982-1986 SME Limb Scattering Profiles, *J. Geophys. Res.* **94**, 3377-3394, 1989.

Global observations of ultraviolet limb radiances from the Solar Mesosphere Explorer (SME) have been analyzed to obtain atmospheric temperature profiles over the altitude range 58-90 km. The temperature analysis is based upon vertical profiles of Rayleigh scattering, which are derived from the SME ultraviolet limb radiances. Comparisons are provided with lidar and Stratosphere and Mesosphere Sounder (SAMS) temperature observations at 65 km altitude, and with previous temperature climatologies of the mesosphere. SME monthly average temperature profiles are presented for 10° latitude intervals between 70°S and 70°N latitudes, over the January 1982 to September 1986 time period. The altitude resolution (~4 km), latitudinal coverage (with 5° resolution), 5-year term, and mesopause coverage of these temperature observations allow new insight into the average mesospheric temperature structure and unique observations of mesospheric temperature trends corresponding to the 1982-1986 solar maximum to solar minimum cycle. The SME temperature observations define large (10-30 K) semiannual oscillations of equatorial mesopause temperatures; mid-latitude temperature inversions in the winter mesosphere accompanied by steep mesospheric temperature gradients at low latitudes, and -1.5 to +1 K/year trends, which suggest an intensification of these latitude-dependent temperature gradients over the 1982-1986 period. The SME temperature trends are ~4 times smaller than those reported by Mohanakumar (*Planet.*

Space Sci. **33**, 795-805, 1985), Groves (*Planet. Space Sci.* **34**, 1037-1041, 1986), and Chanin *et al.* (*J. Geophys. Res.* **90**, 10,933-10,941, 1987) for solar cycle variations of temperatures in the altitude region 65–70 km.

Clancy, R. T., and D. W. Rusch, "Solar Mesosphere Explorer: Temperature Climatology of the Mesosphere as Compared to the CIRA Model," in *COSPAR International Reference Atmosphere* (M. Roemer, ed.), Holland: Pergamon Press, in press, 1989.

Global observations of ultraviolet limb radiances from the Solar Mesosphere Explorer (SME) have been analyzed to obtain atmospheric temperature profiles over the 58-90 km altitude range. The temperature retrievals are based upon analysis of vertical profiles of Rayleigh scattering, which are derived from the SME ultraviolet limb radiances. A complete description of the SME analytical procedures, including error analysis and comparisons to a wider range of mesospheric temperature data sets, may be found in Clancy and Rusch (1989). This current document provides a detailed comparison of SME temperatures to the new CIRA model temperatures over the 60-90 km altitude region.

Clancy, R. T., and D. W. Rusch, "The Relationship between 1982—1986 Trends in Upper Stratospheric Ozone and Temperatures," in *Atmospheric Ozone* (D. Bojkov, ed.), Boston, Mass.: D. Reidel, in press, 1989.

Trends for upper stratospheric temperatures and ozone are calculated from the NMC and SBUV data sets, respectively, over the 1982-1986 period. Latitudinal and longitudinal variations in ozone and temperature trends are found to be anticorrelated. The observed temperature-ozone trends relationship appears consistent with ozone sensitivity to temperature dependent kinetic rate coefficients for ozone formation and destruction. The absolute SBUV ozone trends include a constant 4%/yr decrease at 1.0 mbar, most of which may be due to a calibration drift in the SBUV experiment. The absolute NMC temperature trends indicate $\sim 0.5\text{K/yr}$ global decreases in upper stratospheric temperatures over the 1982-1986 period. Such temperature trends would force $\sim 0.5\%/yr$ global increases in upper stratospheric ozone over the same period, based upon the derived relationship between ozone and temperature trend anticorrelations.

Clancy, R. T., D. W. Rusch, R. J. Thomas, M. Allen and R. S. Eckman, Model Ozone Photochemistry on the Basis of Solar Mesosphere Explorer Mesospheric Observations, *J. Geophys. Res.* **92**, 3067-3080, 1987.

Morning and afternoon mesospheric ozone profiles (50-90 km) measured by the Solar Mesosphere Explorer (SME) satellite are analyzed with one-dimensional photochemical models. The observed ozone abundances are 40% and 100% greater than the model ozone abundances at 50 and 80 km, respectively, assuming standard chemistry and rate coefficients. A Monte Carlo analysis for model ozone abundances that includes uncertainties in kinetic rate coefficients indicates that the model-data disagreement exceeds 2 standard deviations. The majority of the dis-

agreement must be due to errors in the rate of odd-hydrogen catalytic destruction of ozone, unless the rate coefficient for $O+O_2+M \rightarrow O_3+M$ is significantly (>50%) in error. Diurnal model calculations are compared with SME observations of ozone profiles at 0400 and 1400 LT for high northern summer latitudes. Analysis of the ratios of these early morning and midafternoon ozone profiles provides the additional constraint that larger odd-oxygen production rates are required if lower odd-hydrogen activity is invoked to increase model O_3 abundances. The increase in odd-oxygen production must be solar zenith angle independent in the mesosphere, ruling out significant changes in the Schumann-Runge band O_2 opacities from Allen and Frederick (*J. Atmos. Sci.* **39**, 2066-2075, 1982). However, an increase in three-body formation of O_3 is also consistent with the observed morning/afternoon ratios. Any of the above changes are consistent with an improvement in model ozone comparison with stratospheric observations. Finally, we find evidence for diurnal variations in mesospheric ozone above 80 km altitude, which are likely related to diurnal variations in vertical transport.

Dickinson, P. H. G., G. Witt, A. Zuber, D. Murtagh, K. U. Grossman, H. B. Brockelmann, P. Schwabbauer, K. D. Baker, J. C. Ulwick, and R. J. Thomas, Measurements of Odd Oxygen in the Polar Vortex on 10 February 1984 during MAP/WINE, *J. Atmos. Terr. Phys.* **49**, 843-854, 1987.

Donnelly, R. F., D. F. Heath, J. L. Lean, and G. J. Rottman, Differences in the Temporal Variations of Solar UV Flux, 10.7-cm Solar Radio Flux, Sunspot Number, and Ca-K Plage Data Caused by Solar Rotation and Active Region Evolution, *J. Geophys. Res.* **88**, 9883-9888, 1983.

Two types of temporal variations in the solar UV spectral irradiance, caused by solar rotation and active region evolution, are presented and discussed. These particular UV variations differ markedly from the concurrent variations in the 10.7-cm radio flux and sunspot number. The temporal variations of the modeled UV flux based on Ca-K plage data are similar to the observed UV flux. The first type of dissimilar temporal behavior occurs when concentrations of solar active regions evolve at solar longitudes nearly 180° apart. Both the UV observations and modeled UV fluxes based on Ca-K plage data then show strong 13-day periodicity, while the 10.7-cm solar radio flux and sunspot number exhibit quite dissimilar temporal variations. This type of dissimilarity is related to the modeled UV flux, having a dependence on the solar central meridian distance that is narrower than that for the 10.7-cm radio flux or for sunspot numbers. A second case of marked dissimilarity occurs when major new solar active regions arise and dominate the full-disk fluxes for several rotations. The strongest peaks in 10.7 cm and sunspot numbers tend to occur on their first rotation, for example, during major dips in the total solar irradiance, while the Ca-K plages and UV enhancements peak on the next rotation and then decay more slowly on subsequent rotations. This type of dissimilarity is related to major active regions having a more rapid growth, peak, and decay of sunspots, their strong magnetic fields and related coronal radio emission at centimeter wavelengths than for the Ca-K plages and their related UV enhancements.

Eckman, R. S., The Response of Ozone to Short-Term Variations in the Solar Ultraviolet Irradiance. 1. Theoretical Model, *J. Geophys. Res.* **91**, 6695-6704, 1986.

The response of atmospheric ozone and temperature to variations in the solar ultraviolet irradiance over time scales corresponding to the solar rotation period is examined using a one-dimensional, time-dependent radiative-photochemical model of the upper stratosphere and lower mesosphere. The model uses temporally varying measurements of the solar irradiance in the 120- to 300-nm range made by the Solar Mesosphere Explorer satellite. Calculations of the amplitude and phase of the ozone response due to solar UV oscillations made by the model show that the effects of the coupling of radiation and photochemistry in the region near the stratopause may not be neglected. At 0.85 mbar the computed 27-day 0.6 K temperature variation decreases the amplitude of the corresponding ozone response over the solar rotation period by 25%. The occurrence of small phase leads (up to 1.5 days) in the response of ozone with respect to the solar UV variations may also be explained in light of the radiative-photochemical coupling.

Eckman, R. S., The Response of Ozone to Short-term Variations in the Solar Ultraviolet Irradiance. 2. Observations and Interpretations, *J. Geophys. Res.* **91**, 6705-6721, 1986..

An analysis of the response of middle atmospheric ozone to short-term variations in the solar ultraviolet irradiance is presented. Measurements of ozone from the Solar Mesosphere Explorer (SME) ultraviolet spectrometer (UVS) are compared to calculations of a one-dimensional, radiative-photochemical model of the upper stratosphere and lower mesosphere. SME UVS measurements in the 0.1- to 1-mbar range suggest that tropical ozone responds to solar rotational variations when analyzed using both frequency and time domain techniques. Three periods during 1982 and 1983 were selected for the analysis. The solar irradiance during each period exhibited different spectral characteristics. A significant 27-day variation in the solar irradiance at 205 nm was measured during mid-1982, with an amplitude of 2.5%. Observations of ozone near the stratopause during this period showed a corresponding variation, with a 1.3% amplitude. Analysis of ozone variations at extratropical latitudes revealed different periodicities that were not correlated with solar variations. The amplitude of the measured response is, in all cases, systematically larger than theoretical calculations but is nonetheless in agreement when uncertainties in the analysis are considered. However, the observed phase lag of ozone with respect to the solar UV variations is generally not in accord with model predictions.

Fesen, C. G., J-C. Gerard, and D. W. Rusch, Rapid Deactivation of $N(^2D)$ by O; Impact on Thermospheric and Mesospheric Odd Nitrogen., *J. Geophys. Res.* **94**, 5419-5426, 1989.

One- and two-dimensional models of thermospheric odd nitrogen are used to explore the consequences of the recently-measured fast quenching of $N(^2D)$ by O. A large rate coefficient for this reaction profoundly affects the odd nitrogen chemistry by removing $N(^2D)$ as a source of NO and increasing the concentration of

$N(^4S)$, which destroys NO. The model calculations show that, as the quenching rate increases, the NO and $N(^2D)$ densities decrease, while $N(^4S)$ densities increase. Comparisons with Atmosphere Explorer and Solar Mesosphere Explorer satellite observations are made. Use of the fast quenching rate in the models causes the NO peak altitude, typically observed near 110 km, to rise to 140 km. The $N(^2D)$ densities become 20 times smaller than those observed, while the modelled NO ($N(^4S)$) densities are roughly two to three times too small (large). Additional measurements of the $N(^2D) + O$ quenching rate are clearly warranted. If the quenching rate is indeed very rapid, the chemistry of thermospheric odd nitrogen must be completely re-examined. (odd nitrogen, quenching, modelling.)

Gérard, J-C, C. G. Fesen, and D. W. Rusch, Solar cycle variation of chemospheric nitric oxide at solstice, *J. Geophys. Res.*, in press, 1989.

Grossman, K.U., H.G. Brockelmann, D. Offermann, P. Schwabbauer, R. Gyger, K. Kunzi, G.K. Hartmann, C.A. Barth, R. Thomas, A.F. Chijov, S.P. Perov, V.A. Yushkov, F. Glede and K.H. Grasnik, Middle Atmosphere Abundances of Water Vapor and Ozone During MAP/WINE, *J. Atmos. Terr. Phys.* **49**, 827-842, 1987.

Howell, C. D., D. V. Michelangeli, M. Allen, Y. L. Yung, R. J. Thomas, SME Observations of $O_2(^1\Delta_g)$ Nightglow: An assessment of the Chemical Production Mechanisms, *Planet. Space Sci.*, in press, 1989.

Jensen, E. J., and G. E. Thomas, A Growth-Sedimentation Model of Polar Mesospheric Clouds: Comparison with SME Measurements, *J. Geophys. Res.* **93**, 2461-2473, 1988.

A numerical model for the brightness of polar mesospheric clouds (PMC) is described, and is compared with measurements from the Solar Mesosphere Explorer (SME) satellite. These clouds occur during the summer months at polar latitudes where temperatures are known to fall below 140 K. We calculate the optical properties of a cloud by simulating the growth and sedimentation of ice particles at the cold supersaturated mesopause. Time-dependent trajectories of ice particles are calculated from their origin at the temperature minimum region to their demise at the cloud base through evaporation. We consider the effects of the removal of atmospheric water vapor by the growing particles and its restoration by ice evaporation at the cloud base. The "freeze-drying" effect is crucial in limiting the maximum size of the particles and therefore the maximum brightness of the cloud. Assuming spherical particles, Mie-scattering calculations of the directional albedo of a cloud are performed using a range of possible values for the atmospheric variables (water vapor mixing ratio, temperature, upward wind speed, atmospheric pressure, and eddy diffusion coefficient). We find that for a nominal atmospheric case the model predicts a moderately weak cloud at 265 nm, the wavelength of the SME measurements. An extreme model (cold and moist with high vertical wind and eddy transport) is needed to account for the brightest cloud observed. We estimate an upper limit for the water vapor to be of the order of 5 parts per million by volume. Higher values would imply the existence of clouds which exceed in brightness every cloud observed by the satellite over the time

period 1981-1986. SME observations of greater cloud height in the northern hemisphere, despite their greater brightness, possibly imply an excess (by a factor of 2) of northern hemisphere water vapor. This holds if the other atmospheric variables (and cloud particle numbers) are the same in both north and south. Dependence of model cloud brightness on atmospheric pressure ($\sim P^{4.4}$), water vapor mixing ratio ($\sim w^{2.8}$), thickness of the cloud saturation region ($\sim d^4$) and advective wind speed ($\sim v$) are determined. These scalings are shown to result from a calculated proportionality of the cloud brightness of R^6 (R is the maximum particle radius), and from simple considerations of ice layer growth, particle sedimentation, and the mass budget of water. Mie scattering calculations for a wavelength of 550 nm show that SME and OGO-6 data on PMC brightnesses are consistent.

Jensen, E. J., G. E. Thomas, and B. B. Balsley, On the Statistical Correlation between Polar Mesospheric Cloud Occurrence and Enhanced Mesospheric Radar Echoes, *Geophys. Res. Letters* **15**, 315-318, 1988.

Using data from the Poker Flat MST radar and the Solar Mesosphere Explorer Satellite (SME), we demonstrate the existence of a statistically significant correlation between the occurrence of Polar Mesospheric Clouds (PMC) and enhanced VHF radar echoes near the high-latitude summer mesopause. We propose three physical conditions which could explain the coexistence of strong summertime echoes and PMC. First, both the enhanced echoes and the PMC are most likely to occur in the presence of very low mesopause temperatures and associated steep temperature gradients. Second, the presence of PMC ice particles could induce a strong gradient in the electron density profile, which would produce enhancements in the radar echo strength. Third, it is likely that heavy water cluster ions, indicative of PMC particle nucleation, can alter the ambipolar diffusion coefficient, thus allowing the electron density fluctuations to extend down to much smaller vertical scales. Under these conditions, the turbulent power at the 3 meter scale required for the occurrence of the MST radar echoes could be greatly enhanced. Finally, we discuss the possibility of using MST radars as instruments for PMC detection.

Jensen, E. J., G. E. Thomas, and O. B. Toon, On the Diurnal Variation of Noctilucent Clouds, *J. Geophys. Res.*, in press., 1989.

LeTexier, H., S. Solomon, and R. R. Garcia, Seasonal Variability of the OH Meinel Bands, *Planet. Space Sci.* **35**, 911-939, 1987.

LeTexier, H., S. Solomon, R. J. Thomas, and R. R. Garcia, OH*(7-5) Meinel Band Dayglow and Nightglow Measured by the SME Limb Scanning Near Infrared Spectrometer: Comparison of the Observed Seasonal Variability with Two-dimensional Model Simulation, *Annal. Geophys.*, **7**, 365-374, 1989.

London, J., and G. J. Rottman, The Contribution of Solar UV Irradiance Variations to Variations of the Solar Constant, in *IRS '88: Current Problems in Atmospheric Radiation*, (J. Lenoble and J. S. Geleyn, eds.), A. Deepak Pub. Co., 1989.

The total solar irradiance in the wavelength interval 250-330 nm is about 13.25 Wm^{-2} , which represents almost 1% of the solar constant as measured by the Nimbus 7-ERB instrument. In that spectral interval the normalized solar irradiance observed by the Solar Mesosphere Explorer (SME) decreased during the period Jan 1982 to May 1986 (solar minimum) by about 1.3%. The decrease of the SME observed near UV irradiance contributed over 35% to the observed solar constant change for that period, a value that is certainly significant in considering possible atmospheric responses to solar variability. The implications of the observed solar irradiance variation will be discussed.

London, J., G. G. Bjarnason, and G. J. Rottman, Eighteen Months of Ultraviolet Irradiance Observations from the Solar Mesosphere Explorer, *Geophys. Res. Letters* **11**, 54-56, 1984.

Daily solar irradiance measurements in the spectral interval 120-305 nm have been made since 6 October 1981 with an instrument on the Solar Mesosphere Explorer. The instrument operates with a spectral resolution of about 0.75 nm. Analysis of the observed data for the period 6 December 1981 to 3 June 1983 (20 solar rotations) shows that during this period there was an apparent decrease in irradiance at all wavelengths observed ($-19.7\% \pm 9.7\%$ at Lyman alpha) but the decrease was not significantly different from zero at wavelengths longer than 210 nm. The cross correlations between daily values of the solar irradiance and 10.7 cm flux varied from 0.7 (Lyman alpha) to 0.5 (210-215 nm) and ~ 0 (290-295 nm). Calculations of the % range (*i.e.*, highest to lowest value) of the irradiance within each solar rotation showed that for Lyman alpha the range varied between 6% and 30% over the 20 solar rotations studied. At longer wavelengths the % range was smaller — about 7% at 180 nm and about 2% beyond 240 nm. The percent range values indicate representative variations useful as input data for model calculations of stratosphere/mesosphere responses to short period solar variability.

Mount, G. H., and G. J. Rottman, The Solar Absolute Spectral Irradiance at 1216 Å and 1800-3173 Å: January 12, 1983, *J. Geophys. Res.* **88**, 6807, 1983.

Mount, G. H., and G. J. Rottman, The Solar Absolute Spectral Irradiance 1150-3173 Å: May 17, 1982, *J. Geophys. Res.* **88**, 5403-5410, 1983.

The full-disk solar spectral irradiance in the spectral range 1150-3173 Å was obtained from a rocket observation above White Sands Missile Range, New Mexico, on May 17, 1982, halfway in time between solar maximum and solar minimum. Comparison with measurements made during solar maximum in 1980 indicate a large decrease in the absolute solar irradiance at wavelengths below 1900 Å to approximately solar minimum values. No change above 1900 Å from solar maximum to this flight was observed to within the errors of the measurements. We find irradiance values lower than the Broadfoot results in the 2100-

2500 Å spectral range, but we find excellent agreement with Broadfoot between 2500 and 3173 Å. The absolute calibration of the instruments for this flight was accomplished at the National Bureau of Standards Synchrotron Radiation Facility which significantly improves calibration of solar measurements made in this spectral range.

Mount, G. H., and G. J. Rottman, The Solar Absolute Spectral Irradiance 1180-3000 Å: July 25, 1983, *J. Geophys. Res.* **90**, 13,031-13,036, 1985..

Mount, G. H., D. W. Rusch, J. M. Zawodny, J. F. Noxon, C. A. Barth, G. J. Rottman, R. J. Thomas, G. E. Thomas, R. W. Sanders, and G. M. Lawrence, Measurements of NO₂ in the Earth's Stratosphere Using a Limb Scanning Visible Light Spectrometer, *Geophys. Res. Letters* **10**, 265-268, 1983.

NO₂ densities determined from the limb scanning visible light spectrometer on board the Solar Mesosphere Explorer spacecraft are reported for winter 1981/82 in the altitude region 28-40 km. The observational technique utilizes the photoabsorption by NO₂ of Rayleigh scattered sunlight in the 440 nm spectral region. The NO₂ density varies from pole to pole and shows large variations at high northern latitudes during the winter months which are related to both the temperature and flow of air near 30 km.

Mount, G. H., D. W. Rusch, J. F. Noxon, J. M. Zawodny, and C. A. Barth, Measurements of Stratospheric NO₂ from the Solar Mesosphere Explorer Satellite. I. An Overview of the Results, *J. Geophys. Res.* **89**, 1327-1340, 1984.

The visible light spectrometer on board the Solar Mesosphere Explorer spacecraft measures stratospheric NO₂ in the 20-40 km altitude region and provides accurate daytime NO₂ density profiles with nearly complete latitudinal coverage over an extended period of time. The instrument and data analysis are discussed in detail, and NO₂ results for winter/spring 1982 are presented and compared to current theoretical models. Agreement with other measurements is good, and comparison with NO_x models indicates that although the overall agreement is acceptable, improvements in the models are required before good agreement is reached at all latitudes. The data indicate that NO₂ has a strong memory of the physical conditions present in the stratosphere over a time period of several days.

Naudet, J.-P., and G. E. Thomas, Aerosol Optical Depth and Planetary Albedo in the Visible from the Solar Mesosphere Explorer, *J. Geophys. Res.* **92**, 8373-8381, 1987.

The Solar Mesosphere Explorer (SME) satellite has observed the visible sunlight scattered at the earth's limb since early 1982. By using a radiative transfer model including multiple scattering and albedo effects, observations at 20°N latitude have been interpreted in terms of aerosol optical depth. The ratio of aerosol extinction to Rayleigh extinction at 421.8 nm shows a large increase after the eruption of El Chichon. A maximum ratio of 5 at 36 km and larger than 11 at 30 km occurs in the summer of 1982 followed by a decrease through 1983 and 1984. Aspects of

the aerosol time evolution appear to be consistent with other observations and model predictions. Quantitative differences exist between inferred SME and lidar extinction coefficients, possibly due to the different wavelengths of the measurements and to the different scattering phase functions used in the two analyses. It also shows that visible limb radiances provide information on the planetary albedo, which shows an increase from the equator to the poles with a maximum in the winter hemisphere and a minimum in the summer hemisphere.

Naudet, J. P., D. W. Rusch, R. J. Thomas, R. T. Clancy, C. A. Barth, J. Wedding, J. M. Zawodny, P. Fabian, and M. Helten, Stratospheric NO₂ from the Solar Mesosphere Explorer during MAP/GLOBUS 1983, *Planet. Space Sci.* **35**, 631-635, 1987.

Nitrogen dioxide in the altitude range 24-40 km has been observed by the Solar Mesosphere Explorer Satellite during the MAP/GLOBUS campaign in September 1983. Results are presented and compared to other observations. NO₂ from the Solar Mesosphere Explorer appears to be in good agreement with daytime *in situ* balloon measurements in the mid-stratosphere.

Naudet, J.-P., R. J. Thomas, H. K. Roscoe, and J. M. Russell III, About a Possible Reference Model for Stratospheric NO₂, *Adv. Space Sci.* **7**, 919-923, 1987.

Naudet, J.-P., R. J. Thomas, D. W. Rusch, and R. T. Clancy, Distribution of Stratospheric NO₂ at 10 mbar: SME Global Morphology and Comparison to LIMS Observations, *J. Geophys. Res.* **92**, 9863-9867, 1987.

The Solar Mesosphere Explorer Satellite (SME) has measured stratospheric NO₂ since January 1982 using a visible light spectrometer. The presence of large amounts of aerosol injected into the stratosphere by El Chichon on April 4, 1982, temporarily prevented NO₂ data analysis. At the end of 1983 the volcanic aerosol content of the atmosphere, although present, had decreased sufficiently to again allow reliable NO₂ measurements. Monthly average results at 10 mbar are presented for a full year of SME observations, from October 1983 to September 1984. The observed morphology of NO₂ is discussed. Interesting features include large amounts of NO₂ in the summer hemisphere, with more in the south than in the north. A low usually exists in the tropics. A comparison to Nimbus 7 Limb Infrared Spectrometer of the Stratosphere (LIMS) observations shows similar features.

Offermann, D., H. Rippel, P. Aumedieu, W. A. Matthews, G. Mégie, E. Arijs, J. Ingels, D. Nevejans, W. Attmannspacher, J. M. Cisneros, A. W. Dawkins, D. Demuer, P. Fabian, F. Karcher, G. Froment, U. Langematz, R. Reiter, K. W. Rothe, U. Schmidt, and R. J. Thomas, Disturbance of Stratospheric Trace Gas Mixing Ratios During the MAP/GLOBUS 1983 Campaign, *Planet. Space Sci.* **35**, 1987.

Olivero, J. J., and G. E. Thomas, Climatology of Polar Mesospheric Clouds, *J. Atmos. Sci.* **43**, 1263-1274, 1986.

The ultraviolet spectrometer on board the Solar Mesosphere Explorer Satellite has measured solar radiation scattered from a diffuse and patchy layer of material near the summer polar mesopause. We call this scattering layer polar mesospheric clouds (PMC) and present here a first climatology of this phenomenon covering three years (six summer seasons). We address these general questions: How bright are PMC and how frequently do they occur in space and time? Are there year-to-year or hemisphere-to-hemisphere differences in PMC seasons? We find that the brightest PMC are found right where they occur most frequently — above 70°-75° in latitude and in a season of 60 to 80 days duration centered about the peak which occurs about 20 days after the summer solstice. This holds true for both hemispheres. We find variability on time scales from day-to-day to year-to-year; averaging over large time and space scales does, however, reveal a basic underlying symmetry. A major finding is that for three years (six seasons) considered, the Northern Hemisphere clouds are inherently brighter than the Southern Hemisphere ones.

Olivero, J. J., and G. E. Thomas, Clouds of the Polar Middle Atmosphere, *Physica Scripta* **T18**, 276-280, 1987.

Clouds have been observed at great heights in the polar regions for a century or more. Recently this series of ground-based observations has been greatly extended by limb viewing satellite systems. A major result has been the discoveries of more pronounced, more pervasive cloud phenomena extending all the way across the poles themselves. This review focuses on the results of more than three years of observations and analysis of polar mesospheric (or noctilucent) clouds by the Solar Mesosphere Explorer satellite and team. We present an undated climatology of cloud radiances and occurrence frequencies using a conservative background removal process. We also review a quite recent study of cloud heights and show how relatively little variation occurs on all time scales investigated, except perhaps for differences between the hemispheres themselves.

Petzoldt, K., R. Lenschow, A. Hauchecorne, G. A. Kokin, W. Meyer, A. O'Neill, F. Schmidlin, and R. J. Thomas, Large Scale Structure of the Stratosphere and the Lower Mesosphere (20 to 60 km) Over the Northern Hemisphere During the MAP/WINE Campaign, *J. Atmos. Terr. Phys.* **49**, 621-637, 1987.

Rosenlof, K. H., and R. J. Thomas, Five-Day Mesospheric Waves Observed in SME Ozone, *J. Geophys. Res.*, **94**, in press, 1989.

Rottman, G. J., 27-day Variations Observed in Solar Ultraviolet (120-300 nm) Irradiance, *Planet. Space Sci.* **31**, 1001-1007, 1983.

A Fourier transform analysis of 256 days of SME solar irradiance data (115-303 nm) provides an estimate of the root mean square 27-day solar variation. The magnitude of this 27-day variation exceeds $\pm 10\%$ at 120 nm and decreases with

increasing wavelength to less than 1% above 260 nm. Qualitative aspects of the analysis include a striking decrease in the per cent variation across the aluminium absorption edge near 208 nm.

Rottman, G. J., Solar Ultraviolet Irradiance 1982 and 1983 in *Atmospheric Ozone* (ed. C. S. Zerefos), D. Reidel Pub. Co., 1985.

The Solar Mesosphere Explorer (SME) has been in operation since October 6th 1981. In addition to making measurements of ozone and other trace constituents of the earth's atmosphere the observatory includes a small spectrometer to make daily measurements of the solar ultraviolet irradiance in the spectral range 115 to 305 nm. The solar spectra are obtained with 0.75 nm spectral resolution. Examination of the data show a strong signature of the 27-day solar rotation displaying a time varying modulation of incoming solar radiation exceeding $\pm 15\%$ near Lyman alpha, decreasing to a few percent at 200 nm, and less than 1 percent near 300 nm. Long term trends in the data, due both to changes in the instrument and to true long term solar variations, are removed in order to obtain quantitative measure of the intermediate term variations with time periods of a few days to weeks.

Rottman, G. J., Results from Space Measurements of Solar UV and EUV Flux, in *Solar Radiative Output Variation* (P. Foukal, ed), Cambridge Press, 1988

The last major review of observations of solar irradiance in the entire spectral range of 10 to 300 nm was a compilation of papers in *The Solar Output and Its Variation* (White, Colorado Assoc. Press, 1977). During the past eleven years a large amount of effort has been devoted to improved observations, especially in the wavelength interval above Lyman alpha. Recent satellite, sounding rocket, and Shuttle observations show vastly improved absolute and relative accuracy and may significantly change the previous estimates of solar cycle variability. Unfortunately in the EUV, 10 to 120 nm, the same effort has not been forthcoming. Only a single satellite experiment, AE-E, operated for a portion of solar cycle 21 and only two sounding rocket experiments were conducted.

Rottman, G. J., Observations of Solar UV and EUV Variability, *Adv. Space Res.* **8**, (7)53-7)66, 1988.

Solar radiation at wavelengths below 300 nm is almost completely absorbed by the earth's middle and upper atmosphere. Small variations in the solar UV and EUV flux may produce concomitant atmospheric changes. During the past 11 years, major improvements in satellite observations, especially at wavelengths longward of Lyman alpha (121.6 nm), have significantly improved our understanding of short and intermediate term solar variability. Recent Solar Mesosphere Explorer (SME) and NIMBUS-7 SBUV data sets have also improved our understanding of solar cycle variability, significantly reducing previous estimates. Details of this longer period solar variability will require improved precision in the future UV

observations. At wavelengths below 120 nm only a single satellite experiment, AE-E, operated during a portion of solar cycle 21. At these short wavelengths additional measurements over large portions of the solar cycle will be required to provide a definitive estimate of EUV solar variability.

Rottman, G. J., and J. London, Solar UV Irradiance Observations and Evidence for Solar Cycle Variations, *IRS '84: Current Problems in Atmospheric Radiation*, p. 320, (ed. G. Fiocco), A. Deepak Pub. Co., 1984.

The Solar Mesosphere Explorer was launched into a polar orbit on October 6th, 1981. Four limb scanning instruments make measurements of Mesospheric Ozone and other minor atmospheric constituents, for example H₂O and NO₂. The prime objective of the SME is to study the distribution of ozone and, in particular, to study the changes in ozone due to natural effect. Since a major influence on ozone is solar ultraviolet radiation, a spectrometer was included in the observatory to make daily measurements of the incoming solar radiation. This small spectrometer covers the spectral interval 115 to 305 nm with 0.75 nm spectral resolution. The daily solar spectral have high relative accuracy and provide reliable information on intermediate term solar variations. These variations have time scales of several days and are related to the formation and disruption of active areas on the solar disk. The relatively high contrast of these active centers produces an ultraviolet signal that is strongly modulated by the 27-day rotation period of the Sun. Short term variations of the solar output are related to ;disruptive or flare type events and exhibit time scales of minutes to hours. Since the SME measurements are obtained throughout a calendar day and are combined to give a mean daily value, these short term phenomena may produce a few anomalous daily values at some wavelengths which have been ignored in the present data analyses.

Rottman, G. J., C. A. Barth, R. J. Thomas, G. H. Mount, G. M. Lawrence, D. W. Rusch, R. W. Sanders, G. E. Thomas, and J. London, Solar Spectral Irradiance, 120 to 190 nm, October 13, 1981 — January 3, 1982, *Geophys. Res. Letters* 9, 587-590, 1982.

Beginning on October 13, 1981 a two channel spectrometer aboard the Solar Mesosphere Explorer has been obtaining daily measurements of full disc solar irradiance. These observations cover the spectral interval 120 to 305 nm with ± 0.75 nm spectral resolution. The relative accuracy of the measurements from day to day over the first three solar rotations is approximately 1%. In this report we present analyses of Lyman alpha, the integrated Schumann-Runge continuum (130-175 nm), and the integrated Schumann-Runge bands (175-190 nm). All three show a clear variability related primarily to the 27-day solar rotation period. Correlations of these three values of solar irradiance to ground-based indices of solar activity, 10.7 cm flux and sunspot number, are presented.

Rusch, D. W., and R. T. Clancy, Minor Constituent in the Upper Stratosphere and Mesosphere, *Rev. Geophys.* **25**, 479-486, 1987.

This brief review of advances in our understanding of the physical processes important in the upper stratosphere and mesosphere is intended to highlight specific issues and to focus on areas in which further research is needed.

Rusch, D. W., and R. T. Clancy, A Comparison of Ozone Trends from SME and SBUV Satellite Observations and Model Calculations, *Geophys. Res. Letters* **15**, 776-779, 1988.

Trends in the ozone mixing ratio near the stratopause are presented for global observations by the Ultraviolet Spectrometer (UVS) instrument on the Solar Mesosphere Explorer (SME) and the Solar Backscatter Ultraviolet Instrument (SBUV) on NIMBUS-7. The June, September, and January data are separately analyzed for trends as a function of latitude over the 1982-1986 period. The SME UVS data indicate trends in the range $-0.5 \pm 1.3\%/yr$ in ozone for the summer hemisphere at 1.0 mbar for January, June, and for all latitudes in September. The SBUV data show decreases of 2-5%/yr for all three months. Model calculations of ozone trends at 1.0 mb, including 5%/yr Cl_x increases, measured solar flux decreases over the 1982-1986 time period, and measured temperatures, reproduce the SME trends. The solar flux and Cl_x trends contribute equally to the measured changes at 1.0 mb. The SBUV and UVS data exhibit remarkably similar seasonal and latitudinal variations in ozone trends over the five years. The detailed variations of ozone trends from both data sets are reproduced by photochemical model calculations which include latitude-dependent NMC temperature trends over the 1982-1986 period.

Rusch, D. W., and R. T. Clancy, Trends in Atmospheric Ozone: Conflicts between Models and SBUV Data, *J. Geophys. Res.* **93**, 8431-8437, 1988.

Model calculations of ozone trends in the 1982-1986 time period show that interannual stratospheric temperature variations over that period dominate over changes in minor constituents, including Cl_x , in producing trends in ozone. Estimates for upper limits to changes in solar flux over the declining part of the solar cycle and estimates for maximum increases in Cl_x , lead to similar model decreases in upper stratospheric ozone, although the calculated trends from each are less than 1%/yr. Model calculations suggest that long-term increases in Cl_x , may produce decreases in the relative amplitude of the annual variation of ozone near 1.0 mbar that are nearly twice the secular decreases in ozone. However, trends in temperature over the period 1982-1986 lead to predicted decreases in the seasonal amplitude of ozone up to 10%/yr, based upon National Meteorological Center (NMC) observations of upper stratospheric temperatures. The secular and seasonal ozone trends derived from SBUV data for the 1982-1986 time period exhibit poor agreement with model predictions. SBUV data indicate secular trends in ozone which are negative and larger, in an absolute sense, than the largest model trends by a factor of 2 or more, indicating problems with the SBUV data or the model ozone chemistry. SBUV

data also exhibit significantly smaller changes in the amplitude of the annual variation of ozone than the models which include NMC temperatures. At least part of this disagreement may be related to temperature-correlated variations in photochemistry which are not included in the model, such as changes in water vapor or other minor constituent densities. Future efforts to determine ozone trends from satellite measurements should include monitoring of ozone, temperature, and possibly water vapor in the atmospheric pressure region from 10 to 0.1 mb.

Rusch, D. W., and R. S. Eckman, Implications of the Comparison of Ozone Abundances Measured by the Solar Mesosphere Explorer to Model Calculations, *J. Geophys. Res.* **90**, 12991-12998, 1985.

Two years of ozone measurements from the Solar Mesosphere Explorer satellite are compared to the results of a model of lower mesospheric photochemistry. The measured ozone mixing ratios are larger than those predicted by the model by as much as a factor of two at pressures near 0.1 mbar and 1.3 at 1.0 mbar using currently accepted reaction rate coefficients. The model is brought into good agreement with the measurements over a wide range of latitudes and solar zenith angles only if the efficiency of the odd hydrogen catalytic cycle which destroys odd oxygen is decreased by 30-50%.

Rusch, D. W., G. H. Mount, C. A. Barth, G. J. Rottman, R. J. Thomas, G. E. Thomas, R. W. Sanders, G. M. Lawrence, and R. S. Eckman, Ozone Densities in the Lower Mesosphere Measured by a Limb-Scanning Ultraviolet Spectrometer, *Geophys. Res. Letters* **10**, 241-244, 1983.

The ozone content of the earth's atmosphere between 1 mb and 0.08 mb has been measured as a function of latitude and season by an ultraviolet spectrometer on the Solar Mesosphere Explorer spacecraft. The ozone mixing ratio is found to be highly variable in time and space during the winter of 1982 with maxima occurring in the winter hemisphere during January and February at all pressure levels. The latitude gradients near spring equinox are relatively small. A relative maximum occurs at latitudes between 15 and 30°S in January and February.

Rusch, D. W., G. H. Mount, J. M. Zawodny, C. A. Barth, G. J. Rottman, R. J. Thomas, G. E. Thomas, R. W. Sanders, and G. M. Lawrence, Temperature Measurements in the Earth's Stratosphere Using a Limb Scanning Visible Light Spectrometer, *Geophys. Res. Letters* **10**, 261-264, 1983.

The temperature of the earth's atmosphere between 40 and 50 km is inferred from measurements of Rayleigh scattered sunlight by a visible-light spectrometer on the Solar Mesosphere Explorer spacecraft. The RMS deviation of the satellite measurements from conventional rocket measurements is 5°K above 45 km and 2-3°K below 45 km. The satellite data are compared to model temperatures for March 1982.

Rusch, D. W., G. H. Mount, C. A. Barth, R. J. Thomas, and M. T. Callan, Solar Mesosphere Explorer Ultraviolet Spectrometer: Measurements of Ozone in the 1.0 to 0.1 mb Region, *J. Geophys. Res.* **89**, 11677-11687, 1984.

The ozone density of the earth's mesosphere in the 1.0-0.1 mbar (48 to 70 km) region has been measured at sunlit latitudes for the period from December 1981 until the present by an ultraviolet spectrometer on the Solar Mesosphere Explorer satellite. Results for 1982 are reported. The ozone mixing ratios are found to be highly variable in time and place, with maxima occurring in the winter hemispheres. The results show complex time variations at all pressure levels, with annual and semiannual variations apparent at most pressures and latitudes. A relative maximum occurs in July at the equator.

Rusch, D. W., M. P. McCormick, R. T. Clancy, and J. M. Zawodny, A Comparison of SME and SAGE II Ozone Densities near the Stratosopause, *J. Geophys. Res.*, in press, 1989.

Ozone measurements made by the Ultraviolet Spectrometer on the Solar Mesosphere Explorer and those from the Stratosphere Aerosol and Gas Experiment II are compared at 1.0 mbar for the time period from October, 1984, to December, 1986. A model of the diurnal variation of ozone is used to correct for the difference in local times of the two measurements. The two instruments agree to within 5% at all latitudes considered in the comparison. Further, no significant divergence is found between the data sets for the time period of overlap. The results support the accuracy and precision of each instrument and the accuracy of ozone trends derived over the 1982-1986 period from Solar Mesosphere Explorer data. 95, no. D4, 3533-3537

Russell III, J. M., S. Solomon, M. P. McCormick, A. J. Miller, J. J. Barnett, R. L. Jones, and D. W. Rusch, "Middle Atmosphere Revealed by Satellite Observations," in *Middle Atmosphere Program Handbook*, **22**, 1986.

Siskind, D. E., C. A. Barth, and R. G. Roble, The Response of Thermospheric Nitric Oxide on an Auroral Storm, 1, Low and Middle Latitudes, *J. Geophys. Res.* **94**, 16,885-16,898, 1989.

The Solar Mesosphere Explorer (SME) satellite observed thermospheric nitric oxide (NO) during the period September 17-20, 1984, using the resonance fluorescence technique. Altitude profiles from 100 to about 130 km were obtained for 1500 LT along two orbital tracks: one over the United States and one over Europe. An auroral storm occurred on September 19. A comparison of data from September 20 with data from September 18 revealed a factor of 3 increase in NO at mid-latitudes over the United States. Little NO enhancement was seen over Europe or at equatorial latitudes. A larger increase was seen for the higher altitudes (>120 km). The SME observations are compared with the calculations of a one-dimensional photochemical model of the lower thermosphere. The National Center for Atmospheric Research (NCAR) thermospheric general circulation model (TGCM) is used to calculate the response of the background neutral atmosphere to auroral forcings such as Joule and particle heating. The output of the TGCM is used as input to the photochemical model. Calculations of the mid-latitude NO

response show that temperature increases which result from Joule and compressional heating can explain the observed NO enhancements. A larger response is initially seen for altitudes greater than 120 km. After several days, downward diffusion leads to NO increases at lower altitudes. Equatorial NO shows little response because the combined effects of temperature enhancements and atomic oxygen enhancements largely cancel. The best absolute fit of the model to the data is for an $N(^2D) + O$ quenching rate of $5 \times 10^{-13} \text{ cm}^3 \text{ s}^{-1}$, although uncertainties in the neutral composition preclude an exact specification of the quenching rate. The success of the model in reproducing the observed NO altitude and latitude variations argues against the importance of horizontal transport of E region NO.

Siskind, D E., C. A. Barth, D. S. Evans, and R. G. Roble, The Response of Thermospheric Nitric Oxide on an Auroral Storm, 2, Auroral Latitudes, *J. Geophys. Res.* **94**, 16,899-16911, 1989.

An analysis of the response of lower thermospheric nitric oxide (NO) at auroral latitudes to the auroral storm of September 19, 1984, is presented. A comparison of data from the Solar Mesosphere Explorer (SME) taken one day after the storm (September 20) with data obtained one day before the storm (September 18) revealed a factor of 3 increase in NO. In order to model this response, particle data from the NOAA 6 and 7 satellites are used to assess the time history of the auroral energy input along each SME orbital track. The deduced fluxes and characteristic energies are used as input to a time dependent one-dimensional photochemical model. In addition, the NCAR thermospheric general circulation model (TGCM) is used to calculate the response of the background neutral atmosphere to auroral forcings such as Joule and particle heating. It was found that particle precipitation accounted for 90% of the increase in the peak NO density, although Joule heating was more important at the higher altitudes (>140 km). The results of the model calculations predict an NO enhancement; however, the amplitude of the response as well as the absolute magnitude of the calculated NO density greatly exceed the observations. Two possibilities are proposed to explain this discrepancy. The first is that the yield of $N(^2D)$ from electron impact on N_2 may only be 50%, rather than the 60-75% previously assumed. The second is that vertical winds of the order of $1-5 \text{ m s}^{-1}$ may be generated in an E region auroral arc. It is shown that such winds could be important in damping out the NO response to increased particle precipitation.

Solomon, S., G. C. Reid, D. W. Rusch, and R. J. Thomas, Mesospheric Ozone Depletion during the Solar Proton Event of July 13, 1982. Part II. Comparison between Theory and Measurements, *Geophys. Res. Letters* **10**, 257-260, 1983.

The solar proton event of July 13, 1982 was the largest to date in the current solar cycle. Proton fluxes observed by the NOAA-6 satellite have been used to calculate ionization rates during the event, which have been found to be almost as large as

those of the August 1972 event near 70 km, but much smaller at lower altitudes. This ionization leads to the production of odd hydrogen radicals ($H+OH+HO_2$) which catalytically destroy odd oxygen in the mesosphere and stratosphere. A one-dimensional time-dependent model has been used to calculate the percentage change in ozone resulting from this event. The calculated ozone depletion is compared to that observed by the Solar Mesosphere Explorer (SME) satellite.

Solomon, S., D. W. Rusch, R. J. Thomas, and R. S. Eckman, Comparison of Mesospheric Ozone Abundances Measured by the Solar Mesosphere Explorer and Model Calculations, *Geophys. Res. Letters* **10**, 249-252, 1983.

Ozone observations in the mesosphere obtained by the near infrared and ultraviolet spectrometers onboard the Solar Mesosphere Explorer (SME) satellite are compared to two-dimensional model calculations for the month of January. In general, the model calculated abundances are somewhat smaller than those measured, but exhibit similar trends with respect to altitude and latitude. The possible causes of discrepancies include the mesospheric H_2O content and photochemical reaction rates, particularly the rate of O_2 photolysis.

Solomon, S., G. H. Mount, and J. M. Zawodny, Measurements of Stratospheric NO_2 from the Solar Mesosphere Explorer Satellite. 2. General Morphology of Observed NO_2 and derived N_2O_5 , *J. Geophys. Res.* **89**, 7317-7321, 1984.

Observations of NO_2 densities from 28 to 40 km as measured by the Solar Mesosphere Explorer (SME) satellite are compared to model calculations for the month of January. Low densities are obtained in the tropics and in high latitude winter, with much larger values in the summer middle and high latitude regions in both the observations and the model. The reasons for areas of agreement and disagreement between the model and the observations are explored. The observed NO_2 distribution is also used to infer the N_2O_5 distribution based on presently accepted chemistry and suggests that very large amounts of N_2O_5 are present in high latitude winter.

Thomas, G. E., Solar Mesosphere Explorer Measurements of Polar Mesospheric Clouds (Noctilucent Clouds), *J. Atmos. & Terr. Phys.*, **46**, 819-824, 1984.

The Ultraviolet Spectrometer experiment on board the Solar Mesosphere Explorer satellite has measured scattering of sunlight from the polar mesospheric cloud layer in the 0.2-0.3 μm spectral range. The layer is manifested in the limb-scanning measurements as large increases in radiances at heights near 80 km, at latitudes 60-90°N and 60-90°S and during the summer season. They are similar to noctilucent clouds with respect to their height, geometrical thickness (less than 3.5 km) and morphology. However, as shown by Donahue *et al.* (*J. Atmos. Sci.* **29** 1205, 1972), they are much brighter and occupy the entire polar 'cap' region, a region largely inaccessible to ground-based observation. The measurements have revealed a forward-scattering asymmetry, which increases with layer brightness. This

behaviour shows that the brighter clouds are composed of particles with radii according to Mie theory up to $0.07 \mu\text{m}$, at least for the limited set of data studied so far. The variation of layer brightness with asymmetry factor is consistent with the layer being limited by the available water content of the atmosphere. The calculated water content of the particles, assuming them to consist of pure water ice, is about $100 \mu\text{g m}^{-2}$, provided the particle distribution is monodisperse. This corresponds to the total amount of atmospheric water vapor residing in a vertical column above 80 km for a water vapor mixing ratio of 1.2 ppmv. This is consistent with the amount of water vapor believed to exist at mesopause heights (a few ppmv). The large amounts of ice reported by Donahue *et al.* (1972) are too large by a factor of 10. Their corrected values are consistent with the present analysis. A brief description is given concerning additional research topics which are being pursued using the extensive SME data base, which now consists of five complete summer seasons from 1981 to the present.

Thomas, G. E., Trace Constituents in the Mesosphere, *Physica Scripta* **T18**, 281-288, 1987.

Recent observations of selected trace constituents in the mesosphere are reviewed. The review is divided into discussions of some long-lived constituents (CO, NO and H₂O), and short-lived constituents (OH and O₃) that are important for understanding the transport in the lower thermosphere and in the mesosphere. CO and NO are produced in the lower thermosphere and lost in the lower mesosphere and stratosphere. There is now observational evidence that downward transport into the winter polar region, and subsequent "spillage" into the winter mid-latitude regions are important for CO and NO. In comparison with CO and NO the distribution of H₂O is "upside down" in the sense that it is generated in the lower atmosphere and flows upward to its sink. The same transport mechanism may operate for H₂O, but in the opposite sense of moving dry air downward in winter, and moist air upward in summer. The short-lived OH radical is important for understanding the HO_x—O_x mechanism in the middle atmosphere. Unfortunately, there is an almost complete lack of data for its distribution above 50 km. Ozone and water vapor are out-of-phase in their seasonal behavior in the upper mesosphere; the variations in both species provide important clues for understanding the causes of eddy mixing in the mesosphere. The seasonal climatology of mesospheric ozone is now well documented as a result of five years of SME satellite observations.

Thomas, G. E., and C. P. McKay, On the Mean Particle Size and Water Content of Polar Mesospheric Clouds, *Planet. Space Sci.*, **33**, 1209-1224, 1985.

The ultraviolet spectrometer on board the Solar Mesosphere Explorer (SME) satellite has been measuring the scattering of ultraviolet sunlight from optically thin cloud layers in the upper boundary of the mesosphere (85 km) since the launch of the spacecraft in October 1981. These layers are present only at high latitudes during the summer season. During Summer 1983 an observing sequence was undertaken to measure the cloud radiance at two different scattering angles — one in the

forward hemisphere at 50° , the other in the backward hemisphere at 130° . The data show a pronounced tendency for the brighter clouds to exhibit greater forward-scattering behavior, indicating that particle size may be the most important factor in determining the cloud brightness. We conclude that if the particles are monodisperse water ice aggregates, their radii do not exceed 70 nm. Estimates are provided for the water content and column particle number of the clouds, depending upon the unknown shape of the particle size distribution. Characterizing the distribution by two parameters, the spherical equivalent particle radius and the width of the distribution, the bulk cloud properties are shown to be dependent upon the limb radiance and width parameter. For narrow widths the water ice content is less than that expected for the water vapor content at mesopause heights of a few parts per million. This confirms our earlier analysis using a smaller data set and assuming the cloud particles are monodisperse. However if the size dispersion is broad, the implied water ice exceeds the static atmospheric water supply. The calculated column number for the brightest clouds exceeds our estimates for the total supply of condensation nuclei. The alternative is that the brighter clouds are limited to a fairly narrow range of particle sizes from 40 to 60 nm. This conclusion is supported by theoretical time dependent calculations by Turco *et al.* (*Planet. Space Sci.* **30**, 1147, 1982).

Thomas, G. E., and J. J. Olivero, The Heights of Polar Mesospheric Clouds, *Geophys. Res. Letters* **13**, 1403-1406, 1986.

Data from the Solar Mesosphere Explorer satellite of polar mesospheric clouds have been used in determining the variation of cloud height from 1981 to 1985. Applying various corrections to the apparent tangent heights measured at the atmospheric limb, we find no significant variation of height within an individual cloud season (-10 days to +50 days relative to summer solstice) either with latitude or local time. Furthermore, no significant year-to-year variation is found over the 4-year time span. We find significantly higher (2 km) PMC cloud heights in the north than in the south. The average value of 85.0 ± 1.5 km for the northern PMC is in good agreement with measurements from the OGO-6 satellite, rocket-borne photometers and ground-based triangulation of noctilucent clouds.

Thomas, G. E., and J. J. Olivero, Climatology of Polar Mesospheric Clouds: Part II, *J. of Geophys. Res.*, in press, 1989.

Thomas, G. E., C. A. Barth, E. R. Hansen, C. W. Hord, G. M. Lawrence, G. H. Mount, G. J. Rottman, D. W. Rusch, A. I. Stewart, R. J. Thomas, J. London, P.L. Bailey, P. J. Crutzen, R. E. Dickinson, J. C. Gille, S. C. Liu, J. F. Noxon, and C. B. Farmer, Scientific Objectives of the Solar Mesosphere Explorer Mission, *PAGEOPH* **118**, 591-615, 1980.

The 1981-82 Solar Mesosphere Explorer (SME) mission is described. The SME experiment will provide a comprehensive study of mesospheric ozone and the processes which form and destroy it. Five instruments will be carried on the spinning

spacecraft to measure the ozone density and its altitude distribution from 30 to 80 km, monitor the incoming solar ultraviolet radiation, and measure other atmospheric constituents which affect ozone. The polar-orbiting spacecraft will be placed into a 3 PM—3 AM Sun-synchronous orbit. The atmospheric measurements will scan the Earth's limb and measure: (1) the mesospheric and stratospheric ozone density distribution by inversion of Rayleigh-scattered ultraviolet limb radiance, and the thermal emission from ozone at 9.6 μm ; (2) the water vapor density distribution by inversion of thermal emission at 6.3 μm ; (3) the ozone photolysis rate by inversion of the $\text{O}_2(^1\Delta_g)$ 1.27 μm limb radiance; (4) the temperature profile by a combination of narrow-band and wide-band measurements of the 15 μm thermal emission by CO_2 ; and (5) the NO_2 density distribution by inversion of Rayleigh-scattered limb radiance at 0.439 μm . The solar ultraviolet monitor will measure both the 0.2-0.31 μm spectral region and the Lyman-alpha (0.1216 μm) contribution to the solar irradiance. This combination of measurements will provide a rigorous test of the photochemical equilibrium theory of the mesospheric oxygen-hydrogen system, will determine what changes occur in the ozone distribution as a result of changes in the incoming solar radiation, and will detect changes that may occur as a result of meteorological disturbances.

Thomas, G. E., B. M. Jakosky, R. A. West, and R. W. Sanders, Satellite Limb-Scanning Thermal Infrared Observations of the El Chichon Stratospheric Aerosol: First Results, *Geophys. Res. Letters* **10**, 997-1000, 1983.

The Infrared Radiometer experiment on the Solar Mesosphere Explorer satellite has been continuously measuring the 6.8- μm thermal emission from the stratospheric aerosol from the El Chichon volcano since the time of eruption in early April 1982. Inversion results from the zonally-averaged infrared extinction coefficient in height, latitude, and time show that the aerosol increased in mass to a maximum of 8 Tg (8×10^{12} gm) about 15 weeks after the April 4 eruption. It descended in height with an average speed consistent with the gravitational settling time of particles with a diameter of about 1.4 μm .

Thomas, G. E., D. W. Rusch, R. J. Thomas, and R. T. Clancy, "Long-Term Changes in the Stratosphere Due to the 1982 Eruption of El Chichon," in *The Middle Atmosphere Program Handbook*, in press, 1989.

Thomas, R. J., Seasonal Ozone Variations in the Upper Mesosphere, *J. Geophys. Res.* **95**, in press, 1990.

The global daytime ozone was measured by the Solar Mesosphere Explorer satellite (SME) for five years. The measurements extend through the mesosphere, covering from 50 km to over 90 km. The ozone in the upper mesosphere varies annually by up to a factor of 3. The observed seasonal variations may be summarized in several different ways. From year to year there is a great deal of repeatability of these variations. This repeatability occurs in most of the upper mesosphere outside the

tropics. Near 0.01 mbar (80 km) the mid- and high latitude mixing ratio peaks each year in mid April.

A secondary maximum in the altitude profile of ozone density usually occurs near 85 km. Changes in this structure are directly related to the April maximum and other seasonal changes seen at 0.01 mbar. The changing seasonal structure produces a 'bump' at the ozone mixing ratio minimum that is largest just after spring equinox. This perturbation to the mixing ratio profile seems to move upward during the first half of the year.

The seasonal changes of ozone were analyzed in terms of annual and semiannual structure. The variations generally have both an annual and semiannual component depending on altitude and latitude. The phases of the variations change quickly with both altitude and latitude. The semiannual component peaks in April, over most of the upper mesosphere .

Thomas, R. J., Atomic Hydrogen and Atomic Oxygen Density in the Mesopause Region: Global and Seasonal Variations Deduced from SME Near-infrared Emissions, *J. Geophys. Res.* **95**, in press, 1990.

Atomic oxygen and atomic hydrogen have been inferred from the hydroxyl airglow measurements on Solar Mesosphere Explorer spacecraft (SME) between 0.01 and 0.0013 mbar (80-93 km). These constitute the first measurements of the seasonal and latitudinal variations of these atomic species, in the mesopause region. At night atomic oxygen is directly proportional to the Meinel band emission of OH. During the day the emission is proportional to the product of ozone and hydrogen. Since daytime ozone is inferred from the $O_2(^1\Delta_g)$ emission, daytime hydrogen can be inferred. Daytime atomic oxygen is then inferred from the measured hydrogen and ozone. At levels where both methods are valid (at 0.0032-0.0013 mbar or 88-93 km) the day and night atomic oxygen display the same seasonal behavior. Very large annual and semiannual changes are found in the atomic hydrogen density between 80 and 93 km. At 40° N the summer-to-spring ratio of atomic hydrogen exceeds a factor of 4 at 0.01 mbar (80 km). Between 80 and 90 km the odd oxygen family is found to be almost entirely atomic oxygen. Its behavior is characterized by annual variations at 40° north and south, and semiannual changes at the equator; in both cases the changes are a doubling from minimum to maximum. At least part of the mid-latitude semiannual variation in ozone is found to be due to the product of two annually varying functions. The atomic oxygen is annual and maximizes in the winter while the ozone-oxygen partitioning, controlled mostly by temperature, maximizes in the summer due to temperature changes.

Thomas R. J., C. A. Barth, G. J. Rottman, D. W. Rusch, G. H. Mount, G. M. Lawrence, R. W. Sanders, G. E. Thomas, and L. E. Clemens, Mesospheric Ozone Depletion during the Solar Proton Event of July 13, 1982. Part I. Measurement, *Geophys. Res. Letters* **10**, 253-255, 1983.

The near infrared spectrometer and the ultraviolet spectrometer on the Solar Mesosphere Explorer (SME) observed the ozone density as a function of latitude and altitude during the solar proton event of July 18, 1981. Airglow at $1.27 \mu\text{m}$ was observed at the earth's limb. The altitude profiles of the emission were inverted providing ozone densities. The ozone densities observed showed a clear decrease during the event. The maximum depletion seen was 70%. The decrease was observed in the northern high latitudes at mesospheric altitudes. The decrease was very short lived, lasting less than a day.

Thomas R. J., C. A. Barth, G. J. Rottman, D. W. Rusch, G. H. Mount, G. M. Lawrence, R. W. Sanders, G. E. Thomas, and L. E. Clemens, Ozone Density Distribution in the Mesosphere (50-90 km) Measured by the SME Limb-Scanning Near-Infrared Spectrometer, *Geophys. Res. Letters* **10**, 245-248, 1983.

The ozone densities between 50 and 90 km are deduced from $1.27 \mu\text{m}$ airglow measured on the Solar Mesosphere Explorer satellite. The derived densities agree well with those made simultaneously from SME by the ultraviolet spectrometer. The data set extends from pole to pole at about 3 pm, for most sunlit latitudes. At low altitudes, in the mesosphere, there are larger variations in ozone density in the winter latitudes than in the summer. Above the mesopause the day-to-day variation in ozone density is a factor of 2 at most latitudes and times.

Thomas, R. J., C. A. Barth, D. W. Rusch, and R. W. Sanders, Solar Mesosphere Explorer Near-Infrared Spectrometer: Measurements of $1.2 \mu\text{m}$ Radiances and the Inference of Mesospheric Ozone, *J. Geophys. Res.* **89**, 9569-9580, 1984.

Ozone in the mesosphere is determined from observations made by the near-infrared spectrometer experiment on the Solar Mesosphere Explorer satellite (SME) between 50 and 90 km over most latitudes at 3:00 PM local time. The spectrometer measures emission from $\text{O}_2(^1\Delta_g)$ at $1.27 \mu\text{m}$ that is primarily due to the photodissociation of ozone. The instrument consists of a parabolic telescope that limits the field of view to less than 0.1° , an Ebert-Fastie spectrometer, and a passively cooled lead sulfide detector system. The limb radiances, measured as the spacecraft spins, are inverted, producing volume emission rate profiles from which ozone densities are inferred. The vertical resolution is better than 3.5 km. The calculation of ozone accounts for quenching and atmospheric transmission of both solar radiation and $1.27 \mu\text{m}$ radiation. We have established the existence of a secondary maximum of ozone density near 80 km. An error analysis shows that the effects of random errors in the data and in the analysis on the final ozone profile are less than 10% between 50 and 82 km.

Thomas, R. J., C. A. Barth, and S. Solomon, Seasonal Variations of Ozone in the Upper Mesosphere and Gravity Waves, *Geophys. Res. Letters* **11**, 673-676, 1984.

Ozone densities in the upper mesosphere have been measured as a function of time and latitude over a two-year period (1982-1983) by the Solar Mesosphere Explorer (SME) satellite. Large seasonal changes occur, particularly near 80 km where ozone densities at the equinoxes are about 2-3 times those observed at the solstices. The structure of the ozone secondary maximum also fluctuates substantially during the year, with extremes near equinox and solstice. Further, the variations are highly repeatable from year to year and from hemisphere to hemisphere. We propose that the seasonal variability in ozone is produced by the variation of gravity-wave-induced transport in the mesosphere which, in turn, results from the seasonal modulation of the propagation and breaking of small-scale gravity waves.

Thomas, R. J., K. H. Rosenlof, R. T. Clancy, and J. M. Zawodny, Stratospheric NO₂ over Antarctica as Measured by the Solar Mesosphere Explorer during Austral Spring, 1986, *J. Geophys. Res.* **93**, 12,561-12,568, 1988.

The visible spectrometer on the Solar Mesosphere Explorer measured stratospheric NO₂ in the 24- to 40-km region. In September and October 1986 the spatial density of the measurements was increased over Antarctica in order to examine the NO₂ change during the period of the "ozone hole." These measurements are compared with the 1985 austral spring observations, with northern polar spring measurements for both years, and with model results. A polar low in NO₂ is seen between 10 and 24 mbar. The geographic extent of the low decreases as hours of sunlight increase, in marked contrast to the behavior of the total ozone column during the same period. The latitude and time dependence of the NO₂ is similar for both years, and during the same season, in the northern hemisphere. Comparison of measurements and model imply that much of the odd nitrogen is converted to HNO₃ during the polar night. Observed vertical profiles and comparison to measurements from the ground indicate that the bulk of the NO₂ column lies above 24 km. The observed behavior does not appear to be anomalous when compared to simple model calculations, indicating no obvious connection between the polar stratospheric NO_x above 24 km and the development of the ozone hole below 24 km.

Tobiska, W. K., R. D. Culp, and C. A. Barth, Predicted Solar Cycle 22 10.7 cm Flux and Satellite Orbit Decay, *J. Astron. Sci.* **35** (4), 419-433, 1987.

This study develops an empirical model of the 10.7 cm solar flux ($F_{10.7}$) through solar cycle twenty-two as it relates to the problem of a low-Earth orbiting satellite and its orbit decay. A comparison between the predicted orbit decay using the model and the first thirty-seven months of actual altitude of the Solar Mesosphere Explorer (SME) satellite is conducted. The predicted orbit semimajor axis is solved as a function of atmospheric density using a modified Jacchia 1971 atmospheric model (J71). J71 densities vary based on the empirically modeled $F_{10.7}$ of solar cycle twenty-two. The derivation of the orbit radius, r , related to atmospheric mass

density, ρ , is outlined, as are the simplifications made in this study for atmospheric density modeling. The $F_{10.7}$ model for solar cycle twenty-two is then detailed with a comparison of one other model. Finally, the results of the predicted SME orbit decay are evaluated against the actual orbit decay.

Zawodny, J. M., Short-Term Variability of Nitrogen Dioxide in the Winter Stratosphere, *J. Geophys. Res.* **91**, 5439-5450, 1986.

Zawodny, J. M., and D. W. Rusch, Seasonal Behavior of NO_2 in the Winter Stratosphere: Infrared NO_x , *J. Geophys. Res.* **91**, 5451-5454, 1986.

The long-term seasonal trend in NO_2 density near 10 mbar, as measured by the Solar Mesosphere Explorer (SME), is compared to photochemical model predictions of the trend throughout the first 3 months of 1982. The general increase in the observed NO_2 is found to be caused by a shift in the partitioning of odd nitrogen in favor of NO_2 . The model is also used to infer the odd nitrogen (NO_x : $\text{NO} + \text{NO}_2 + \text{NO}_3 + 2 \times \text{N}_2\text{O}_5$) mixing ratio, which is seen to decrease rapidly throughout the period. This rapid decrease is found to be caused in part by improper modeling of the photodissociation rate of NO_2 . Indirect measurements of the photodissociation rate of NO_2 from SME show the rate to change with solar zenith angle at angles greater than 70° . Only when this dependence is taken into account do the variations in the odd nitrogen mixing ratio become consistent with theory.

Rec Jan 89
81-100A-01F,01G

LABORATORY FOR ATMOSPHERIC AND SPACE PHYSICS

SOLAR MESOSPHERE EXPLORER

ORBIT TRACK NITRIC OXIDE DATA FOR THE

NATIONAL SPACE SCIENCE DATA CENTER

1982-1986 DATA

The SOLAR MESOSPHERE EXPLORER (SME) orbit track NO data was derived from the ultra-violet spectrometer radiance measurements. A description of the mission, the instruments, the scientific objectives, and the initial results is contained in a series of articles in the April 1983 issue of Geophysical Research Letters (10:237-267).

The nitric oxide densities are given on altitude surfaces from 100 to 160 km. There are 2 sets of NO densities, one on a grid of magnetic latitudes, and the other on geographic latitudes. Each set also includes longitudes and solar zenith angles.

Dr. C.A. Barth is the principal investigator for the SME experiment. Co-investigators Drs. R.J. Thomas, D.W. Rusch, G.E. Thomas, and G.J. Rottman are resident at the Laboratory for Atmospheric and Space Physics at the University of Colorado, Boulder, Colorado, 80309.

This set of data consists of 6 tapes. The tapes labeled NOMX, where X goes from 1 to 3, contain NO density data on a magnetic latitude grid. The tapes labeled NOGX contain NO density data on a geographic latitude grid. NOM1 and NOG1 both contain 3 files, covering the time period 1982006 to 1983181. NOM2 and NOG2 have 4 files each, covering the time period 1983182 to 1985181. NOM3 and NOG3 have 3 files each, covering the time period 1985182 to 1986245.

The blocksize on these tapes is 456. The logical record length is 456. A description of the tape characteristics is given in the appendix.

These data, derived from the UV spectrometer on SME, are orbit track NO densities. They cover the years 1982 through 1986. The data given is number density, (cm⁻³).

SME NO DENSITY DATA, 1981 - 1986

TAPE	FILE	NO.BLOCKS	CONTENTS	FIRST ORBIT
MAGNETIC LATITUDE GRIDDED NO DENSITY TAPES				
NOM_1	NOM82A.DAT	10718	1/ 6/82 - 6/30/82	1387
	NOM82B.DAT	9269	7/ 1/82 - 12/31/82	4046
	NOM83A.DAT	7774	1/ 1/83 - 6/30/83	6834
NOM_2	NOM83B.DAT	7843	7/ 1/83 - 12/31/83	9576
	NOM84A.DAT	7889	1/ 1/84 - 6/29/84	12365
	NOM84B.DAT	5267	6/30/84 - 12/31/84	15110
	NOM85A.DAT	3703	1/ 1/85 - 6/30/85	17915
NOM_3	NOM85B.DAT	3979	7/ 1/85 - 12/31/85	20659
	NOM86A.DAT	4048	1/ 1/86 - 6/30/86	23451
	NOM86B.DAT	2323	7/ 1/86 - 12/11/86	26211
GEOGRAPHIC LATITUDE GRIDDED NO DENSITY TAPES				
NOG_1	NOG82A.DAT	10718	1/ 6/82 - 6/30/82	1387
	NOG82B.DAT	9269	7/ 1/82 - 12/31/82	4046
	NOG83A.DAT	7774	1/ 1/83 - 6/30/83	6834
NOG_2	NOG83B.DAT	7843	7/ 1/83 - 12/31/83	9576
	NOG84A.DAT	7889	1/ 1/84 - 6/29/84	12365
	NOG84B.DAT	5267	6/30/84 - 12/31/84	15110
	NOG85A.DAT	3703	1/ 1/85 - 6/30/85	17915
NOG_3	NOG85B.DAT	3979	7/ 1/85 - 12/31/85	20659
	NOG86A.DAT	4048	1/ 1/86 - 6/30/86	23451
	NOG86B.DAT	2323	7/ 1/86 - 12/11/86	26211

The following format describes the file NOM82A.DAT. The format is applicable for all the files in this dataset consisting of SME NO density data on magnetic latitudes and

those on geographic latitudes. Missing data is indicated by -1.0. The altitude ranges from 100 to 160 km. The altitude grid increment is 3 1/3 km. There are 19 altitude levels and 37 latitudes. Latitudes range from 90 S to 90 N in 5 degree increments.

First orbit=1387, date=1982006 (Jan. 6, 1982)

Record	Format	Description
1	2(1X,I5),1X,F7.2	Orbit, Date(YYYYY), Equatorial Long.
2	1X,F6.2,37E12.5	Altitude(km), 37 NO density values for latitudes from -90 to 90 in 5 degree increments. Alt=160.00 km.
3	1X,F6.2,37E12.5	Altitude(km), 37 NO density values for latitudes from -90 to 90 in 5 degree increments. Alt=156.67 km.
4	1X,F6.2,37E12.5	Altitude(km), 37 NO density values for latitudes from -90 to 90 in 5 degree increments. Alt=153.33 km.
.		
.		
.		
19	1X,F6.2,37E12.5	As in previous data records for Alt=100.00 km.
20	7X,37(F12.3)	37 latitude values.
21	7X,37(F12.3)	37 longitude values.
22	7X,37(F12.3)	37 solar zenith angle values.

Second orbit=1388, date=1982006 (Jan. 6, 1982)

23	2(1X,I5),1X,F7.2	Orbit, Date(YYYYY), Equatorial Long.
24	1X,F6.2,37E12.5	Altitude(km), 37 NO density values for latitudes from -90 to 90 in 5 degree increments. Alt=160.00 km.
25	1X,F6.2,37E12.5	Altitude(km), 37 NO density values for latitudes from -90 to 90 in 5 degree increments. Alt=156.67 km.
26	1X,F6.2,37E12.5	Altitude(km), 37 NO density values for latitudes from -90 to 90 in 5 degree increments. Alt=153.33 km.
.		
.		
.		
41	1X,F6.2,37E12.5	As in previous data records for Alt=100.00 km.
42	7X,37(F12.3)	37 latitude values.
43	7X,37(F12.3)	37 longitude values.
44	7X,37(F12.3)	37 solar zenith angle values.

etc., for subsequent orbits for which there is SME NO data.

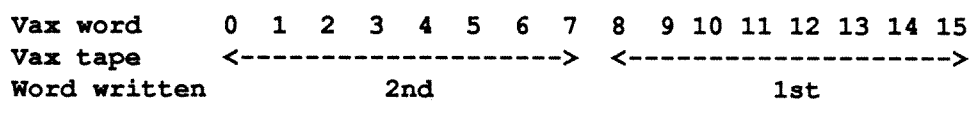
-01F,G
P.4

LABORATORY FOR ATMOSPHERIC AND SPACE PHYSICS
SOLAR MESOSPHERE EXPLORER
ORBIT TRACK NITRIC OXIDE DATA FOR THE
NATIONAL SPACE SCIENCE DATA CENTER

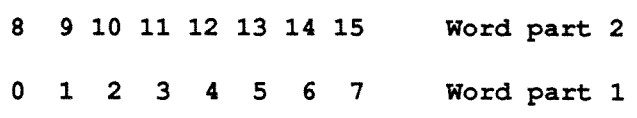
APPENDIX

The enclosed tapes have the following characteristics:

1. 9-track, 1600 bpi. Written on a Digital TU77 drive.
2. ANSI STANDARD tape headers and End-of-File (EOF) structure (7-bit ASCII characters) as per VAX 11/780 system software. After the Volume Header record (80 bytes), there are four File Header records (80 bytes each), one EOF, the data records (456 bytes each), one EOF, four File Trailer records (80 bytes each), and one EOF for each of the data files on this tape.
3. These tapes were made using the VMS COPY command after first initializing each tape.
4. Physical data blocks are 456 bytes long; each block contains one logical record.
5. The VAX writes bytes onto a 9-track tape in the following order:



The resulting tape (up is the tape beginning direction)



6. An annotated dump is attached which shows the contents of the first ten physical blocks for the first tape. The left side of the dump shows the hexadecimal word (read from right to left) and the right side of the dump shows the ASCII equivalent word contents (read from left to right). The last column on the right is the hexadecimal 4-byte word number for the rightmost four bytes in the hexadecimal dump section.

01F,G
P.5

DUMP OF FIRST 10 blocks
tape NDM-1

Dump of device MTA2: on 20-JAN-1989 20:43:02.40

Block number 1 (00000001), 30 (0050) bytes

20202020	20202020	20202020	20202020	20202020	20202031	5F404F4F	314C4F56	VOL1NDM_1		000000
20202020	20202020	20202020	20202020	20202020	20202020	20202020	20202020			000020
				33202020	20202020	20202020	20202020		3.....	000040

Block number 2 (00000002), 30 (0050) bytes

30313030	3020315F	4D4F4E20	20202020	20205441	442F4132	39404F4F	31524448	HDR1NDM82A.DAT	NDM_1 00010	000000	
46434544	30303030	30302030	32303938	20303230	39382030	30312030	30313030	001000100	89020 89020	000000DECF	000020
				20202020	20202020	20204131	31454C49	ILE11A	000040	

Block number 3 (00000003), 80 (0050) bytes

20202020	20202020	20202020	20202020	20313534	30303635	34303046	32524448	HDR2F0045600451		000000
20202020	20202020	20202020	30302020	20202020	20202020	20202020	20202020		00	000020
				20202020	20202020	20202020	20202020		000040

Block number 4 (00000004), 80 (0050) bytes

30303030	30303030	31303030	30303030	30303030	31303230	33433130	33524448	HDR301C3020100000000000100000000		000000
30303030	30303030	30303030	30303030	30303030	33433130	30303030	30303030	0000000001C300000000000000000000		000020
				20202020	20202020	20202020	30303030	0000	000040

Block number 5 (00000005), 80 (0050) bytes

20202020	20202020	20202020	20202020	20202020	20202020	20202020	20202020	34524448	HDR4	000000	
20202020	20202020	20202020	20202020	20202020	20202020	20202020	20202020	20202020		000020	
				20202020	20202020	20202030	30202020		00	000040

*** End of file ***
Dump of device MTA2: on 20-JAN-1989 20:43:02.40

Block number 6 (00000006), 456 (01C8) bytes

20202020	20202020	20202020	35322F39	38202020	36303032	38203739	33312020	1387 82006	89.25	000000
20202020	20202020	20202020	20202020	20202020	20202020	20202020	20202020			000020
20202020	20202020	20202020	20202020	20202020	20202020	20202020	20202020			000040
20202020	20202020	20202020	20202020	20202020	20202020	20202020	20202020			000060
20202020	20202020	20202020	20202020	20202020	20202020	20202020	20202020			000080
20202020	20202020	20202020	20202020	20202020	20202020	20202020	20202020			0000A0
20202020	20202020	20202020	20202020	20202020	20202020	20202020	20202020			0000C0
20202020	20202020	20202020	20202020	20202020	20202020	20202020	20202020			0000E0
20202020	20202020	20202020	20202020	20202020	20202020	20202020	20202020			000100
20202020	20202020	20202020	20202020	20202020	20202020	20202020	20202020			000120
20202020	20202020	20202020	20202020	20202020	20202020	20202020	20202020			000140
20202020	20202020	20202020	20202020	20202020	20202020	20202020	20202020			000160
20202020	20202020	20202020	20202020	20202020	20202020	20202020	20202020			000180
20202020	20202020	20202020	20202020	20202020	20202020	20202020	20202020			0001A0
					5E5E5E5E	5E202020			0001C0

Block number 7 (00000007), 456 (01C8) bytes

20363028 45323431 31352E36 20363028 45387235 36372E35 2030302E 30363120 160.00 5.78528E+06 5.51142E+06 000000
45323836 33332E36 20363028 45353739 36312E36 20363028 45353833 38372E35 5.78385E+06 6.16975E+06 6.38682E 000020
35362E36 20363028 45363431 36352E35 20363028 45323238 35332E36 20363028 +06 6.35622E+06 5.56146E+06 6.65 000040
20363028 45373437 37362E36 20363028 45343430 31382E35 20363028 45333336 633E+06 5.81044E+06 6.67747E+06- 000060
45303030 30302E31 20303028 45303030 30302E31 20363028 45303030 30302E31 1.00000E+00-1.00000E+00-1.00000E 000080
32392E33 20303028 45303030 30302E31 20303028 45303030 30302E31 20303028 +00-1.00000E+00-1.00000E+00 3.92 0000A0
20303028 45303030 30302E31 20303028 45303030 30302E31 20363028 45343037 704E+06-1.00000E+00-1.00000E+00 0000C0
45323037 35342E33 20363028 45393735 32392E33 20363028 45393232 31342E34 4.41228E+06 3.92579E+06 3.45702E 0000E0
31302E33 20363028 45303030 35332E33 20363028 45363832 34342E32 20363028 +06 3.44286E+06 3.35930E+06 3.01 000100
20303028 45303030 30302E31 20363028 45382731 39352E32 20363028 45373432 247E+06 2.39178E+06-1.00000E+00- 000120
45303030 30302E31 20303028 45303030 30302E31 20303028 45303030 30302E31 1.00000E+00-1.00000E+00-1.00000E 000140
30302E31 20303028 30302E31 20303028 30302E31 20303028 30302E31 20303028 +00-1.00000E+00-1.00000E+00-1.00 000160
20303028 45303030 30302E31 20303028 45303030 30302E31 20303028 45303030 000E+00-1.00000E+00-1.00000E+00- 000180
45303030 30302E31 20303028 45303030 30302E31 20303028 45303030 30302E31 1.00000E+00-1.00000E+00-1.00000E 0001A0
5E5E5E5E 5E303028 +00^^^^^..... 0001C0

Block number 8 (00000008), 456 (01C8) bytes

20363028 45303235 37392E36 20363028 45393639 38332E36 2037362E 36353120 156.67 6.39969E+06 6.97520E+06 000000
45323031 39352E37 20363028 45323639 34322E37 20363028 45333335 36322E36 6.36533E+06 7.24962E+06 7.59102E 000020
36302E33 20363028 45393932 34322E36 20363028 45343635 39312E37 20363028 +06 7.19564E+06 6.24298E+06 8.06 000040
20363028 45333235 37392E37 20363028 45393737 31352E36 20363028 45393032 209E+06 6.51779E+06 7.87523E+06 000060
45393939 33342E36 20363028 45313030 32302E36 20363028 45363437 36342E37 7.46746E+06 6.02001E+06 6.43998E 000080
32352E34 20363028 45383337 31362E34 20363028 45333737 30352E35 20363028 +06 5.50773E+06 4.61738E+06 4.52 0000A0
20363028 45373839 33322E35 20363028 45363135 35312E35 20363028 45313038 801E+06 5.15516E+06 5.23987E+06 0000C0
45393131 32322E34 20363028 45353938 37362E34 20363028 45393031 39312E35 5.19109E+06 4.67895E+06 4.22118E 0000E0
31332E33 20363028 45383531 33372E33 20363028 45393736 31302E34 20363028 +06 4.01679E+06 3.73158E+06 3.31 000100
20363028 45393639 34362E32 20363028 45393234 35362E32 20363028 45373130 017E+06 2.65429E+06 2.64969E+06 000120
45303030 30302E31 20363028 45343831 35392E31 20363028 45373733 38372E31 1.78377E+06 1.85184E+06-1.00000E 000140
30302E31 20303028 45303030 30302E31 20303028 45303030 30302E31 20303028 +00-1.00000E+00-1.00000E+00-1.00 000160
20303028 45303030 30302E31 20303028 45303030 30302E31 20303028 45303030 000E+00-1.00000E+00-1.00000E+00- 000180
45303030 30302E31 20303028 45303030 30302E31 20303028 45303030 30302E31 1.00000E+00-1.00000E+00-1.00000E 0001A0
5E5E5E5E 5E303028 +00^^^^^..... 0001C0

Block number 9 (00000009), 456 (01C8) bytes

20363028 45343838 30342E37 20363028 45393531 37302E37 2033332E 33353120 153.33 7.07159E+06 7.40884E+06 000000
45353537 30372E38 20363028 45343630 33332E39 20363028 45333533 34392E36 6.94353E+06 8.33064E+06 8.70755E 000020
39322E39 20363028 45383433 33392E36 20363028 45303332 34362E37 20363028 +06 7.84230E+06 6.93348E+06 9.29 000040
20363028 45323836 32392E38 20363028 45373733 33322E37 20363028 45343435 544E+06 7.23377E+06 8.92682E+06 000060
45353035 36342E37 20363028 45373533 33302E37 20363028 45343138 34342E38 8.44814E+06 7.03357E+06 7.46505E 000080
34312E35 20363028 45353034 38332E35 20363028 45313531 39372E35 20363028 +06 5.79151E+06 5.38405E+06 5.14 0000A0
20363028 45323038 38382E35 20363028 45313031 34352E35 20363028 45323935 592E+06 5.54101E+06 5.88802E+06 0000C0
45353930 36392E34 20363028 45343136 31332E35 20363028 45313733 36382E35 5.86371E+06 5.31614E+06 4.96095E 0000E0
35342E33 20363028 45373335 30392E33 20363028 45303637 38342E34 20363028 +06 4.48760E+06 3.90937E+06 3.45 000100
20363028 45343639 32312E33 20363028 45383537 31382E32 20363028 45393639 969E+06 2.91758E+06 3.12984E+06 000120
45303030 30302E31 20363028 45323738 39312E32 20363028 45303935 34302E32 2.04590E+06 2.19872E+06-1.00000E 000140
30302E31 20303028 45303030 30302E31 20303028 45303030 30302E31 20303028 +00-1.00000E+00-1.00000E+00-1.00 000160
20303028 45303030 30302E31 20303028 45303030 30302E31 20303028 45303030 000E+00-1.00000E+00-1.00000E+00- 000180
45303030 30302E31 20303028 45303030 30302E31 20303028 45203030 30302E31 1.00000E+00-1.00000E+00-1.00000E 0001A0
5E5E5E5E 5E303028 +00^^^^^..... 0001C0

Block number 10 (0000000A), 456 (01C8) bytes

20363028 45393131 33382E37 20363028 45394433 37372E37 2030302E 33353120 150.00 7.77389E+06 7.83119E+06 000000
45363536 33352E39 20363028 45333233 33322E39 20363028 45373834 32352E37 7.52487E+06 9.29322E+06 9.59656E 000020
32302E31 20363028 45313237 33362E37 20363028 45353136 38312E38 20363028 +06 8.18615E+06 7.53721E+06 1.02 000040
20363028 45393131 31372E39 20363028 45342631 30392E37 20373028 45323930 052E+07 7.92168E+06 9.71118E+06 000060
45343933 31332E38 20363028 45303030 37392E37 20363028 45203936 32312E39 9.12690E+06 7.97000E+06 9.31394E 000080

-01F, G P.6

-01F, G
P. 7

31372E35	20363028	45363131	38312E35	20363028	45313230	35392E35	20363028	+06	5.95021E+06	6.18116E+06	5.71	0000A0
20363028	45393132	30332E36	20363028	45373429	39762E35	20363028	45303936	690E+06	5.69947E+06	6.30219E+06		0000C0
45343739	35352E35	20363028	45373131	34372E35	20363028	45323531	34332E36	6.34182E+06	5.74117E+06	5.55974E		0000E0
34342E33	20363028	45373734	35322E33	20363028	45323536	36372E34	20363028	+06	4.76682E+06	3.85477E+06	3.44	000100
20363028	45343231	32352E33	20363028	45383930	33782E32	20363028	45333638	863E+06	2.83698E+06	3.52124E+06		000120
45303030	30302E31	20363028	45393236	35352E32	20363028	45343538	34332E32	2.34854E+06	2.55629E+06	-1.00000E		000140
30302E31	20303028	45303030	30302E31	20303028	45303030	30302E31	20303028	+00	-1.00000E+00	-1.00000E+00	-1.00	000160
20303028	45303030	30302E31	20303028	45303030	30302E31	20303028	45303030	000E+00	-1.00000E+00	-1.00000E+00		000180
45303030	30302E31	20303028	45303030	30302E31	20303028	45303030	30302E31	1.00000E+00	-1.00000E+00	-1.00000E		0001A0
						5E5E5E5E	5E30302E	+00	^^^^^		0001C0

81-100A-02A

LABORATORY FOR ATMOSPHERIC AND SPACE PHYSICS
SOLAR MESOSPHERE EXPLORER
PROCESSED IRR ORBIT DATA (1982-1985)
FOR THE
NATIONAL SPACE SCIENCE DATA CENTER

The SOLAR MESOSPHERE EXPLORER (SME) infrared radiometer (IRR) orbit data consists of limb radiance profiles measured at two wavelengths (6.8 μm and 9.6 μm). Each radiance profile is the average of four to six individual limb profiles measured at 12 second intervals, each of which has had an assumed instrument background subtracted (the average of all measurements above 70 km), and has been interpolated to a standard 2-km altitude grid. The merged profiles have been calibrated to $\text{W m}^{-2} \text{sr}^{-1}$. Each profile consists of 46 radiance values covering an altitude range of 100 km down to 10 km at 2 km intervals, and 14 items of additional information such as time, latitude, longitude, and background radiance. The profiles have not been interpolated to a standard latitude grid, as have most other SME final science products. A detailed description of the IRR instrument and data analysis is given in Jakosky *et al.*, 1986.

The IRR data supplied here are from the period Jan. 1982 to Sept. 1985. The data are contained on eight tapes, one for each wavelength (6 μm , 9 μm) and for each year (1982-1985). The contents of the tapes are summarized in Table 1. (The term "Tape Label" refers to the actual paper label on the tape reel; there are no ANSI standard labels written on the tapes themselves.)

Table 1. IRR Tape Contents

Tape Label	λ	Year	First Orbit	Last Orbit	No. Records
SMEIRR 1	6 μm	1982	1316	6825	111289
SMEIRR 2	9 μm	1982	1316	6825	103988
SMEIRR 3	6 μm	1983	6830	12355	98680
SMEIRR 4	9 μm	1983	6830	12355	96708
SMEIRR 5	6 μm	1984	12364	17906	74577
SMEIRR 6	9 μm	1984	12364	17906	69020
SMEIRR 7	6 μm	1985	17913	21987	99594
SMEIRR 8	9 μm	1985	17913	21987	83493

Each tape contains a single unlabeled file consisting of unformatted records of 60 VAX 4-byte floating point words (see appendix 1). The tapes are 9-track tapes written at a density of 1600 bytes/inch with a block size (physical record size) of 24000 bytes (100 logical records). There are two types of records, orbit header records (identified by a zero in word 51), and profile records. The contents of the two types of records are described in Table 2.

-02A
p.2

Table 2. IRR Record Contents

Orbit Header Record:

Word No.	Description
1	orbit number
2	year
3	day of year (1 to 366)
4	Universal Time (secs) of orbit start
5	total number of spins in orbit
6	no. rejected for non-limb view
7	no. rejected for incomplete altitude range
8	no. rejected for telemetry error or bit error
9	limb view code, sum of 1-lead, 2-nadir, 4-trail
10	no. of merged profiles (NO. RECORDS THIS ORBIT)
11	no. of leading limb profiles
12	no. of trailing limb profiles
13	no. of mixed-limb profiles (rejected)
14	no. of short profiles (1-3 spins; rejected)
15	mean spin set variance
16	orbital variance of spin set variances

Profile Record:

Word No.	Description
1	calibrated radiance at 100 km
2	calibrated radiance at 98 km
:	:
45	calibrated radiance at 12 km
46	calibrated radiance at 10 km
47	background radiance
48	std dev of background
49	no. background points
50	detector temperature (K)
51	standard spin set number
52	latitude (deg., - for south)
53	longitude (deg., - for west)
54	Universal Time (secs)
55	limb code (0 trailing, 1 leading)
56	UVS altitude correction code (1=yes, 0=no)
57	UVS altitude correction added (km)
58	number of profiles merged (4 to 6)
59	spin set variance
60	spin no. of worst spin (< 0 if rejected)

- 02A
P.3

A second appendix contains three listings of VAX Fortran codes which illustrate the use of these tapes. Listing 1. (PROGRAM irr_nssdc) is the code which was actually used to write the tapes from the unformatted disk files. Listing 2. (PROGRAM irt_nssdc) is a code which will create VAX disk files from the tape which will be identical to the original files. Notice that the number of records in each orbit is variable, and must be read from the header record (record(10)); there are no end-of-file marks except the one following the last record on each tape. Listing 3. (SUBROUTINE getrad) is the routine used at LASP to access the disk files.

A description of the SME mission, the instruments, the scientific objectives, and the initial results is contained in a series of papers in the April 1983 issue of *Geophysical Research Letters*. In *JGR* in 1984 there are more comprehensive papers on the instruments and data analysis.

Dr. C. A. Barth is the principal investigator for the SME experiment. Co-investigators are Drs. R. J. Thomas, D. W. Rusch, G. E. Thomas, and G. J. Rottman, all at the Laboratory for Atmospheric and Space Physics at the University of Colorado, Boulder, Colorado, 80309.

References

- Barth, C. A., R. W. Sanders, G. E. Thomas, G. J. Rottman, D. W. Rusch, R. J. Thomas, G. H. Mount, G. M. Lawrence, J. M. Zawodny, R. A. West and J. London, Solar Mesosphere Explorer Measurements of the El Chichón Volcanic Cloud, *Bull. Amer. Meteor. Soc.*, **63**, 1314, 1982.
- Barth, C. A., D. W. Rusch, R. J. Thomas, G. H. Mount, G. J. Rottman, G. E. Thomas, R. W. Sanders, G. M. Lawrence, Solar Mesosphere Explorer: Scientific Objectives and Results, *Geophys. Res. Lett.*, **10**, 237-240, 1983.
- Jakosky, B. M., G. E. Thomas, D. W. Rusch, C. A. Barth, G. M. Lawrence, J. J. Olivero, R. T. Clancy, R. W. Sanders, B. G. Knapp, M. T. Callan, Solar Mesosphere Explorer Thermal-infrared Observations of Stratospheric and Mesospheric Water Vapor and Aerosol, submitted to *J. Geophys. Res.*, Nov. 1986.
- Mount, G. H., D. W. Rusch, J. M. Zawodny, J. F. Noxon, C. A. Barth, G. J. Rottman, R. J. Thomas, G. E. Thomas, R. W. Sanders, G. M. Lawrence, Measurements of NO₂ in the Earth's Stratosphere Using a Limb Scanning Visible Light Spectrometer, *Geophys. Res. Lett.*, **10**, 265-268, 1983.
- Mount, G. H., D. W. Rusch, J. F. Noxon, J. M. Zawodny, and C. A. Barth, Measurements of Stratospheric NO₂ from the Solar Mesosphere Explorer Satellite. 1. An Overview of the Results, *J. Geophys. Res.*, **89**, 1327-1340, 1984.

- 02A
p.4
- Rottman, G. J., "Solar Ultraviolet Irradiance 1982 and 1983" in *Atmospheric Ozone* (ed. C.S. Zerefos) D. Reidel Pub. Co., 1985.
- Rottman, G. J., C. A. Barth, R. J. Thomas, G. H. Mount, G. M. Lawrence, D. W. Rusch, R. W. Sanders, G. E. Thomas, and J. London: Solar Spectral Irradiance, 120 to 190 nm, October 13, 1981 - January 3, 1982, *Geophys. Res. Lett.*, **9**, 587-590, 1982.
- Rusch, D. W., R. S. Eckman, and S. Solomon, Implications of the Comparison of Ozone Abundances Measured by the Solar Mesosphere Explorer to Model Calculations, *J. Geophys. Res.*, **90**, 12991-12998, 1985.
- Rusch, D. W., G. H. Mount, C. A. Barth, G. J. Rottman, R. J. Thomas, G. E. Thomas, R. W. Sanders, G. M. Lawrence, R. S. Eckman, Ozone Densities in the Lower Mesosphere Measured by a Limb Scanning Ultraviolet Spectrometer, *Geophys. Res. Lett.*, **10**, 241-244, 1983.
- Rusch, D. W., G. H. Mount, C. A. Barth, R. J. Thomas, and M. T. Callan, Solar Mesosphere Explorer Ultraviolet Spectrometer: Measurements of Ozone in the 1.0 to 0.1 mb Region, *J. Geophys. Res.*, **89**, 11677-11687, 1984.
- Rusch, D. W., G. H. Mount, J. M. Zawodny, C. A. Barth, G. J. Rottman, R. J. Thomas, G. E. Thomas, R. W. Sanders, G. M. Lawrence, Temperature Measurements in the Earth's Stratosphere Using a Limb Scanning Visible Light Spectrometer, *Geophys. Res. Lett.*, **10**, 261-264, 1983.
- Solomon, S., G. H. Mount, and J. M. Zawodny, Measurements of Stratospheric NO₂ from the Solar Mesosphere Explorer Satellite. 2. General Morphology of observed NO₂ and derived N₂O₅, *J. Geophys. Res.*, **89**, 7317-7321, 1984.
- Thomas, G. E., C. A. Barth, E. R. Hansen, C. W. Hord, G. M. Lawrence, G. H. Mount, G. J. Rottman, D. W. Rusch, A. I. Stewart, R. J. Thomas, J. London, P. L. Bailey, P. J. Crutzen, R. E. Dickenson, J. C. Gille, S. C. Liu, J. F. Noxon, and C. B. Farmer: Scientific Objectives of the Solar Mesosphere Explorer Mission, *Pageoph*, **118**, 591-615, 1980.
- Thomas, R. J., C. A. Barth, G. J. Rottman, D. W. Rusch, G. H. Mount, G. M. Lawrence, R. W. Sanders, G. E. Thomas, L. E. Clemens, Ozone Density Distribution in the Mesosphere (50-90 km) Measured by the SME Limb Scanning Near Infrared Spectrometer, *Geophys. Res. Lett.*, **10**, 245-248, 1983.
- Thomas, R. J., C. A. Barth, G. J. Rottman, D. W. Rusch, G. H. Mount, G. M. Lawrence, R. W. Sanders, G. E. Thomas, L. E. Clemens, Mesospheric Ozone Depletion During the Solar Proton Event of July 13, 1982, Part I Measurement, *Geophys. Res. Lett.*, **10**, 253-255, 1983.

-02A
p.5

Thomas, R. J., C. A. Barth, D. W. Rusch, and R. W. Sanders, Solar Mesosphere Explorer Near Infrared Spectrometer: Measurements of 1.2 μm Radiances and the Inference of Mesospheric Ozone, *J. Geophys. Res.*, **89**, 9569-9580, 1984.

Thomas, R. J., C. A. Barth, and S. Solomon, Seasonal Variations of Ozone in the Upper Mesosphere and Gravity Waves, *Geophys. Res. Lett.*, **11**, 673-676, 1984.

-02A
P.7

APPENDIX II

Listing 1.

```

PROGRAM irr_nssdc

C   Make tape of unlabelled, unformatted files of IRR orbit track
C   radiance data for NSSDC.

C   B. G. Knapp, 86/11/05

C   Tape unit must be $ASSIGNED to the logical "NSSDC"

IMPLICIT NONE      !VAX-11 Fortran 77!

CHARACTER*22      fname
INTEGER           i,chan
INTEGER           n,nrecs,nblocks
INTEGER           maxblocks      /1600/
REAL*4           blocksize      /100./
INTEGER*4         ceil          !ceil(x) = least integer >= x

CHARACTER*13      froot(4)      !file name root
1                 /' 03_RAD:IRR9_',
2                 '          ',
3                 '          ',
4                 'H20_RAD:IRR6_/'

INTEGER*4         begorb,endorb,orb
REAL*4           record(60)

WRITE(*,10) ' Enter beginning, ending orbits: '
10 FORMAT('$',A)
READ *,begorb,endorb
WRITE(*,10) ' Channel (1 for 9-micron, 4 for 6-micron)? '
READ *,chan

OPEN(2,FILE='NSSDC',STATUS='NEW',ACCESS='SEQUENTIAL',
1     FORM='UNFORMATTED',RECORDTYPE='FIXED',RECL=60)

nrecs = 0
nblocks = 0
DO 100 orb=begorb,endorb

    write(fname,20) froot(chan),orb
20    FORMAT(A13,I5.5,'.RAD')

    OPEN(1,FILE=fname,STATUS='OLD',FORM='UNFORMATTED',
1       ORGANIZATION='SEQUENTIAL',ACCESS='SEQUENTIAL',
2       RECORDTYPE='FIXED',RECL=60,READONLY,ERR=100)

    READ(1,ERR=100,END=100) record
    WRITE(2) record

    n = NINT(record(10))
    DO i=1,n

```

-02A
p. 8

```
        READ(1) record
        WRITE(2) record
ENDDO
CLOSE(1)
nrecs = nrecs+n+1
nblocks = ceil(nrecs/blocksize)

        WRITE(*,30) orb,n,nrecs,nblocks
30      FORMAT(4I10)

        IF (nblocks .GE. maxblocks) GOTO 200

100 CONTINUE

200 CLOSE(2)

END
```

02A
P.9

Listing 2.

PROGRAM irt_nssdc

C Recover IRR orbit-track radiance files from NSSDC unformatted
C tapes.

C B. G. Knapp, 86/11/06

C Tape unit must be \$ASSIGNED to the logical "NSSDC"

IMPLICIT NONE !VAX-11 Fortran 77!

CHARACTER*22 fname
INTEGER i,chan,n,nfiles,nskip
CHARACTER*13 froot(4) !file name root
1 /' 03_RAD:IRR9_',
2 ' ',
3 ' ',
4 'H20_RAD:IRR6_'/'

INTEGER*4 begorb,endorb,orb
REAL*4 record(60)
LOGICAL header

WRITE(*,10) ' Enter beginning, ending orbits: '
10 FORMAT('\$',A)
READ *,begorb,endorb
WRITE(*,10) ' Channel (1 for 9-micron, 4 for 6-micron)? '
READ *,chan

OPEN(1,FILE='NSSDC',STATUS='OLD',ACCESS='SEQUENTIAL',FORM=
1 'UNFORMATTED',READONLY,RECORDTYPE='FIXED',RECL=60)

orb = begorb
nfiles = 0
DOWHILE (orb.LT.endorb)

header = .FALSE.
nskip = -1
DOWHILE (.NOT. header)
READ(1,END=100) record
nskip = nskip+1
header = (record(51).LE.0.)

ENDDO
IF (nskip.GT.0) WRITE(*,20) nskip
20 FORMAT(' Records skipped searching for header record:',I4)

orb = NINT(record(1))
n = NINT(record(10))

IF ((orb.GE.begorb).AND.(orb.LE.endorb)) THEN
write(fname,30) froot(chan),orb

-02A
p.10

```
30     FORMAT(A13,I5.5, '.RAD')

      OPEN(2,FILE=fname,STATUS='NEW',FORM='UNFORMATTED',
1         ORGANIZATION='SEQUENTIAL',ACCESS='SEQUENTIAL',
2         RECORDTYPE='FIXED',RECL=60)

      WRITE(2) record
      DO i=1,n
        READ(1) record
        WRITE(2) record
      ENDDO
      CLOSE(2)
      nfiles = nfiles+1

      WRITE(*,40) orb,n,i-1
40     FORMAT(3I10)
      ELSE
        DO i=1,n
          READ(1) record
        ENDDO
      ENDIF
    ENDDO

100  WRITE(*,50) nfiles
50   FORMAT('/'  Number of files copied from tape:',I5//)
      CLOSE(1)

      END
```

-02A
p.11

Listing 3.

SUBROUTINE getrad(ichan,orbit,a,retcode)

C Programmer: Barry G. Knapp, LASP, May 1986.

C Returns array a of IRR merged, altitude-corrected radiances for
C the specified channel. The array a must be declared by caller to
C be REAL*4, with 81 rows and 60 columns. Each row of a returns
C one merged radiance profile (cols 1-46) as well as the following
C additional information:

C	Col #	Data
C	-----	----
C	47	background
C	48	std dev of background
C	49	number of background points
C	50	detector (patch) temperature (K)
C	51	standard spin set number
C	52	latitude
C	53	longitude
C	54	Universal Time (secs)
C	55	limb code (0 trailing, 1 leading)
C	56	UVS altitude correction code (1=yes, 0=no)
C	57	UVS altitude correction added (km)
C	58	number of profiles merged (4,5, or 6)
C	59	variance in col. norms of co-distance matrix
C	60	spin no. of worst spin (< 0 if rejected)

C Row 81 contains the standard altitudes from 10 to 100 km in
C cols 1-46, and the following additional information:

C	Col #	Data
C	-----	----
C	47	orbit
C	48	channel
C	49	yearday (YYYYDDD)
C	50	UT (secs)
C	51	number of spins in orbit
C	52	number rejected for non-limb view
C	53	number rejected for incomplete altitude range
C	54	number rejected for bad data start or bit error
C	55	limb view code, sum of 1-lead, 2-nadir, 4-trail
C	56	number of profiles returned
C	57	number of leading limb profiles
C	58	number of trailing limb profiles
C	59	number of mixed-limb profiles (rejected)
C	60	number of short profiles (1-3 spins; rejected)

IMPLICIT NONE

C Input:
INTEGER*4 ichan

-02A
p.12

```
INTEGER*4 orbit

C   Output:
REAL*4      a(81,60)
INTEGER     retcode

C   Local:
INTEGER     nalt
PARAMETER   (nalt=46)           !number of altitudes

REAL*4      prof(nalt)         !holds one profile
REAL*4      bkgd,sigma,nbkgd   !background info
REAL*4      tdet               !detector temp.
REAL*4      set                !set number
REAL*4      ncor,delz          !alt cor. info
REAL*4      lat,lon,secs,limb  !"file2" info
REAL*4      ngood,pdpa,kd      !merge info
REAL*4      horb,hyr,hday,hsecs,hview !header info
REAL*4      hnspins,hnlrej,haltrej,hwrej !spin classes
REAL*4      hn,hnle,hntr,hnmx,hnshort !profile classes
REAL*4      missing_data/-1E6/ !represents missing data
```

```
INTEGER i,j,n
```

```
CHARACTER*13 fname(4)           !file name root
1              /' 03_RAD:IRR9_',
2              '          ',
3              '          ',
4              'H20_RAD:IRR6_'/
```

```
CHARACTER*22 radfile           !raw radiance file name
```

C >>> Execution begins here <<<

```
DO i=1,81
  DO j=1,56
    a(i,j) = missing_data
  ENDDO
ENDDO
```

```
WRITE(radfile,10) fname(ichan),orbit           !internal write
10 FORMAT(A13,I5.5, '.RAD')
```

```
i = 1           !next row to fill
retcode = 1     !default: no return
```

```
OPEN(1,FILE=radfile,STATUS='OLD',FORM='UNFORMATTED',
1  ORGANIZATION='SEQUENTIAL',ACCESS='SEQUENTIAL',
2  RECORDTYPE='FIXED',RECL=60,READONLY,SHARED,ERR=100)
```

```
C   Read header
READ(1,ERR=100) horb,hyr,hday,hsecs,hnspins,hnlrej,haltrej,
1  hwrej,hview,hn,hnle,hntr,hnmx,hnshort
```

-02A
p.13

n = INT(hn)

C Read & stuff profiles

```
DO i=1,n
  READ(1,ERR=100) prof,bkgd,sigma,nbkgd,tdet,set,
1      lat,lon,secs,limb,ncor,delz,ngood,pdpa,kd
  DO j=1,nalt
    a(i,j) = prof(nalt-j+1)
  ENDDO
  a(i,nalt+1) = bkgd
  a(i,nalt+2) = sigma
  a(i,nalt+3) = nbkgd
  a(i,nalt+4) = tdet
  a(i,nalt+5) = set
  a(i,nalt+6) = lat
  a(i,nalt+7) = lon
  a(i,nalt+8) = secs
  a(i,nalt+9) = limb
  a(i,nalt+10) = ncor
  a(i,nalt+11) = delz
  a(i,nalt+12) = ngood
  a(i,nalt+13) = pdpa
  a(i,nalt+14) = kd
ENDDO
```

```
DO j=1,nalt
  a(81,j) = 10.+(j-1)*2.
ENDDO
a(81,nalt+1) = orbit
a(81,nalt+2) = ichan
a(81,nalt+3) = 1000.*hyr+hday
a(81,nalt+4) = hsecs
a(81,nalt+5) = hnspins
a(81,nalt+6) = hnlrej
a(81,nalt+7) = haltrej
a(81,nalt+8) = hwrej
a(81,nalt+9) = hview
a(81,nalt+10) = hn
a(81,nalt+11) = hnle
a(81,nalt+12) = hntr
a(81,nalt+13) = hnmX
a(81,nalt+14) = hnshort
```

```
CLOSE(1)
retcode = 0      !good data returned
```

```
100 CONTINUE
RETURN
END
```

SOLAR MESOSPHERE EXPLORER
INFRARED RADIANCE DATA

1981-1987

In the normal data mode the spectrometer samples data at two wavelengths, 1.27 micrometers and 1.87 micrometers. The limb altitude radiance profiles with identifying data are on the tapes. See Thomas et al., 1984 for more informaton.

Dr. C. A. Barth is the principal investigator for the SME experiment. Co-investigators Drs. R. J. Thomas, D. W. Rusch, G. E. Thomas, R. W. Sanders, and G. J. Rottman are resident at the laboratory for Atmospheric and Space Physics at the University of Colorado, Boulder, Colorado 80309.

The radiance data from the near infrared spectrometer is written in standard ASCII labeled format with one orbit per file. Each orbit consists of 20 to 60 (approximate range) merged spin sets. Filenames are of the format RMxxxxx.NSS, where xxxxx is the orbit number. The data set consists of 52 tapes containing radiance data from Day 350, 1981 through Day 280, 1983. The following is a listing of tapes and orbit intervals contained on tapes:

Tape Label	Orbit Interval	No. Orbits on Tape
AG0001	1074 - 1952	300
AG0002	1953 - 2693	306
AG0003	2701 - 3399	301
AG0004	3403 - 4055	306
AG0005	4065 - 4675	308
AG0006	4676 - 5189	300
AG0007	5190 - 5750	300
AG0008	5751 - 6286	303
AG0009	6294 - 6832	314
AG0010	6835 - 7377	308
AG0011	7379 - 7914	314
AG0012	7921 - 8459	307
AG0013	8466 - 9004	314
AG0014	9007 - 9543	295
AG0015	9950 - 10091	281
AG0016	10095 - 10629	278
AG0017	10637 - 11066	213
AG0018	10900 - 11698	329
AG0019	11699 - 12455	339
AG0020	12456 - 13001	254
AG0021	13006 - 13306	144
AG0022	13309 - 13608	137
AG0023	13612 - 14010	184
AG0024	14017 - 14418	189
AG0025	14426 - 14823	183
AG0026	14826 - 15117	136
AG0027	15124 - 15520	185
AG0028	15524 - 15921	184
AG0029	15928 - 16502	255
AG0030	16515 - 17399	313

-03B
p.2

Tape Label	Orbit Interval	No. Orbits on Tape
AG0031	17404 - 18193	296
AG0032	18200 - 18799	298
AG0033	18800 - 19299	336
AG0034	19300 - 19899	379
AG0035	19900 - 20296	318
AG0036	20300 - 20797	325
AG0037	20800 - 21198	316
AG0038	21202 - 21599	311
AG0039	21600 - 22051	346
AG0052	22052 - 22499	311 ** Tape is out of sequential order
AG0040	22502 - 23095	408
AG0041	23102 - 23699	411
AG0042	23700 - 24096	296
AG0043	24100 - 24499	297
AG0044	24500 - 24977	395
AG0045	25000 - 25493	370
AG0046	25500 - 25941	310
AG0047	26000 - 26499	310
AG0048	26500 - 26999	341
AG0049	27000 - 27499	441
AG0050	27500 - 27999	382
AG0051	28000 - 28813	290

The first step in the analysis of the raw science data from the near infrared spectrometer is to merge the spins, data collection rotations of the SME satellite, into groups of 1 to 6 spins. The data consists of long (1.87 micron) and short (1.27 micron) channel radiances and information to identify merged spin set position. The ASCII format of a merged spin set follows:

Format	Description
1X,I3,1X	Julian Day
32(E9.2,1X)	Long channel radiances (wavelength = 1.87 μ , units = MR)
32(E9.2,1X)	Short channel radiances (wavelength = 1.27 μ , units = MR)
F7.1	Seconds into day (GMT)
1X,F8.3	Latitude of merged spin set
1X,F8.3	Longitude of merged spin set
1X,F5.0	Highest altitude (106 km)
1X,F3.0	Number of spins in merged set (1-6)
1X,F3.0	Sampling limb (+1 leading, -1 trailing)
1X,F5.0	Chronological order in orbit of last spin merged into set

The physical characteristics of the tapes are:

Density	1600 bytes per inch
Tracks	9
Blocksize	796 bytes
Label	AGxxxx, where xxxx is the tape # in the series.

Rusch, D.W., G.H. Mount, J.M. Zawodny, C.A. Barth, G.J. Rottman, R.J. Thomas, G.E. Thomas, R.W. Sanders, G.M. Lawrence, Temperature Measurements in the Earth's Stratosphere Using a Limb Scanning Visible Light Spectrometer, Geophys. Res. Lett. 10, 261-264, 1983.

Solomon, S., G.H. Mount, and J.M. Zawodny, Measurements of Stratospheric NO2 from the Solar Mesosphere Explorer Satellite. 2. General Morphology of observed NO2 and derived N2O5, J. Geophys. Res. 89, 7317-7321, 1984.

Thomas, G.E., C.A. Barth, E.R. Hansen, C.W. Hord, G.M. Lawrence, G.H. Mount, G.J. Rottman, D.W. Rusch, A.I. Stewart, R.J. Thomas, J. London, P.L. Bailey, P.J. Crutzen, R.E. Dickenson, J.C. Gille, S.C. Liu, J.F. Noxon, and C.B. Farmer: Scientific Objectives of the Solar Mesosphere Explorer Mission, Pageoph 118, 591-615, 1980.

Thomas, R.J., C.A. Barth, G.J. Rottman, D.W. Rusch, G.H. Mount, G.M. Lawrence, R.W. Sanders, G.E. Thomas, L.E. Clemens, Ozone Density Distribution in the Mesosphere (50-90 km) Measured by the SME Limb Scanning Near Infrared Spectrometer, Geophys. Res. Lett. 10, 245-248, 1983.

Thomas, R.J., C.A. Barth, G.J. Rottman, D.W. Rusch, G.H. Mount, G.M. Lawrence, R.W. Sanders, G.E. Thomas, L.E. Clemens, Mesospheric Ozone Depletion During the Solar Proton Event of July 13, 1982, Part I Measurement, Geophys. Res. Lett. 10, 253-255, 1983.

Thomas, R.J., C.A. Barth, D.W. Rusch, and R.W. Sanders, Solar Mesosphere Explorer Near Infrared Spectrometer: Measurements of 1.2 μ m Radiances and the Inference of Mesospheric Ozone, J. Geophys. Res. 89, 9569-9580, 1984.

Thomas, R.J., C.A. Barth, and S. Solomon, Seasonal Variations of Ozone in the Upper Mesosphere and Gravity Waves, Geophys. Res. Lett. 11, 673-676, 1984.

-03B
p.4

SME REFERENCES

- Barth, C.A., R.W. Sanders, G.E. Thomas, G.J. Rottman, D.W. Rusch, R.J. Thomas, G.H. Mount, G.M. Lawrence, J.M. Zawodny, R.A. West and J. London, Solar Mesosphere Explorer Measurements of the El Chicon Volcanic Cloud, Bull. Amer. Meteor. Soc. 63, 1314, 1982.
- Barth, C.A., D.W. Rusch, R.J. Thomas, G.H. Mount, G.J. Rottman, G.E. Thomas, R.W. Sanders, G.M. Lawrence, Solar Mesosphere Explorer: Scientific Objectives and Results, Geophys. Res. Lett. 10, 237-240, 1983.
- Mount, G.H., D.W. Rusch, J.M. Zawodny, J.F. Noxon, C.A. Barth, G.J. Rottman, R.J. Thomas, G.E. Thomas, R.W. Sanders, G.M. Lawrence, Measurements of NO₂ in the Earth's Stratosphere Using a Limb Scanning Visible Light Spectrometer, Geophys. Res. Lett. 10, 265-268, 1983.
- Mount, G.H., D.W. Rusch, J.F. Noxon, J.M. Zawodny, and C.A. Barth, Measurements of Stratospheric NO₂ from the Solar Mesosphere Explorer Satellite. 1. An Overview of the Results, J. Geophys. Res. 89, 1327-1340, 1984.
- Rottman, G.J., "Solar Ultraviolet Irradiance 1982 and 1983" in Atmospheric Ozone (ed. C.S. Zerefos) D. Reidel Pub. Co., 1985.
- Rottman, G.J., C.A. Barth, R.J. Thomas, G.H. Mount, G.M. Lawrence, D.W. Rusch, R.W. Sanders, G.E. Thomas, and J. London: Solar Spectral Irradiance, 120 to 190 nm, October 13, 1981 - January 3, 1982, Geophys. Res. Lett. 9, 587-590, 1982.
- Rusch, D.W., R.S. Eckman, and S. Solomon, Implications of the Comparison of Ozone Abundances Measured by the Solar Mesosphere Explorer to Model Calculations, J. Geophys. Res., in press, 1985.
- Rusch, D.W., G.H. Mount, C.A. Barth, G.J. Rottman, R.J. Thomas, G.E. Thomas, R.W. Sanders, G.M. Lawrence, R.S. Eckman, Ozone Densities in the Lower Mesosphere Measured by a Limb Scanning Ultraviolet Spectrometer, Geophys. Res. Lett. 10, 241-244, 1983.
- Rusch, D.W., G.H. Mount, C.A. Barth, R.J. Thomas, and M.T. Callan, Solar Mesosphere Explorer Ultraviolet Spectrometer: Measurements of Ozone in the 1.0 to 0.1 mb Region, J. Geophys. Res. 89, 11677-11687, 1984.

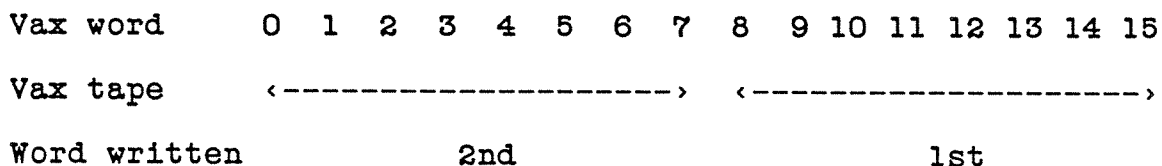
-03B
p.6

LABORATORY FOR ATMOSPHERIC AND SPACE PHYSICS
SOLAR MESOSPHERE EXPLORER
AIRGLOW SPECTROMETER RADIANCE DATA FOR THE
NATIONAL SPACE SCIENCE DATA CENTER

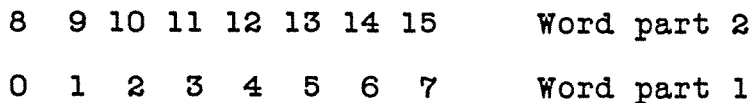
APPENDIX

Each of the enclosed tapes has the following characteristics:

1. 9-track, 1600 bpi. Written on a Digital TU77 drive.
2. ANSI STANDARD tape headers and End-of-File (EOF) structure (7-bit ASCII characters) as per VAX 11/780 system software. After the Volume Header record (80 bytes), there are four File Header records (80 bytes each), one EOF, the data records (796 bytes each), one EOF, four File Trailer records (80 bytes each), and one EOF for each of the data files on this tape.
3. Physical data blocks are 796 bytes long; each block contains one logical record. If the logical record is less than 796 bytes long, a hexadecimal value of 5E is used as fill from the end of the logical record to the end of the physical record.
4. The VAX writes bytes onto a 9-track tape in the following order:



The resulting tape (up is the tape beginning direction)



5. An annotated dump is attached which shows the contents of the first eight physical blocks. The left side of the dump shows the hexadecimal word (read from right to left) and the right side of the dump shows the ASCII equivalent word contents (read from left to right). The last column on the right is the hexadecimal 4-byte word number for the rightmost four bytes in the hexadecimal dump section.

B R I E F D E S C R I P T I O N

SME, Visible Nitrogen Dioxide

81-100A-04

NO NEW I.D.

The objective of the Visible Nitrogen Dioxide Experiment was to measure the distribution of nitrogen dioxide in the 25- to 40-km altitude region. This was done by measuring the differential absorption of scattered sunlight by NO₂ at two wavelengths near 4400 A. A dual-channel Ebert-Fastie spectrometer operated in the following wavelength intervals: 4390 to 4420 A and 3200 to 6400 A. The signal at half maximum had a full width of 9.8 A and 19.6 A, respectively. There were 512 and 438 grating steps per scan, respectively. The instrument line of sight was normal to the spin axis.

M A T E R I A L S F O R D I S T R I B U T I O N

81-100A-04B

Orbital Nitrogen Dioxide Pfl, Tape

Laboratory for Atmospheric and Space Physics Solar Mesosphere Explorer
Orbit Track NO2 Data for the National Space Science Data Center
1982-1986 Data (12 pp.)

A C K N O W L E D G E M E N T S

When using the data in any reports, publications, or presentations, please
acknowledge the National Space Science Data Center and the following
individuals or groups:

81-100A-04B The Principal Investigator, Dr. C. A. Barth

DEC, 88
81-100A-04B

LABORATORY FOR ATMOSPHERIC AND SPACE PHYSICS

SOLAR MESOSPHERE EXPLORER

ORBIT TRACK NO2 DATA FOR THE

NATIONAL SPACE SCIENCE DATA CENTER

1982-1986 DATA

The SOLAR MESOSPHERE EXPLORER (SME) orbit track NO2 data was derived from the visible spectrometer radiance measurements. A description of the mission, the instruments, the scientific objectives, and the initial results is contained in a series of articles in the April 1983 issue of Geophysical Research Letters (10:237-267). In Mount et al. (JGR 89: 1327-1340, 1984) there is a more comprehensive paper on the visible instrument and data analysis.

The nitrogen dioxide mixing ratios in parts per billion by volume are given on pressure surfaces from about 24 to 40 km between 120 degrees South and 120 degrees North at each 5 degrees. Latitudes between 90 S and 90 N indicate normal data, taken at an afternoon local time. During times when the pole is sunlit, SME was able to take data on both sides of the pole. Crossing the pole gives an early morning local time. In order to differentiate between data taken at these different local times, latitude labeling was extended beyond 90 degrees. So, latitudes greater than 90 indicate morning data, while latitudes less than 90 indicate afternoon data. For example, a latitude of 110 N would indicate data taken at 70 N in the morning.

Dr. C.A. Barth is the principal investigator for the SME experiment. Co-investigators Drs. R.J. Thomas, D.W. Rusch, G.E. Thomas, and G.J. Rottman are resident at the Laboratory for Atmospheric and Space Physics at the University of Colorado, Boulder, Colorado, 80309.

This set of data consists of 2 tapes. The first tape, labeled NO201, has 3 files covering the years 1982 through 1984. The second tape, labeled NO202, has 2 files covering the years 1985 through 1986.

The blocksize on these tapes is 2048. The logical record length is 490. A description of the tape characteristics is given in the appendix.

These data, derived from the visible spectrometer on SME, are orbit track NO2 mixing ratios. They cover the years 1982 through 1986. Units are parts per billion by volume.

SME NO2 MIXING RATIO DATA, 1981 - 1986

TAPE	FILE	NO. BLOCKS	CONTENTS
NO201	NO282.DAT	4137	2/17/82 - 12/31/82
	NO283.DAT	3237	1/ 1/83 - 12/31/83
	NO284.DAT	2829	1/ 1/84 - 12/31/84
NO202	NO285.DAT	3335	1/ 1/85 - 12/31/85
	NO286.DAT	4683	1/ 1/86 - 12/ /86

The following format describes the file NO282.DAT. The format is applicable for the 5 files in this dataset consisting of SME NO2 mixing ratios (ppbv) on orbit tracks. Missing data is indicated by -1.0. The pressure in millibars ranges from 31.6228 to 4.217 mb. There are 8 pressure levels and 48 latitudes. Pressure levels are evenly spaced in terms of LOG(pressure). The LOG values range from 1.5 to .625 in increments of .125. $P(mb) = 10.**(1.5 - (level-1)*.125)$, where level goes from 1 to 8. Latitudes range from 120 S to 120 N in 5 degree increments. Values of latitude greater than 90 indicate morning data, while data between 90S and 90N was taken in the afternoon. Data at 120 S would be in the morning at 60S, while data at 60 S would be in the afternoon.

First orbit=2021, date=1982048 (Feb. 17, 1982)

Record	Format	Description
1	3I5,F10.2	Orbit, Year, Day, Equatorial Long.
2	49E10.3	For pressure = 31.6 mb Field 1: Latitude = -120. Field 2: Latitude = -115. ... Field N: Latitude = (N-25)*5. ...
3	49E10.3	Field 49: Latitude = 120. For pressure = 23.7 mb Field 1: Latitude = -120. Field 2: Latitude = -115. ... Field N: Latitude = (N-25)*5.

```

...
4          49E10.3      Field 35:Latitude = 120.
                    For pressure = 17.8 mb
...
.
.
.
9          49E10.3      For pressure = 4.2 mb
10         49F7.2       Longitudes
11         49F7.2       Solar zenith angles
12         49F9.2       Seconds of day
13         49F6.2       Roll angles

```

Second orbit=2022, date=1982048 (Feb. 17, 1982)

```

14         3I5,F10.2    Orbit, Year, Day, Equatorial Long.
15         49E10.3     For pressure = 31.6 mb
                    Field 1: Latitude = -120.
                    Field 2: Latitude = -115.
                    ...
                    Field N: Latitude = (N-25)*5.
                    ...
16         49E10.3     Field 49:Latitude = 120.
                    For pressure = 23.7 mb
                    Field 1: Latitude = -120.
                    Field 2: Latitude = -115.
                    ...
                    Field N: Latitude = (N-25)*5.
                    ...
17         49E10.3     Field 35:Latitude = 120.
                    For pressure = 17.8 mb
                    ...
.
.
.
22         49E10.3     For pressure = 4.2 mb
23         49F7.2       Longitudes
24         49F7.2       Solar zenith angles
25         49F9.2       Seconds of day
26         49F6.2       Roll angles

```

etc., for subsequent orbits for which there is SME NO2 data.

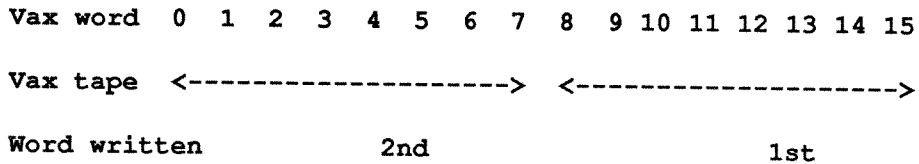
-048
p.4

LABORATORY FOR ATMOSPHERIC AND SPACE PHYSICS
SOLAR MESOSPHERE EXPLORER
PROCESSED DATA FOR THE
NATIONAL SPACE SCIENCE DATA CENTER

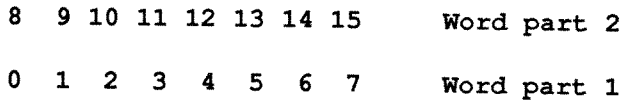
APPENDIX

Each of the enclosed tapes has the following characteristics:

1. 9-track, 1600 bpi. Written on a Digital TU77 drive.
2. ANSI STANDARD tape headers and End-of-File (EOF) structure (7-bit ASCII characters) as per VAX 11/780 system software. After the Volume Header record (80 bytes), there are four File Header records (80 bytes each), one EOF, the data records (2048 bytes each), one EOF, four File Trailer records (80 bytes each), and one EOF for each of the data files on this tape.
3. Physical data blocks are 2048 bytes long; data files are 7-bit ASCII records containing a four byte "control" word followed by the ASCII bytes. The control word consists of two bytes of End-of-Text characters (hexidecimal=0) followed by a two byte logical record length value. The length refers to the total number of bytes and includes the 4-byte control word. Logical records are blocked into physical records and a hexidecimal value of 5E is used as fill from the end of the last logical record to the end of the physical record.
4. The VAX writes bytes onto a 9-track tape in the following order:



The resulting tape (up is the tape beginning direction)



5. An annotated dump is attached which shows the contents of the first six physical blocks. The left side of the dump shows the hexidecimal word (read from right to left) and the right side of the dump shows the ASCII equivalent word contents (read from left to right). The last column on the right is the hexidecimal 4-byte word number for the rightmost four bytes in the hexidecimal dump section.

-048 45

Dump of device MTA0: on 14-DEC-1988 23:33:22.03

Block number 1 (00000001), 80 (0050) bytes

20202020	20202020	20202020	20202020	20202020	20202031	30324F4E	314C4F56	VOLIND201	000000
20202020	20202020	20202020	20202020	20202020	20202020	20202020	20202020		000020
				33202020	20202020	20202020	20202020	3.....	000040

Block number 2 (00000002), 80 (0050) bytes

30313030	30203130	324F4E20	20202020	20202054	41442E32	38324F4E	31524448	HDRIND282.DAT	ND201 00010 000000
46434544	30303030	30302039	34333838	20393433	38382030	30313030	30313030	001000100 88349 88349	000000DECF 000020
				20202020	20202020	20204131	31454C49	ILE11A 000040

Block number 3 (00000003), 80 (0050) bytes

20202020	20202020	20202020	20202020	20343934	30303834	30323044	32524448	HDR2D0204800494	000000
20202020	20202020	20202020	30302020	20202020	20202020	20202020	20202020	00	000020
				20202020	20202020	20202020	20202020	000040

Block number 4 (00000004), 80 (0050) bytes

30303030	30303030	31303030	30303030	30303030	32303230	41453130	33524448	HDR301EA020200000000000100000000	000000
30303030	30303030	30303030	30303030	30303030	30303030	30303030	30303030	00000000000000000000000000000000	000020
				20202020	20202020	20202020	30303030	0000 000040

Block number 5 (00000005), 80 (0050) bytes

20202020	20202020	20202020	20202020	20202020	20202020	20202020	34524448	HDR4	000000
20202020	20202020	20202020	20202020	20202020	20202020	20202020	20202020		000020
				20202020	20202020	20202030	30202020	00 000040

*** End of file ***

Header info

Dump of tape N02 01 pg 1

Dump of device MTA0: on 14-DEC-1988 23:33:22.03

Block number 6 (00000006), 2048 (0800) bytes

39343037	362E9399	20202020	20383420	20203238	39312031	32303220	39323030	0029 2021 1982	48	99.67049	000000	
20303028	45303030	2E312030	30284530	30302E31	20303028	45303030	2E312034	4-1.000E+00	-1.000E+00	-1.000E+00	000020	
2E322030	30284537	39342E32	20303028	45303030	2E312030	30284530	30302E31	1.000E+00	-1.000E+00	2.497E+00	2.000040	
33352E31	20303028	45383536	2E312030	30284537	32312E32	20303028	45363333	336E+00	2.127E+00	1.658E+00	1.53000060	
45363537	2E312030	30284536	32372E31	20303028	45303036	2E312030	30284531	1E+00	1.600E+00	1.726E+00	1.756E000080	
30284533	39312E31	20303028	45383833	2E312030	30284534	31362E31	20303028	+00	1.614E+00	1.388E+00	1.193E+00	0000A0
20313020	45333732	2E392030	30284535	34302E31	20303028	45313031	2E312030	0	1.101E+00	1.045E+00	9.273E-01	0000C0
2E312031	30204531	35382E31	20313020	45383439	2E332031	30204533	33382E36	6.833E-01	3.948E-01	1.851E-01	1.0000E0	
30302E31	20313020	45323239	2E322031	30204532	30332E32	20313020	45373135	517E-01	2.302E-01	2.922E-01	-1.00	000100
45303030	2E312030	30284530	30302E31	20303028	45303030	2E312030	30284530	0E+00	-1.000E+00	-1.000E+00	-1.000E+00	000120
30284530	30302E31	20303028	45303030	2E312030	30284530	30302E31	20303028	+00	-1.000E+00	-1.000E+00	-1.000E+00	000140
20303028	45303030	2E312030	30284530	30302E31	20303028	45303030	2E312030	0	-1.000E+00	-1.000E+00	-1.000E+00	000160
2E312030	30284530	30302E31	20303028	45303030	2E312030	30284530	30302E31	1.000E+00	-1.000E+00	-1.000E+00	-1.000E+00	000180
30302E31	20303028	45303030	2E312030	30284530	30302E31	20303028	45303030	000E+00	-1.000E+00	-1.000E+00	-1.000E+00	0001A0
45303030	2E312030	30284530	30302E31	20303028	45303030	2E312030	30284530	0E+00	-1.000E+00	-1.000E+00	-1.000E+00	0001C0
30284530	30302E31	20303028	45303030	2E312030	30302E31	20303028	45333337	+00	-1.000E+00	-1.000E+00	-1.000E+00	0001E0
45303030	2E312030	30284530	30302E31	20343934	30303028	45303030	2E312030	0	-1.000E+00	0.494E+00	-1.000E+00	000200
30284530	30302E31	20303028	45303030	2E312030	30284530	30302E31	20303028	+00	-1.000E+00	-1.000E+00	-1.000E+00	000220
20303028	45393531	2E332030	30284535	38342E33	20303028	45333337	2E332030	0	3.733E+00	3.485E+00	3.159E+00	000240
2E322030	30284539	30352E32	20303028	45303932	2E322030	30284537	33342E32	2.437E+00	2.290E+00	2.509E+00	2.000260	
35352E32	20303028	45353638	2E322030	30284536	30302E33	20303028	45303438	840E+00	3.006E+00	2.865E+00	2.55000280	
45353539	2E312030	30284532	38302E32	20303028	45323532	2E322030	30284532	2E+00	2.252E+00	2.082E+00	1.955E0002A0	
30204539	39362E38	20303028	45323433	2E312030	30284538	33372E31	20303028	+00	1.738E+00	1.342E+00	8.699E-00	0002C0
20313020	45313635	2E322031	30204534	38392E32	20313020	45393937	2E342031	1	4.799E-01	2.984E-01	2.561E-01	0002E0
2E312030	30284530	30302E31	20303028	45303030	2E312031	30204537	36302E32	2.067E-01	-1.000E+00	-1.000E+00	-1.000E+00	000300
30302E31	20303028	45303030	2E312030	30284530	30302E31	20303028	45303030	000E+00	-1.000E+00	-1.000E+00	-1.000E+00	000320
45313438	2E332030	30284530	30302E31	20303028	45303030	2E312030	30284530	0E+00	-1.000E+00	-1.000E+00	3.841E	000340
30284530	30302E31	20313020	45353334	2E382031	30204536	33312E36	20313020	-01	6.136E-01	8.435E-01	-1.000E+00	000360
20303028	45303030	2E312030	30284530	30302E31	20303028	45303030	2E312030	0	-1.000E+00	-1.000E+00	-1.000E+00	000380
2E312030	30284530	30302E31	20303028	45303030	2E312030	30284530	30302E31	1.000E+00	-1.000E+00	-1.000E+00	-1.000E+00	0003A0
30302E31	20303028	45303030	2E312030	30284530	30302E31	20303028	45303030	000E+00	-1.000E+00	-1.000E+00	-1.000E+00	0003C0
2E312034	39343030	30284530	30302E31	20303028	45303030	2E312030	30284530	0E+00	-1.000E+00	-1.000E+00	0.494E-01	0003E0
30302E31	20303028	45303030	2E312030	30284530	30302E31	20303028	45303030	000E+00	-1.000E+00	-1.000E+00	-1.000E+00	000400
45323339	2E342030	30284539	34322E35	20303028	45303030	2E312030	30284530	0E+00	-1.000E+00	5.249E+00	4.932E	000420
30284536	35332E33	20303028	45373035	2E332030	30284531	30352E34	20303028	+00	4.501E+00	3.507E+00	3.356E+00	000440
20303028	45323438	2E342030	30284535	36342E34	20303028	45363138	2E332030	0	3.816E+00	4.465E+00	4.842E+00	000460
2E332030	30284532	32382E33	20303028	45323732	2E342030	30284537	30372E34	4.707E+00	4.272E+00	3.822E+00	3.000480	
39372E32	20303028	45393631	2E332030	30284538	38332E33	20303028	45373535	557E+00	3.388E+00	3.169E+00	2.790004A0	
45303130	2E322030	30284530	38302E32	20303028	45303833	2E322030	30284538	8E+00	2.380E+00	2.080E+00	2.010E0004C0	
30284530	30302E31	20303028	45343635	2E312030	30284533	35392E31	20303028	+00	1.953E+00	1.564E+00	-1.000E+00	0004E0
20303028	45303030	2E312030	30284530	30302E31	20303028	45303030	2E312030	0	-1.000E+00	-1.000E+00	-1.000E+00	000500
2E312030	30284530	30302E31	20303028	45303030	2E312030	30284530	30302E31	1.000E+00	-1.000E+00	-1.000E+00	-1.000E+00	000520
33392E31	20303028	45303637	2E312030	30284537	38352E31	20303028	45303030	000E+00	1.587E+00	1.760E+00	1.93000540	
45303030	2E312030	30284530	30302E31	20303028	45303030	2E312030	30284532	2E+00	-1.000E+00	-1.000E+00	-1.000E+00	000560
30284530	30302E31	20303028	45303030	2E312030	30284530	30302E31	20303028	+00	-1.000E+00	-1.000E+00	-1.000E+00	000580
20303028	45303030	2E312030	30284530	30302E31	20303028	45303030	2E312030	0	-1.000E+00	-1.000E+00	-1.000E+00	0005A0
2E312030	30284530	30302E31	20303028	45303030	2E312030	30284530	30302E31	1.000E+00	-1.000E+00	-1.000E+00	-1.000E+00	0005C0
20303028	45303030	2E312030	30284530	30302E31	20343934	30303028	45303030	000E+00	0.494E-01	-1.000E+00	-1.000E+00	0005E0
2E372030	30284530	30302E31	20303028	45303030	2E312030	30284530	30302E31	1.000E+00	-1.000E+00	-1.000E+00	7.000600	
30382E34	20303028	45303431	2E362030	30284537	35362E36	20303028	45373030	007E+00	6.657E+00	6.140E+00	4.80000620	
45343632	2E362030	30284537	38322E35	20303028	45323935	2E342030	30284538	8E+00	4.592E+00	5.287E+00	6.264E000640	
30284539	36392E35	20303028	45353935	2E362030	30284537	31382E36	20303028	+00	6.817E+00	6.595E+00	5.969E+00	000660
20303028	45303134	2E352030	30284536	30332E35	20303028	45383234	2E352030	0	5.428E+00	5.306E+00	5.410E+00	000680
2E342030	30284539	34372E34	20303028	45383631	2E352030	30284537	33342E35	5.437E+00	5.168E+00	4.749E+00	4.0006A0	
34372E34	20303028	45353935	2E342030	30284536	31342E34	20303028	45313334	431E+00	4.416E+00	4.595E+00	4.740006C0	
45303028	2E312030	30284530	30302E31	20303028	45303030	2E312030	30284530	0E+00	-1.000E+00	-1.000E+00	-1.000E+00	0006E0
30284530	30302E31	20303028	45303030	2E312030	30284530	30302E31	20303028	+00	-1.000E+00	-1.000E+00	-1.000E+00	000700
20303028	45383337	2E322030	30284530	30302E31	20303028	45303030	2E312030	0	-1.000E+00	-1.000E+00	2.738E+00	000720
2E312030	30254530	30302E31	20303028	45353034	2E332030	30284532	37302E33	3.072E+00	3.405E+00	-1.000E+00	-1.000E+00	000740

Start of
1/16/2021

Dump of tape N0201 p52

-DAB
P.7

```
30302E31 2D30302B 45303030 2E312D30 302B4530 30302E31 2D30302B 45303030 000E+00-1.000E+00-1.000E+00-1.00 000760
45303030 2E312D30 302B4530 30302E31 2D30302B 45303030 2E312D30 302B4530 0E+00-1.000E+00-1.000E+00-1.000E 000780
302B4530 30302E31 2D30302B 45303030 2E312D30 302B4530 30302E31 2D30302B +00-1.000E+00-1.000E+00-1.000E+0 0007A0
5E5E5E5E 5E5E5E5E 5E5E5E30 302B4530 30302E31 2D30302B 45303030 2E312D30 0-1.000E+00-1.000E+00^^^^^^^^^^^^ 0007C0
5E5E5E5E 5E5E5E5E 5E5E5E5E 5E5E5E5E 5E5E5E5E 5E5E5E5E 5E5E5E5E 5E5E5E5E ^^^^^^^^^^^^^^^^^^^^^^^^^^^^^^^^^^^^^ 0007E0
```

Dump of tape 110241 p53

-04B
P.8

Dump of device MTA1: on 15-DEC-1988 17:03:51.63

Block number 1 (00000001), 80 (0050) bytes

```
20202020 20202020 20202020 20202020 20202020 20202032 30324F4E 314C4F56 VOL1N0202 000000
20202020 20202020 20202020 20202020 20202020 20202020 20202020 20202020 000020
33202020 20202020 20202020 20202020 3..... 000040
```

Block number 2 (00000002), 80 (0050) bytes

```
30313030 30203230 324F4E20 20202020 20202054 41442E35 38324F4E 31524448 HDR1N0285.DAT N0202 00010 000000
46434544 30303030 30302030 35333838 20303533 38382030 30313030 30313030 001000100 88350 88350 000000DEC F 000020
20202020 20202020 20204131 31454C49 ILE11A ..... 000040
```

Block number 3 (00000003), 80 (0050) bytes

```
20202020 20202020 20202020 20202020 20343934 30303834 30323044 32524448 HDR2D0204800494 000000
20202020 20202020 20202020 30302020 20202020 20202020 20202020 20202020 00 000020
20202020 20202020 20202020 20202020 ..... 000040
```

Block number 4 (00000004), 80 (0050) bytes

```
30303030 30303030 31303030 30303030 30303030 32303230 41453130 33524448 HDR301EA0202000000000000100000000 000000
30303030 30303030 30303030 30303030 30303030 30303030 30303030 30303030 00000000000000000000000000000000 000020
20202020 20202020 20202020 30303030 0000 ..... 000040
```

Block number 5 (00000005), 80 (0050) bytes

```
20202020 20202020 20202020 20202020 20202020 20202020 20202020 34524448 HDR4 000000
20202020 20202020 20202020 20202020 20202020 20202020 20202020 20202020 000020
20202020 20202020 20202030 30202020 00 ..... 000040
```

*** End of file ***

Header information

Dump of tape N0202

Block number 6 (00000006), 2048 (0800) bytes

39343032	332E3235	2D202020	20312020	20203538	39312031	32393731	39323030	002917921	1985	1	-52.32049	000000
2030302B	45353735	2E322030	302B4534	35382E32	2030302B	45303030	2E312D34	4-1.000E+00	2.854E+00	2.575E+00	000020	000020
2E312030	302B4533	33392E31	2030302B	45313331	2E322030	302B4536	33332E32	2.336E+00	2.131E+00	1.933E+00	1.000040	000040
37312E32	2030302B	45333939	2E312030	302B4535	34382E31	2030302B	45313638	861E+00	1.845E+00	1.993E+00	2.17	000060
45303937	2E312030	302B4531	31312E32	2030302B	45393532	2E322030	302B4537	7E+00	2.259E+00	2.111E+00	1.790E	000080
302B4535	30332E31	2030302B	45303233	2E312030	302B4532	37342E31	2030302B	+00	1.472E+00	1.320E+00	1.305E+0	0000A0
2031302D	45333135	2E322031	302D4537	30332E38	2030302B	45333132	2E312030	0	1.213E+00	8.307E-01	2.513E-01-	0000C0
2E312030	302B4530	30302E31	2031302D	45313338	2E352033	302D4530	33332E31	1.330E-03	5.831E-01-	1.000E+00-1.	0000E0	0000C0
34322E34	2030302B	45303030	2E312030	302B4530	30302E31	2D30302B	45303030	000E+00-	1.000E+00-	1.000E+00	4.24	000100
45323030	2E342031	302D4531	36312E34	2031302D	45323832	2E342031	302D4530	0E-01	4.282E-01	4.161E-01	4.002E	000120
302B4530	30302E31	2D30302B	45303030	2E312031	302D4538	39302E34	2031302D	-01	4.098E-01-	1.000E+00-	1.000E+00	000140
2D30302B	45303030	2E312030	302B4530	30302E31	2D30302B	45303030	2E312030	0-1.000E+00-	1.000E+00-	1.000E+00-	1.000E+00-	000160
2E312030	302B4530	30302E31	2D30302B	45303030	2E312030	302B4530	30302E31	1.000E+00-	1.000E+00-	1.000E+00-	1.000E+00-	000180
30302E31	2D30302B	45303030	2E312030	302B4530	30302E31	2D30302B	45303030	000E+00-	1.000E+00-	1.000E+00-	1.000E+00-	0001A0
45303030	2E312030	302B4530	30302E31	2D30302B	45303030	2E312030	302B4530	0E+00-	1.000E+00-	1.000E+00-	1.000E+00-	0001C0
302B4530	30302E31	2D30302B	45303030	2E312030	302B4530	30302E31	2D30302B	+00-	1.000E+00-	1.000E+00-	1.000E+00-	0001E0
45303333	2E342030	302B4530	30302E31	2D343934	3030302B	45303030	2E312030	0-1.000E+00	4.94-1.000E+00	4.330E	000200	000200
302B4538	39332E33	2030302B	45363237	2E332030	302B4531	34302E34	2030302B	+00	4.041E+00	3.726E+00	3.398E+0	000220
2030302B	45303737	2E322030	302B4536	36382E32	2030302B	45303330	2E332030	0	3.030E+00	2.866E+00	2.770E+00	000240
2E332030	302B4531	31332E33	2030302B	45373531	2E332030	302B4530	31392E32	2.910E+00	3.157E+00	3.311E+00	3.	000260
38322E32	2030302B	45393934	2E322030	302B4533	36382E32	2030302B	45363931	198E+00	2.863E+00	2.499E+00	2.28	000280
45313136	2E312030	302B4531	34302E32	2030302B	45383931	2E322030	302B4533	3E+00	2.198E+00	2.041E+00	1.611E	0002A0
302B4533	30352E31	2031302D	45323630	2E382030	302B4538	31302E31	2030302B	+00	1.018E+00	8.062E-01	1.503E+0	0002C0
2D30302B	45303030	2E312030	302B4530	30302E31	2D30302B	45303030	2E312030	0-1.000E+00-	1.000E+00-	1.000E+00-	1.000E+00-	0002E0
2E322031	302D4539	39382E31	2031302D	45323532	2E322030	302B4530	30302E31	1.000E+00	2.252E-01	1.899E-01	2.	000300
31322E35	2031302D	45303930	2E342031	302D4533	33382E32	2031302D	45393530	059E-01	2.833E-01	4.090E-01	5.21	000320
45343133	2E332031	302D4535	30372E34	2031302D	45373335	2E352031	302D4535	5E-01	5.537E-01	4.705E-01	3.314E	000340
302B4530	30302E31	2D30302B	45303030	2E312030	302B4530	30302E31	2D31302D	-01-	1.000E+00-	1.000E+00-	1.000E+00-	000360
2D30302B	45303030	2E312030	302B4530	30302E31	2D30302B	45303030	2E312030	0-1.000E+00-	1.000E+00-	1.000E+00-	1.000E+00-	000380
2E312030	302B4530	30302E31	2D30302B	45303030	2E312030	302B4530	30302E31	1.000E+00-	1.000E+00-	1.000E+00-	1.000E+00-	0003A0
30302E31	2D30302B	45303030	2E312030	302B4530	30302E31	2D30302B	45303030	000E+00-	1.000E+00-	1.000E+00-	1.000E+00-	0003C0
2E312034	39343030	302B4530	30302E31	2D30302B	45303030	2E312030	302B4530	0E+00-	1.000E+00-	1.000E+00	4.94-	0003E0
32362E35	2030302B	45343939	2E352030	302B4531	37312E36	2030302B	45303030	000E+00	6.171E+00	5.994E+00	5.62	000400
45383732	2E342030	302B4535	36352E34	2030302B	45363431	2E352030	302B4533	3E+00	5.146E+00	4.565E+00	4.278E	000420
302B4530	35332E34	2030302B	45323031	2E342030	302B4536	35302E34	2030302B	+00	4.056E+00	4.102E+00	4.350E+0	000440
2030302B	45363733	2E342030	302B4538	37352E34	2030302B	45323735	2E342030	0	4.572E+00	4.578E+00	4.376E+00	000460
2E332030	302B4530	35362E33	2030302B	45343438	2E332030	302B4531	39302E34	4.091E+00	3.844E+00	3.650E+00	3.	000480
39302E32	2030302B	45393336	2E322030	302B4532	30312E33	2030302B	45303334	430E+00	3.102E+00	2.639E+00	2.09	0004A0
45303030	2E312030	302B4530	30302E31	2D30302B	45313335	2E312030	302B4536	6E+00	1.531E+00-	1.000E+00-	1.000E+00-	0004C0
302D4537	31352E37	2030302B	45303030	2E312030	302B4530	30302E31	2D30302B	+00-	1.000E+00-	1.000E+00	7.517E-0	0004E0
2031302D	45353636	2E392031	302D4533	35322E37	2031302D	45313837	2E362031	1	6.781E-01	7.253E-01	9.665E-01	000500
2E312030	302B4534	38392E31	2030302B	45383937	2E312030	302B4538	38332E31	1.388E+0D	1.798E+00	1.984E+00	1.	000520
30302E31	2D30302B	45303030	2E312030	302B4533	35332E31	2030302B	45373038	807E+00	1.353E+00-	1.000E+00-	1.000E+00-	000540
45303030	2E312030	302B4530	30302E31	2D30302B	45303030	2E312030	302B4530	0E+00-	1.000E+00-	1.000E+00-	1.000E+00-	000560
302B4530	30302E31	2D30302B	45303030	2E312030	302B4530	30302E31	2D30302B	+00-	1.000E+00-	1.000E+00-	1.000E+00-	000580
2D30302B	45303030	2E312030	302B4530	30302E31	2D30302B	45303030	2E312030	0-1.000E+00-	1.000E+00-	1.000E+00-	1.000E+00-	0005A0
2E312030	302B4530	30302E31	2D30302B	45303030	2E312030	302B4530	30302E31	1.000E+00-	1.000E+00-	1.000E+00-	1.000E+00-	0005C0
2030302B	45333539	2E372030	302B4530	30302E31	2D343934	3030302B	45303030	000E+00	4.94-	1.000E+00	7.953E+00	0005E0
2E362030	302B4530	32302E37	2030302B	45323036	2E372030	302B4537	37392E37	7.977E+00	7.602E+00	7.020E+00	6.	000600
39352E35	2030302B	45393236	2E352030	302B4534	33392E35	2030302B	45393932	299E+00	5.934E+00	5.629E+00	5.59	000620
45343931	2E362030	302B4531	39302E36	2030302B	45313338	2E352030	302B4538	8E+00	5.831E+00	6.091E+00	6.194E	000640
302B4535	34392E35	2030302B	45323230	2E362030	302B4537	33312E36	2030302B	+00	6.137E+00	6.022E+00	5.945E+0	000660
2030302B	45323932	2E352030	302B4531	31372E35	2030302B	45353838	2E352030	0	5.885E+00	5.711E+00	5.292E+00	000680
2E312030	302B4536	31352E33	2030302B	45353739	2E332030	302B4530	34362E34	4.640E+00	3.975E+00	3.516E+00-	1.	0006A0
30302E31	2D30302B	45303030	2E312030	302B4530	30302E31	2D30302B	45303030	000E+00-	1.000E+00-	1.000E+00-	1.000E+00-	0006C0
45373333	2E332030	302B4535	33342E33	2030302B	45343235	2E332030	302B4530	0E+00	3.524E+00	3.435E+00	3.337E	0006E0
302B4537	30392E33	2030302B	45323636	2E332030	302B4539	39332E33	2030302B	+00	3.399E+00	3.662E+00	3.907E+0	000700
2D30302B	45363138	2E322030	302B4536	35342E33	2030302B	45343838	2E332030	0	3.884E+00	3.456E+00	2.816E+00-	000720
2E312030	302B4530	30302E31	2D30302B	45303030	2E312030	302B4530	30302E31	1.000E+00-	1.000E+00-	1.000E+00-	1.	000740

04B
P.9

Start of orbit 17921

Dump of tape 00242 pg 2

-04 B
p.10

30302E31 2D30302B 45303030 2E312D30 302B4530 30302E31 2D30302B 45303030 00E+00-1.000E+00-1.000E+00-1.00 000760
45303030 2E312D30 302B4530 30302E31 2D30302B 45303030 2E312D30 302B4530 0E+00-1.000E+00-1.000E+00-1.000E 000780
302B4530 30302E31 2D30302B 45303030 2E312D30 302B4530 30302E31 2D30302B +00-1.000E+00-1.000E+00-1.000E+0 0007A0
5E5E5E5E 5E5E5E5E 5E5E5E30 302B4530 30302E31 2D30302B 45303030 2E312D30 0-1.000E+00-1.000E+00^^^^^^^^^^^^ 0007C0
5E5E5E5E 5E5E5E5E 5E5E5E5E 5E5E5E5E 5E5E5E5E 5E5E5E5E 5E5E5E5E 5E5E5E5E ^^^^^^^^^^^^^^^^^^^^^^^^^^^^^^^^^^^^^ 0007E0

Dumpof tape 00202 pg 3

-048
p. 11

SME VISIBLE SPECTROMETER REFERENCES

Barth, C.A., R.W. Sanders, G.E. Thomas, G.J. Rottman, D.W. Rusch, R.J. Thomas, G.H. Mount, G.M. Lawrence, J.M. Zawodny, R.A. West and J. London, Solar Mesosphere Explorer measurements of the El Chicon volcanic cloud, *Bull. Amer. Meteor. Soc.*, *63*, 1314, 1982.

Barth, C.A., D.W. Rusch, R.J. Thomas, G.H. Mount, G.J. Rottman, G.E. Thomas, R.W. Sanders, G.M. Lawrence, Solar Mesosphere Explorer: Scientific objectives and results, *Geophys. Res. Lett.* *10*, 237-240, 1983.

Clancy, R.T., El Chichon and "mystery cloud" aerosols between 30 and 55 km: Global observations from the SME visible spectrometer, *Geophys. Res. Lett.* *13*, 937-940, 1986.

Mount, G.H., D.W. Rusch, J.M. Zawodny, J.F. Noxon, C.A. Barth, G.J. Rottman, R.J. Thomas, G.E. Thomas, R.W. Sanders, G.M. Lawrence, Measurements of NO₂ in the Earth's stratosphere using a limb scanning visible light spectrometer, *Geophys. Res. Lett.* *10*, 265-268, 1983.

Mount, G.H., D.W. Rusch, J.F. Noxon, J.M. Zawodny, and C.A. Barth, Measurements of stratospheric NO₂ from the Solar Mesosphere Explorer satellite. 1. An overview of the results, *J. Geophys. Res.* *89*, 1327-1340, 1984.

Naudet, J.P. and G.E. Thomas, Aerosol optical depth and planetary albedo in the visible from the Solar Mesosphere Explorer, *J. Geophys. Res.* *92*, 8373-8381, 1987.

Naudet, J.P., R.J. Thomas, D.W. Rusch and R.T. Clancy, Distribution of Stratospheric NO₂ at 10 mbar: SME global morphology and comparison to LIMS observations, *J. Geophys. Res.* *92* 9863-9867, 1987.

-04 B
p.12

Naudet, J.P., D.W. Rusch, R.J. Thomas, R.T. Clancy, C.A. Barth, J. Wedding, J.M. Zawodny, P. Fabian and M. Helten, Stratospheric NO₂ from the Solar Mesosphere Explorer during MAP/GLOBUS 1983, *Planet. Space Sci.* 35, 631-6635, 1987.

Rusch, D.W., G.H. Mount, J.M. Zawodny, C.A. Barth, G.J. Rottman, R.J. Thomas, G.E. Thomas, R.W. Sanders, G.M. Lawrence, Temperature measurements in the Earth's stratosphere using a limb scanning visible light spectrometer, *Geophys. Res. Lett.* 10, 261-264, 1983.

Solomon, S., G.H. Mount, and J.M. Zawodny, Measurements of stratospheric NO₂ from the Solar Mesosphere Explorer satellite. 2. General morphology of observed NO₂ and derived N₂O₅, *J. Geophys. Res.* 89, 7317-7321, 1984.

Thomas, G.E., C.A. Barth, E.R. Hansen, C.W. Hord, G.M. Lawrence, G.H. Mount, G.J. Rottman, D.W. Rusch, A.I. Stewart, R.J. Thomas, J. London, P.L. Bailey, P.J. Crutzen, R.E. Dickenson, J.C. Gille, S.C. Liu, J.F. Noxon, and C.B. Farmer: Scientific objectives of the Solar Mesosphere Explorer mission, *Pageoph*, 118, 591-615, 1980.

Thomas, R.J., K.H. Rosenlof, R.T. Clancy and J.M. Zawodny, Stratospheric NO₂ over Antarctica as measured by the Solar Mesosphere Explorer during austral spring, 1986. *J. Geophys. Res.* 93, 12561-12568, 1988.

Zawodny, J.M., Short-term variability of nitrogen dioxide in the winter stratosphere, *J. Geophys. Res.* 91, 5439-5450, 1986.

Zawodny, J.M., and D.W. Rusch, Seasonal behavior of NO₂ in the winter stratosphere: Inferred NO_x, *J. Geophys. Res.* 91, 5451-5454, 1986.

81-1007-072
Dec 88

LABORATORY FOR ATMOSPHERIC AND SPACE PHYSICS

SOLAR MESOSPHERE EXPLORER

MONTHLY AVERAGE NO2 DATA FOR THE

NATIONAL SPACE SCIENCE DATA CENTER

1982-1986 DATA

The SOLAR MESOSPHERE EXPLORER (SME) monthly average data was derived from the visible spectrometer radiance measurements. A description of the mission, the instruments, the scientific objectives, and the initial results is contained in a series of articles in the April 1983 issue of Geophysical Research Letters (10:237-267). In Mount et al. (JGR 89: 1327-1340, 1984) there is a more comprehensive paper on the visible instrument and data analysis.

The nitrogen dioxide mixing ratios in parts per billion by volume are given on pressure surfaces from about 24 to 40 km between 120 degrees South and 120 degrees North at each 5 degrees. Latitudes between 90 S and 90 N indicate normal data, taken at an afternoon local time. During times when the pole is sunlit, SME was able to take data on both sides of the pole. Crossing the pole gives an early morning local time. In order to differentiate between data taken at these different local times, latitude labeling was extended beyond 90 degrees. So, latitudes greater than 90 indicate morning data, while latitudes less than 90 indicate afternoon data. For example, a latitude of 110 N would indicate data taken at 70 N in the morning.

Dr. C.A. Barth is the principal investigator for the SME experiment. Co-investigators Drs. R.J. Thomas, D.W. Rusch, G.E. Thomas, and G.J. Rottman are resident at the Laboratory for Atmospheric and Space Physics at the University of Colorado, Boulder, Colorado, 80309.

-040
p.2

There is one file on this tape. The tape is labeled NO2MON, and the file is SMENO2M.DAT. The blocksize on this tape is 396. There is one physical record per block.

These data, derived from the visible spectrometer on SME, are monthly average NO2 mixing ratios. They cover the years 1982 through 1986. Units are parts per billion by volume. The data record format is described in the following table.

Description of SMENO2M.DAT, monthly averages of NO2 mixing ratios in ppbv. Missing data is indicated by -1.0. The pressure in millibars ranges from 31.6228 to 4.217 mb. There are 8 pressure levels and 48 latitudes. Pressure levels are evenly spaced in terms of LOG(pressure). The LOG values range from 1.5 to .625 in increments of .125. The pressure in mb is given on the tape. Latitudes range from 120 S to 120 N in 5 degree increments. Values of latitude greater than 90 indicate morning data, while data between 90S and 90N was taken in the afternoon. Data at 120 S would be in the morning at 60S, while data at 60 S would be in the afternoon.

DATE: 1982 MONTH 1

Record	Format	Description
1	1X,I4,1X,I2	Year, Month
2	1X,F8.4,3X,48(F7.3,1X)	Pressure, NO2MR(48), this is for pressure=31.6 mb.
3	1X,F8.4,3x,48(F7.3,1X)	Pressure, NO2MR(48), this is for pressure=23.7 mb.
.	.	.
9	1X,F8.4,3x,48(F7.3,1X)	Pressure, NO2MR(48), this is for pressure=4.217 mb.
10	12X,48(1X,F6.1,1X)	XLAT(48), latitudes which correspond to 48 NO2 values in each record.
11	1X,I4,1X,I2	IDUM1, IDUM2...these are both equal to 0, this signifies the end of the month.

DATE: 1982 MONTH 2

12	repeat record 1
13	repeat record 2

etc., the first 11 records repeat through 1986 MONTH 12. Please note: Data for Jan. 1982 and Dec. 1986 are missing. The records for this data exist on the tape, they are filled with -1.0s. All other months in the range given do contain data, although not for all latitudes and pressures.

04C
p. 3

LABORATORY FOR ATMOSPHERIC AND SPACE PHYSICS

SOLAR MESOSPHERE EXPLORER

MONTHLY AVERAGE NITROGEN DIOXIDE DATA FOR THE

NATIONAL SPACE SCIENCE DATA CENTER

APPENDIX

The enclosed tape has the following characteristics:

1. 9-track, 1600 bpi. Written on a Digital TU77 drive.
2. ANSI STANDARD tape headers and End-of-File (EOF) structure (7-bit ASCII characters) as per VAX 11/780 system software. After the Volume Header record (80 bytes), there are four File Header records (80 bytes each), one EOF, the data records (396 bytes each), one EOF, four File Trailer records (80 bytes each), and one EOF for each of the data files on this tape.
3. These tapes were made using the VMS COPY command after first initializing each tape.
4. Physical data blocks are 396 bytes long; each block contains one logical record.
5. The VAX writes bytes onto a 9-track tape in the following order:

Vax word	0	1	2	3	4	5	6	7	8	9	10	11	12	13	14	15
Vax tape	<----->								<----->							
Word written	2nd								1st							

The resulting tape (up is the tape beginning direction)

8	9	10	11	12	13	14	15	Word part 2
0	1	2	3	4	5	6	7	Word part 1

6. An annotated dump is attached which shows the contents of the first twenty physical blocks for this tape. The left side of the dump shows the hexadecimal word (read from right to left) and the right side of the dump shows the ASCII equivalent word contents (read from left to right). The last column on the right is the hexadecimal 4-byte word number for the rightmost four bytes in the hexadecimal dump section.

Block number 1 (00000001), 80 (0050) bytes

20202020	20202020	20202020	20202020	20202020	20204E4F	4D324F4E	314C4F56	VOL1ND2MDN	000000
20202020	20202020	20202020	20202020	20202020	20202020	20202020	20202020		000020
				33202020	20202020	20202020	20202020	3.....	000040

Header information

Block number 2 (00000002), 80 (0050) bytes

30313030	304E4F4D	324F4E20	20202020	20544144	2E4D324F	4E454D53	31524448	HDR1SHEND2M.DAT	ND2MDN00010	000000		
46434544	30303030	30302039	34333838	20393433	38382036	30313030	30313030	001000106	88349	88349	000000DEC	000020
				20202020	20202020	20204131	31454C49	ILE11A				000040

Block number 3 (00000003), 80 (0050) bytes

20202020	20202020	20202020	20202020	20363933	30303639	33303046	32524448	HDR2F0039600396		000000
20202020	20202020	20202020	30302020	20202020	20202020	20202020	20202020		00	000020
				20202020	20202020	20202020	20202020			000040

Block number 4 (00000004), 80 (0050) bytes

30303030	30303030	31303030	30303030	30303030	31303230	43383130	33524448	HDR3018C020100000000000100000000	000000	
30303030	30303030	30303030	30303030	30303030	43383130	30303030	30303030	0000000018C000000000000000000000	000020	
				20202020	20202020	20202020	30303030	0000		000040

Block number 5 (00000005), 80 (0050) bytes

20202020	20202020	20202020	20202020	20202020	20202020	20202020	20202020	34524448	HDR4	000000
20202020	20202020	20202020	20202020	20202020	20202020	20202020	20202020	20202020		000020
				20202020	20202020	20202030	30202020		00	000040

*** End of file ***

*040
P.7*

Dump of device MTA0: on 14-DEC-1988 18:24:27.27

Block number 15 (0000000F), 396 (018C) bytes

31312020	20302E35	31312020	20302E30	32312020	20202020	20202020	20202020			-120.0	-115.0	-11	000000
392D2020	20302E35	392D2020	20302E30	30312020	20302E35	30312020	20302E30	0.0	-105.0	-100.0	-95.0	-9	000020
372D2020	20302E35	372D2020	20302E30	382D2020	20302E35	382D2020	20302E30	0.0	-85.0	-80.0	-75.0	-7	000040
352D2020	20302E35	352D2020	20302E30	362D2020	20302E35	362D2020	20302E30	0.0	-65.0	-60.0	-55.0	-5	000060
332D2020	20302E35	332D2020	20302E30	342D2020	20302E35	342D2020	20302E30	0.0	-45.0	-40.0	-35.0	-3	000080
312D2020	20302E35	312D2020	20302E30	322D2020	20302E35	322D2020	20302E30	0.0	-25.0	-20.0	-15.0	-1	0000A0
31202020	20302E35	20202020	20302E30	20202020	20302E35	20202020	20302E30	0.0	-5.0	0.0	5.0	1	0000C0
33202020	20302E35	32202020	20302E30	32202020	20302E35	31202020	20302E30	0.0	15.0	20.0	25.0	3	0000E0
35202020	20302E35	34202020	20302E30	34202020	20302E35	33202020	20302E30	0.0	35.0	40.0	45.0	5	000100
37202020	20302E35	36202020	20302E30	36202020	20302E35	35202020	20302E30	0.0	55.0	60.0	65.0	7	000120
39202020	20302E35	38202020	20302E30	38202020	20302E35	37202020	20302E30	0.0	75.0	80.0	85.0	9	000140
31312020	20302E35	30312020	20302E30	30312020	20302E35	39202020	20302E30	0.0	95.0	100.0	105.0	11	000160
					20302E35	31312020	20302E30	0.0	115.0	000180

Block number 16 (00000010), 396 (018C) bytes

20202020	20202020	20202020	20202020	20202020	20202020	30202030	20202020	0	0				000000
20202020	20202020	20202020	20202020	20202020	20202020	20202020	20202020						000020
20202020	20202020	20202020	20202020	20202020	20202020	20202020	20202020						000040
20202020	20202020	20202020	20202020	20202020	20202020	20202020	20202020						000060
20202020	20202020	20202020	20202020	20202020	20202020	20202020	20202020						000080
20202020	20202020	20202020	20202020	20202020	20202020	20202020	20202020						0000A0
20202020	20202020	20202020	20202020	20202020	20202020	20202020	20202020						0000C0
20202020	20202020	20202020	20202020	20202020	20202020	20202020	20202020						0000E0
20202020	20202020	20202020	20202020	20202020	20202020	20202020	20202020						000100
20202020	20202020	20202020	20202020	20202020	20202020	20202020	20202020						000120
20202020	20202020	20202020	20202020	20202020	20202020	20202020	20202020						000140
20202020	20202020	20202020	20202020	20202020	20202020	20202020	20202020						000160
20202020	20202020	20202020	20202020	20202020	20202020	20202020	20202020						000180

Block number 17 (00000011), 396 (018C) bytes

20202020	20202020	20202020	20202020	20202020	20202020	32202032	38393120	1982	2				000000
20202020	20202020	20202020	20202020	20202020	20202020	20202020	20202020						000020
20202020	20202020	20202020	20202020	20202020	20202020	20202020	20202020						000040
20202020	20202020	20202020	20202020	20202020	20202020	20202020	20202020						000060
20202020	20202020	20202020	20202020	20202020	20202020	20202020	20202020						000080
20202020	20202020	20202020	20202020	20202020	20202020	20202020	20202020						0000A0
20202020	20202020	20202020	20202020	20202020	20202020	20202020	20202020						0000C0
20202020	20202020	20202020	20202020	20202020	20202020	20202020	20202020						0000E0
20202020	20202020	20202020	20202020	20202020	20202020	20202020	20202020						000100
20202020	20202020	20202020	20202020	20202020	20202020	20202020	20202020						000120
20202020	20202020	20202020	20202020	20202020	20202020	20202020	20202020						000140
20202020	20202020	20202020	20202020	20202020	20202020	20202020	20202020						000160
20202020	20202020	20202020	20202020	20202020	20202020	20202020	20202020						000180

end Jan 1982

start Feb 1982

8d
-040

Block number 18 (00000012), 396 (018C) bytes

2E312D20	20303030	2E312D20	20303030	2E312D20	20202038	3232362E	31332020	31.6228	-1.000	-1.000	-1.000000	
2E312D20	20303030	2E312D20	20303030	2E312D20	20303030	2E312D20	20303030	000	-1.000	-1.000	-1.000020	
2E322020	20303030	2E312D20	20303030	2E312D20	20303030	2E312D20	20303030	000	-1.000	-1.000	2.000040	
2E312020	20363836	2E312020	20363737	2E312020	20333638	2E312020	20333430	043	1.863	1.776	1.686	1.000060
2E302020	20303636	2E302020	20313739	2E302020	20393832	2E312020	20353435	545	1.289	0.971	0.660	0.000080
2E302020	20343833	2E302020	20323633	2E302020	20393633	2E302020	20323534	452	0.369	0.362	0.384	0.0000A0
2E302020	20303333	2E302020	20363433	2E302020	20353833	2E302020	20343933	394	0.385	0.346	0.330	0.0000C0
2E312020	20323137	2E302020	20303735	2E302020	20313334	2E302020	20303333	330	0.431	0.570	0.712	-1.0000E0
2E312020	20303030	2E312020	20303030	2E312020	20303030	2E312020	20303030	000	-1.000	-1.000	-1.000	-1.000100
2E312020	20303030	2E312020	20303030	2E312020	20303030	2E312020	20303030	000	-1.000	-1.000	-1.000	-1.000120
2E312020	20303030	2E312020	20303030	2E312020	20303030	2E312020	20303030	000	-1.000	-1.000	-1.000	-1.000140
2E312020	20303030	2E312020	20303030	2E312020	20303030	2E312020	20303030	000	-1.000	-1.000	-1.000	-1.000160
2E312020	20303030	2E312020	20303030	2E312020	20303030	2E312020	20303030	000	-1.000	-1.000	-1.000	-1.000180

Block number 19 (00000013), 396 (018C) bytes

2E312D20	20303030	2E312D20	20303030	2E312D20	20202037	3331372E	33322020	23.7137	-1.000	-1.000	-1.000000	
2E332020	20383339	2E332020	20303030	2E312D20	20303030	2E312D20	20303030	000	-1.000	-1.000	3.938	3.000020
2E332020	20393531	2E332020	20363933	2E332020	20333437	2E332020	20393538	859	3.743	3.396	3.159	3.000040
2E322020	20343938	2E322020	20353030	2E332020	20373430	2E332020	20343630	064	3.047	3.005	2.894	2.000060
2E312020	20383634	2E312020	20313239	2E312020	20313533	2E322020	20333936	693	2.351	1.921	1.468	1.000080
2E302020	20313936	2E302020	20343737	2E302020	20353438	2E302020	20333830	083	0.845	0.774	0.691	0.0000A0
2E302020	20303831	2E302020	20343433	2E302020	20353035	2E302020	20303036	600	0.505	0.344	0.180	0.0000C0
2E312020	20373930	2E312020	20303135	2E302020	20343031	2E302020	20373730	077	0.104	0.510	1.097	1.0000E0
2E312020	20313932	2E312020	20353934	2E312020	20383336	2E312020	20303734	470	1.638	1.495	1.291	1.000100
2E302020	20323734	2E302020	20313436	2E302020	20393739	2E302020	20303231	120	0.979	0.641	0.472	0.000120
2E312020	20303030	2E312020	20303030	2E312020	20303030	2E312020	20363033	306	-1.000	-1.000	-1.000	-1.000140
2E312020	20303030	2E312020	20303030	2E312020	20303030	2E312020	20303030	000	-1.000	-1.000	-1.000	-1.000160
2E312020	20303030	2E312020	20303030	2E312020	20303030	2E312020	20303030	000	-1.000	-1.000	-1.000	-1.000180

Block number 20 (00000014), 396 (018C) bytes

2E312D20	20303030	2E312D20	20303030	2E312D20	20202038	3238372E	37312020	17.7828	-1.000	-1.000	-1.000000	
2E342020	20333030	2E352020	20303030	2E312020	20303030	2E312020	20303030	000	-1.000	-1.000	5.003	4.000020
2E342020	20373533	2E342020	20333734	2E342020	20383239	2E342020	20353339	935	4.828	4.473	4.357	4.000040
2E342020	20353136	2E342020	20383038	2E342020	20393237	2E342020	20333934	493	4.728	4.808	4.615	4.000060
2E322020	20393831	2E332020	20373035	2E332020	20393938	2E332020	20383832	288	3.899	3.507	3.189	2.000080
2E312020	20303431	2E322020	20353933	2E322020	20383336	2E322020	20333938	893	2.638	2.395	2.140	1.0000A0
2E302020	20393237	2E302020	20363533	2E312020	20353337	2E312020	20333639	963	1.735	1.356	0.729	0.0000C0
2E322020	20373332	2E322020	20333531	2E312020	20373434	2E302020	20303134	410	0.447	1.153	2.237	2.0000E0
2E322020	20343132	2E322020	20333435	2E322020	20353738	2E322020	20303739	970	2.875	2.543	2.214	2.000100
2E302020	20343433	2E312020	20313936	2E312020	20353339	2E312020	20323430	042	1.935	1.691	1.344	0.000120
2E312020	20303030	2E312020	20303030	2E312020	20303030	2E312020	20363239	926	-1.000	-1.000	-1.000	-1.000140
2E312020	20303030	2E312020	20303030	2E312020	20303030	2E312020	20303030	000	-1.000	-1.000	-1.000	-1.000160
2E312020	20303030	2E312020	20303030	2E312020	20303030	2E312020	20303030	000	-1.000	-1.000	-1.000	-1.000180

042
19

-04c
p. 10

SME VISIBLE SPECTROMETER REFERENCES

- Barth, C.A., R.W. Sanders, G.E. Thomas, G.J. Rottman, D.W. Rusch, R.J. Thomas, G.H. Mount, G.M. Lawrence, J.M. Zawodny, R.A. West and J. London, Solar Mesosphere Explorer measurements of the El Chicon volcanic cloud, *Bull. Amer. Meteor. Soc.*, *63*, 1314, 1982.
- Barth, C.A., D.W. Rusch, R.J. Thomas, G.H. Mount, G.J. Rottman, G.E. Thomas, R.W. Sanders, G.M. Lawrence, Solar Mesosphere Explorer: Scientific objectives and results, *Geophys. Res. Lett.* *10*, 237-240, 1983.
- Clancy, R.T., El Chichon and "mystery cloud" aerosols between 30 and 55 km: Global observations from the SME visible spectrometer, *Geophys. Res. Lett.* *13*, 937-940, 1986.
- Mount, G.H., D.W. Rusch, J.M. Zawodny, J.F. Noxon, C.A. Barth, G.J. Rottman, R.J. Thomas, G.E. Thomas, R.W. Sanders, G.M. Lawrence, Measurements of NO₂ in the Earth's stratosphere using a limb scanning visible light spectrometer, *Geophys. Res. Lett.* *10*, 265-268, 1983.
- Mount, G.H., D.W. Rusch, J.F. Noxon, J.M. Zawodny, and C.A. Barth, Measurements of stratospheric NO₂ from the Solar Mesosphere Explorer satellite. 1. An overview of the results, *J. Geophys. Res.* *89*, 1327-1340, 1984.
- Naudet, J.P. and G.E. Thomas, Aerosol optical depth and planetary albedo in the visible from the Solar Mesosphere Explorer, *J. Geophys. Res.* *92*, 8373-8381, 1987.
- Naudet, J.P., R.J. Thomas, D.W. Rusch and R.T. Clancy, Distribution of Stratospheric NO₂ at 10 mbar: SME global morphology and comparison to LIMS observations, *J. Geophys. Res.* *92* 9863-9867, 1987.

-04c
p.11

Naudet, J.P., D.W. Rusch, R.J. Thomas, R.T. Clancy, C.A. Barth, J. Wedding, J.M. Zawodny, P. Fabian and M. Helten, Stratospheric NO₂ from the Solar Mesosphere Explorer during MAP/GLOBUS 1983, *Planet. Space Sci.* 35, 631-6635, 1987.

Rusch, D.W., G.H. Mount, J.M. Zawodny, C.A. Barth, G.J. Rottman, R.J. Thomas, G.E. Thomas, R.W. Sanders, G.M. Lawrence, Temperature measurements in the Earth's stratosphere using a limb scanning visible light spectrometer, *Geophys. Res. Lett.* 10, 261-264, 1983.

Solomon, S., G.H. Mount, and J.M. Zawodny, Measurements of stratospheric NO₂ from the Solar Mesosphere Explorer satellite. 2. General morphology of observed NO₂ and derived N₂O₅, *J. Geophys. Res.* 89, 7317-7321, 1984.

Thomas, G.E., C.A. Barth, E.R. Hansen, C.W. Hord, G.M. Lawrence, G.H. Mount, G.J. Rottman, D.W. Rusch, A.I. Stewart, R.J. Thomas, J. London, P.L. Bailey, P.J. Crutzen, R.E. Dickenson, J.C. Gille, S.C. Liu, J.F. Noxon, and C.B. Farmer: Scientific objectives of the Solar Mesosphere Explorer mission, *Pageoph*, 118, 591-615, 1980.

Thomas, R.J., K.H. Rosenlof, R.T. Clancy and J.M. Zawodny, Stratospheric NO₂ over Antarctica as measured by the Solar Mesosphere Explorer during austral spring, 1986. *J. Geophys. Res.* 93, 12561-12568, 1988.

Zawodny, J.M., Short-term variability of nitrogen dioxide in the winter stratosphere, *J. Geophys. Res.* 91, 5439-5450, 1986.

Zawodny, J.M., and D.W. Rusch, Seasonal behavior of NO₂ in the winter stratosphere: Inferred NO_x, *J. Geophys. Res.* 91, 5451-5454, 1986.

SOLAR MESOPHERE EXPLORE
VISIBLE SPECTROMETER RADIANCE DATA
1982-1986

The visible spectrometer samples data at two wavelengths at a given time. The limb altitude radiance profiles from the visible spectrometer with identifying data are on the tapes. See Mount et. al., 1984 for additional information about the data.

The visible spectrometer was designed to observe limb radiances at two wavelengths simultaneously. There is a short channel radiance and a long channel radiance given for each merged spinset. Data exists for altitudes from 20 to 76 km. Several grating positions have been used, none is continuous throughout the mission. The wavelengths corresponding to the two channels are dependent on which grating position was used. Possible grating positions and the corresponding wavelengths are:

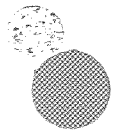
<u>Grating position</u>	<u>long channel</u>	<u>short channel</u>
333	431.84 nm	428.75 nm
344	435.59 nm	432.50 nm
364	442.38 nm	439.31 nm
363	442.04 nm	438.92 nm

Individual spin radiances were calibrated and had a background subtracted before merging. We actually merge the long channel and the ratio of the two channels, the short channel included on the tapes was reconstructed from those two profiles. Radiances are also adjusted for instrument polarization.

After calibrating, the spins (which are data collection rotations of the SME satellite) are merged into groups of up to six spins. Wildpoint and wild spin checking occurs before merging. In order to average together six spin radiance profiles, each profile was interpolated onto a standard altitude grid. This data was then averaged together. The latitude resolution of the merged profiles is about five degrees. These merged profiles are later used as input for the nitrogen dioxide inversion routine.

The radiance data from the visible spectrometer is written in standard ASCII labeled format with one orbit per file. Each orbit consists of 20 to 60 (approximate range) merged spin sets. Filenames are of the format VSxxxxx.NSS, where xxxxx is the orbit number. The data set consists of 23 tapes containing radiance data from Day 1, 1982 through Day 354, 1986. The following is a listing of tapes and orbit intervals contained on the tapes:

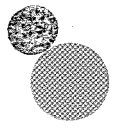
<u>Tape Label</u>	<u>Orbit Interval</u>	<u>Number of Orbits on Tape</u>
VIS001	1316-1999	253
VIS002	2000-2999	358
VIS003	3003-3996	426
VIS004	4000-4898	408
VIS005	4901-5997	381
VIS006	6001-6997	281
VIS007	7002-7996	331
VIS008	8001-8991	323
VIS009	9001-9996	323
VIS010	10001-10991	324
VIS011	11000-11992	326
VIS012	12002-12993	319
VIS013	13001-13994	324
VIS014	14002-15298	424
VIS015	15306-16890	420
VIS016	16903-18997	480
VIS017	19000-20758	399
VIS018	20800-22594	461
VIS019	22606-23996	454
VIS020	24000-25493	447
VIS021	25501-26899	467
VIS022	26900-27699	591
VIS023	27700-28786	311



The ASCII format of the merged spin set data files follows:

FIRST RECORD IN EACH FILE:

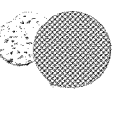
<u>Format</u>	<u>Description</u>
1X,I5	Orbit number
1X,I4	Year
1X,I3	Julian Day
1X,F8.2	Seconds into day (GMT) at start of orbit
1X,F7.2	Longitude of equatorial crossing
23(1X,F5.2)	Altitude profile (note: The grid interval is not constant, it is 1.75 km in the lower part of the profile, and 3.5 km in the upper part.)
1X,I2	Number of profiles in this orbit



MERGED SPIN RECORDS:

<u>Format</u>	<u>Description</u>
1X,I4	Year
I3	Julian Day
F8.2	Seconds into day (GMT)
F6.2	Latitude of merged spin set
F7.2	Longitude of merged spin set
F5.2	Solar zenith angle
I2	Number of spins in merged set (1-6)
I3	Grating position of merged set
23F8.2	Long channel radiances
23F8.2	Short channel radiances

NOTES ABOUT THE DATA

- 
1. An altitude shift has been applied to the data to put it on the best altitude grid

that we can determine. A good assumption is that the altitudes are correct within ± 1 km.

2. Missing radiance data is set to 0. Negative data is a consequence of the data reduction in that a background had to be calculated and then subtracted off. Negative values should only occur at high altitudes. If it does occur at lower altitudes, it would be best to ignore the profile.

3. The altitude scale is actually made up of 2 scales, a lower one with a spacing of 1.75 km and an upper one with a spacing of 3.5 km. This was done to make the NO₂ inversions easier.

4. A value of -1 for equatorial longitude indicates missing data.

NOTES ABOUT THE TAPE

The physical characteristics of the tapes are:

Density	1600 bytes per inch
Tracks	9
Blocksize	408 bytes
Label	VISxxx, where xxx is the tape # in the series

SME VISIBLE SPECTROMETER REFERENCES

- Barth, C.A., R.W. Sanders, G.E. Thomas, G.J. Rottman, D.W. Rusch, R.J. Thomas, G.H. Mount, G.M. Lawrence, J.M. Zawodny, R.A. West and J. London, Solar Mesosphere Explorer measurements of the El Chicon volcanic cloud, *Bull. Amer. Meteor. Soc.*, *63*, 1314, 1982.
- Barth, C.A., D.W. Rusch, R.J. Thomas, G.H. Mount, G.J. Rottman, G.E. Thomas, R.W. Sanders, G.M. Lawrence, Solar Mesosphere Explorer: Scientific objectives and results, *Geophys. Res. Lett.* *10*, 237-240, 1983.
- Mount, G.H., D.W. Rusch, J.M. Zawodny, J.F. Noxon, C.A. Barth, G.J. Rottman, R.J. Thomas, G.E. Thomas, R.W. Sanders, G.M. Lawrence, Measurements of NO₂ in the Earth's stratosphere using a limb scanning visible light spectrometer, *Geophys. Res. Lett.* *10*, 265-268, 1983.
- Mount, G.H., D.W. Rusch, J.F. Noxon, J.M. Zawodny, and C.A. Barth, Measurements of stratospheric NO₂ from the Solar Mesosphere Explorer satellite. 1. An overview of the results, *J. Geophys. Res.* *89*, 1327-1340, 1984.
- Naudet, J.P. and G.E. Thomas, Aerosol optical depth and planetary albedo in the visible from the Solar Mesosphere Explorer, *J. Geophys. Res.* *92*, 8373-8381, 1987.
- Naudet, J.P., R.J. Thomas, D.W. Rusch and R.T. Clancy, Distribution of Stratospheric NO₂ at 10 mbar: SME global morphology and comparison to LIMS observations, *J. Geophys. Res.* *92* 9863-9867, 1987.
- Naudet, J.P., D.W. Rusch, R.J. Thomas, R.T. Clancy, C.A. Barth, J. Wedding, J.M. Zawodny, P. Fabian and M. Helten, Stratospheric NO₂ from the Solar Mesosphere Explorer during MAP/GLOBUS 1983, *Planet. Space Sci.* *35*, 631-6635, 1987.

Rusch, D.W., G.H. Mount, J.M. Zawodny, C.A. Barth, G.J. Rottman, R.J. Thomas, G.E. Thomas, R.W. Sanders, G.M. Lawrence, Temperature measurements in the Earth's stratosphere using a limb scanning visible light spectrometer, *Geophys. Res. Lett.* 10, 261-264, 1983.

Solomon, S., G.H. Mount, and J.M. Zawodny, Measurements of stratospheric NO₂ from the Solar Mesosphere Explorer satellite. 2. General morphology of observed NO₂ and derived N₂O₅, *J. Geophys. Res.* 89, 7317-7321, 1984.

Thomas, G.E., C.A. Barth, E.R. Hansen, C.W. Hord, G.M. Lawrence, G.H. Mount, G.J. Rottman, D.W. Rusch, A.I. Stewart, R.J. Thomas, J. London, P.L. Bailey, P.J. Crutzen, R.E. Dickenson, J.C. Gille, S.C. Liu, J.F. Noxon, and C.B. Farmer: Scientific objectives of the Solar Mesosphere Explorer mission, *Pageoph*, 118, 591-615, 1980.

Zawodny, J.M., Short-term variability of nitrogen dioxide in the winter stratosphere, *J. Geophys. Res.* 91, 5439-5450, 1986.

Zawodny, J.M., and D.W. Rusch, Seasonal behavior of NO₂ in the winter stratosphere: Inferred NO_x, *J. Geophys. Res.* 91, 5451-5454, 1986.

LABORATORY FOR ATMOSPHERIC AND SPACE PHYSICS

SOLAR MESOSPHERE EXPLORER

VISIBLE SPECTROMETER RADIANCE DATA FOR THE

NATIONAL SPACE SCIENCE DATA CENTER

APPENDIX

Each of the enclosed tapes has the following characteristics:

1. 9-track, 1600 bpi. Written on a Digital TU77 drive.
2. ANSI STANDARD tape headers and End-of-File (EOF) structure (7-bit ASCII characters) as per VAX 11/780 system software. After the Volume Header record (80 bytes), there are four File Header records (80 bytes each), one EOF, the data records (408 bytes each), one EOF, four File Trailer records (80 bytes each), and one EOF for each of the data files on this tape.
3. These tapes were made using the VMS COPY command after first initializing each tape.
4. Physical data blocks are 408 bytes long; each block contains one logical record.
5. The VAX writes bytes onto a 9-track tape in the following order:

Vax word	0	1	2	3	4	5	6	7	8	9	10	11	12	13	14	15
Vax tape	←-----→							←-----→								
Word written	2nd							1st								

The resulting tape (up is the tape beginning direction)

8	9	10	11	12	13	14	15	Word part 2
0	1	2	3	4	5	6	7	Word part 1

6. An annotated dump is attached which shows the contents of the first eight physical blocks for each tape in the series. The left side of the dump shows the hexadecimal word (read from right to left) and the right side of the dump shows the ASCII equivalent word contents (read from left to right). The last column on the right is the hexadecimal 4-byte word number for the rightmost four bytes in the hexadecimal dump section.

JULY '88

81-100A-05A
(replacement)

Solar Mesosphere Explorer (SME)
Solar Ultraviolet Spectrometer
Daily Solar Flux Measurements, 115 nm to 302 nm, 1 nm resolution
1982 January 1 through 1988 June 30

Data Tape for NSSDC Archive

The SME Solar UVS daily solar irradiance data are reduced from multiple scans, in 0.25 nm steps, of the full disk solar irradiance at the SME by a spectrometer with a full-width half-maximum resolution of 0.75 nm (Rottman *et al*, 1982). That is, multiple measurements at a resolution of 0.25 nm are convolved with an instrument response function and integrated to a resolution of 1 nm. The data supplied here are computed by a new algorithm which attempts to account for gaps in the measurements by substituting for a missing 0.25 nm grating position a time-averaged mean of the most recent measurements (over several days) at that grating position. Thus there are no "missing" data.* Instead, for each 1-nm datum, a *quality* index is provided which indicates what fraction (0 to 1) of the given datum was derived from actual measurements. For example, a quality index greater than 0.9 indicates that the reduced datum was little influenced by "fill" data, whereas a quality index of less than 0.8 indicates that at least one grating position was probably missed.

The absolute flux is normalized to a rocket experiment of 17 May 1982 (Mount and Rottman, 1983) and is accurate to $\pm 15\%$. The relative accuracy should not be considered better than $\pm 2\%$ per year, and long term solar variability should not be extracted from the data.

The SME Solar UVS wavelength calibration is subject to a systematic error (probably temperature-related) which is seen as an accumulated error in the 1-nm integrated irradiances of a few percent. In cases of single emission lines, the effect is magnified. The width of a daily Gaussian fit to the Lyman-alpha line has declined by about 30 percent from 1982 to 1988. A dataset processed with an improved wavelength calibration function will be available later this year. In the meantime, we have developed an interim Lyman-alpha dataset based on the amplitudes of the daily Gaussian fit mentioned above, normalized to the rocket flight measurement of 17 May 1982. (Since the Lyman-alpha spectral feature is much narrower than SME's slit function, the Gaussian amplitude is independent of any error in the dispersion calibration.) This dataset is for the three wavelengths 120, 121, and 122 nm only; the error (of unknown magnitude and sign) is still present at other wavelengths.

* Due to operational constraints, we have been unable to obtain spectra in the 250-300 nm region since 1 May 1988, so these data *are* missing and have been assigned the value 0.

The measurements are given as photons $\text{cm}^{-2} \text{sec}^{-1} \text{nm}^{-1}$, adjusted to a solar distance of 1 AU, and are supplied for the 188 1-nm bins centered at 115.5 through 302.5 nm. Thus, for example, the Lyman- α emission (121.6 nm) is contained almost entirely in the seventh bin (121.5 nm). (The solar distance used to normalize the flux to 1 AU is given for each day, so the observed absolute flux may be retrieved by the relation $\text{obs} = \text{adj}/\text{dist}^2$.)

The data are supplied here in a single file named SMESOL.TXT, on a single 1200-foot tape with the volume label SMESOL. The data are written to the tape (9-track, 1600 bpi) in formatted logical records (of 7-bit ASCII characters), one record per day, 3040 bytes per record. There are 2373 logical records, one for each day from 1982 January 1 through 1988 June 30. Each logical record contains the following data, in the indicated format: year (I6), month (I3), day (I3), day-of-year (I4), Julian Day Number of Julian Day which begins at noon, UT, of the calendar date (I8), solar distance [AU] (F8.5), flux (188E10.3), and the quality index (188F6.3). The first record, for 1982 Jan 1, is appended, printed out at 80 characters per line.

To illustrate the Fortran statements needed to access the data in this file, a small ANSI-standard Fortran-77 program is appended which will create an unformatted direct-access file from the formatted text file.

References

- Rottman, G. J., C. A. Barth, R. J. Thomas, G. H. Mount, G. M. Lawrence, D. W. Rusch, R. W. Sanders, G. E. Thomas, and J. London: Solar Spectral Irradiance, 120 to 190 nm, October 13, 1981 - January 3, 1982, *Geophys. Res. Lett.*, **9**, 587-590, 1982.
- Mount, G. H., and G. J. Rottman, The Solar Absolute Spectral Irradiance 1150-3173 Å: May 17, 1982, *J. Geophys. Res.*, **88**, 5403-5410, 1983.

PROGRAM TXTDAT

C

CREATE AN UNFORMATTED DIRECT-ACCESS FILE, SMESOL.DAT,
FROM THE FORMATTED FILE, SMESOL.TXT.

C

C

INTEGER YEAR,MONTH,DAY,DOY,JULDAY,J
REAL DIST,FLUX(188),QUAL(188)

C

OPEN(UNIT=5,FILE='SMESOL.TXT',STATUS='OLD',FORM='FORMATTED',
* RECL=3040)
OPEN(UNIT=6,FILE='SMESOL.DAT',STATUS='NEW',FORM='UNFORMATTED',
* ACCESS='DIRECT',RECL=382)

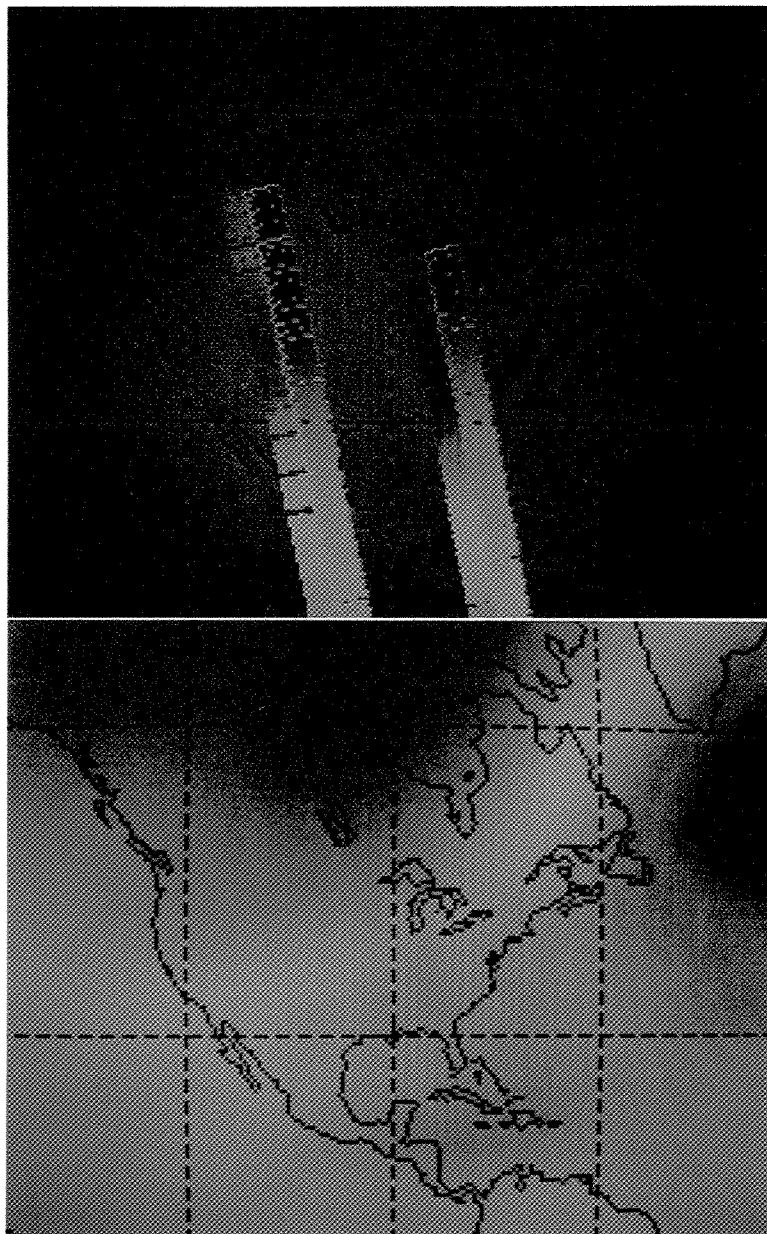
C

J=0
10 READ(5,20,END=30) YEAR,MONTH,DAY,DOY,JULDAY,DIST,FLUX,QUAL
20 FORMAT(I6,2I3,I4,I8,F8.5,188E10.3,188F6.3)
J=J+1
WRITE(6,REC=J) YEAR,MONTH,DAY,DOY,JULDAY,DIST,FLUX,QUAL
GOTO 10

C

30 WRITE(*,40) J,YEAR,MONTH,DAY,DOY,JULDAY
40 FORMAT(' End of File reached. '/
* ' Number of Records:',I6/
* ' Year, Month, Day:',I6,2I3/
* ' Day of Year, Julian Day:',I5,I9)
CLOSE(5)
CLOSE(6)
END

Geophysical Research Letters



APRIL
1983

volume 10
number 4

AMERICAN GEOPHYSICAL UNION

SOLAR MESOSPHERE EXPLORER: SCIENTIFIC OBJECTIVES AND RESULTS

C.A. Barth^{1,2}, D.W. Rusch^{1,2}, R.J. Thomas^{1,2}, G.H. Mount^{1,2}, G.J. Rottman^{1,2}
G.E. Thomas^{1,2}, R.W. Sanders¹, G.M. Lawrence^{1,2}

¹Laboratory for Atmospheric and Space Physics
University of Colorado, Boulder, Colorado 80309

²Department of Astro-Geophysics
University of Colorado, Boulder, Colorado 80309

Abstract. Instruments on the Solar Mesosphere Explorer simultaneously measure ozone density, temperature, and solar ultraviolet flux. Results from six months of observations show that ozone density in the mesosphere changes from day-to-day and with the seasons and that the principal cause of these changes is the variation in atmospheric temperature. The dependence between ozone density and temperature is inverse, with a decrease in temperature producing an increase in ozone density. This dependence is observable in the seasonal patterns and also in orbit-to-orbit observations during dramatic atmosphere changes such as stratospheric warmings.

Introduction

The Solar Mesosphere Explorer (SME) is a satellite that has the objective of studying ozone in the Earth's upper stratosphere and mesosphere with the intent of determining the cause of changes in ozone density. In the altitude region between 50 and 80 km, the chemical time constants are sufficiently short that the ozone density should respond rapidly to changes in atmospheric temperature, solar ultraviolet flux, water vapor density, and to solar proton events. This altitude region is ideally suited for testing the photochemical theory without the additional variable of atmospheric transport. In the analysis of SME data, the photochemical theory is tested by comparing model calculations of ozone density to the observations and, also, by calculating the time response of the model to changes in atmospheric temperature, solar ultraviolet flux, and water vapor density. For a more complete description of the scientific objectives, see Thomas et al., (1980).

Four limb scanning instruments are used to measure ozone density, ozone photodissociation rate, temperature, water vapor thermal emission, and nitrogen dioxide density. A fifth instrument monitors ultraviolet radiation from the sun. Solar proton events are detected by still another instrument. This paper will present a summary of results from several of the instruments during the first year of operation. Additional papers in this issue will show detailed data and analysis of the principal findings.

Orbit Geometry

The Solar Mesosphere Explorer spacecraft was launched from the Western Test Range on a Delta

Copyright 1983 by the American Geophysical Union.

Paper number 3L0322.
0094-8276/83/003L-0322\$3.00

launch vehicle on October 6, 1981. A sun-synchronous, circular orbit was achieved with an altitude of 534 km, an inclination of 97.5°, and a period of 96 minutes. The satellite spins at a rate of 5rpm with the spin axis perpendicular to the orbit plane so that the four limb-scanning instruments measure a vertical profile of the atmosphere every twelve seconds. The vertical extent of the field of view of the instruments is 3.5 km at a range of 2700 km. Individual profiles are averaged and sorted into 5° latitude bins. The sun-synchronous, polar orbit enables the instruments to obtain latitude-altitude cross sections of the atmosphere along the orbit track which crosses the equator at a local time of approximately 3 P.M. Successive orbits are displaced 24° in longitude to the west.

Instruments

Ozone density between 50 and 70 km is determined with an ultraviolet spectrometer. The instrument measures solar radiation at two wavelengths (265 and 297nm) which has been scattered by the atmospheric molecules. Differential absorption by ozone at these two wavelengths produces an absolute measurement of the density of ozone along the line of sight of the limb viewing instrument. A mathematical inversion is used to calculate the ozone density as a function of altitude through the region of the atmosphere that has been scanned by the instrument (Rusch et al., 1983a).

Ozone density is also determined with a near-infrared spectrometer which measures the airglow at 1.27 μ m. This emission is the result of the photodissociation of ozone which produces oxygen molecules in excited states. When the effects of quenching of the excited molecules and radiative transfer of the 1.27 μ m radiation are taken into account, these observations provide a measure of the ozone density between 50 and 90 km (Thomas et al., 1983a).

From SME, ozone is measured simultaneously with both the ultraviolet and near-infrared instruments. Over the altitude range where the observations overlap, the results from the ultraviolet instrument are used to adjust the absolute calibration of the near-infrared instrument. The results from both instruments have been compared with earlier rocket observations of ozone.

Temperature is determined between 36 and 50 km by the measurement of the local scale height of the radiation scattered by atmospheric molecules at 440nm. Temperature profiles obtained using this technique have been compared with those measured simultaneously by sounding rockets (Rusch et al., 1983b).

Observations

SME observations of ozone and temperature which have been made for six months, from January 1, 1982 to June 30, 1982 are described here. The data set for these observations consists of the mixing ratio of ozone and the temperature as a function of altitude, latitude, and time.

A time-latitude plot of the ozone mixing ratio at an altitude of 64 km is shown in Figure 1 (Rusch et al., 1983a). At this level in the mesosphere, the ozone density shows systematic seasonal behavior. For this data set, the seasons are winter and spring in the north and summer and fall in the south. During the first three months, the ozone mixing ratio is greater in the south than in the north. At the equinox, the mixing ratio in the north and south are nearly equal, but there is an increase in ozone mixing ratio near the equator. In the tropical region the ozone increases during the spring/fall season. In the latter half of the northern spring, the ozone mixing ratio increases at high latitudes. This data set shows day-to-day variations of ozone mixing ratio of 20% and seasonal variations of 50%.

Figure 2 shows a time-latitude plot of ozone mixing ratio at 48 km. A comparison of the data in these two figures shows distinctly different behavior at these two altitudes which are approximately two scale heights apart. At 48 km, the high-latitude maxima occur in northern winter and southern fall, opposite to the behavior at 64 km. At this altitude, the day-to-day ozone variations are 10% with seasonal changes of 25%.

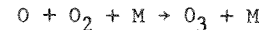
The temperature behavior of the 48 km level of the atmosphere during this same time period is shown in a time-latitude plot in Figure 3 (Rusch et al., 1983b). The atmosphere at high latitudes is hotter in the southern summer than in the northern winter and in the northern spring than the southern fall. The north tropical region is cooler in May and June than in January - March period. At the 48 km level, the seasonal variations in temperature are 12%, from 290° K in northern spring to 255° K in northern winter.

Figure 4 shows a time-latitude plot of the ozone mixing ratio at 90 km as measured by the near-infrared spectrometer (Thomas et al., 1983a). Ozone at this altitude varies drastically from day-to-day (sometimes a factor of 2) and shows seasonal variations as well. There is increased ozone at high latitudes in southern summer and northern late spring. There is a distinctive latitudinal pattern near the time of northern spring equinox.

Results

The day-to-day and seasonal changes in ozone in the lower region of the mesosphere are caused by variations in the atmospheric temperature (Rusch et al., 1983a; Solomon et al., 1983a). The dependence is inverse. When the temperature decreases, the ozone density increases and when the temperature increases, ozone becomes less dense. This inverse dependence is illustrated by a comparison of Figures 2 and 3. The winter and fall increases in ozone at high latitudes is caused by a decrease in the temperature of the atmosphere. Changes in temperature affect both

the three-body reaction that converts atomic oxygen into ozone (inverse temperature dependence)



and the two-body reaction between atomic oxygen and ozone that converts odd-oxygen into even-oxygen (direct temperature dependence)



Laboratory measurements of these reactions give a rate coefficient of the three-body reaction of $6.2 \times 10^{-34} (T/300)^{-2} \text{ cm}^6 \text{ s}^{-1}$ and of the two-body reaction $1.5 \times 10^{-11} \exp(-2218/T) \text{ cm}^3 \text{ s}^{-1}$ (NASA, 1979). Both reactions produce an inverse dependence between ozone density and temperature. Ozone density is directly proportional to the three-body reaction which has the inverse temperature dependence and it is inversely proportional to the two-body reaction which has a direct temperature dependence. Odd-hydrogen reactions which also destroy ozone in the mesosphere are relatively independent of temperature. Consideration of all of these processes leads to an inverse relationship between ozone density and temperature. The magnitude of this relationship depends on the relative strength of the odd-hydrogen catalytic destruction of ozone (Solomon et al., 1983a).

The inverse dependence of ozone density on temperature may also be seen in the observations from individual orbits. A stratospheric warming began on January 25, 1982 and lasted until January 30, 1982. During this event, the temperature at the 30 km level of the stratosphere was higher at high latitudes than at low latitudes. SME observations show that at the 48 km level the temperature at high latitudes decreased. Simultaneous SME observations of ozone show an increase in ozone at 48 km, the result of the decrease in temperature at this altitude. A stratospheric warming leads to a mesospheric cooling which in turn produces an increase in the ozone mixing ratio.

Above the mesopause at 90 km, the dramatic day-to-day variations in ozone are most likely produced by vertical motions in the thermosphere transporting odd oxygen from above into this region. The distinctive patterns in ozone mixing ratio that appear in Figure 4 are indicators of the dynamics of the lower thermosphere.

Summary

The results of the Solar Mesosphere Explorer show that the principal cause of changes in ozone density in the mesosphere is atmospheric temperature. The photochemical time constants are sufficiently short that the ozone density responds quickly to changes in physical conditions. In the mesosphere, temperature changes produce an inverse change in ozone density both through the three-body reaction that produces ozone and the two-body reactions that destroy ozone. The ozone patterns in the mesosphere reflect the temperature structure of the atmosphere.

Changes in the ozone density that are produced by temperature changes are much larger than changes induced in ozone density by variations in

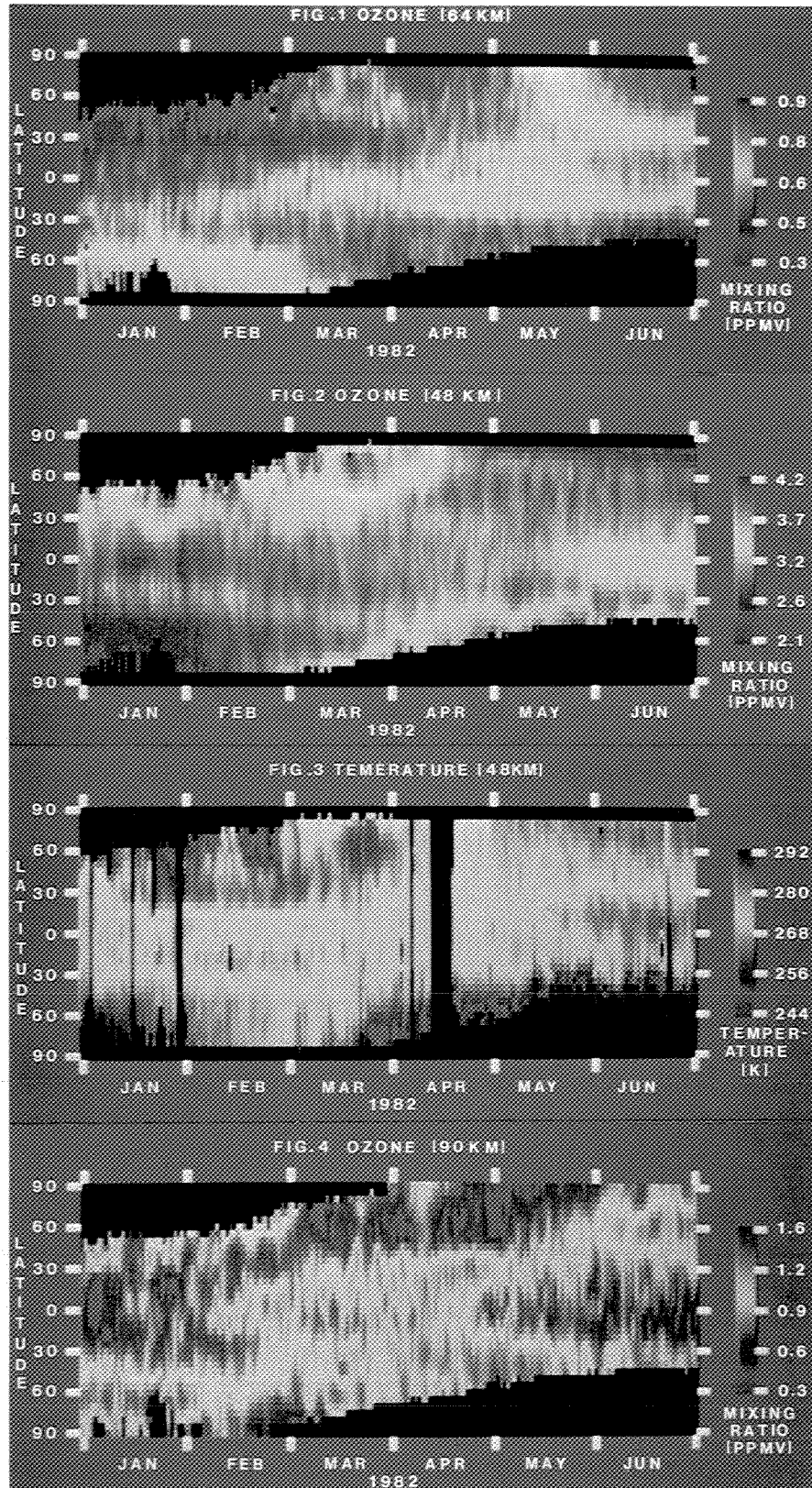


Figure 1. Time-latitude plot of the ozone mixing ratio at 64 km.
 Figure 2. Time-latitude plot of the ozone mixing ratio at 48 km.
 Figure 3. Time-latitude plot of the temperature at 48 km.
 Figure 4. Time-latitude plot of the ozone mixing ratio at 90 km.

the solar ultraviolet flux which caused variations in photodissociation processes in the mesosphere (see Rottman et al., 1982).

Solar Mesosphere Explorer observations show that even with the day-to-day temperature variations in the mesosphere that the results of other physical phenomena on ozone density are readily observed. A dramatic example is the depletion of ozone at 78 km that was produced by the July 13, 1982 solar proton event (Thomas, et al., 1983b; Solomon et al., 1983b).

Acknowledgements

The Solar Mesosphere Explorer is a NASA satellite project that is managed by the Jet Propulsion Laboratory. The JPL Project Manager and Assistant Project Manager are Mr. John J. Paulson and Dr. James R. Stuart. The NASA Headquarters Program Scientist is Dr. Shelby G. Tilford and the Program Manager is Mr. Marius B. Weinreb.

References

- NASA Reference Publication 1049, The Stratosphere: Present and Future, December, 1979.
- Rottman, G.J., C.A. Barth, R.J. Thomas, G.H. Mount, G.M. Lawrence, D.W. Rusch, R.W. Sanders, G.E. Thomas, and J. London, Solar Spectral Irradiance, 120 to 190 nm, October 13, 1981 - January 3, 1982, Geophys. Res. Lett., 9, 587-590, 1982.
- Rusch, D.W., G.H. Mount, C.A. Barth, G.J. Rottman, R.J. Thomas, G.E. Thomas, R.W. Sanders, G.M. Lawrence and R.S. Eckman, Ozone Densities in the Lower Mesosphere Measured by a Limb Scanning Ultraviolet Spectrometer, Geophys. Res. Lett., this issue, 1983a.
- Rusch, D.W., G.H. Mount, J.M. Zawodny, C.A. Barth, G.J. Rottman, R.J. Thomas, G.E. Thomas, R.W. Sanders, G.M. Lawrence, Temperature Measurements in the Earth's Stratosphere Using a Limb Scanning Visible Light Spectrometer, Geophys. Res. Lett., this issue, 1983b.
- Solomon, S., D.W. Rusch, R.J. Thomas, R.S. Eckman, Comparison of Mesospheric Ozone Abundances Measured by the Solar Mesosphere Explorer and Model Calculations, Geophys. Res. Lett., this issue, 1983a.
- Solomon, S., G.C. Reid, D.W. Rusch, R.J. Thomas, Mesospheric Ozone Depletion During the Solar Proton Event of July 13, 1982 Part II. Comparison Between Theory and Measurements, Geophys. Res. Lett., this issue, 1983b.
- Thomas, G.E., C.A. Barth, E.R. Hansen, C.W. Hord, G.M. Lawrence, G.H. Mount, G.J. Rottman, D.W. Rusch, A.I. Stewart, R.J. Thomas, J. London, P.L. Bailey, P.J. Crutzen, R.E. Dickenson, J.C. Gille, S.C. Liu, J.F. Noxon, and C.B. Farmer, Scientific Objectives of the Solar Mesosphere Explorer Mission, Pageoph, 118, 591-615, 1980.
- Thomas, R.J., C.A. Barth, G.J. Rottman, D.W. Rusch, G.H. Mount, G.M. Lawrence, R.W. Sanders, G.E. Thomas and L.E. Clemens, Ozone Density Distribution in the Mesosphere (50-90 KM) Measured by the SME Limb Scanning Near Infrared Spectrometer, Geophys. Res. Lett., this issue, 1983a.
- Thomas, R.J., C.A. Barth, G.J. Rottman, D.W. Rusch, G.H. Mount, G.M. Lawrence, R.W. Sanders, G.E. Thomas, and L.E. Clemens, Mesospheric Ozone Depletion During the Solar Proton Event of July 13, 1982, Part I Measurement, Geophys. Res. Lett., this issue, 1983b.

(Received December 21, 1982;
accepted January 31, 1983.)

OZONE DENSITIES IN THE LOWER MESOSPHERE
MEASURED BY A LIMB SCANNING ULTRAVIOLET SPECTROMETER

D.W. Rusch^{1,2}, G.H. Mount^{1,2}, C.A. Barth^{1,2}, G.J. Rottman^{1,2}, R.J. Thomas^{1,2}
G.E. Thomas^{1,2}, R.W. Sanders¹, G.M. Lawrence^{1,2}, R.S. Eckman^{1,2}

¹Laboratory for Atmospheric and Space Physics, University of Colorado, Boulder, Colorado 80309

²Department of Astro-Geophysics, University of Colorado, Boulder, Colorado 80309

Abstract. The ozone content of the earth's atmosphere between 1 mb and 0.08 mb has been measured as a function of latitude and season by an ultraviolet spectrometer on the Solar Mesosphere Explorer spacecraft. The ozone mixing ratio is found to be highly variable in time and space during the winter of 1982 with maxima occurring in the winter hemisphere during January and February at all pressure levels. The latitude gradients near spring equinox are relatively small. A relative maximum occurs at latitudes between 15 and 30°S in January and February.

Introduction

The Solar Mesosphere Explorer (SME) spacecraft was launched on October 6, 1981 from the Western Test Range into a nearly circular, sun-synchronous orbit. The north equator crossing occurs near 3:00 pm. The scientific objectives of SME have been reviewed by Thomas et al. (1980) and Barth et al., (1983) and include studies of ozone photochemistry in the 50-70 km region where the oxygen-hydrogen photochemistry is dominant in establishing the ozone density distribution. The combination of spacecraft instruments is designed to measure ozone, its variations in time and space, and correlate these changes to changes in the relevant solar flux (Rottman et al., 1982) and other important atmospheric constituents, e.g. water vapor, and to the temperature. In this paper we report on initial results from the ultraviolet spectrometer on SME which measures ozone in the 50-70 km region. A near infrared spectrometer on SME also infers the ozone density in the atmosphere by measuring the 1.27 μm emission from molecular oxygen. The ozone densities resulting from each instrument are compared in a companion paper (Thomas et al., 1983).

Observations and Data Analysis

The ultraviolet instrument on SME (UVS) is a two-channel spectrometer with a programmable wavelength drive. The instrument collecting optics are an f/5 25 cm focal length off-axis parabolic telescope which feeds an f/5 12.5 cm focal length Ebert-Fastie spectrometer. The field of view is 0.074×0.074 which projects to 3.5km X 35km at the earth's limb. The instrument employs a 3600 groove/mm grating blazed at 240nm and two EMR type 510F photomultiplier tubes used in pulse counting mode. The spectral resolution is 15Å and the channels are separated by 300Å.

The wavelength coverage for channel 1 and channel 2 are 1880-3100Å and 2230-3404Å, respectively. The integrated internal instrument scattered light from all wavelengths relative to the intensity at 2660 Å is less than 0.5%.

The grating may be operated either in a scanning mode with 4.9 or 96Å steps or commanded to any of 256 grating positions. The data reported here were obtained on the earth's limb at fixed grating position at wavelengths 2650 and 2964Å. The instrument sensitivity is 5.5×10^3 (counts/sec)/(KR/Å) at 2650Å and 1.4×10^3 (counts/sec)/(KR/Å) at 2960.

The absolute direction of the line of sight of the scientific instruments is determined from a history of averaged pitch angles derived from the four horizon sensor crossings each spin. This analysis leads to limb altitude determinations with residuals of the order of one kilometer at a slant distance of 2550 km (Cowley and Lawrence, 1983). The limb altitudes are further refined by comparisons of the Rayleigh scattered intensity measured by the UVS with expectations from modeling of this signal using the relevant solar fluxes, cross sections, and the model atmosphere of Cole and Kantor (1978).

The period of ozone observations reported here extend from January 1, 1982 to November 30, 1982. The primary orbits cover the longitude range from 40 W to 100 W each day during local afternoon.

Altitude profiles of counts per integration period (IP) for a typical set of six spins is shown in Figures 1a and b. The data taken at 2650Å are shown in Figure 1a where the maximum count rate is about 300 per IP for each of the six spins and the 2964Å data shown in Figure 1b have a maximum count rate of about 600 per IP. The data show an increase in the counting rate as the line of sight penetrates the atmosphere and the Rayleigh scattering intensity increases. This exponential increase is interrupted by the absorption of scattered solar radiation by ozone. The shape of the emission profile is determined by the amount of ozone along the viewing path and the ozone cross-section. The adopted absorption cross-sections for ozone are from Bass and Paur (Private Communication) and when averaged over the instrument bandpass are 9.6×10^{-18} and 5.84×10^{-19} cm^2 at 2650Å and 2964Å, respectively. As a result the Rayleigh scattering maximizes at about 62 km at 2650Å and about 51 km at 2964Å for a typical ozone profile.

The data are then calibrated taking into account instrument dead-time, sensitivity and polarization. The calibrated radiance profiles resulting from the data of Figure 1 are shown in Figure 2 as the asterisks after averaging over six limb scans ($\sim 5^\circ$ along the orbit). The data

Copyright 1983 by the American Geophysical Union.

Paper number 3L0318.
0094-8276/83/003L-0318\$3.00

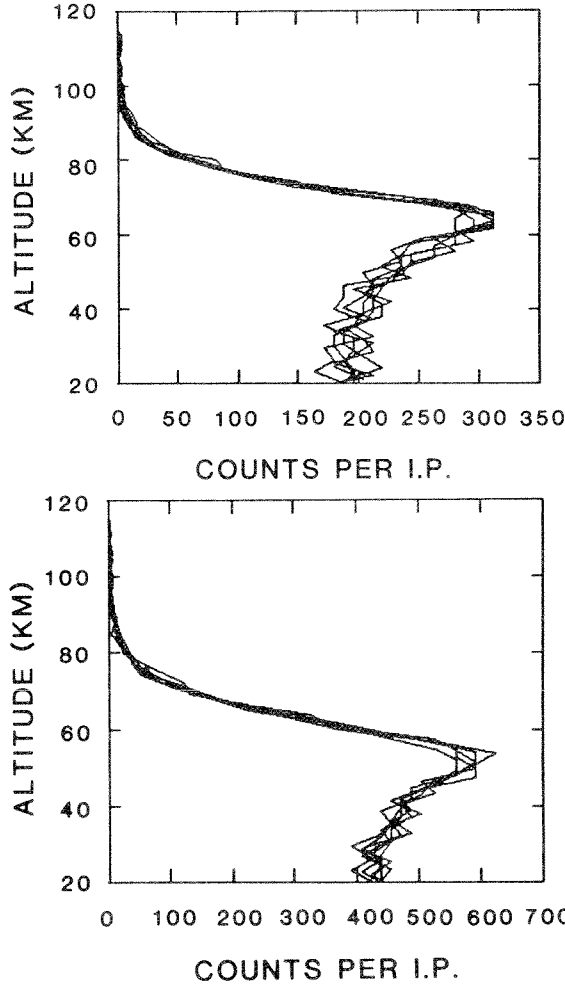


Figure 1: Altitude profiles of counts per integration period vs altitude on orbit 2405, 82073, at 14.0° latitude (a) 2650A, (b) 2964A.

are then fed into a radiative transfer inversion code which we briefly describe here.

Let the intensity as measured by the instrument be $I(\lambda, \ell)$, which is a function of wavelength (λ) and altitude above the limb (ℓ). We approximate I by a linear expansion in the layer values of the unknowns A (the ozone densities)

$$I(\lambda, \ell) = I^M(\lambda, \ell) + \sum_{i=1}^m \frac{\partial I^M(\lambda, \ell)}{\partial A_i} \cdot (A_i^{(n)} - A_i^{(n-1)}) \quad (1)$$

where I^M is calculated from a radiative transfer model, and the derivatives are evaluated at $A_i^{(n-1)}$.

The radiative transfer model used in the calculation assumes single scattering of solar photons and uses the model atmosphere of Cole and Kantor (1978). The use of a single scattering model is justified at the chosen wavelengths because neither penetrate to altitudes where scattering by clouds or snow occur. In addition we have measured the albedo of the atmosphere by looking directly down at the surface of the earth

and have established that the counting rate is a factor of 20 or more lower than the counting rate measured on the limb. Thus the multiple scattering contribution to the signal is insignificant.

We then define the matrix of the derivatives of the intensities by the unknowns.

$$F = \frac{\partial I^M(\lambda, \ell)}{\partial A_i} \quad (2)$$

Equation (1) can then be inverted to give

$$A^{(n)} - A^{(n-1)} = (F^T F)^{-1} [F^T (I(\lambda, \ell) - I^M(\lambda, \ell))] \quad (3)$$

where the I^M 's are evaluated at $A^{(n-1)}$. The relationship between the intensities and the ozone densities is not linear and equation 3 is solved numerically by iteration.

A further complication arises near the end points of the selected data set where the S/N is small. Here the solution can become unstable and the instability may propagate into the region when the S/N is large. Mathematically, the matrix $(F^T F)^{-1}$ can become singular. This situation is avoided by constraining the solution and directing it back to the initial value or preconceived solution if the noise is large. We introduce the γ -factor, a vector quantity which is a function of altitude, to prevent instabilities in the solution. Including $\gamma(\ell)$ in equation (3) we have

$$A^{(n)} - A^{(n-1)} = (F^T F + \gamma I)^{-1} [F^T (I(\lambda, \ell) - I^M(\lambda, \ell) + \gamma(A^{(0)} - A^{(n-1)}))] \quad (4)$$

where I is the identity matrix, $A_i^{(0)}$ is the preconceived or initial solution. If $\gamma=0$, this becomes equation (3), but as γ becomes large, the solution becomes the preconceived solution $A^{(0)}$. Thus it is possible to overcome the problem of noise at the endpoints and by suitable choice of γ allow the data with large S/N to fully influence the solution. A new set of A 's is given by equation (4) and the solution is iterated until the differences between I and I^M are small. In Figure 2 the radiance data, the radiance calculated from the derived ozone den-

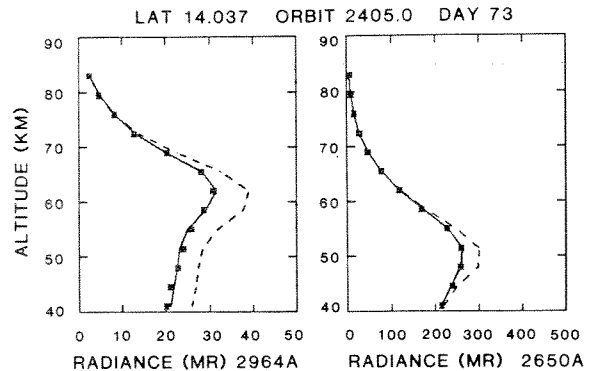


Figure 2: Altitude profiles of the measured radiance (*), the calculated radiance using the initial guess ozone profile (---) and the calculated radiance after the inversion (—).

sities and the radiance calculated from the initial ozone profile are shown for each channel. The dashed lines are the radiance calculated from the initial ozone profile. Note the convergence at high altitudes for all three profiles where no ozone absorption is present. The agreement between the data and the final radiances is excellent after the inversion processes.

The resulting ozone density and mixing ratio profiles are shown in Figure 3a and b for 14° latitude, orbit 2405 on March 14. The ozone density decreases from about $1 \times 10^{11} \text{ cm}^{-3}$ at 48 km to about 1×10^9 at 68 km with an average scale height of 4.5 km. The mixing ratios are 3.2 ppmv at 48 and 0.43 ppmv at 68 for this low latitude case near equinox.

The density profiles shown in Figures 3 are similar to other published ozone measurements. The ozone densities and mixing ratios are 10% smaller than the mid-latitude ozone model of Krueger and Minzner (1976) at 50 km and 20% at 64 km for this one comparison. The results are also within 10% of the measurements of Aikin et al., (1982) who used the Solar Maximum Mission spacecraft in an occultation mode to derive equatorial ozone profiles at dusk. Other measurements of ozone by limb scanning instruments have measured thermal emission from the ozone molecule (see e.g., Gille et al., 1980) or have used stars as occultation sources (Hays and Roble, 1973).

An error analysis was performed to determine the statistical uncertainty of the derived ozone densities. The calculation was done by comparing the inversion of perfect data to those performed with noisy data. In no case did the difference between the ozone densities derived from the noise-free data and the noisy data exceed 10% in the altitude range between 50 and 68 km. We estimate that the total error derived from consideration of inaccurate knowledge of the altitude of the line of sight, internal scattering in the instrument, and errors inherent in the inversion technique are $\pm 15\%$ over the altitude range considered.

The monthly averaged mixing ratios are displayed in Figure 4 in pressure and latitude for January, February and March of 1982. The January data show smaller mixing ratios in mid-latitudes in summer than in winter at pressures above about 0.2 mb with the gradient becoming less or even reversing at lower pressures. Near 0.9 mb the winter latitudinal gradient is large with the

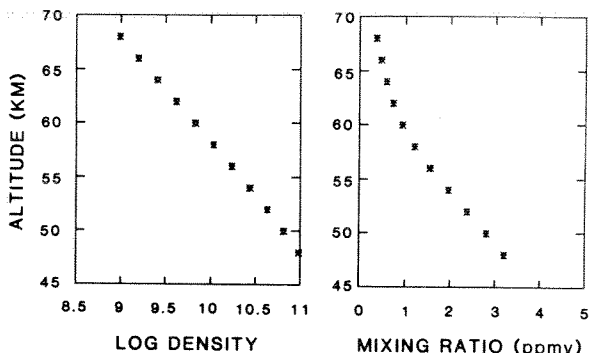


Figure 3: (a) Log of the ozone density as a function of altitude for the radiance data of Figure 2, (b) the ozone mixing ratio profile.

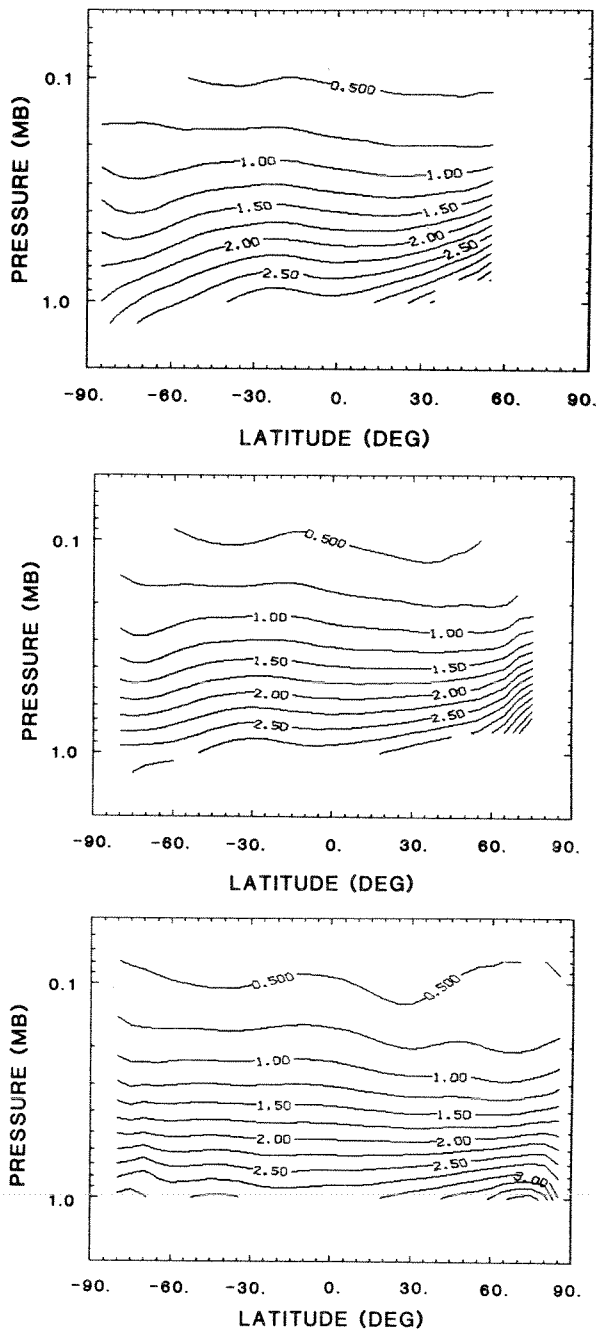


Figure 4: Monthly average value of mixing ratio vs pressure and latitude. (a) January, (b) February, (c) March.

mixing ratios increasing from about 3 ppmv at 20°N to 3.5 ppmv at 50°N. Theoretical comparisons to this data are discussed in a companion paper in this issue (Solomon et al., 1983). The gradients tend to lessen at all levels in February but maintain the general features of the previous month. In March the large gradients at high latitudes have disappeared and a large meridional wave appears at low pressures. An interesting feature in the data is the relative maximum occurring at nearly all levels in January and February between 15°S and 30°S.

The standard deviations from the monthly means

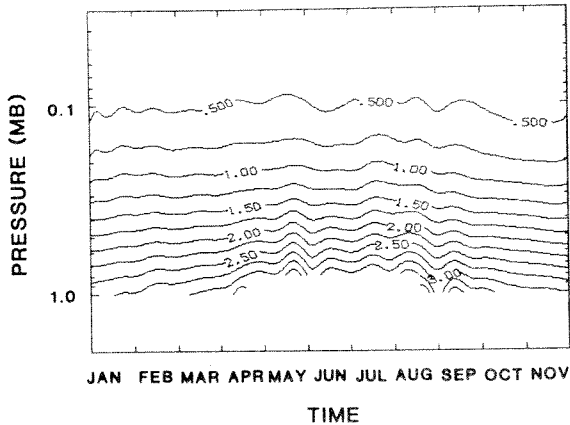


Figure 5: Contours of ozone mixing ratio in pressure and time for eight months of 1982. The data are for 45°S latitude.

shown in Figures 4a, b, and c range from about 5% of the monthly average values at pressures greater than 0.5 mb in the summer hemisphere and up to latitudes near 30°N to about 10% in regions of lower pressure. In January and February, the standard deviations increase toward the winter pole at pressures greater than 0.4 mb to 10 to 15% at 50°N. This reflects the rather large variability of ozone in the winter hemisphere caused by dynamics. This trend continues even into March as a result of including ozone mixing ratios in the average measured during a stratospheric warming event.

In Figure 5 contours of ozone mixing ratio are plotted in pressure and time for January through November of 1982, at 45°S latitude. The data have been smoothed by an eleven day running average. The ozone increases through the first six months reaching a maximum value at all pressures in June or July. Note also the high variability of ozone in the southern winter and the smoothness of the contours in southern spring and summer. The opposite trend is apparent in the northern hemisphere. Much of the variability near 1.0 mb is due to thermal events such as stratospheric warmings.

Summary

The ozone content of the lower mesosphere has been mapped by an orbiting ultraviolet spectrometer. The results reveal ozone variability in latitude and season and demonstrate the validity of the ultraviolet limb scanning technique for measuring mesospheric ozone.

References

- Aikin, A.C., B. Woodgate, and H.J.P. Smith, Atmospheric ozone determination by solar occultation using the UV spectrometer on the Solar Maximum Mission, *Applied Optics* **21**, 3, pp 2421-2424, 1982.
- Barth, C.A., D.W. Rusch, R.J. Thomas, G.H. Mount, G.J. Rottman, G.E. Thomas R.W. Sanders and G.M. Lawrence, Solar Mesosphere Explorer: Scientific Objectives and Results, *Geophys. Res. Lett.*, this issue, 1983.
- Cole, A.E., and A.J. Kantor, "Airforce Reference Atmosphere", Air Force Geophysical Laboratory, Project 6670, 1978.
- Cowley, J.R., Jr., and G.M. Lawrence, Earth limb altitude determination for the Solar Mesosphere Explorer, AIAA 21st Aerospace Sciences Meeting, January 10-13, 1983, Reno, Nevada.
- Gille, J.C., P.L. Bailey, and J.M. Russell III, Temperatures and composition measurements from the I.R.I.R. and I.I.M.S. experiments on NIMBUS 6 and 7, *Phil. Trans. R. Soc. Lond. A.*, 296, pp 205-218, 1980.
- Hays, P.B., and R.G. Roble, Observation of mesospheric ozone at low latitudes, *Planet. Space Sci.*, **21**, pp 273, 279, 1973.
- Krueger, A.J., and R.A. Minzner, A mid-latitude ozone model for the 1976 U.S. Standard Atmosphere, *J. Geophys. Res.*, **81**, pp 4477-4481, 1976.
- Rottman, G.J., C.A. Barth, R.J. Thomas, G.H. Mount, G.M. Lawrence, D.W. Rusch, R.W. Sanders, G.E. Thomas, J. London, Solar Spectral Irradiance, 120 to 190nm, October 13, 1981 - January 3, 1982, *Geophys. Res. Lett.*, **9**, 587-590, 1982.
- Solomon, S., D.W. Rusch, R.J. Thomas, and R.S. Eckman, Comparison of mesospheric ozone abundances measured by the Solar Mesosphere Explorer and model calculations, *Geophys. Res. Lett.*, this issue, 1983.
- Thomas, G.E., C.A. Barth, E.R. Hansen, C.W. Hord, G.M. Lawrence, G.H. Mount, D.W. Rusch, A.I. Stewart, R.J. Thomas, J. London, P.L. Bailey, P.J. Crutzen, R.E. Dickenson, J.C. Gille, S.C. Liu, J.F. Noxon, and C.B. Farmer, Scientific Objectives of the Solar Mesosphere Explorer Mission, *Pageoph*, **118**, 591-615, 1980.
- Thomas, R.J., C.A. Barth, G.J. Rottman, D.W. Rusch, G.H. Mount, G.M. Lawrence, R.W. Sanders, G.E. Thomas, and L.E. Clemens, Ozone density distribution in the mesosphere (50-90 km) measured by the SME limb scanning infrared spectrometer, *Geophys. Res. Lett.*, This issue, 1983.

(Received December 21, 1982;
accepted February 15, 1983.)

OZONE DENSITY DISTRIBUTION IN THE MESOSPHERE (50-90 KM) MEASURED BY THE SME
LIMB SCANNING NEAR INFRARED SPECTROMETERR.J. Thomas^{1,2}, C.A. Barth^{1,2}, G.J. Rottman^{1,2}, D.W. Rusch^{1,2}, G.H. Mount^{1,2},
G.M. Lawrence^{1,2}, R.W. Sanders¹, G.E. Thomas^{1,2}, L.E. Clemens¹¹Laboratory for Atmospheric and Space Physics University of Colorado, Boulder, Colorado 80309²Department of Astro-Geophysics University of Colorado, Boulder, Colorado 80309

Abstract. The ozone densities between 50 and 90 km are deduced from 1.27 μm airglow measured on the Solar Mesosphere Explorer satellite. The derived densities agree well with those made simultaneously from SME by the ultraviolet spectrometer. The data set extends from pole to pole at about 3 pm, for most sunlit latitudes. At low altitudes, in the mesosphere, there are larger variations in ozone density in the winter latitudes than in the summer. Above the meso-pause the day-to-day variation in ozone density is a factor of two at most latitudes and times.

Introduction

The Solar Mesosphere Explorer (SME) spacecraft was launched on October 6, 1981 into a nearly circular, sun-synchronous orbit, so that the subsatellite local time is near 3:00 pm or 3:00 am. The scientific objectives of SME include studies of ozone photochemistry in the mesosphere. The combination of spacecraft instruments is designed to measure ozone, its variations in time and space, and correlate these to changes in the relevant solar flux, the temperature, and other important atmospheric constituents, e.g. water vapor (Barth et al., 1983).

The near infrared instrument measures emission from $\text{O}_2(^1\Delta_g)$ at 1.27 μm . In the dayglow the oxygen molecule is excited to this state primarily by photodissociation of ozone and emits at 1.27 and 1.58 μm . The emission at 1.58 μm was first observed from the ground in the evening twilight by Vallance Jones and Harrison (1958). The emission at 1.27 μm is stronger, but is absorbed in the troposphere by molecular oxygen. Vallance Jones and Gattinger (1963) proposed that the emission was due to ozone photodissociation. A rocket profile of the dayglow was made by Evans et al. (1968). Their analysis indicated that the emission was due to ozone photodissociation, except possibly above 80 km where the excess emission required either more ozone than predicted at that time, or another source of $\text{O}_2(^1\Delta_g)$ molecules. Our analysis indicates that both are true; there is, at times, a secondary peak of ozone density near 85 km, while near 80 km often only about half the emission is due to ozone.

In this paper we report on initial results from the near infrared spectrometer on SME which measures ozone in the 50-90 km region. We will discuss the methods that are used to invert the observed intensities giving the volume emission

rate. The ozone densities are then inferred assuming several sources for the emission. The general behavior of the ozone with altitude, latitude, and time will be shown and discussed.

Observations and Data Analysis

The near infrared instrument on SME is a two-channel Ebert-Fastie spectrometer with a programmable wavelength drive. The collecting optics are an f/5 25 cm focal length off-axis parabolic telescope which feeds an f/5 12.5 cm focal length Ebert-Fastie spectrometer. The field of view is $0.074^\circ \times 0.74^\circ$ which projects to 3.5 km X 35 km at the earth's limb. The instrument employs a 200 groove/mm grating blazed at 1.8 μm and two passively cooled lead sulfide detectors. The spectral resolution is 12.25 nm and the channels are separated by 0.6 μm . The wavelength coverage for channel 1 and channel 2 are 1.1-2.6 μm and 1.1-3.2 μm respectively. The grating may be operated either in a scanning mode with 44 nm steps or commanded to any of 512 positions. The data reported here were obtained on the Earth's limbs with a fixed grating position at 1.27 μm .

The SME spacecraft spins in cartwheel fashion once every 12 seconds with the spin axis perpendicular to the orbit plane. Thus, one scan of the Earth's limb is accomplished every 12 seconds, or about 1 degree of latitude along the orbit path. During each scan of the Earth's limb, 31 data samples are collected. The integration period of 2.44 ms gives 3.5 km resolution on the limb and 31 samples cover the altitude region from about 30 to 130 km. Most of the data were taken on the orbits that cover the longitude range from 40 to 100 degrees west each day during local afternoon.

The altitude profile of typical radiance data is shown in Figure 1. The radiance measurements taken on the limb forward of the spacecraft in the orbit plane begin at the highest altitude with a measurement of the dark sky background. The signal increases above the noise between 90 and 100 km. Often an inflection or even a relative minimum in the signal is seen near 80 km. The signal reaches a peak near 45 km and then falls off until the Rayleigh scattering from the lower atmosphere, scattering from clouds, and reflection from the earth's surface are seen. During the day, the maximum airglow signal is between 250 and 350 data numbers or DN (600 and 800 MR), while at night the maximum signal is about 1 DN (2.3 MR). The instrument sensitivity is about 2 MR per data number and the noise on one sample is about 1.5 DN. Thus, the day signals have a very good signal-to-noise ratio while at night it is poor. The 8-bit data compression adds an error of up to $\pm 3\%$ to all data points.

Copyright 1983 by the American Geophysical Union.

Paper number 3L0301.
0094-8276/83/003L-0301\$3.00

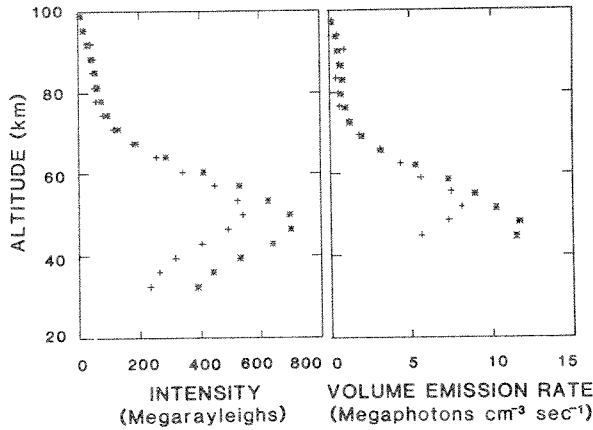


Figure 1: Data measured by the limb scanning near infrared spectrometer on SME on 14 March, 1982 on the left. These profiles are six data scans that have been merged and calibrated. The inverted data, 1.27 μm volume emission rate, is on the right. (+) -data at 66.2°S latitude and a solar zenith angle = 74.1°. (*) -data at 12.5°N and a solar zenith angle = 44.1°.

The data are calibrated by taking into account the instrument and detector temperatures which are included in the telemetry. In order to decrease the noise and the volume of data storage, we merge 6 calibrated profiles together taking into account any changes in pointing and timing.

The observed slant intensity along the line of sight path ℓ with a tangent altitude of h is

$$S(h) = \int_0^{\infty} V(\ell)T(\ell)d\ell$$

Where $V(\ell)$ is the volume emission rate. The 1.27 μm emission is self absorbed by O₂. $T(\ell)$ is the atmospheric transmission of 1.27 μm radiance between the emission point and SME and depends on the column density of O₂ and the emission and absorption temperatures.

The volume emission rate $V(h)$, at any altitude h , is retrieved using an onion peel method assuming that the atmosphere is uniformly stratified. Two inverted profiles are shown in Figure 1.

During the day, the dominant production mechanisms of O₂(¹Δ) are ozone photodissociation and collisional transfer of energy from O₂(¹Σ). We examined the photochemical reactions (using cur-

TABLE 1 REACTION RATES AND CONSTANTS

ϵ	0.9	1
J_3	$8.0 \times 10^{-3} \text{ sec}^{-1}$	2
J_{∞}	$6.3 \times 10^{-9} \text{ sec}^{-1}$	3
$A_{S_{\infty}}$	0.085 sec^{-1}	3
A_D	$2.58 \times 10^{-4} \text{ sec}^{-1}$	4
k_D	$2.22 \times 10^{-18} (T/300)^{0.78} \text{ cm}^3 \text{ sec}^{-1}$	5
k_n	$2.0 \times 10^{-11} \exp(-107/T) \text{ cm}^3 \text{ sec}^{-1}$	6
k_o	$2.9 \times 10^{-11} \exp(-67/T) \text{ cm}^3 \text{ sec}^{-1}$	6
k_s	$2.0 \times 10^{-15} \text{ cm}^3 \text{ sec}^{-1}$	7

1. Fairchild et al. 1978, 2. See text, 3. Wallace and Hunten 1968, 4. Badger et al. 1965, 5. Findlay and Snelling 1971, 6. Streit et al. 1976, 7. Becker et al. 1971.

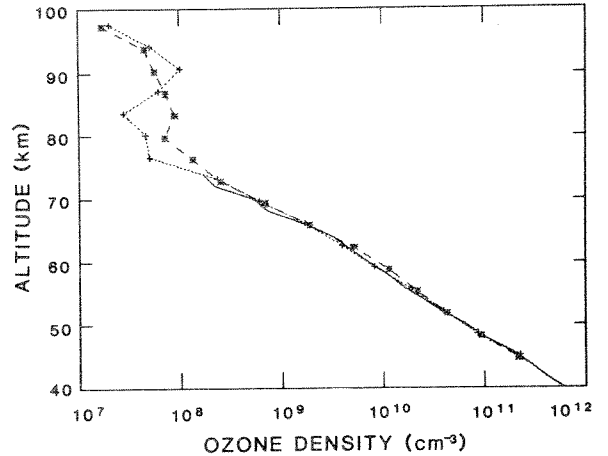
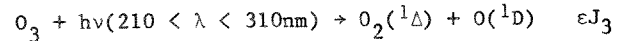
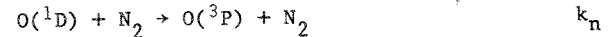
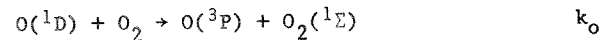


Figure 2: Ozone density at 65°S and 10°N corresponding to the profiles of Figure 1. The solid line ending at 72 km is the average data of Krueger and Minzner (1967).

rent rate constants) that could produce O₂(¹Δ) (Evans et al., 1968 and Han et al. 1973) and found only those discussed below were significant during the day.



The production efficiency ϵ is about 90% and the number of ozone dissociations per second per molecule is J_3 . J_3 is calculated using temperature dependent cross sections of Bass and Paur (1982) and the solar flux of Mount and Rottman (1983) corrected for the sun-earth distance and the overhead ozone. The excited oxygen atom can transfer its energy to O₂ or be quenched by N₂.



The O₂(¹Σ) molecule in turn is de-excited by

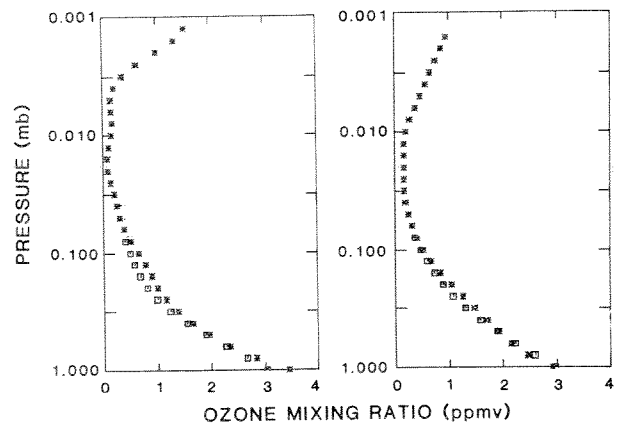
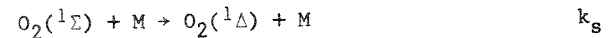


Figure 3: The same ozone densities as in Figure 2 but plotted as mixing ratio in parts per million by volume vs. pressure. 65°S is on the left and 10°N is on the right. The small squares are ozone data from the UV absorption experiment (Rusch et al., 1983).

where M is any molecule, usually N₂. All de-excitation reactions of O₂(¹Σ) produce an O₂(¹Δ) (Ogryzlo and Thrush, 1974). Deactivation of O₂(¹Σ) effectively adds 30% to the photodissociation production of O₂(¹Δ), making the efficiency about 117%. O₂(¹Σ) is also produced by resonance absorption of sunlight at 762nm which is then collisionally converted to O₂(¹Δ) below about 90 km. Above that altitude more O₂(¹Σ) is lost by radiation than by quenching. The excitation rate is J_s.

O₂(¹Δ) molecules either radiate or are quenched by O₂



Hence the volume emission rate is given by

$$V(h) = \left\{ \frac{P_s k_s [M]}{A_s + k_s [M]} + J_3 \epsilon [O_3] \right\} \frac{A_D}{A_D + k_D [O_2]}$$

A_s and A_D are the Einstein coefficients for O₂(¹Σ) and O₂(¹Δ) respectively, and P_s is the production rate of O₂(¹Σ)

$$P_s = J_s [O_2] + J_3 \epsilon [O_3] K_o / (K_o + 3.76 K_n)$$

The above equations are then solved for the ozone density and mixing ratio. The background atmospheric density and temperature are taken from Cole and Kantor (1978). Rates and constants used are given in Table 1. The transmission function for resonance-band absorption by O₂ molecules was taken to be a weighted-sum over all lines of the transmission function for a pure Doppler line (Holstein, 1947). The weighting

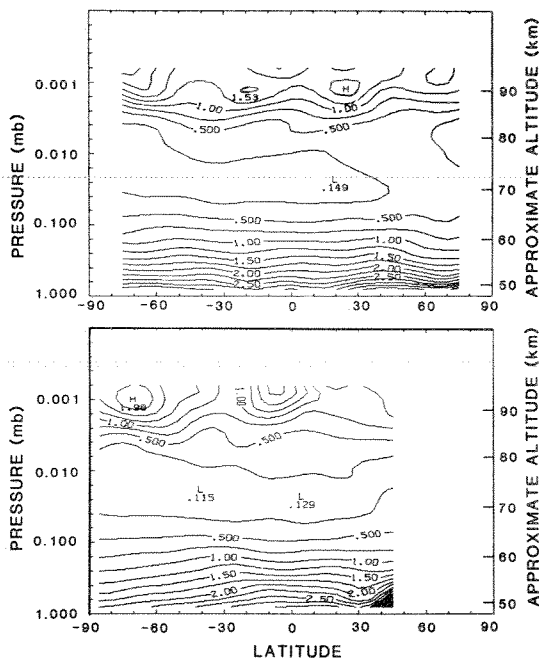


Figure 4: Contour plots of ozone mixing ratio for the orbit of 14 March, 1982, top, and 22 December, 1981 on the bottom. The upper plot contains data shown in Figure 3. Negative value of latitude indicates the southern hemisphere.

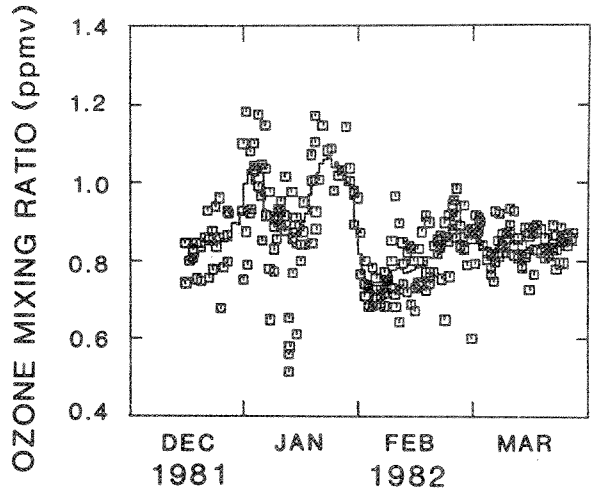


Figure 5: Ozone mixing ratio as a function of time at 40°N and about 60 km (0.159 mb). Each square is one orbit while the solid line is a five day running average.

factor is the normalized Boltzmann distribution function evaluated at the temperature of the model atmosphere evaluated at the limb point (Wallace and Hunten, 1968).

Results and Discussion

The ozone densities and mixing ratios derived from the intensity measurements of Figure 1 are shown in Figures 2 and 3. In Figure 2 the logarithm of the ozone density is plotted against altitude. Below 70 km the ozone follows an exponential behavior and shows a good agreement with the rocket model of Krueger and Minzer (1976). Above 70 km the scale height increases and often there is a secondary maximum of the ozone density. The mixing ratios are shown in Figure 3 with total pressure as the vertical coordinate. The profiles are representative of March conditions. Figure 3 also includes data from the SME UV measurement of ozone that shows the good agreement of ozone altitude profiles.

The ozone inferred from the measurements exhibits a considerable variation with latitude and time. The latitude variation of the ozone mixing ratio by volume for two orbits is represented by contour maps in Figure 4. In the winter, the mixing ratio is enhanced in the northern mid latitudes. Above 70 km (0.03 mb), there is a good deal of structure in each map. The mixing ratio above 80 km has a maximum near the summer pole.

The variation of ozone with time can be seen in Figure 5 for 40°N latitude at 60 km. The changes from orbit to orbit are due to longitudinal variations and random noise in the inversion. In Figure 6, the 5 day running average is shown for several pressure levels at 40°S. At high pressures (1.0 and 0.8 mb) ozone mixing ratio increases throughout the period up to the beginning of May when large winter variability becomes apparent. The dotted line at 0.8 mb represents ozone measured by the UV spectrometer. The agreement between the two instruments is very good. The ozone at 0.3, 0.1, and 0.01 mb

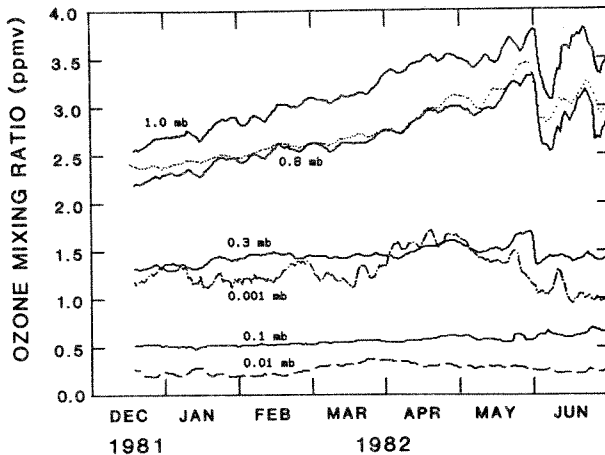


Figure 6: Ozone five day running average at several pressure levels at 40°S.

appears less variable except in June. The variability returns at 0.001 mb throughout the entire period, possibly indicating a region of control of ozone different than that at higher pressures.

Satellite measurements of the 1.27 μm airglow on the Earth's limb are currently being made from the SME spacecraft. Most of the emission is due to ozone photodissociation. A small amount of the emission is due to transfer of energy from $\text{O}_2(^1\Sigma)$ which is resonantly excited by sunlight at 762 nm. Taking into account quenching of both $\text{O}_2(^1\Sigma)$ and $\text{O}_2(^1\Delta)$, the atmospheric transmission of the UV, of 762 nm and of 1.27 μm radiation, we infer the ozone densities from 50 to 90 km during the daylight portion of the orbit.

We have shown that the derived ozone density is consistent with that measured previously by rockets and with the UV absorption measurements of ozone on SME. The ozone above 80 km is highly variable while that at 60 km shows seasonal trends and winter variability.

References

- Badger, R.M., A.C. Wright, and R.F. Whitlock, "Absolute Intensities of the Discrete and Continuous Absorption Bands of Oxygen Gas at 1.26 and 1.065 μ and the Radiative Lifetime of the $^1\Delta$ State of Oxygen", *J. Chem. Phys.* **43**, 4345, 1965.
- Barth, C.A., D.W. Rusch, R.J. Thomas, G.H. Mount, G.J. Rottman, G.E. Thomas, R.W. Sanders, G.M. Lawrence, Solar Mesosphere Explorer: Scientific Objectives and Results, *Geophys. Res. Lett.*, this issue, 1983.
- Bass, A.M. and R.J. Paur, Personal Communications, 1982.
- Becker, K.H., W. Groth, and V. Schurath, "The Quenching of Metastable $\text{O}_2(^1\Delta_g)$ and $\text{O}_2(^1\Sigma_g^+)$ Molecules", *Chem. Phys. Lett.* **8**, 259, 1971.
- Cole, A.E., and A.J. Kantor, "Airforce Reference Atmosphere", Air Force Geophysical Laboratory, Project 6670, 1978.
- Evans, W.F.J., D.M. Hunten, E.J. Llewellyn, and A. Vallance Jones, "Altitude Profile of the Infrared Atmospheric System of Oxygen in the Dayglow", *J. Geo. Res.* **73**, 2885, 1968.
- Fairchild, C.E., E.J. Stone, and G.M. Lawrence, "Photofragment Spectroscopy of Ozone in the UV Region 270-310nm and at 600nm", *J. Chem. Phys.* **69**, 3632, 1978.
- Findlay, F.D., and D.R. Snelling, Collisional Deactivation of $\text{O}_2(^1\Delta_g)$, *J. Chem. Phys.*, **55**, 545, 1971.
- Han, R.Y., L.R. Megill, and C.L. Wyatt, "Rocket Observation of the Equatorial $\text{O}_2(^1\Delta_g)$ Emission After Sunset", *J. Geo. Res.*, **78**, 6140, 1973.
- Holstein, T., "Imprisonment of Resonance Radiation in Gases", *Phys. Rev.*, **72**, 1212, 1947.
- Krueger, A.J., and R.A. Minzner, "A Mid-Latitude Ozone Model for 1976 U.S. Standard Atmosphere", *J. Geo. Res.*, **81**, 4477, 1976.
- Mount, G.H., and G.J. Rottman, "The Solar Spectral Irradiance 1150-3173 Å 17 May 1982", to be published *J. Geo. Res.*, 1983.
- Ogryzlo, E.A. and B.A. Thrush, "The Vibrational Excitation of H_2O and $\text{CO}_2(^1\Sigma_g^+)$ ", *Chem. Phys. Lett.*, **24**, 314, 1974.
- Rusch, D.W., G.H. Mount, C.A. Barth, G.J. Rottman, R.J. Thomas, G.E. Thomas, G.E. Thomas, R.W. Sanders, G.M. Lawrence & R.S. Eckman, Ozone Densities in the Lower Mesosphere Measured by a Limb Scanning Ultraviolet Spectrometer, *Geophys. Res. Lett.* this issue, 1983.
- Streit, G.E., C.J. Howard, A.L. Schmeltekopf, J.A. Davidson, and H.I. Schiff, "Temperature Dependence of $\text{O}(^1\text{D})$ Rate Constants for Reactions with O_2 , N_2 , CO_2 , O_3 and H_2O ", *J. Chem. Phys.*, **65**, 4761, 1976.
- Vallance Jones, A., and A.W. Harrison, " $^1\Delta_g - ^3\Sigma_g^-$ - O_2 Infrared Emissions Band in the Twilight Airglow Spectrum", *J. Atm. Terr. Phys.*, **13**, 45, 1958.
- Vallance Jones, A., and R.L. Gattinger, "The Seasonal Variation and Excitation Mechanism of the 1.58 μ $^1\Delta_g - ^3\Sigma_g^-$ Twilight Airglow Band", *Planet. Space Sci.*, **11**, 961, 1963.
- Wallace, L., and D.M. Hunten, "Dayglow of the Oxygen A Band", *J. Geo. Res.*, **73**, 4813, 1968.

(Received December 22, 1982;
accepted February 4, 1983.)

TABLE 1. Calculated monthly mean H₂O mixing ratios and O₂ and H₂O photolysis rates in the equatorial mesosphere

Pressure (mb)	Approximate Altitude (km)	H ₂ O (ppmv)	R1 (sec ⁻¹)	R7 (sec ⁻¹)
0.75	50	5.2	1.0(-9)*	2.3(-8)
0.37	55	5.2	1.2(-9)	6.0(-8)
0.18	60	5.3	1.4(-9)	9.3(-8)
0.09	65	5.2	2.0(-9)	2.8(-7)
0.04	70	4.8	2.9(-9)	8.6(-7)
0.02	75	4.3	5.1(-9)	2.1(-6)
0.01	80	3.2	8.5(-9)	3.6(-6)

* Read 1.0(-9) as 1.0×10^{-9}

tropical mesosphere, and these are consistent with the detailed calculations mentioned above when differences in solar flux are considered. Further description of the model is provided by Garcia and Solomon (1983). The satellite data which will be displayed represent averages for the month of January, 1982.

Figure 1 shows calculated and observed mixing ratios from the ultraviolet spectrometer versus latitude for two pressure levels. (Our model is

formulated in pressure coordinates). The latitude trends which appear in the data are generally similar to those obtained in the model. Ozone data obtained by Krueger and Minzner (1976) (mostly at Wallops Island, Virginia) are also shown for comparison. The indicated error bars represent one sigma standard deviations about the observed means. The Krueger-Minzner data include observations at various seasons and local times, as well as some twilight data, while the SME data are for January at 3PM local time. At twilight, conversion of atomic oxygen to ozone may occur, yielding larger ozone densities (especially at higher altitudes) and larger variability when averaged together with daytime data. The variability observed by SME does not change much with latitude at these heights, as indicated. The specific differences will be discussed in more detail below.

Figure 2 presents the monthly averaged profile

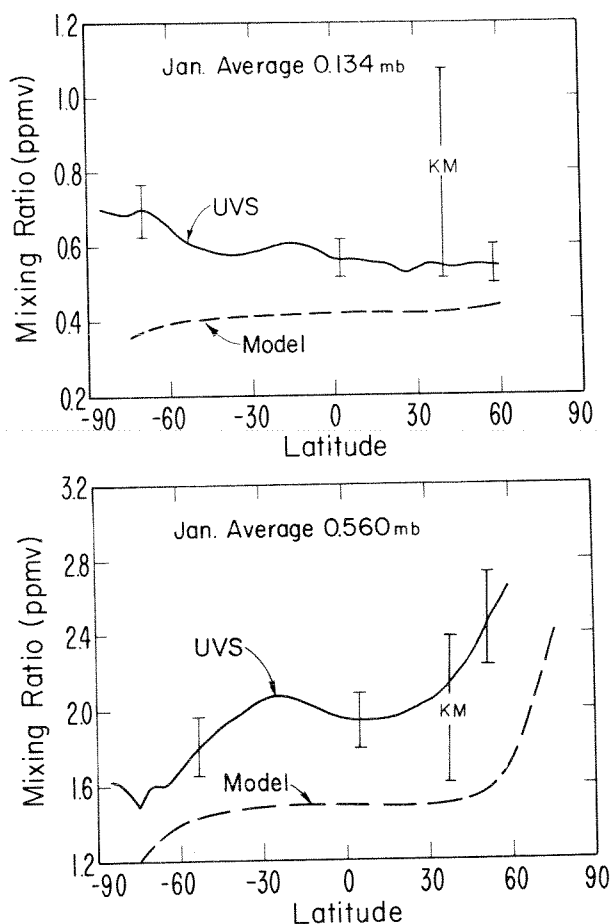


Figure 1. Ozone mixing ratios observed by the UVS instrument in January versus latitude at 0.56 and 0.13 mb and those obtained in the "standard" model B (see text).

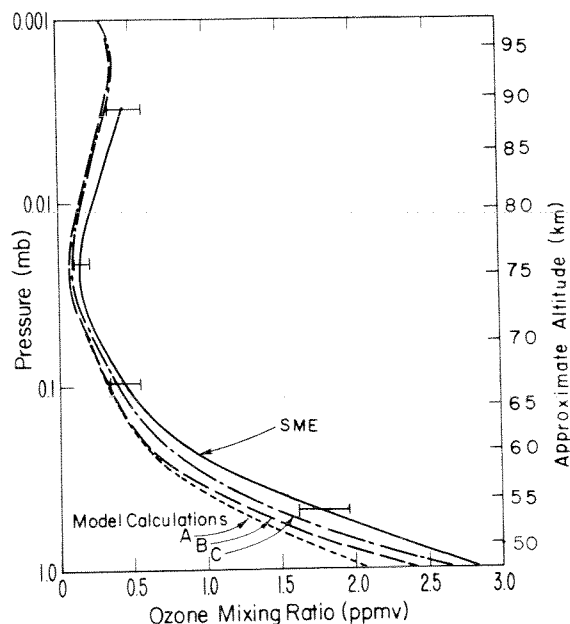


Figure 2. Ozone profiles observed at the equator by SME in January along with several model calculations. Model B employs standard chemistry. Model C uses a slower rate for R3 discussed in the text. Model A shows the effects of reduced cross sections for O₂ in the Herzberg continuum.

obtained with the SME instruments at the equator along with a number of model calculations. The SME UV spectrometer obtains ozone data from about 1.0 to 0.1 mb, while the near infrared spectrometer operates from about 1.0 to .002 mb. In the overlap region from 1.0 to 0.1 mb, the two instruments generally agree to within 15%. The profile displayed in Figure 2 represents a mean of the data of both instruments from 1.0 to 0.1 mb, and near infrared data above 0.1 mb. One sigma standard deviation about the observed means provide an estimate of the uncertainty in the measurements. This is a smoothly varying function of altitude between the indicated points. Systematic errors in the measurements are discussed by Rusch et al., (1983) and Thomas et al., (1983). The different calculations are intended to provide an indication of areas of uncertainty in model parameters. The "standard chemistry" (model B) is given by Garcia and Solomon (1983) except that the rate coefficient for reaction R9 was increased to $1.0 (-10) \text{ cm}^3 \text{ s}^{-1}$ in these calculations as an upper limit consistent with recent recommendations (JPL, 1982). A reaction coefficient of $7.0(-11) \text{ cm}^3 \text{ s}^{-1}$ is employed for R3₃. Use of a slower rate constant of $4.0(-11) \text{ cm}^3 \text{ s}^{-1}$ for this reaction yields an increase in the calculated ozone abundance as shown in model C. Recently, Herman and Mentall (1982) and Frederick and Mentall (1982) have deduced O₂ absorption cross sections near 200 nm from balloon observations of the solar irradiance, and these values are smaller than those obtained from laboratory studies. Use of these cross sections (model A) reduces the rate of O₂ photolysis (R1) in the Herzberg continuum, and has its largest effects on ozone density near 1 mb, where these wavelengths provide the dominant source of odd oxygen.

The use of the "standard chemistry" (model B) results in ozone mixing ratios which are about 10% and 30% below those obtained with SME near 1 mb and .1 mb, respectively. The general shape of the calculated profile is quite similar to that obtained in the measurements at all altitudes.

Discussion

We now examine the latitudinal trends in the data and comparison to the model in more detail. At low pressures (near 0.1 mb), odd oxygen production is believed to be due solely to R1 and odd oxygen loss is dominated by R2-R4, which depend on the odd hydrogen abundance. Neither of these exhibits much latitude dependence at 3 PM local time in the sunlit atmosphere and as a result the distribution at these altitudes is relatively flat with respect to latitude. At lower altitudes near 0.5 mb, R5 begins to play a role in odd oxygen loss along with R2-R4. R5 has a large energy of activation and is thus rapid near the hot summer stratopause and slow near the cold winter stratopause, contributing to a substantial difference in ozone abundance from one pole to the other at solstice. These seasonal trends have been noted previously by both observational and theoretical studies (see e.g. Cunnold et al., 1980; McPeters, 1980).

In spite of the good overall agreement between the observed and calculated latitudinal trends in ozone, however, it is clear that there are some differences between the absolute abundances pre-

dicted by theory and measurements in the mesosphere. The differences near 1 mb are relatively small and could well be due to minor differences in temperatures calculated in the model versus those which existed when the measurements were made. The differences which exist between about 1 and 0.1 mb are sensitive to several poorly known model parameters. For example, ozone mixing ratios slightly larger than those of model C could be obtained using model B chemistry if the Frederick and Hudson (1980) parameterization for H₂O photolysis in the Schumann Runge bands were used rather than that of Nicolet (1981). The differences between these two parameterizations lie at least in part in the adopted solar fluxes in the Schumann Runge band region (which are at present uncertain by at least 10%). At higher altitudes, however, the differences appear to be more significant, particularly when faster values are assumed for R3 as indicated by recent laboratory studies. It must be mentioned, however, that the ozone mixing ratios derived from the near infrared instrument are sensitive to the adopted chemistry for O₂(¹Δ_g) as discussed by Thomas et al. (1983).

The temperature dependence of ozone near the stratopause can be used to provide an indication of which model parameters may be responsible for the apparent discrepancies between calculated and observed mean ozone mixing ratios in the mesosphere. Barnett et al., (1975) examined the correlation between ozone density and temperature at 1 mb during a stratospheric warming, and found that the logarithm of the ozone density varies as 967/T. A similar analysis by Krueger et al., (1980) yielded a temperature coefficient of 1067/T. The magnitude of this temperature sensitivity depends largely on the relative amounts of odd oxygen destruction by R5 (which has a temperature sensitivity of about 2200/T) versus R2-R4, which are almost temperature insensitive. Our model with "standard chemistry" yields a temperature coefficient of about 1080/T, in reasonable agreement with the measured values cited above, but also predicts mean ozone abundances in the mesosphere which are below observations by SME as well as other investigators such as Krueger and Minzner (1976) (see Figure 1) or Gille et al. (1980). In order to obtain mean odd oxygen abundances as large as those inferred by SME, we must either decrease the rate of odd oxygen loss (R2-R5) or increase the rate of odd oxygen production (R1 or some other process). We could achieve agreement with the measured ozone densities by reducing the rate constants of R2 and R3 by about a factor of 2 below current recommendations. However, such a change would yield an ozone temperature coefficient of 1250/T near 1 mb, which is significantly higher than that suggested by the measurements unless those rate coefficients varied rapidly with altitude, presumably as a result of temperature sensitivity. This is not consistent with laboratory studies which indicate very little temperature dependence for R2 or R3. Similarly, agreement between the mean measured and calculated ozone mixing ratios could be obtained by reducing the water vapor mixing ratios near 0.1 to 0.01 mb to about 1 ppmv, but this would also result in an unacceptably large temperature sensitivity for ozone at the stratopause, unless the H₂O mixing ratio profile decreases extremely steeply with altitude above 0.1

mb. Alternatively, an increase in the rate of odd oxygen production by about 30% near 0.1 to 0.01 mb would reconcile the discrepancies. Indeed, Cicerone and McCrumb (1980) suggested that the calculated rate of O_2 photolysis should be larger than present estimates in the Schumann-Runge bands due to the isotopic shift of heavy oxygen. However, their current estimate of the magnitude of this effect is only 10% near 70 km, which is too small to account for the discrepancies discussed here. There could also be other odd oxygen producing reactions in addition to R1 which are not at present considered in mesospheric models, such as the photolysis of excited states of oxygen.

It is important to examine a more extensive data set to determine if the discrepancies between theory and observation obtained here are indeed representative, and not a result of natural variability in the atmospheric water vapor content or temperature. For example, Gibbins et al., (1981) emphasized the large time variation of water vapor abundance near the stratopause deduced from a long time series of microwave measurements.

In summary, we have compared the ozone abundances measured by the SME satellite in the mesosphere to those obtained in a two dimensional theoretical model. The present comparison implies that the mesospheric odd oxygen production rates may be underestimated with present photochemistry, but we note the existence of numerous uncertainties in photochemical parameters, particularly in the rate of H_2O photolysis in the Schumann Runge band region. Further data are needed to establish whether the apparent discrepancies are typical at all seasons and years. In spite of these differences in absolute amount, the trends in the data with respect to latitude and altitude are similar to those obtained in the model calculations.

Acknowledgements

Helpful discussions with R. Cicerone, M. Allen and S. Liu are gratefully acknowledged.

References

- Barnett, J.J., J.T. Houghton and J.A. Pyle, The temperature dependence of the ozone concentration near the stratopause. Quart. J. Roy. Met. Soc., 101, 245, 1975.
- Brasseur, G. Physique et chimie de l'atmosphère moyenne, Masson, Paris, 1982.
- Cicerone, R.J. and J.L. McCrumb, Photodissociation of isotopically heavy O_2 as a source of atmospheric O_3 , Geophys. Res. Lett. 7, 251, 1980.
- Cogley, A.C. and W.J. Borucki, Exponential approximation for daily average solar heating and photolysis, J. Atmos. Sci., 33, 1347, 1976.
- Cunnold, D.M. F.N. Alyea and R.G. Prinn, Preliminary calculations concerning the maintenance of the zonal mean ozone distribution in the Northern hemisphere, Pageoph, 118, 329, 1980.
- Frederick, J.E., and R.D. Hudson, Atmospheric opacity in the Schumann Runge bands and the aeronomical dissociation of water vapor., J. Atmos. Sci., 37, 1088, 1980a.
- Frederick, J.E. and R.D. Hudson, Dissociation of molecular oxygen in the Schumann Runge bands, J. Atmos. Sci., 37, 1099, 1980b.
- Frederick, J.E. and J.E. Mentall, Solar irradiance in the stratosphere: implications for the Herzberg continuum absorption of O_2 , Geophys. Res. Lett. 9, 461, 1982.
- García, R.R. and S. Solomon, A numerical model of the zonally averaged dynamical and chemical structure of the middle atmosphere, J. Geophys. Res., 88, 1379, 1983.
- Gibbins, C.J., P.R. Schwartz, D.L. Thacker and R.M. Bevilacqua, The variability of mesospheric water vapor, Geophys. Res. Lett. 8, 1059, 1981.
- Gille, J.C., P.L. Bailey and J.M. Russell, Temperature and composition measurements from the LRIR and LIMS experiments on Nimbus 6 and 7, Phil. Trans. Roy. Soc. London A, 296, 205, 1980.
- Herman, J.R. and J.E. Mentall, O_2 absorption cross sections (190-225 nm) from stratospheric solar flux measurements, J. Geophys. Res., in press, 1982.
- JPL, Chemical kinetic and photochemical data for use in stratospheric modeling, NASA panel for data evaluation, JPL 82-3, 1982.
- Krueger, A.J. and R.A. Minzner, A mid latitude ozone model for the 1976 U.S. Standard Atmosphere, J. Geophys. Res. 81, 4477, 1976.
- Krueger, A.J., B. Guenther, A.J. Fleig, D.F. Heath, E. Hilsenrath, R. McPeters, and C. Prabhakara, Satellite ozone measurements, Phil. Trans. R. Soc. London, Ser. A, 296, 191, 1980.
- McPeters, R.D., The behavior of ozone near the stratopause from two years of UV: observations, J. Geophys. Res., 85, 4545, 1980.
- Mount, G.H. and G.J. Rottman, The Solar Spectral Irradiance 1200-3184 Å Near Solar Maximum: 15 July, 1980, J. Geophys. Res., 86, 9193, 1981.
- Nicolet, M., The photodissociation of water vapor in the mesosphere, J. Geophys. Res., 86, 5203, 1981.
- Nicolet, M. and W. Peetermans, Atmospheric absorption in the O_2 Schumann Runge band spectral range and photodissociation in the stratosphere and mesosphere, Planet. Space Sci., 28, 85, 1980.
- Prather, M.J., Ozone in the upper stratosphere and mesosphere, J. Geophys. Res., 86, 5325, 1981.
- Rottman, G.J., C.A. Barth, R.J. Thomas, G.H. Mount, G.M. Lawrence, D.W. Rusch, R.W. Sanders, G.E. Thomas, and J. London, Solar Spectral Irradiance, 120 to 190nm, October 13, 1981 - January 3, 1982, Geophys. Res. Lett., 9, 587-590, 1982.
- Rusch, D.W., G.H. Mount, C.A. Barth, G.J. Rottman, R.J. Thomas, G.E. Thomas, R.W. Sanders, G.M. Lawrence, R.S. Eckman, Ozone Densities in the Lower Mesosphere Measured by a Limb Scanning Ultraviolet Spectrometer, Geophys. Res. Lett., this issue, 1983.
- Thomas, R.J., C.A. Barth, G.J. Rottman, D.W. Rusch, G.H. Mount, G.M. Lawrence, R.W. Sanders, G.E. Thomas, L.E. Clemens, Ozone Density Distribution in the Mesosphere (50-90 KM) Measured by the SME Limb Scanning Near Infrared Spectrometer, Geophys. Res. Lett., this issue.

(Received December 22, 1982;
revised February 17, 1983;
accepted March 3, 1983.)

MESOSPHERIC OZONE DEPLETION DURING THE
SOLAR PROTON EVENT OF JULY 13, 1982
PART I MEASUREMENT

R. J. Thomas^{1,2}, C.A. Barth^{1,2}, G.J. Rottman^{1,2}, D.W. Rusch^{1,2}, G.H. Mount^{1,2},
G.M. Lawrence^{1,2}, R.W. Sanders¹, G.E. Thomas^{1,2}, L.E. Clemens¹

¹Laboratory for Atmospheric and Space Physics
University of Colorado, Boulder, Colorado 80309

²Department of Astro-Geophysics
University of Colorado, Boulder, Colorado 80309

Abstract. The near infrared spectrometer and the ultraviolet spectrometer on the Solar Mesosphere Explorer (SME) observed the ozone density as a function of latitude and altitude during the solar proton event of July 13, 1982. Airglow at 1.27 μm was observed at the earth's limb. The altitude profiles of the emission were inverted providing ozone densities. The ozone densities observed showed a clear decrease during the event. The maximum depletion seen was 70%. The decrease was observed in the northern high latitudes at mesospheric altitudes. The decrease was very short lived, lasting less than a day.

Introduction

Solar proton events can inject a large number of high energy protons into the earth's middle atmosphere ionizing molecules and thereby changing the amounts of odd hydrogen, nitrogen, and oxygen. These changes then will alter the ozone destruction rate and thus its density. A change in the ozone density has been measured during several previous proton events. During the solar proton event of November 1969, decreased ozone concentrations were observed in the 50-70 km region at Fort Churchill, Canada (Weeks et al., 1972). After the large event of August 1972 an ozone depletion of up to 30% was seen between 30 and 55 km (Heath et al., 1977). McPeters, et al., (1981) observed an ozone depletion during two other solar proton events; one in January, 1971 and the other in September, 1971. One of the goals of SME was to measure the ozone changes during proton events and on July 13, 1982 an event occurred with a very large number of low energy protons that penetrated the atmosphere to about 70 km. The near infrared spectrometer was observing emission at 1.27 μm due to ozone photodissociation. The instrument, the inversion, and the resulting ozone data are discussed in this issue (Thomas et al., 1983). In this paper we will describe the measured depletion, examining the time, altitude, and latitude behavior. We will show that the ozone depletion is significantly larger than the noise and natural variations in the data. We will show data from the SME Ultraviolet Spectrometer that also shows the ozone decrease (Rusch et al., 1983). In a companion paper, Solomon et al. (1983) will examine model predictions of the ozone changes.

Copyright 1983 by the American Geophysical Union.

Paper number 3L0325.
0094-8276/83/003L-0325\$3.00

The Data

The data presented will be in the northern hemisphere. Since the event occurred in July, the southern pole was in darkness and thus no ozone measurements were made. The northern pole was almost completely sunlit giving good observation over the entire polar cap. SME is in a polar orbit (97° inclination) and observes in the orbit plane. Thus each polar latitude is seen at two different solar zenith angles. We found the largest depletion where the solar zenith angle was near 90°. We will refer to the data taken on the daytime side of the pole, where most of the data are near 3 PM local time, as PM data. These data are taken over the American continent. Data on the other side of the pole, still sunlit, will be referred to as AM data. The geometry described here is illustrated in Figure 1.

A time series of data for 21 days is shown in Figure 2. These are data at 70° and 76 km for both sides of the pole. The ozone depletion on July 13 is easily seen on the AM side. The ozone for each orbit in the 21 day period illustrates the natural variation, both in time and longitude, and noise due to instrumentation and the inversion. The entire data set was then averaged over the 20 day period, excluding July 13th, for each altitude and latitude. Figure 3 shows the depletion as a function of altitude for

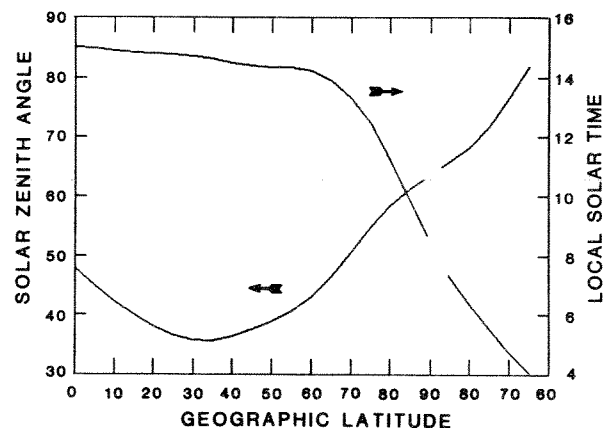


Figure 1. Solar zenith angle and local time. The local time of the observation near the equator is about 3 PM (1500 hours). Over the pole the local time changes rapidly to 3 AM. The geographic latitude of the observation never quite reaches 90°. The solar zenith angle depends on the season and orbit track.

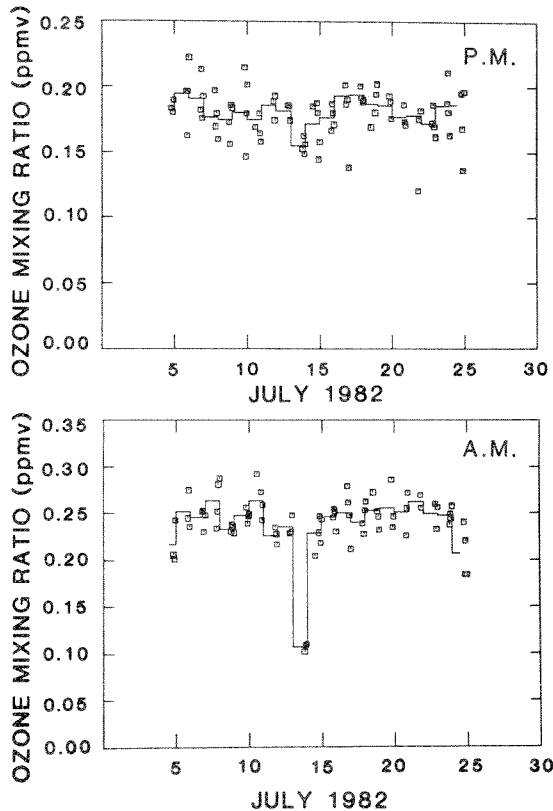


Figure 2. Ozone mixing ratio, in parts per million by volume, during July at 70° latitude and 76 km. The upper data are on the PM side of the pole and the lower are on the AM side. Each square is one orbit. There are 3 to 5 orbits near the end of each day. The solid line is the daily average of mixing ratio. The proton event occurred on July 13, 1982.

70° geographic latitude on both sides of the pole. On the AM side the depletion reaches a maximum of 60% near 78 km, while it is 10 to 20% on the PM side. The plot also shows the ozone depletion measured by the UV absorption experiment on SME. The agreement between the two techniques is very good. The geomagnetic latitude is about 60° on the AM side and 75° on the PM side. Since the three orbits averaged together on the 13th of July pass over North America the geomagnetic coordinates are shifted about 10° toward the equator.

The bars here and on other figures represent two standard deviations from the daily average estimated from the variations in the 20 days of data analysed. The variance was calculated in the following manner,

$$\sigma^2 = \frac{\sum (A_i - AVE)^2}{N-1}$$

where A_i is a matrix containing the mixing ratios of ozone at all latitudes and altitudes for the i th orbit. Most of the other quantities in these equations are similar matrices. The sum includes N ($N \approx 77$) orbits from July 3 to July 23 except those on the 13th. AVE is the average over the same data set. Assuming that the expected varia-

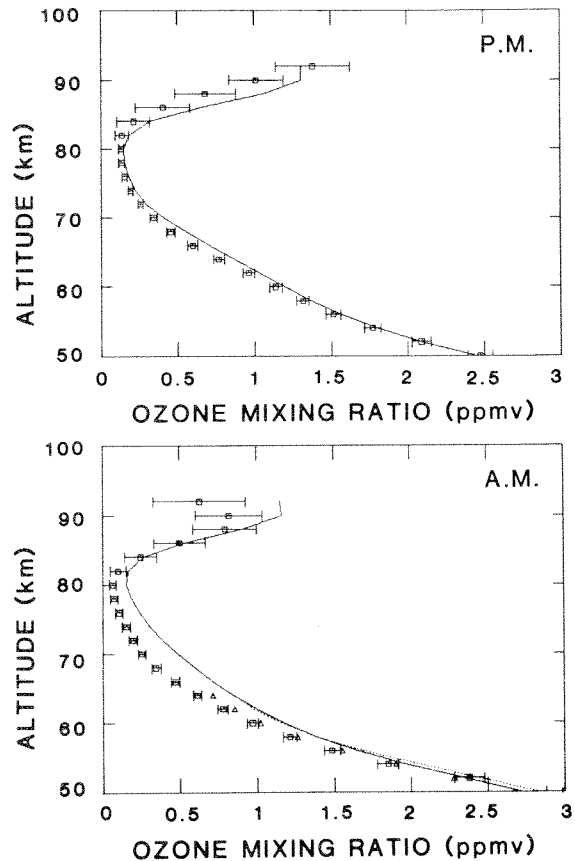


Figure 3. Ozone depletion due to the solar proton event. Both plots include the daily average on July 13 (squares) and the average for the period (—) for 70° latitude. The upper one is on the PM side of the pole and the lower is on the AM side. The bars are the two-sigma estimate of the natural variation and noise in the data. Data for the UV absorption experiment on SME is also shown for the AM side. The UV 20-day average (...) extends from 50 to 64 km as do the measurements for the 13th (triangles).

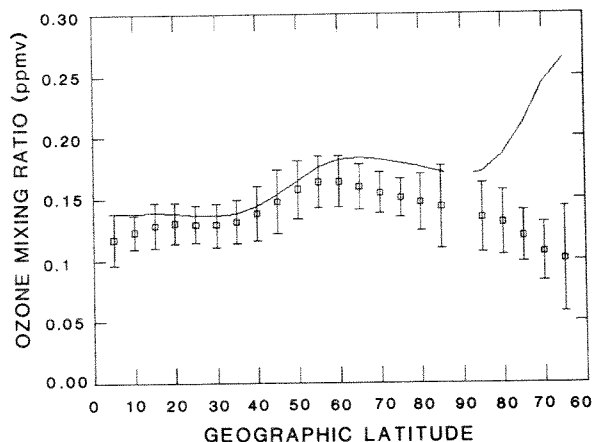


Figure 4. Latitude variation of the ozone mixing ratio at 76 km. The solid line is the average from July 3 to July 23, excluding July 13. The squares are the ozone on July 13. The bars are the same as in figure 3.

tion on the 13th is the same, the variance of the average on the 13th is

$$\sigma_{13} = \left(\frac{\sigma^2}{N_{13}} \right)^{1/2}$$

where N_{13} is the number of orbits used in the average for the 13th. The variance depends on

altitude and latitude ranging from 5% at 50 km to 30 or 40% at 90 km.

The latitudinal (or solar zenith angle) variation of the ozone changes is shown in figure 4. At 76 km, as the satellite moves north from the equator, the ozone mixing ratio increases with a plateau at high latitudes and another increase on the other side of the pole. The depletion begins as we enter the polar cap near 60° (about 65° geomagnetic) and becomes larger as we approach the terminator. The natural variability of the ozone during this period also can be seen to be a function of latitude. We again see the largest depletions on the AM side.

These data can be combined into contour plots in Figure 5 where the data grid is 5° in latitude and 2 km in altitude. The three plots show the average mixing ratio, the ratio of the depletion to the normal variation, and the percent depletion on the 13th. The top contour of Figure 5 is the average mixing ratio for the 20-day period. The plot represents a mixture of the latitudinal variations as well as some diurnal variations across the north pole. The center contours show the size of depletion in relationship to normal variation. North of 60° the depletion exceeds 2-sigma over a region between 55 and 80 km. At 65 km and 70° on the AM side the depletion exceeds 18 times the natural variation. Near the equator the ozone changes are near that expected and thus not affected by the proton event. The lower contour shows the ozone depletion in percent. The maximum depletion is 70% at 65° and 78 km on the AM side. On the PM side the depletion is only 10 to 20% but it exceeds the natural variation by 4-sigma. Thus we see a significant depletion of ozone over the north polar cap at mesospheric altitudes.

References

- Heath, D. F., O. J. Krueger, and P. J. Crutzen, Solar proton event: influence on stratospheric ozone., *Science*, 197, 886, 1977.
- McPeters, R.D., C.H. Jackman, and E.G. Stassinopoulos, Observations of ozone depletion associated with solar proton events, *J. Geophys. Res.*, 86, 12071-12081, 1981.
- Rusch, D., G.H. Mount, C.A. Barth, G.J. Rottman, R.J. Thomas, G.E. Thomas, R.W. Sanders, and G.M. Lawrence, Ozone Densities in the Lower Mesosphere Measured by a Limb Scanning Ultraviolet Spectrometer, *Geophys. Res. Lett.*, this issue, 1983.
- Solomon, S., Mesospheric ozone depletion during the solar proton event of July 13, 1982 part II theory. *Geophys. Res. Lett.* this issue, 1983.
- Thomas, R. J., C.A. Barth, G.J. Rottman, D.W. Rusch, G.H. Mount, G.M. Lawrence, R.W. Sanders, G.E. Thomas & L.E. Clemens, Ozone density distribution in the mesosphere (50-90 km) measured by the SME limb scanning near infrared spectrometer., *Geophys. Res. Lett.*, 1983, this issue.
- Weeks, L. H., R. S. Cuikay, and J. R. L. Corbin, Ozone measurement in the mesosphere during the solar proton event of 2 November 1969. *J. Atmos. Sci.*, 29, 1138, 1972.

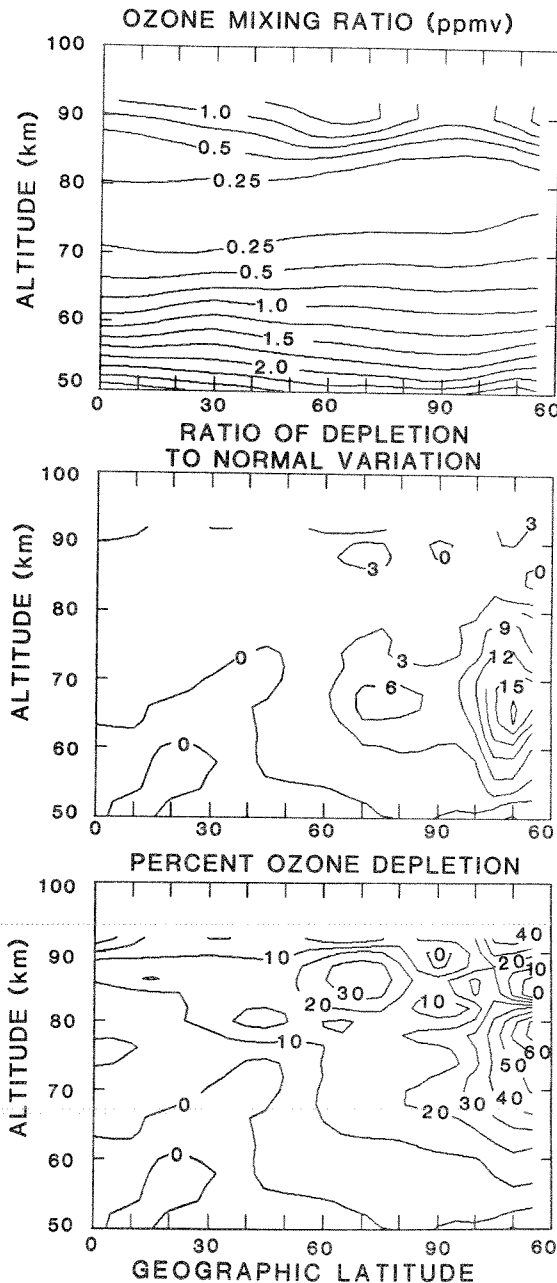


Figure 5. Contour plots of the average mixing ratio, the ratio of the depletion to normal variation, and the percent depletion on July 13. The upper plot shows the average mixing ratio during this period in parts per million by volume. The center plot is the ratio of the measured depletion to the rms variation of the daily average. In the lower plot we show the percent depletion of ozone on the day of the proton event.

(Received December 22, 1982;
accepted January 26, 1983.)

MESOSPHERIC OZONE DEPLETION DURING THE SOLAR PROTON EVENT OF JULY 13, 1982
PART II. COMPARISON BETWEEN THEORY AND MEASUREMENTS

S. Solomon^{1,3}, G.C. Reid¹, D.W. Rusch^{2,3}, R.J. Thomas^{2,3}

¹Aeronomy Laboratory, NOAA/ERL
Boulder, Colorado 80303

²Laboratory for Atmospheric and Space Physics
University of Colorado, Boulder, Colorado 80309

³Department of Astro-Geophysics
University of Colorado, Boulder, Colorado 80309

Abstract. The solar proton event of July 13, 1982 was the largest to date in the current solar cycle. Proton fluxes observed by the NOAA-6 satellite have been used to calculate ionization rates during the event, which have been found to be almost as large as those of the August, 1972 event near 70 km, but much smaller at lower altitudes. This ionization leads to the production of odd hydrogen radicals (H+OH+HO₂) which catalytically destroy odd oxygen in the mesosphere and stratosphere. A one-dimensional time-dependent model has been used to calculate the percentage change in ozone resulting from this event. The calculated ozone depletion is compared to that observed by the Solar Mesosphere Explorer (SME) satellite.

Introduction

The first observations of the depletion of mesospheric ozone during a solar proton event (hereafter referred to as SPE) were obtained by Weeks et al., (1972) using a pair of rocket probes. Swider and Keneshea (1973) suggested that these observed changes in mesospheric ozone could be due to the production of odd hydrogen formed as a by product of ion-neutral reactions under disturbed conditions. Later studies of the response of mesospheric species to SPE's include those of McPeters et al., (1981), Crutzen and Solomon (1980), Reagan et al., (1981), Rusch et al., (1981) and Solomon et al., (1981).

On July 13, 1982, the largest SPE to date in the present solar cycle occurred. Incoming proton fluxes above thresholds of 0.25, 0.8, 2.5, 16.0, 32.0, and 80.0 MeV were measured as a function of time during the event by the NOAA-6 satellite (D. Evans, H. Sauer, private communication), and a proton spectrum was constructed by fitting a series of exponential rigidity segments (Freier and Webber, 1963) to the data. Ionization rates in the polar mesosphere were then calculated by the method outlined by Reid (1974), assuming isotropy of the proton flux over the upward looking hemisphere. The rate of ionization by energetic electrons measured on the same satellite was estimated approximately and found to be negligible compared to the proton ionization. It is expected that ionization occurs over the entire polar cap (geomagnetic latitude greater

than about 55 to 60°). Figure 1 shows the observed proton spectrum and calculated ionization rate during the most intense part of the event compared to those of some of the other large events of recent solar cycles.

During this period, ozone was continuously monitored in the mesosphere by the near infrared airglow and ultraviolet spectrometers onboard the SME satellite. Thomas et al., (1983) have shown that significant depletions of high latitude ozone were observed on July 13, and that these changes were well outside the natural variability of ozone as observed by the satellite since its launch in October, 1981. In this paper, we compare the observed changes in mesospheric ozone to those calculated using a one dimensional time dependent model including full photochemistry and eddy diffusion. Use of the one dimensional approximation is valid here because we will be examining perturbations to the chemistry over a period of a few days, which is much shorter than the time scales of meridional motion in the mesosphere (of the order of weeks).

The model has been applied previously to the study of SPE's as described by Crutzen and Solomon (1980), Solomon and Crutzen (1981), Rusch et al., (1981), and Solomon et al. (1981). H₂O and H₂ distributions with altitude are taken from the two dimensional model calculations described by Solomon et al. (1982a,b) for high latitude summer. Water vapor photolysis rates are calculated using the formulas described by Nicolet (1981).

Photochemistry

The production of positive ions during particle precipitation leads to the formation of proton hydrates (H⁺(H₂O)_n) and odd hydrogen. This process may be interrupted, however, if the precursor ions (such as O₂⁺H₂O) recombine rather than reacting with H₂O. Solomon et al., (1981) discussed this ion chemistry in detail, and pointed out that below about 80 km nearly 2 odd hydrogen particles should be formed per ionization, but that above that altitude odd hydrogen production is effectively blocked by the recombination of precursor ions as a result of large electron densities and low water vapor concentrations there. Figure 2 shows the calculated number of odd hydrogen particles produced per ionization for various altitudes during this event. A sharp cutoff occurs above 80 km which will be discussed later. The location of this cutoff corresponds to the altitude where cluster ions are replaced

Copyright 1983 by the American Geophysical Union.

Paper number 3L0396
0094-8276/83/003L-0396\$3.00

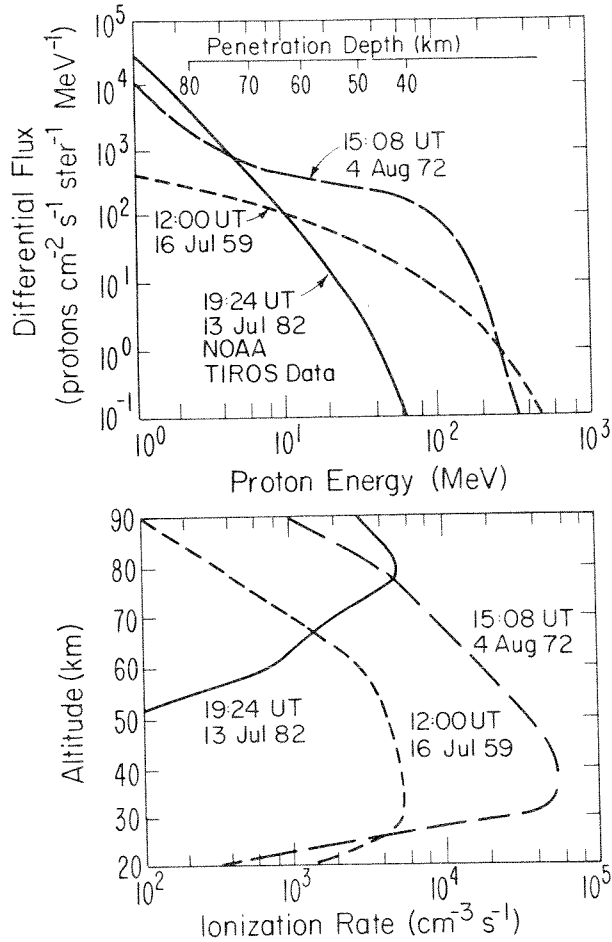
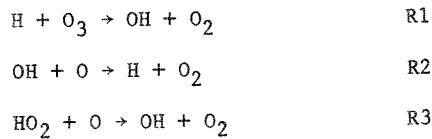


Figure 1. Differential proton energy spectra and resulting ionization rates for the July 1959, August 1972, and July 1982 solar proton events. (After Reagan et al., 1978).

by molecular ions as the dominant positive ion species, and is somewhat dependent on the assumed temperature and water vapor mixing ratio profiles (see for example, Reid, 1970).

If odd hydrogen is produced, odd oxygen can be destroyed by the following catalytic processes:



A review of the photochemistry of odd hydrogen and odd oxygen is provided, for example by Nicolet (1975). The lifetimes of odd oxygen and odd hydrogen are of the order of hours between 50 and 85 km, so that both of these species will rapidly come to equilibrium with respect to the perturbation induced by incoming particles and will return to normal within a few hours after the particle precipitation is over. For purposes of illustration only, we present below some simple photochemical arguments which can be used to estimate the response of mesospheric ozone to such an event. Assuming HO_x is in steady state near 70 km, it can be shown that for these altitudes

$$(\text{HO}_x) = \left(\frac{2J(\text{H}_2\text{O})}{2k_1\text{AB} + 2k_2\text{BC}} \right)^{1/2} \quad (1)$$

where J represents the rate of photolysis of H_2O , k_1 and k_2 are the rate constants of reaction of HO_2 with OH and H respectively, and A , B , and C represent the fraction of odd hydrogen which resides as OH , HO_2 and H , respectively. During perturbed conditions, we find

$$(\text{HO}_x)' = \left(\frac{2J(\text{H}_2\text{O}) + \text{FQ}}{2k_1\text{AB} + 2k_2\text{BC}} \right)^{1/2} \quad (2)$$

where F = number of odd hydrogen particles produced per ionization and Q = ionization rate. To a first approximation, odd oxygen is inversely proportional to the local odd hydrogen concentration. Therefore

$$\begin{aligned}
 (\text{O}_x)' / (\text{O}_x) &= (\text{HO}_x) / (\text{HO}_x)' \\
 &= \left(\frac{2J(\text{H}_2\text{O})}{2J(\text{H}_2\text{O}) + \text{FQ}} \right)^{1/2} \quad (3)
 \end{aligned}$$

and finally

$$\begin{aligned}
 &\% \text{ decrease in } \text{O}_x \\
 &= \left\{ 1 - \left(\frac{2J(\text{H}_2\text{O})}{2J(\text{H}_2\text{O}) + \text{FQ}} \right)^{1/2} \right\} \times 100 \quad (4)
 \end{aligned}$$

and we can see that the expected change in ozone during a SPE should be roughly related to the relative magnitudes of odd hydrogen production by the ions versus the normal background production due to photolysis of water vapor. Therefore, the computed depletion will depend on the adopted water vapor mixing ratios, and we show below the

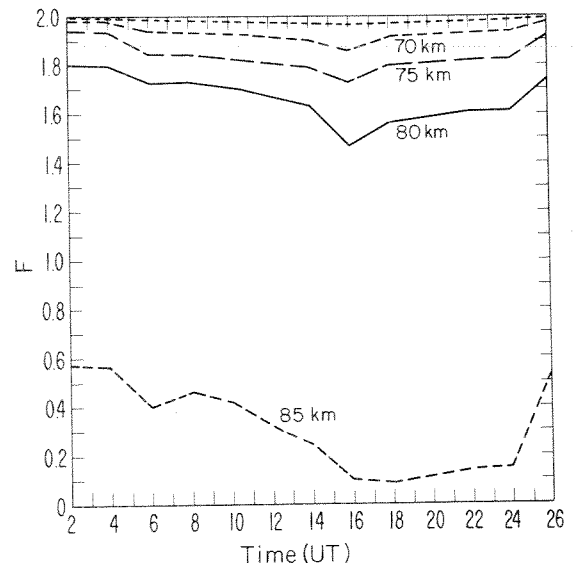


Figure 2. Number of odd hydrogen particles produced per ionization for various altitudes during the July 1982 SPE at 70° latitude.

sensitivity of our analysis to the assumed water vapor content. We have found that this simple formula yields results which are within 10% of the results of the complete time dependent calculations from 70 to 80 km. At lower altitudes, the production of odd hydrogen from the reaction of $O(^1D)$ with H_2O introduces an additional complication and more detailed calculations must be made. Also, the relative abundances of OH, HO_2 , and H (A, B, and C in equations (1) and (2) above) are dependent on the atomic oxygen and ozone densities and may therefore change during the event as large amounts of odd oxygen are destroyed. All of these effects are considered in our model.

Results And Discussion

Figure 3 presents the observed depletions of the mesospheric ozone profiles obtained by SME on July 13, 1982 along with model calculations for 70° latitude on the PM and AM sides of the orbit as discussed by Thomas et al., 1983. The differences between these two cases are principally due to the effect of changing solar zenith angle on the rate of H_2O photolysis (cf., eqn 3 above).

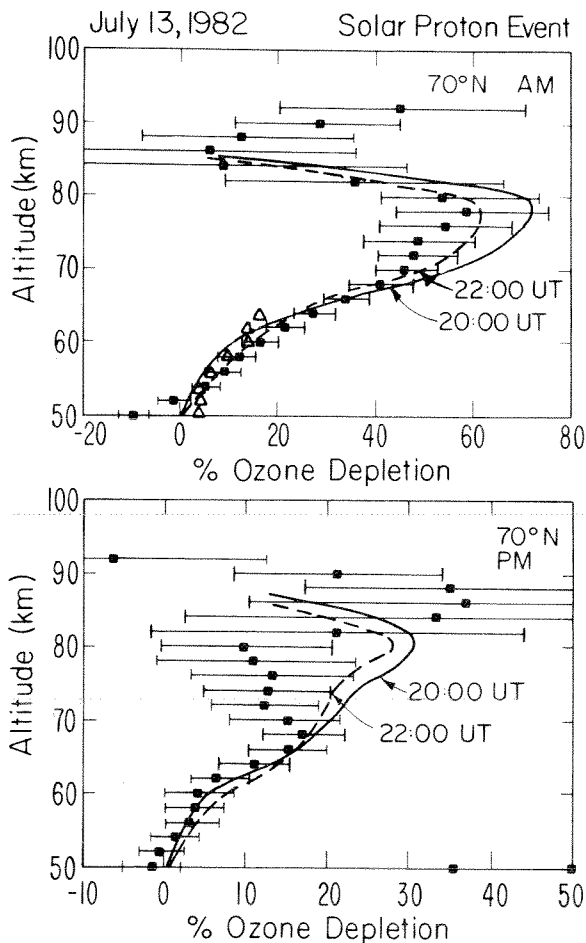


Figure 3. Observed ozone depletion on July 13, 1982 at 70°N latitude on the AM and PM portions of the SME orbit (each point represents a mean of three orbits on July 13, 1982 near 1830, 2120 and 2206 UT). Triangles denote data from the UV spectrometer. Model calculated profiles for 2000 and 2200 UT are shown.

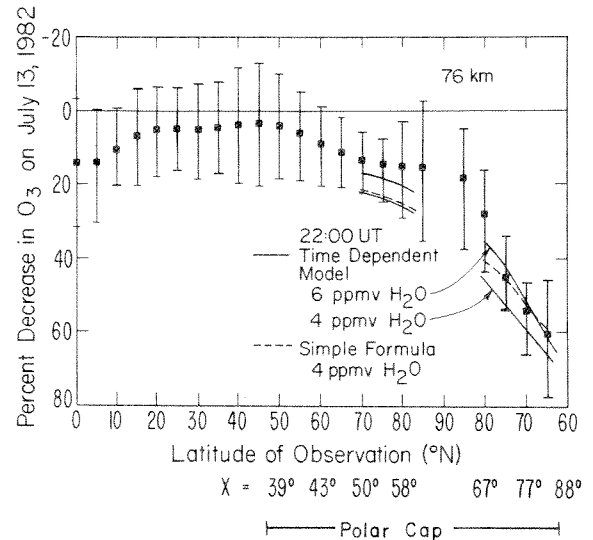


Figure 4. Observed depletion in ozone at 76 km on July 13, 1982 as a function of latitude on the SME orbit. Solar zenith angles are also shown. Time dependent model calculations employing 4 and 6 ppmv H_2O as well as the values obtained with the simple formula (4) (see text) with 4 ppmv H_2O are displayed.

At larger solar zenith angles, the rate of production of HO_x due to water vapor photolysis is proportionately smaller compared to the production of HO_x by the ionization, which is independent of zenith angle. The agreement between theory and observation is somewhat better on the AM than on the PM side of the orbit. It is possible that local variations in H_2O density or temperatures contribute to these differences particularly since the altitude of the cutoff in ozone depletion appears to be different in the two cases shown. It should be noted that there is some uncertainty in the computed ionization rates and in the assumed water vapor mixing ratio. If we adopt a 30% uncertainty in the ionization rate and a 1.0 ppmv uncertainty in the H_2O mixing ratio, then the calculated depletion varies by roughly plus or minus 10% near 75 km, so that the apparent differences may not be significant. The effect of solar zenith angle is illustrated more clearly in Figure 4, which displays the calculated and measured depletions at 76 km as a function of solar zenith angle. The agreement between measurement and theory suggests that the computed behavior of optical depth for the wavelengths responsible for H_2O photolysis (primarily Lyman alpha radiation) is approximately correct. Results are shown for two different values adopted for the water vapor mixing ratio. Figure 4 also shows the calculated depletion at this altitude using the simple formula (4) above.

The marked reduction in ozone depletion observed above 80 km is well reproduced by the model. As discussed above, this feature is probably due to the lack of odd hydrogen production by ions at high altitudes, and provides an indication that our understanding of the ion chemistry is qualitatively correct.

McPeters et al., (1981) presented a study of the ozone depletion observed near 1 mb by the

backscatter ultraviolet ozone instrument during SPE's and concluded that the observed depletion was greater than predicted. Similar conclusions were inferred from the limited rocket data of Weeks et al., (1972) by Swider et al., (1978) and by Solomon et al., (1981) who also pointed out that fluctuating temperatures could be responsible for the apparent changes. Further observations may be required to determine whether or not inconsistencies exist at these lower altitudes.

The data base provided by SME furnishes an opportunity to study the effect of particle precipitation much more comprehensively than has been possible before. The July 13, 1982 SPE was an ideal event for purposes of examining mesospheric ozone chemistry. The observed ozone depletion has been examined here as a function of latitude, altitude, and local time, and has been shown to be in good agreement with model calculations. This suggests that the mesospheric response to an impulsive injection of odd hydrogen is quite similar to theoretical expectation.

Acknowledgement. We gratefully acknowledge D. Evans and H. Sauer of the NOAA Space Environment Laboratory for making the satellite particle data available to us. This research was partly supported by a grant from the Defense Nuclear Agency.

References

- Crutzen, P.J., and S. Solomon, Response of mesospheric ozone to particle precipitation, Planet. Space Sci., 28, 1147, 1980.
- Freier, P.S., and W.R. Webber, Exponential rigidity spectra for solar flare cosmic rays, J. Geophys. Res., 68, 1605, 1963.
- McPeters, R.D., C.H. Jackman and C.G. Stassinopoulos, Observations of ozone depletion associated with solar proton events, J. Geophys. Res., 86, 12, 071, 1981.
- Nicolet, M., Stratospheric ozone: an introduction to its study, Rev. Geophys. Space Phys., 13, 593, 1975.
- Nicolet, M., The photodissociation of water vapor in the mesosphere, J. Geophys. Res., 86, 5203, 1981.
- Reagan, J.B., R.W. Nightingale, R.E. Meyerott, R.C. Gunton, R.G. Johnson, J.E. Evans, and W.L. Imhof, Lockheed report #LMSC-D630455, 1978.
- Reagan, J.B., R.E. Meyerott, R.W. Nightingale, R.C. Gunton, R.G. Johnson, J.E. Evans and W.L. Imhof, Effects of the August 1972 Solar particle events on stratospheric ozone, J. Geophys. Res., 86, 1473, 1981.
- Reid, G.C., Production and loss of electrons in the quiet daytime D-region of the ionosphere, J. Geophys. Res., 75, 2551, 1970.
- Reid, G.C., Polar cap absorption-observations and theory, Fund. Cosmic Phys., 1, 167, 1974.
- Rusch, D.W., J.C. Gerard, S. Solomon, P.J. Crutzen, and G.C. Reid, The effect of particle precipitation on the neutral and ion chemistry of the middle atmosphere I. Odd nitrogen, Planet. Space Sci., 29, 767, 1981.
- Solomon, S. and P.J. Crutzen, Analysis of the August, 1972 solar proton including chlorine chemistry, J. Geophys. Res., 86, 1140, 1981.
- Solomon, S., D.W. Rusch, J.C. Gerard, G.C. Reid, and P.J. Crutzen, The Effect of particle precipitation on the neutral and ion chemistry of the middle atmosphere II. Odd hydrogen, Planet. Space Sci., 29, 885, 1981.
- Solomon, S., P.J. Crutzen and R.G. Roble, Photochemical coupling between the thermosphere and the lower atmosphere I. Odd nitrogen from 50 to 120 km, J. Geophys. Res., 87, 7206, 1982a.
- Solomon, S., E.E. Ferguson, D.W. Fahey and P.J. Crutzen, On the chemistry of H₂O, H₂, and meteoritic ions in the mesosphere and lower thermosphere, Planet. Space Sci., 30, 1117, 1982b.
- Swider, W. and T.J. Keneshea, Decrease of ozone and atomic oxygen in the lower mesosphere during a PCA event, Planet. Space Sci., 21, 1969, 1973.
- Swider, W., T.J. Keneshea and C.I. Foley, An SPE disturbed D-region model, Planet. Space Sci., 26, 883, 1978.
- Thomas, R.J., C.A. Barth, G.J. Rottman, D.W. Rusch, G.H. Mount, G.M. Lawrence, R.W. Sanders, G.E. Thomas, L.E. Clemens, Mesospheric Ozone Depletion During the Solar Proton Event of July 13, 1982 Part I Measurement, Geophys. Res. Lett. this issue, 1983.
- Weeks, C.H., R.S. Cuikay and J.R. Corbin, Ozone measurements in the mesosphere during the solar proton event of 2 November, 1969, J. Atmos. Sci., 29, 1138, 1972.

(Received December 22, 1982;
revised February 17, 1983;
accepted March 3, 1983.)

TEMPERATURE MEASUREMENTS IN THE EARTH'S STRATOSPHERE
 USING A LIMB SCANNING VISIBLE LIGHT SPECTROMETER

D. W. Rusch^{1,2}, G.H. Mount^{1,2}, J.M. Zawodny^{1,2}, C.A. Barth^{1,2}, G.J. Rottman^{1,2},
 R.J. Thomas^{1,2}, G.E. Thomas^{1,2}, R.W. Sanders¹, G.M. Lawrence^{1,2}

¹Laboratory for Atmospheric and Space Physics and
 University of Colorado, Boulder, Colorado 80309

²Department of Astro-Geophysics
 University of Colorado, Boulder, Colorado 80309

Abstract. The temperature of the earth's atmosphere between 40 and 50 km is inferred from measurements of Rayleigh scattered sunlight by a visible-light spectrometer on the Solar Mesosphere Explorer spacecraft. The RMS deviation of the satellite measurements from conventional rocket measurements is 5°K above 45 km and 2-3°K below 45 km. The satellite data are compared to model temperatures for March, 1982.

Introduction

In this paper we report on a method of temperature profile retrieval using an instrument on the Solar Mesosphere Explorer (SME) satellite which accurately measures the shape of the Rayleigh scattering profile in the stratosphere. The primary purpose of the visible light spectrometer is to determine the NO₂ density in the 20-40 km region (see Thomas et al., 1980, Barth et al., 1983, and Mount et al., 1983). In the 40-50 km altitude region, the data from this instrument are used to retrieve the ambient temperature profile. We validate the method by comparing our results to several sounding rocket retrievals of temperature during near coincident SME measurements. Below we describe the instrument, the observations, and the comparisons to rocket data and models. The objective of this analysis is to determine temporal and geographical changes in temperature and relate them to other atmospheric measurements made on the Solar Mesosphere Explorer satellite.

Instrument Description

The visible light instrument on SME is a two channel, programmable Ebert-Fastie spectrometer which employs dual silicon diode detectors and an f/5 25 cm focal length off-axis parabolic telescope. The field of view is 0°.074 x 0°.74 giving a height resolution on the earth's limb of 3.5 km. The wavelength coverage is from 312.6nm to 647.2nm. The data reported on here were all obtained near 440.0nm. A more detailed description of the instrument is given in an accompanying paper in this issue (Mount et al., 1983).

Observations

The line of sight penetrates the earth's limb once each spin of the spacecraft. The operating

mode of the instrument allows the Rayleigh scattering in the two channels to be measured simultaneously on each scan. For the temperature calculations, six limb scans are averaged to form a single radiance profile to improve the signal to noise of the data. In addition, the data from both channels are used to increase the statistical accuracy of the result.

In Figure 1 we display data from six consecutive limb scans as a function of altitude for the long wavelength channel at 442.0nm. The data numbers decrease from about 350 at 30 km to about 10 at 50 km. The statistical error on any sample is less than 1 data number and was established during pre-launch calibration. The short wavelength channel is set at 439nm. An error analysis will be presented later. The method provides one temperature profile for each 5° of latitude from about 40 to 50 km.

The temperature profile is derived from measuring the pressure scale height of the atmosphere. At each altitude the slant intensity data are corrected for the presence of a non-zero lapse rate by the Chapman function which is proportional to (T)^{1/2}. The expression for the temperature is

$$T(z+\Delta z/2) = C/\ln\{(I(z)/T(z))/(I(z+\Delta z)/T(z+\Delta z))\} \quad (1)$$

and

$$C = \Delta zmg/k \quad (2)$$

Here T is the temperature and I the radiance which has been corrected for atmospheric trans-

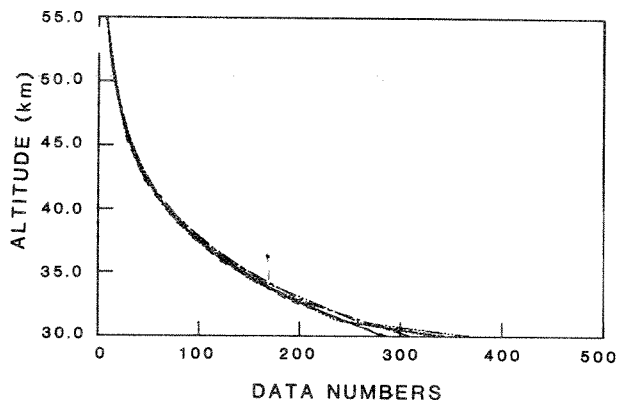


Figure 1: Data numbers as a function of altitude for six consecutive limb scans of the visible light spectrometer at 4420 A over Natal on January 25, 1982.

Copyright 1983 by the American Geophysical Union.

Paper number 3L0409
 0094-8276/83/003L-0409\$3.00

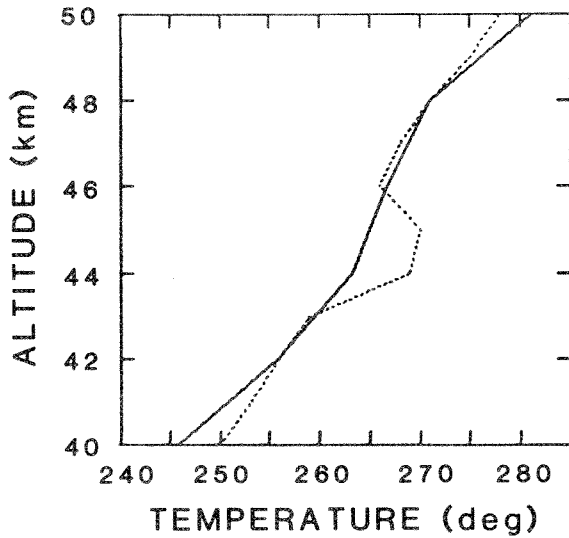


Fig. 2a

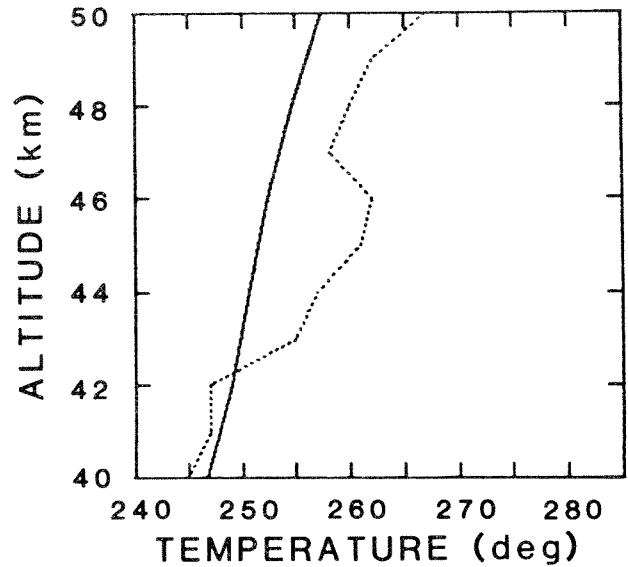


Fig. 2d

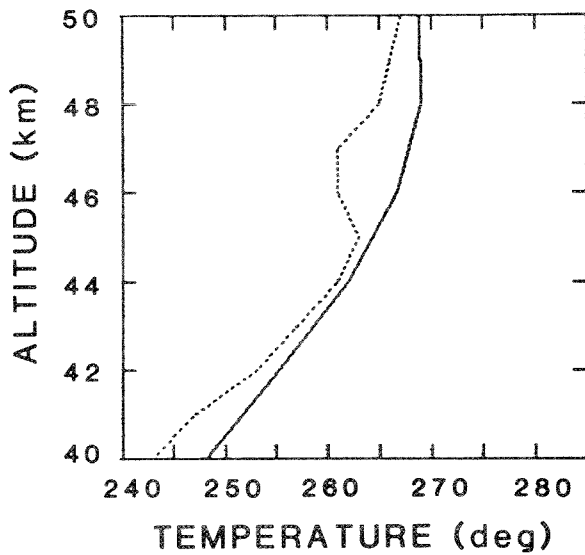


Fig. 2b

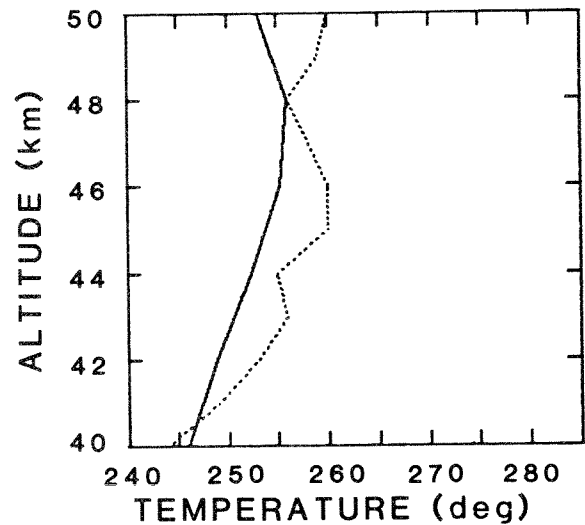


Fig. 2e

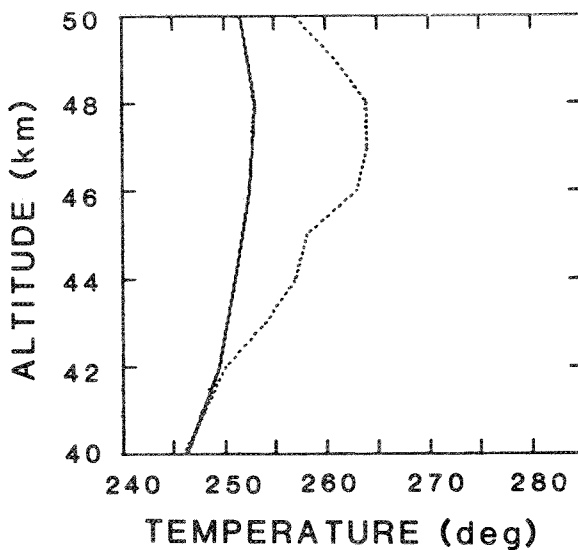


Fig. 2c

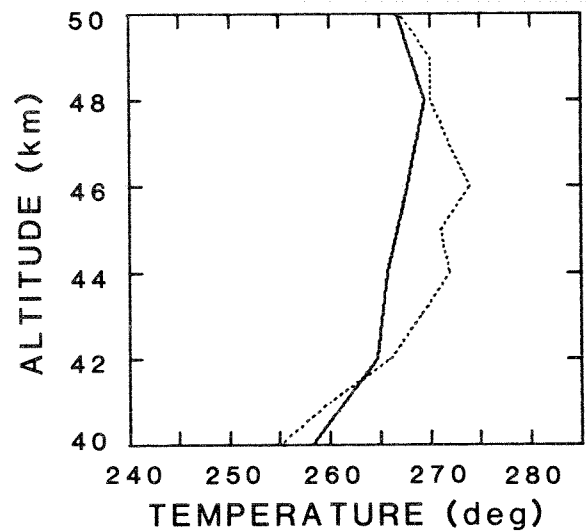


Fig. 2f

Figure 2a-f) Comparison of temperature data from the visible spectrometer (—) with a conventional rocketsonde (---) at Natal; b) at Wallops Island on Day 56; c) Day 65; d) Day 66; e) Day 77; f) Day 174.

TABLE 1. Details of SME-Rocket temperature comparisons

ROCKETS			SME OVERPASS		
PLACE	DAY OF YEAR	TIME (UT)	TIME (UT)	LAT	LONG
Natal	25	1520	1700	5.00	-30.27
Wallops	56	1900	1954	40.00	-76.98
Wallops	65	1902	1953	40.00	-76.75
Wallops	66	1901	1942	40.00	-74.07
Wallops	77	1901	1917	40.00	-68.60
Wallops	110	1737	1928	40.00	-72.99*
Wallops	174	1600	1944	40.00	-78.16

* Not shown

mission. The temperature is calculated at the meshed altitude grid points and a model profile is used as the initial guess. Because only relative intensities are used, the calculated temperature is completely independent of the absolute calibration of the instrument. The calculation is iterated until the temperatures converge to less than the statistical accuracy of the measurement (See Figure 3).

Figures 2a to f compare the temperature profiles derived from the visible light spectrometer data to conventional rocketsonde data. The profile in Figure 2a was deduced from data obtained over Natal, Brazil on January 25, 1982 (Figure 1). The remaining profiles were all taken over Wallops Island, Virginia. Details of the comparisons are given in Table 1. The rocket data are provided every km whereas the altitude resolution of the SME spectrometer is 3.5 km and the detail shown in the rocket profiles is smoothed over latitude and altitude in the satellite data.

The RMS deviation between the rocket and satellite profiles is shown in Figure 3 as the solid line for the seven comparisons. A Wallops Island comparison on Day 110 which is included in the RMS deviation is not shown in Figure 2. The

result gives an RMS deviation of 5°K above 45 km and about 3°K below 45 km. The rocket data have been smoothed over 3.5 km for this calculation. The dashed line is the calculated error on the satellite measurements assuming the laboratory established error of one data number per sample. The error is calculated from the following expression which was derived from Equation 1 by taking into account the statistical error in the measurement of the radiance.

$$\Delta T(z + \frac{1}{2} \Delta z) = C \left(\left[\left(\frac{\Delta I_1}{I_1} \right)^2 + \left(\frac{\Delta I_2}{I_2} \right)^2 \right] / [\ln(I_1/I_2)]^4 \right)^{1/2} \quad (3)$$

where C is as defined in equation 2, ΔI is at most one data number, and I ranges from 120 to 4000 data numbers over the altitude region 50 to 36 km for 12 merged radiance profiles. The error shown in Figure 3 is about 0.25°C at 40 km and increases to about 2.5°C at 50 km. The quoted precision on the rocket profiles is ±2°C (Schmidlen, 1981) over the altitude range presented.

In Figure 4 we present a cross-section of temperature versus altitude and latitude for March, 1982 derived from the SME data. The March data show an area of maximum temperatures between 0° and 30°S near 48 km of about 275°K, with decreasing temperatures southward. Northward of 30°N the monthly average shows very cold temperatures due to a displaced cold polar vortex for

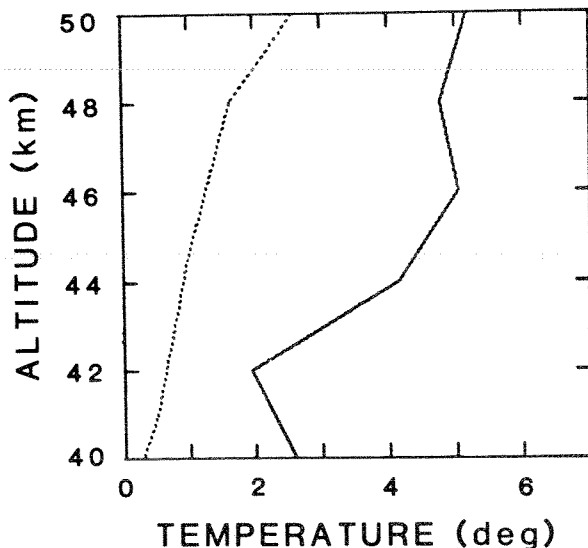


Figure 3: The RMS deviation of the satellite temperature from the rocket data for the seven comparisons of Figures 2-4 (—). The dashed line is the error introduced in the satellite retrievals from the statistical uncertainty of the data.

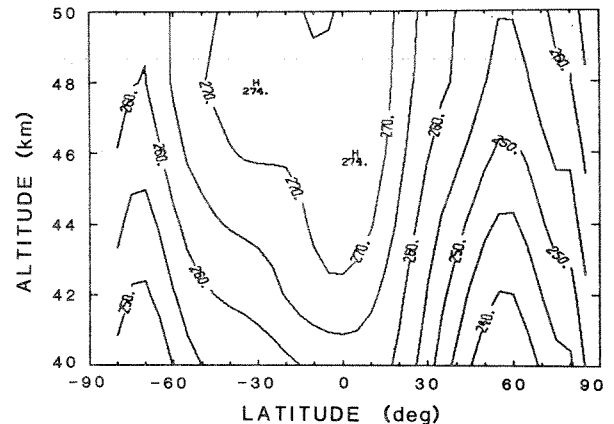


Figure 4: Monthly averaged temperatures in altitude and latitude for March, 1982 for the SME measurements.

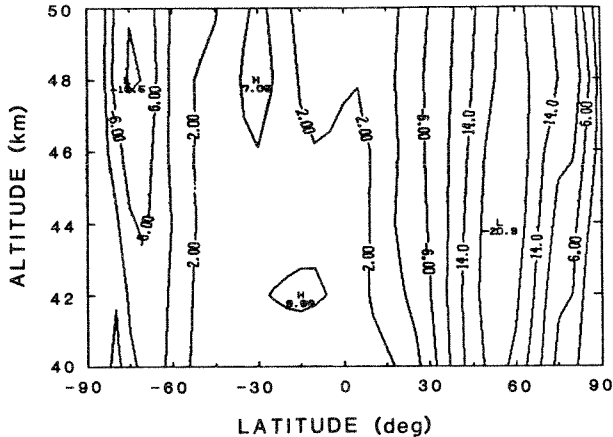


Figure 5: The difference between the SME March average temperature and the model of Cole and Kantor (1978). Positive differences imply the SME data are warmer than the model.

almost the entire month. In Figure 5, contours of temperature difference between the SME data and the model of Cole and Kantor (1978) are displayed. A positive temperature difference means the SME data are warmer than the model. In the southern hemisphere the maximum differences occur near 30°S where SME is warmer than the model by about 7°K and at 70°S where SME is cooler by about 10° at 48 km. In the north, the SME data are cooler everywhere. The temperature difference is 20° at 50°N for all altitudes. Data from the National Meteorological Center (NMC) support the cooler SME temperatures and show the polar vortex stably positioned over Canada in North America where the SME data were taken. For example, the SME daily average temperatures have been compared to the NMC temperatures for the period from January 25, to March 26, 1982 for 50°N at 40 km. The maximum difference between the two data sets is 7°K and the average temperatures over the period agree to within 3°K.

Summary

A technique for measuring the temperature of the earth's atmosphere between 40 and 50 km by a satellite instrument which accurately measures

the Rayleigh scattering scale height has been compared to rocket data and agree well, even considering the small number of comparisons available. The satellite measurements of temperature as a function of latitude when averaged monthly agree well with the Air Force model in the southern hemisphere for winter of 1982. The results shown in Figures 3 and 5 indicate that from the SME data we are able to determine changes in atmospheric temperature in the 40-50 km region of the order of 3-5° K and detect and track the presence of large scale dynamic systems such as stratospheric warmings and movements of the winter polar vortex.

References

- Barth, C.A., D.W. Rusch, R.J. Thomas, G.H. Mount, G.J. Rottman, G.E. Thomas, R.W. Sanders, G.M. Lawrence, *Solar Mesosphere Explorer: Scientific Objectives and Results*, *Geophys. Res. Lett.*, this issue, 1983.
- Cole, A.E., and A.J. Kantor, *Air Force reference atmospheres*, Air Force Geophysics Laboratory, Project 6670, 1978.
- Mount, G.H., J.F. Noxon, D.W. Rusch, J.M. Zawodny, C.A. Barth, G.J. Rottman, R.J. Thomas, G.E. Thomas, R.W. Sanders and G.M. Lawrence, *Measurements of NO₂ in the Earth's stratosphere using a limb scanning visible light spectrometer*, *Geophys. Res. Lett.*, this issue, 1983.
- Schmidlen, F.J., *Repeatability and measurement uncertainties of United States meteorological rockets*, *J. Geophys. Res.*, 86, 9599-9603, 1981.
- Thomas, G.E., C.A. Barth, E.R. Hansen, C.W. Hord, G.M. Lawrence, G.H. Mount, G.J. Rottman, D.W. Rusch, A.I. Stewart, R.J. Thomas, J. London, P.L. Bailey, P.J. Crutzen, R.E. Dickenson, J.C. Gille, S.C. Liu, J.F. Noxon, and C.B. Farmer, *Scientific Objectives of the Solar Mesosphere Explorer Mission*, *Pageoph.*, 118, 591-615, 1980.

(Received December 22, 1982;
accepted March 8, 1983.)

MEASUREMENTS OF NO₂ IN THE EARTH'S STRATOSPHERE USING A LIMB SCANNING VISIBLE LIGHT SPECTROMETER

G.H. Mount^{1,2}, D.W. Rusch^{1,2}, J.M. Zawodny^{1,2}, J.F. Noxon³, G.A. Barth^{1,2}, G.J. Rottman^{1,2}, R.J. Thomas^{1,2}, G.E. Thomas^{1,2}, R.W. Sanders¹, G.M. Lawrence^{1,2}

¹Laboratory for Atmospheric and Space Physics University of Colorado, Boulder, Colorado 80309

²Department of Astro-Geophysics University of Colorado, Boulder, Colorado 80309

³Aeronomy Laboratory, NOAA/ERL Boulder, Colorado 80303

Abstract. NO₂ densities determined from the limb scanning visible light spectrometer on board the Solar Mesosphere Explorer spacecraft are reported for winter 1981/82 in the altitude region 28-40 km. The observational technique utilizes the photoabsorption by NO₂ of Rayleigh scattered sunlight in the 440nm spectral region. The NO₂ density varies from pole to pole and shows large variations at high northern latitudes during the winter months which are related to both the temperature and flow of air near 30 km.

Introduction

The importance of NO₂ as a catalytic destroyer of ozone in the stratosphere was first pointed out by Crutzen (1970). Since then, the global and seasonal behavior of the column abundance of stratospheric NO₂ have been studied by Noxon and co-workers (1979a,b, 1982) and Coffey et al., (1981). The measurements reported in the literature are inherently limited to the collection of data sporadic in both time and location. A recent theoretical treatment has appeared which compares these measurements and model calculations of the distribution of nitrogen species in the stratosphere (Solomon and Garcia, 1982).

We report here on NO₂ density profiles obtained during winter 1981/82 from the Visible Light Spectrometer on board the Solar Mesosphere Explorer (SME) spacecraft. Data collected by SME provide complete latitude coverage over the Western Hemisphere and Western Europe during daytime. Profiles are retrieved on one degree latitude centers in the 20-45 km altitude region, and are averaged to a standard geophysical data base on 5 degree latitude centers and a 2 km altitude grid. We describe the measurement technique, observations, and comparison with other data. The scientific aspects of SME are discussed by Thomas et al., (1980) and Barth et al., (1983).

Measurement Technique

Figure 1 shows the absorption cross section of NO₂ (Johnston, 1982) in the visible region of the

Copyright 1983 by the American Geophysical Union.

Paper number 3L0328. 0094-8276/83/003L-0328\$3.00

spectrum convolved with the 1nm resolution of the SME instrument. Considerable variation in the cross section exists in the region near 440nm. By making radiance measurements, at the limb, of Rayleigh scattered sunlight at two wavelengths from the same scattering element, one where NO₂ has maximum absorption and one where it has minimum absorption, it is possible to deduce the slant column effect of NO₂ on the Rayleigh scattered signal. Measurements made simultaneously at wavelength pairs marked "normal" or "inverted" result in a radiance ratio characteristic of NO₂. Measurements made at pairs marked "null" return a radiance ratio of the background atmosphere. By comparing normal or inverted pair ratios with null ratios one may obtain a profile of NO₂ slant column abundance as seen from the satellite.

The instrument used to make the NO₂ measurements is a two channel visible light spectrometer programmable in wavelength from 320-640nm in 0.3nm steps. The spectrometer is a 12.5 cm focal length Ebert-Fastie design with a grating chosen to put a 1nm triangular bandwidth onto dual silicon diode detectors in the exit plane at a wavelength separation of 3nm near 440nm (see figure 1). The telescope is a single-element f/5 off-axis paraboloid. Its 25 cm focal length gives a projected slit width at the earth's limb as seen from the satellite of 3.5 km perpendicular to the limb and 35 km tangent to the limb. The telescope was carefully designed and tested to minimize spatially off-axis scattered light, and the observations indicate that the flight performance

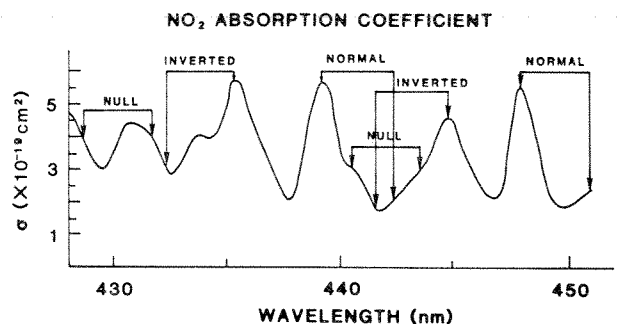


Figure 1. The photoabsorption cross section of NO₂ from 430-450nm (Johnston, 1982). The wavelength pairs used for making the NO₂ measurements are indicated as "normal", "inverted" and "null".

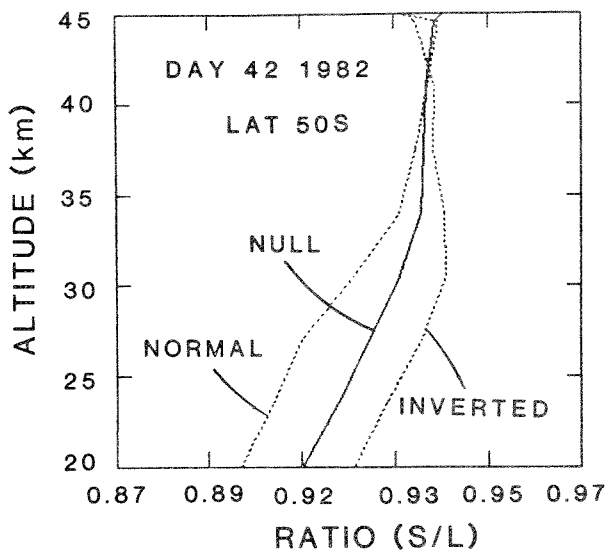


Figure 2.. The ratio of short wavelength (S) to long wavelength (L) "normal", "inverted", and "null" wavelength pairs as observed on Day 42 1982. The null ratio is characteristic of a Rayleigh scattering atmosphere with no NO₂ present. The other pairs are inverses of each other in the NO₂ cross section and are symmetric about the null line.

is excellent. The silicon diode detectors, which were etched as exit slits, feed an analog electronic circuit which measures each channel output and the difference between the channels such that the ratio of the two channel output can be determined to an accuracy of 0.2% in the 20-40 km altitude region. This high degree of precision is required since the differential absorption in the ratio due to NO₂ in the Rayleigh scattered signal rarely exceeds 3%.

Figure 2 shows raw unsmoothed measurements of a null ratio, a normal and inverted pair. The lack of noise in these profiles demonstrates the high precision of the instrument. The null curve lies between the others and the separation of the null and the normal (or inverted) curves depends on the relative NO₂ cross-sections in these wavelength pairs. While Figure 2 shows how the various choices of grating position allow detection of NO₂ some comment on the shape of the null curve seems called for. At the wavelengths we use (~440nm) the atmosphere has unit optical depth for a tangent ray whose minimum altitude is 23 km. At much higher altitudes the satellite views along a path of low optical depth and receives a signal which consists almost entirely of singly scattered solar photons. Under these conditions two neighboring wavelengths will exhibit a ratio characterized by the λ^4 (blue) Rayleigh scattering dependence. At the other extreme of altitude, well below 23 km, the signal consists of photons which have been scattered many times before re-emerging from the atmosphere and the spectral dependence will be that of the incident white sunlight. The expected change in ratio between these two extremes is close to 3% and the null curve in Figure 2 exhibits this. Above ~32 km the signal ratio shows the pure Rayleigh "blue" value; at lower altitude one sees the transition to the "white" limit of multiple

scattering. Above ~28 km the optical depth along a ray path is small enough to permit an analysis only in terms of single scattering. Below this altitude multiple scattering is important and, indeed, prevents a clear quantitative measurement of NO₂. We thus, at present, restrict our analysis to the region >28 km.

Observations

Thirty-two 2.5 msec samples (each 3.5 km projected at the earth's limb) are taken each spin of the spacecraft (approximately one degree of latitude travel). Six spins are averaged together to put the data onto a standard 5° latitude grid producing radiance profiles of high statistical precision.

Instrument calibrations are used to produce radiance profiles which are ratioed and averaged in 5 degree latitude bins. An "onion peel" radiative transfer inversion code then retrieves NO₂ density profiles. The altitude profile of the differences between an NO₂ radiance ratio data set ("normal" or "inverted" pairs) and the pure Rayleigh ratio ("null pair") measured on the 3.5 km grid is input to the inversion routine and is interpolated to an 0.5 km grid for inversion stability. Inversion begins at 41 km where the NO₂ density is known to be small and the inversion code calculates the overhead column abundance of NO₂ at the layer of interest. For each successive 0.5 km layer below 41 km, the measured difference in the ratios is corrected for the column of NO₂ above that layer. The residual difference is then assumed to be due to NO₂ column abundance in that layer. Model scale heights (Solomon and Garcia, 1982) are used to start the inversion. In the analysis account must be taken of a small but non-negligible effect due to ozone absorption (Johnston, 1982)

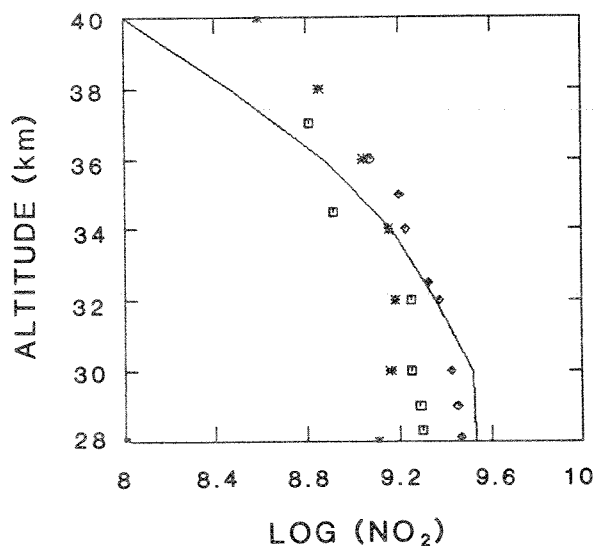


Figure 3. An NO₂ density profile taken at 40°S latitude on Day 42 1982 from SME (solid line). Comparison data is from Ackerman et al. (1975) (squares) and Kerr and McElroy (1976) diamonds taken 40°-60°N latitude in spring and summer. A model calculation by Solomon (1982) (*) is shown also.

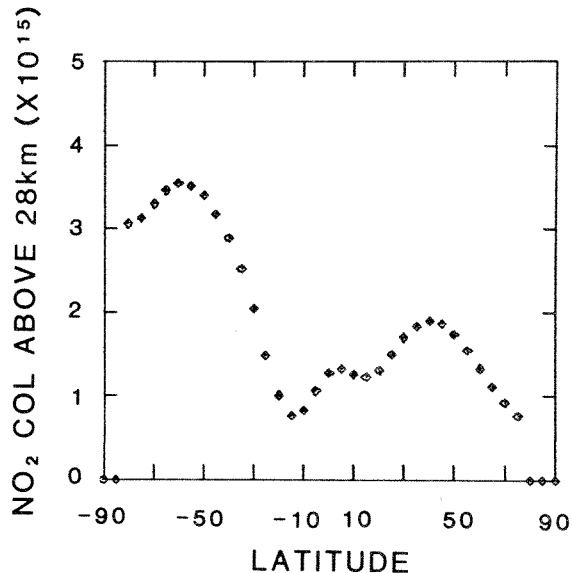


Figure 4. NO₂ column abundance above 28 km for Day 42 1982.

which requires correction below ~30 km. The effect of this correction on the NO₂ densities is never in excess of 20% and only achieves this value near 28 km and at high winter latitude where the NO₂ density is very small. NO₂ densities are calculated to $\pm 20\%$ at 28 km and $\pm 50\%$ at 38 km. Most of this error is normally due to inaccuracies in determining the instrument line of sight.

Figure 3 shows a typical NO₂ profile taken during January 1982. NO₂ profiles from Kerr and McElroy (1976), Ackerman et al., (1975), and Solomon and Garcia (1982) are shown for comparison. The SME and Solomon profiles are for January 1982 at 40°S and the others are for summer at 40°N, a set that should be comparable. This comparison shows a satisfying agreement between the SME profile and the earlier measurements; all three measured profiles also appear to be in harmony with the shape and magnitude of the model profile.

Figure 4 shows NO₂ column abundance above 28 km for Day 42 from south pole to northern terminator. The large amounts of NO₂ in the summer hemisphere, the equatorial minimum, and a variation in the winter hemisphere, resemble what was reported by Noxon (1979). A detailed theoretical discussion of this general behavior may be found in Solomon and Garcia (1982).

In Figure 5 we show a time and latitude display of the integrated column abundance of NO₂ above 28 km during the first quarter of 1982. Very prominent is the great degree of variability in the winter hemisphere and the relative invariance south of ~20°S. Noxon's studies (1979a,b, 1982) have already given hints of this seasonal effect which reflects the much larger degree of meridional movement of air in the winter stratosphere, at least in the northern hemisphere. The NMC maps during this period confirm the inference from Figure 5 that south of 20°S the stratospheric air flow at ~10mbar is highly zonal in comparison with the disturbed flow in the northern hemisphere.

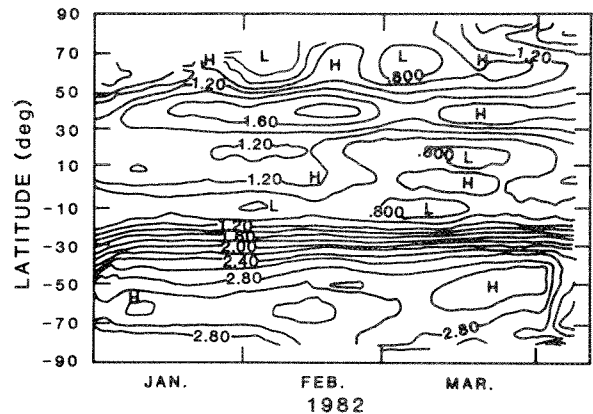


Figure 5. Integrated column abundance of NO₂ above 28 km in units of 10^{15} cm^{-2} as a function of latitude and time.

Of particular interest is the behavior near 60°N where we can discern the appearance and disappearance of a marked gradient in NO₂ with latitude; the "cliff" discussed by Noxon (1979a). The NMC maps confirm that the periods of high NO₂ at high latitudes occur when air flow is from midlatitude to high latitude; low NO₂ occurs when the flow is reversed. These oscillating air flow regimes occur in association with springtime warmings in the high latitude northern stratosphere.

A further example of the "Noxon Cliff" is shown in Figure 6 where the NO₂ column abundances above 28 km are proportional to the length of the line segments for two orbits on day 42. There is a clear difference between the latitude dependence of the two column abundances at high northern latitudes. The equatorial edge of the polar vortex was over Hudson Bay just where the abrupt decrease in NO₂ column is observed. We

NO₂ COL ABOVE 28 km DAY 42 1982

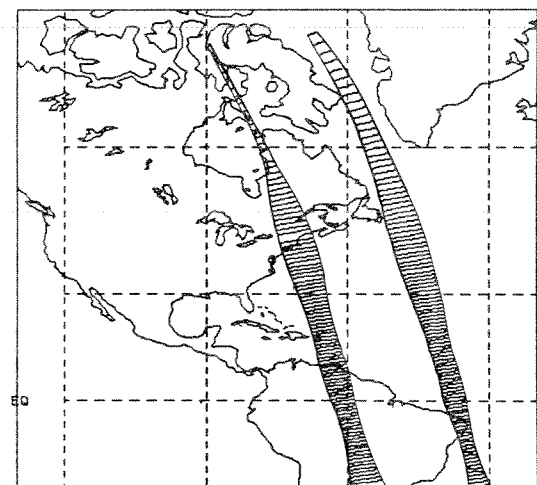


Figure 6. NO₂ column abundance above 28 km on Day 42 1982 for two consecutive orbits showing a cliff over Hudson Bay, Canada. The equatorial edge of the polar vortex is over Hudson Bay just where the abrupt decrease in NO₂ column is observed.

have numerous other examples which confirm this "cliff" behavior which will be discussed in detail elsewhere.

Conclusions

Measurements of the NO₂ density between 28 and 40 km have been made by the visible light instrument on board the Solar Mesosphere Explorer spacecraft during winter 1981/82. Daily profiles of NO₂ are being collected on 5 degree latitude centers over the Western Hemisphere and Western Europe with a high degree of accuracy.

References

- Ackerman, M. J. Fontanella, D. Frimout, A. Girard, N. Louisnard and C. Muller Simultaneous measurements of NO and NO₂ in the stratosphere, Atmospheric & Space Sci., 23, 651, 1975.
- Barth, C.A., D.W. Rusch, R.J. Thomas, G.H. Mount, G.J. Rottman, G.E. Thomas, R.W. Sanders, G.M. Lawrence, Solar Mesosphere Explorer: Scientific Objectives and Results, Geophys. Res. Lett., this issue, 1983.
- Coffey, M.T., W.G. Mankin and A. Goldman, Simultaneous Spectroscopic Determination of the Latitudinal, Seasonal, and Diurnal Variability of Stratospheric N₂O, NO, NO₂, and HNO₃, J. Geophys. Res., 86, 7331, 1981.
- Crutzen, P. Influence of Nitrogen Oxides on the Atmospheric Ozone Content, Quart. J. Roy. Meteorol. Soc. 96, 320, 1970.
- Johnston, H., Private Communication, 1982.
- Kerr, J. and C. McElroy, Measurement of stratospheric nitrogen dioxide from the AES stratospheric balloon program, Atmosphere 14, 166, 1976.
- Noxon, J.F., Stratospheric NO₂, 2. Global Behavior, J. Geophys. Res., 84, 5067, 1979a.
- Noxon, J.F., E.C. Whipple and R. Hyde, Stratospheric NO₂, 1. Observational Method and Behavior at Mid-Latitude, J. Geophys. Res., 84, 5047, 1979b.
- Noxon, J.F., W.R. Henderson, and R.B. Norton, Stratospheric NO₂, 3. The effects of Large Scale Horizontal Transport. J. Geophys. Res., submitted, 1982.
- Solomon, S. and R. Garcia, On the Distribution of NO₂ in the High Latitude Stratosphere, J. Geophys. Res., submitted, 1982.
- Thomas, G.E., C.A. Barth, E.R. Hansen, C.W. Hord, G.M. Lawrence, G.H. Mount, G.J. Rottman, D.W. Rusch, A.I. Stewart, R.J. Thomas, J. London, P.L. Bailey, P.J. Crutzen, R.E. Dickenson, J.C. Gille, S.C. Liu, J.F. Noxon, and C.B. Farmer, Scientific Objectives of the Solar Mesosphere Explorer Mission, Pageoph, 118, 591-615, 1980.

(Received December 22, 1982;
accepted January 25, 1983.)

SOLAR SPECTRAL IRRADIANCE, 120 to 190nm, October 13, 1981 - January 3, 1982

G.J. Rottman, C.A. Barth, R.J. Thomas, G.H. Mount, G.M. Lawrence,
D.W. Rusch, R.W. Sanders, G.E. Thomas, and J. London

Laboratory for Atmospheric and Space Physics and Department of
Astro-Geophysics, University of Colorado, Boulder, Colorado 80309

ABSTRACT. Beginning on October 13, 1981 a two channel spectrometer aboard the Solar Mesosphere Explorer has been obtaining daily measurements of full disc solar irradiance. These observations cover the spectral interval 120 to 305nm with ≈ 0.75 nm spectral resolution. The relative accuracy of the measurements from day to day over the first three solar rotations is approximately 1%. In this report we present analyses of Lyman-alpha, the integrated Schumann-Runge continuum (130-175nm), and the integrated Schumann-Runge bands (175 to 190nm). All three show a clear variability related primarily to the 27-day solar rotation period. Correlations of these three values of solar irradiance to ground-based indices of solar activity, 10.7cm flux and sunspot number, are presented.

Introduction

Solar ultraviolet radiation between 120 and 300nm is completely absorbed in the earth's upper atmosphere. Although the ultraviolet comprises only 1% of the total solar irradiance, it is largely responsible for the photochemistry and dynamics of the upper stratosphere, mesosphere and lower thermosphere.

The Solar Mesosphere Explorer (SME) is a satellite designed to study ozone in the atmosphere of the earth including the processes that create and destroy it. In addition to four limb-scanning instruments measuring temperature, pressure, ozone and other trace gases, the SME includes a small ultraviolet spectrometer taking daily measurements of full-disc solar irradiance.

In this letter we present the observations of solar Lyman-alpha at 121.6nm which influences ozone in the mesosphere primarily through its interaction with water vapor; irradiance in the Schumann-Runge continuum (130-175nm), a source of thermospheric atomic oxygen which is transported into the mesosphere; and irradiance in the Schumann-Runge bands (175-190nm) which penetrates into the mesosphere providing a direct source of atomic oxygen. We expect that the observed changes in solar ultraviolet produce a direct and measureable response of middle atmosphere ozone densities.

The SME was launched on October 6, 1981 from the Western Test Range into a nearly-circular, sun-synchronous orbit at an altitude of 534km with the north equator crossing occurring near 3:00PM local time. The scientific objectives of the SME mission are described in Thomas, *et al.*, (1980).

Copyright 1982 by the American Geophysical Union.

Paper number 2L0465.
0094-8276/82/002L-0465\$3.00

Observations

Solar data have been obtained on a routine basis starting on October 11, 1981 (day number 81284). In this brief letter we present irradiance data for three full solar rotations, a period from October 13, 1981 through January 3, 1982.

The solar instrument consists of an Ebert-Fastie spectrometer measuring solar radiation scattered from a small scattering screen. There are two separate spectral channels each with its own pulse counting photomultiplier tube. The G-channel is used in the spectral interval 120 to 200nm and the F-channel obtains useful data over the interval 174 to 305nm. The photometric sensitivity was determined in the laboratory relative to NBS photodiode standards. These laboratory measurements were made one year prior to launch and our absolute accuracy on-orbit is estimated to be $\pm 30\%$. The overall goal of the SME irradiance measurement is ± 15 to $\pm 20\%$ and will be achieved through comparison to sounding rocket experiments (see for example, Mount and Rottman, 1981). However, it is evident from the first 90 days of solar data that the instrument is extremely stable with little or no on-orbit degradation. This allows us to meet a primary goal of the solar instrument: to follow changes at or below the 1% relative accuracy level over time scales of days to weeks. Solar variations at these intermediate time scales are related to solar rotation and/or the development and disappearance of active regions. Long time scales of solar variability related to the 11 year sunspot cycle or 22 year magnetic field cycle can only be addressed after an extended period (> 3 years) of SME operations coupled with a successful sounding rocket (or shuttle) cross calibration effort.

Each channel of the solar spectrometer measures radiation from the full solar disc scattered from a small diffusing screen. The SME instrument was designed to include an additional set of screens used only for calibration. The calibration screens were used on day 81301 and day 82006, a time period spanning the three solar rotations discussed in this report. The short wavelength G-channel screen showed no change to within 0.4% and the long wavelength F-channel screen showed degradation of less than 1%.

The spectrometer has a spectral resolution of ≈ 0.75 nm with approximately three wavelength steps per instrument bandpass. The spacecraft spin rate is ≈ 12 seconds and the sun passes through a plane normal to the scattering screen once for each rotation of the satellite. At this point in the satellite rotation, a small solar sensor clocks out a single data sample and the grating

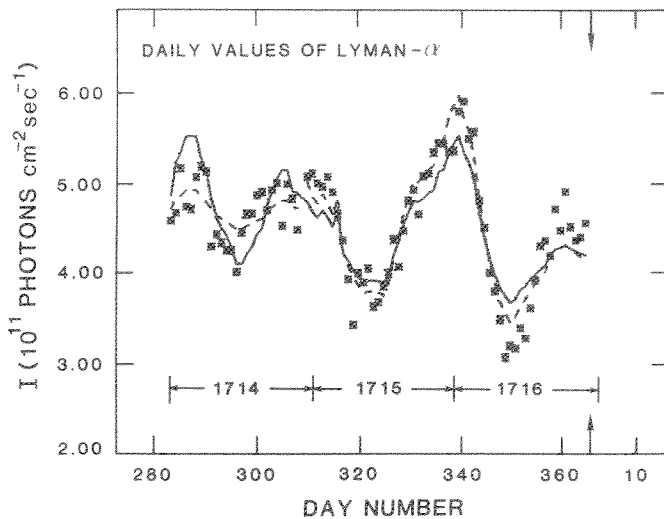


Figure 1. Daily values of solar Lyman-alpha irradiance and the linear regression on 10.7 cm flux (Table 1).

drive is incremented. For each calendar day portions of F and G spectra are pieced together to form a best average spectrum for that 24 hour period.

The sun was relatively active during the first three months of operation. The Zurich Sunspot number ranged from approximately 100 to almost 400 and the 10.7cm flux (in units of $10^{-22} \text{ Wm}^{-2}\text{Hz}^{-1}$) varied between 150 and 300. Both indices show a mixture of active and quiet solar behavior, typical for this time in the solar cycle. In particular two large flare periods (days 81286-81290 and 81344-81345) produced solar proton events while the last three weeks of this period had little or no solar activity. We have chosen to model the solar irradiance as a function of 10.7cm flux. This radio emission (2800MHz) is a ground-based index observed in Ottawa and is reported on a daily basis by NOAA. It has been employed in the past to model EUV solar flux variability with considerable success (Hinteregger, 1980). The source of the radio emission is high in the solar atmosphere, at the temperature level of the high transition region: $T \sim 10^6 \text{ K}$. The UV (140-300nm) emission is formed in the solar atmosphere at or near the temperature minimum and it is not unreasonable to find that the 10.7cm flux emission is only a marginal indicator of UV variability. Still, to the extent that the 10.7cm flux clearly tracks solar activity, we use it for this first investigation. The daily Zurich sunspot number is an alternate ground-based indicator of solar activity and we include the correlation of the UV irradiance to sunspot number. Our impression is that below 200nm the correlation with 10.7cm flux is somewhat higher.

Results

A) Lyman-alpha

Figure 1 shows the Lyman-alpha irradiance (10^{11} photons $\text{cm}^{-2}\text{sec}^{-1}$) measured from day 81286 through day 82003. These data have not been

adjusted for the change in earth-sun distance (from 0.998 to 0.983 AU). The calibration of the Lyman-alpha data set is based on a sounding rocket (27.052) experiment of November 23, 1981. This solar rocket experiment included a small NO cell with a MgF_2 window. The NO cell was calibrated in our laboratory against the same NBS standard photodiode used for the SME calibrations. The cross calibration is accurate to $\pm 20\%$ and establishes a value of 3.85 (11) photons $\text{cm}^{-2}\text{sec}^{-1}$ for day 327.

Variability due to the twenty-seven day solar rotation is clearly seen in Figure 1. The overplot of adjusted 10.7cm flux (solid line) more or less tracks the Lyman-alpha data through all three rotations. To examine the data more closely, they are subdivided into three individual rotation periods. The least-squares linear regression of Lyman-alpha on 10.7cm flux for the entire data set is given by.

$$F_{\text{Ly}\alpha} = 3.08(11) + 5.59(8)*F_{10.7} \quad (1)$$

A similar relationship was found in the OSO-5 data (Vidal-Madjar and Phissamay, 1980) and, in addition they found the coefficients varied over the solar cycle. The extended OSO-5 data set (1969-72 and 1974-75) allows analysis relative to slowly varying parameters, for example yearly means of 10.7cm flux. Future analysis of the SME data will study such long term effects. For the time being it is of interest to compare the SME regression (equation 1) with the relation found by Vidal-Madjar and Phissamay (1980) for medium to high levels of solar activity. If we substitute our 83 day mean value for 10.7cm flux (214) for their suggested yearly mean value we obtain:

$$F_{\text{Ly}\alpha} = 2.87(11) + 4.8(8)*F_{10.7} \quad (\text{V-M})$$

The linear regressions determined from the two data sets are remarkably similar. Comparison of the SME data set and the Vidal-Madjar results indicates that the absolute accuracies of the two data sets differ by less than 10%.

If we return to the SME Lyman-alpha data of Figure 1 and consider each solar rotation separately we obtain the statistical parameters shown in Table 1. Examination of Figure 1 (dashed lines give the 10.7cm flux scaled to the Lyman-alpha rotation by rotation) and of the correlation coefficients of Table 1 show that agreement of 10.7 variability and Lyman-alpha variability is quite good for rotation 2 and 3, but poor for rotation 1. In general we expect to see such differences from one period of solar activity to another. We will continue to model irradiance changes over individual rotations as well as over longer time periods.

B) Schumann-Runge Continuum

We refer to radiation in the spectral interval 130 to 175nm as Schumann-Runge Continuum (SRC) since this is the approximate spectral range of the corresponding molecular oxygen absorption feature. Essentially all of this radiation is absorbed in the thermosphere and is the source of atomic oxygen atoms which are transported into the mesosphere where

TABLE 1 Least-squares linear regression data for Lyman-alpha, integrated Schumann-Runge Continuum (130-175nm) and integrated Schuman-Runge bands (175-190nm) on 10.7cm flux and sunspot number. Analysis is carried out for the three individual solar rotations and for the entire period of 83 days.

	1	2	3	TOTAL
Carrington Rotation	1714	1715	1716	
Time Period (Days)	81286-81312	81313-81339	81340-82003	81286-82003
Lyman-alpha				
Regression on 10.7cm				
Constant Term (10^{11})	3.78 ±.15	2.71 ±.12	2.74 ±.11	3.08 ±.09
Linear Term (10^8)	2.35 ±.62	7.62 ±.59	7.40 ±.54	5.59 ±.40
Standard Error (10^{11})	.14	.11	.15	.18
Correlation Coefficient	.62	0.93	.94	0.84
Regression on Sunspot Number				
Constant Term (10^{11})	4.11 ±.08	3.61 ±.09	3.43 ±.07	3.70 ±.06
Linear Term (10^8)	0.94 ±.28	3.38 ±.44	4.01 ±.35	2.65 ±.24
Standard Error (10^{11})	.14	.16	.17	.21
Correlation Coefficient	0.56	0.84	0.92	0.78
Schumann-Runge Continuum				
Regression on 10.7cm				
Constant Term (10^{12})	1.29 ±.04	1.08 ±.02	1.17 ±.02	1.20 ±.02
Linear Term (10^9)	.13 ±.14	1.29 ±.09	.86 ±.09	.60 ±.08
Standard Error (10^{11})	.27	.15	.23	.33
Correlation Coefficient	0.22	0.94	0.90	0.67
Regression on Sunspot Number				
Constant Term (10^{12})	1.29 ±.02	1.23 ±.02	1.24 ±.01	1.26 ±.01
Linear Term (10^9)	.11 ±.06	.49 ±.08	.47 ±.05	.31 ±.04
Standard Error (10^{11})	.25	.28	.25	.33
Correlation Coefficient	0.42	0.79	0.89	0.67
Schumann-Runge Bands				
Regression on 10.7cm				
Constant Term (10^{12})	2.94 ±.07	2.63 ±.05	2.73 ±.05	2.79 ±.04
Linear Term (10^9)	0.0 ±.28	1.56 ±.26	1.33 ±.24	.79 ±.18
Standard Error (10^{11})	.57	.48	.62	.72
Correlation Coefficient	0.0	0.77	0.78	0.46
Regression on Sunspot Number				
Constant Term (10^{12})	2.92 ±.03	2.83 ±.03	2.84 ±.03	2.88 ±.02
Linear Term (10^9)	0.07 ±.13	.60 ±.16	.78 ±.13	.41 ±.09
Standard Error (10^{11})	.57	.60	.58	.72
Correlation Coefficient	0.13	0.60	0.81	0.47

recombination occurs. We have normalized the SME data of day 319 to the Mount-Rottman (1981) rocket data from July 15, 1980. Day 319 was selected because the 10.7cm flux and Zurich

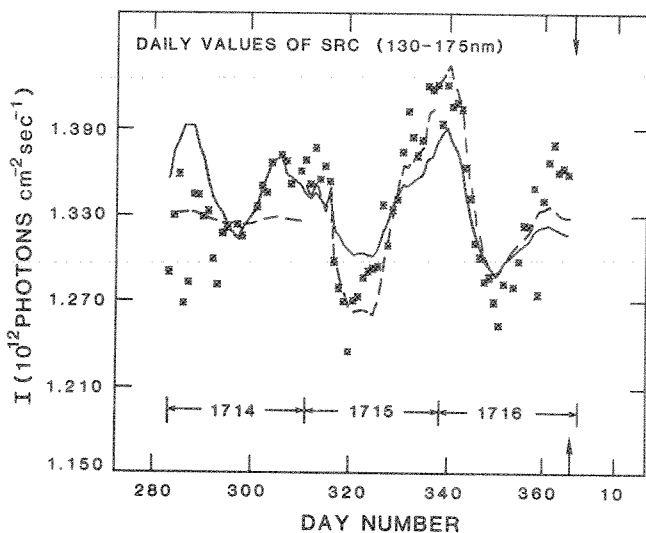


Figure 2. Daily values of the integrated irradiance in the Schumann-Runge Continuum (130-175nm).

sunspot number of that day are similar to the day of the rocket flight.

Figure 2 shows the integrated irradiance (130-175nm) from day 81286 to day 82003. The solid line is the 10.7cm flux scaled to the SRC data according to the least-squares linear regression of the entire data set:

$$F_{\text{SRC}} = 1.20(12) + 6.00(8) * F_{10.7} \quad (2)$$

When a rotation-by-rotation statistical analysis is performed we obtain the dashed lines of Figure 2 and the statistical parameters in Table 1. The correlation coefficient of the entire data set is only 0.67 and again it is clear that the trend to follow 10.7cm flux is stronger for rotations 2 and 3 than for rotation 1.

The ±6% percent variability seen in the integrated SRC is not the mean variability but is clearly weighted by the longer wavelengths where the bulk of the energy resides. In fact the shorter wavelengths, characterized by strong emission lines, show larger variations.

C) Schumann-Runge Bands

We define the spectral interval of the Schumann Runge Bands (SRB) of O_2 absorption to

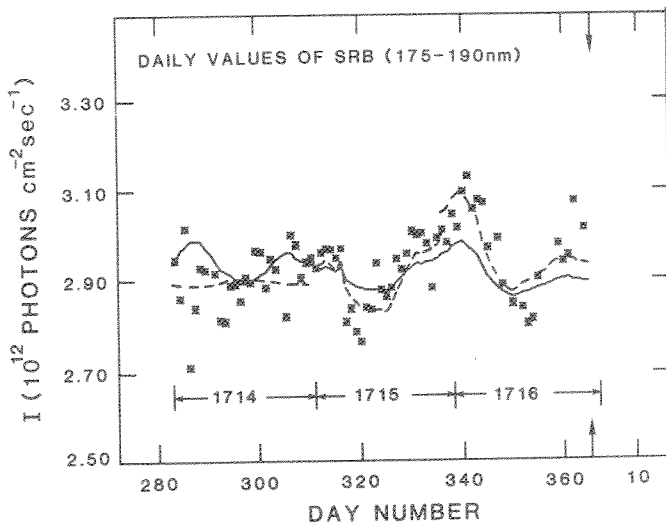


Figure 3. Daily values of the integrated irradiance in the Schumann-Runge Bands (175-190nm).

be 175 to 190nm. The absolute irradiance values have been established by normalizing the SME data of day 319 to the Mount-Rottman (1981) rocket data of July 15, 1980. The daily value of SRB is shown in Figure 3 and also shows the 27 day solar rotation effect (Heath, 1980). The least-squares linear regression of the entire data set is given by:

$$F_{\text{SRB}} = 2.79(12) + 7.90(8) * F_{10.7} \quad (3)$$

When the data are analyzed separately for each rotation we obtain the statistical parameters shown in Table 1. The correlation coefficients for rotation 2 and 3 are moderately high but the overall correlation coefficient is only 0.46. This is due primarily to rotation 1 which has no statistical correlation to 10.7cm flux. We find that the 10.7cm flux is only a marginal indicator of the solar variability at wavelengths above 175nm. As mentioned earlier this is not surprising since the layers of radio emission and UV emission are widely separated in the solar atmosphere and only weakly connected.

Summary

The solar instrument on SME provides a daily measurement of full disc solar irradiance in the spectral interval 120 to 305nm. The instrument has shown little or no degradation during the first three months of operations. We believe that the instrument stability is adequate to accurately follow changes in solar ultraviolet radiation over time periods of days to weeks. Data from the first 83 days of the SME mission, a time period covering three complete solar rotations, have been correlated with ground-based indices of solar activity. In this first report, we present irradiance measurements at Lyman-alpha showing a clear 27-day variability of $\pm 15\%$. The correlation of Lyman-alpha data to 10.7cm radio flux and to

sunspot number are quite high for two of the rotation periods, but only marginal for the third.

Solar irradiance in the integrated Schumann-Runge continuum (130-175nm) shows 27-day variability of $\pm 6\%$ and the longer wavelength interval of the Schumann-Runge bands (175-190nm) give a variability of $\pm 5\%$. Similar to the Lyman-alpha results we find a high correlation of solar UV irradiance in these wavelength intervals to the 10.7cm flux and sunspot number for only two of the three solar rotations. To the extent that these three solar rotations are typical for this period in the solar cycle, we conclude that ground-based indices, for example 10.7cm flux, can only be used to model the average variability of ultraviolet irradiance. The correlations are not always strong and for certain periods the models break down altogether. The objective of the SME solar spectrometer is to accurately measure changes in solar irradiance at or near the one percent level, far more accurately than present empirical correlations can predict. Since the ozone distribution of the middle atmosphere is sensitive to day-to-day variations in solar irradiance, the SME investigations make direct use of these daily solar measurements.

Acknowledgements

The solar irradiance data described in this paper is stored in the SME data base and is available from computer files or in printed form. The SME project is managed by the Jet Propulsion Laboratory for the National Aeronautics and Space Administration. The preliminary ground-based solar indices were obtained from the Space Environment Services Center of the National Oceanic and Atmospheric Administration.

References

- Heath, D.F., A review of observational evidence for short and long term ultraviolet flux variability of the sun, *Sun and Climate*, Toulouse, France, 447, 1980.
- Hinteregger, H.E., Representations of solar EUV fluxes for aeronautical applications, *Adv. Space Res.*, Vol. 1, 39, 1981.
- Mount, G.H., and G.J. Rottman, The Solar Spectral Irradiance 1200-3184A near Solar Maximum, *J. Geophys. Res.*, 86, 9193, 1981.
- Vidal-Madjar, A. and B. Phissamay, The Solar Ly α Flux near Solar Minimum, *Solar Physics*, 66, 259, 1980.
- Thomas, G.E., C.A. Barth, E.R. Hansen, C.W. Hord, G.M. Lawrence, G.H. Mount, G.J. Rottman, D.W. Rusch, A.I. Stewart, R.J. Thomas, J. London, P.L. Bailey, P.J. Crutzen, R.E. Dickenson, J.C. Gille, S.C. Liu, J.F. Noxon, and C.B. Farmer, Scientific Objectives of the Solar Mesosphere Explorer Mission, *Pageoph*, Vol. 118, 591-615, 1980.

(Received February 17, 1982;
accepted March 12, 1982.)

DUMP OF TAPE SO-1

INPUT TAPE SO-1 ON TB1
DATA INPUT H9 NF 1124 SR 2 1 1 SR 1124 LAST 1

Spacecraft SME
DATA Set 81-100A-0
D # 64437
Time span
12/10/81 - 1/22/82

FILE INPUT DATA RECORDS MAX. READ ERROR SUMMARY INPUT RETRIES
RECS. INPUT SIZE PERM ZERO B SHORT UNDEF. #RECS. TOTAL#
1 4 4 80 0 0 0 0 0 0

FILE	RECORD	LENGTH	304BYTES
(0)	20203130	373420B3	35205139
(40)	20202020	20202020	20202020
(80)	20202020	20202020	20202020
(120)	20202020	20202020	20202020
(160)	20202020	20202020	20202020
(200)	20202020	20202020	20202020
(240)	20202020	20202020	20202020
(280)	20202020	20202020	20202020

FILE INPUT DATA RECORDS MAX. READ ERROR SUMMARY INPUT RETRIES
RECS. INPUT SIZE PERM ZERO B SHORT UNDEF. #RECS. TOTAL#
2 36 36 304 0 0 0 0 0 0

FILE	RECORD	LENGTH	304BYTES
(0)	20353120	2037302E	33202131
(40)	36203220	20312E32	35452B31
(80)	2B313020	20312E38	37452B31
(120)	2B313020	20322E30	30452B31
(160)	2B303920	20332E30	38452B30
(200)	2B313120	20322E32	36452B31
(240)	2B313130	20372E32	36452B31
(280)	2B313020	20392E32	39452B30

FILE INPUT DATA RECORDS MAX. READ ERROR SUMMARY INPUT RETRIES
RECS. INPUT SIZE PERM ZERO B SHORT UNDEF. #RECS. TOTAL#
1124 42 43 304 0 0 0 0 0 0

EOJ DUMP STOPPED AFTER FILE 1124 # OF PERMANENT READ ERRORS 0

START TIME 01/31/85 14:20:29 STOP TIME 01/31/85 14:26:01